



The University of  
**Nottingham**

School of Molecular Medical Science

**PRE-CLINICAL DEVELOPMENT OF  
HUMAN APURINIC/APYRIMIDINIC ENDONUCLEASE (APE1)  
INHIBITORS FOR CANCER THERAPY**

*By*

Mohammed Zubair Khuder Mohammed

MBChB, MSc

**MEDICAL LIBRARY**  
QUEENS MEDICAL CENTRE

**Thesis submitted to the University of Nottingham for  
the degree of Doctor of Philosophy**

**July 2011**

بسم الله الرحمن الرحيم

(أقرأ باسم ربك الذي خلق \* خلق الإنسان من علق \* اقرأ  
وربك الأكرم \* الذي علم بالقلم \* علم الإنسان ما لم يعلم)

***In the name of God, Most Gracious, Most Merciful***

*(Read in the name of your Lord, Who created \* Created  
man, out of a (mere) clot of congealed blood \* Proclaim!  
And thy Lord is Most Bountiful, \* He Who taught (the use  
of) the pen \* Taught man that which he knew not.)*

*To My Father Zubair Khuder Mohammed*  
*&*  
*In Memory of My Mother Maryam Abdullah Mohammed (1951 – 1997)*

## Abstract

Modulation of DNA base excision repair (BER) has the potential to enhance response to chemotherapy and improve outcomes in tumours such as melanoma, glioma and pancreatic cancer. APE1, a critical protein in BER that processes potentially cytotoxic abasic sites (AP sites), is a promising new target in cancer. In the current study, my aim was to develop small molecule inhibitors of APE1 for cancer therapy. An industry-standard high throughput virtual screening strategy was adopted. The SYBYL8.0 (Tripos, St Louis, MO, USA) molecular modelling software suite was used to build inhibitor templates. Similarity searching strategies were then applied using ROCS 2.3 (Open Eye Scientific, Santa Fe, NM, USA) to extract pharmacophorically related subsets of compounds from a chemically diverse database of 2.6 million compounds. The compounds in these subsets were subjected to docking against the active site of the APE1 model, using the genetic algorithm-based programme GOLD2.7 (CCDC, Cambridge, UK). Predicted ligand poses were ranked on the basis of several scoring functions. The top virtual hits with promising pharmaceutical properties underwent detailed *in vitro* analyses using fluorescence-based APE1 AP-site cleavage assays and counter screened using endonuclease IV AP-site cleavage assays, fluorescence quenching assays and Whole cell extract AP-site cleavage assays. Biochemical APE1 inhibitors were then subjected to detailed cytotoxicity analyses. Several specific APE1 inhibitors were isolated by this approach. The IC<sub>50</sub> for APE1 inhibition ranged between 50 nM and 25 µM. I also demonstrated that APE1 inhibitors lead to accumulation of AP sites in genomic DNA and potentiated the cytotoxicity of alkylating agents in melanoma, glioma and pancreatic cancer cell lines. I have



also shown that APE1 inhibitors induce delay in cell cycle progression and caused delay in cancer cell growth. I also demonstrated that APE1 knockdown by shRNA results in decrease cancer cell growth and enhanced cell killing by alkylating agent in Glioma cell line. This PhD project provides evidence that APE1 is an emerging drug target and could have therapeutic application in patients with melanoma, glioma and pancreatic cancer.

## **Publications arising from this thesis**

### **Peer reviewed publications**

**Mohammed Z. Mohammed**, Vaddadi N. Vyjayanti, Charles A. Laughton, Lodewijk V. Dekker, Peter M. Fischer, David M. Wilson III, Rachel Abbotts, Suharsh Shah, Poulam M. Patel, Ian D. Hickson, and Srinivasan Madhusudan. 'Development and evaluation of (APE1) inhibitors in melanoma and glioma cell lines.' *British Journal of Cancer* 2011 Feb 15; 104(4): 653-663.

Al-Attar A, Gossage L, Fareed KR, Shehata M, **Mohammed M**, Zaitoun AM, Soomro IN, Lobo DN, Abbotts R, Chan S, Madhusudan S. 'Human apurinic/apyrimidinic endonuclease (APE1) is a potential drug target in melanoma, ovarian, gastric and pancreatobiliary cancers.' *British Journal of Cancer* 2010 Feb 16; 102(4): 704-709.

Gossage L., **Mohammed M**, Madhusudan S. 'Clinical implications of DNA repair genetic alterations in cancer.' *MEMO – Magazine of European Medical Oncology* Volume 2, Number 1, 15-19, DOI: 10.1007/s12254-009-0093-y

### **Oral presentation**

**Mohammed M**, Laughton C, Dekker L, Fischer P, Abbotts R, Patel P, and Madhusudan S. 'Development of Human Apurinic/Apyrimidinic Endonuclease

1 (APE1) inhibitors for cancer therapy.’ National Cancer Research Institute (NCRI), Cancer Conference. Birmingham, UK (Oct 2009).

#### **Poster presentations**

**Mohammed M, Vyjayanti V, Laughton C, Dekker L, Fischer P, David Wilson D III, Patel P, and Madhusudan S.** ‘Structure-based design, discovery, and pharmacological profiling of human AP endonuclease (APE1) inhibitors for cancer therapy.’ AACR 101<sup>st</sup> annual meeting. Washington DC, USA (April 2010).

**Mohammed M, Laughton C, Dekker L, Fischer P, Abbotts R, Patel P, and Madhusudan S.** ‘Development of Human Apurinic/Apyrimidinic Endonuclease 1 (APE1) inhibitors for cancer therapy.’ National Cancer Research Institute (NCRI), Cancer Conference. Birmingham, UK (Oct 2009).

**Mohammed M, Laughton C, Hickson I, and Madhusudan S.** ‘Development of Human Apurinic/Apyrimidinic Endonuclease 1 (APE1) inhibitors for cancer therapy.’ Annual Symposium of Biochemical society: DNA damage: from causes to cures. Robinson College, Cambridge, UK (Dec 2008).

#### **Prices won from work arising from this thesis**

**Travel prize:** Graduate School, University of Nottingham, Nottingham, UK. (July 2010).

**1<sup>st</sup> prize:** Postgraduate day, Molecular Medical School, University of Nottingham, Nottingham, UK. (June 2010).

## **Acknowledgements**

I would like to express my deepest gratitude to my supervisor Dr Srinivasan Madhusudan for his patience, support, enthusiasm and encouragement that was essential to completing this thesis. His advice and friendship has been invaluable on both an academic and personal level. I would also like to thank Dr Charlie Laughton, Dr Lodewijk Dekker and Professor Peter Fischer, School of Pharmacy, University of Nottingham for their interest and support of the project.

I am indebted to Dr Roger McGilvray and Khaleel Fareed for their interest, Lab support and invaluable contributions which made the completion of this thesis possible.

I would also like to thank many of the other members of the Academic and Clinical Department of Oncology for their technical support, advice and friendship during my time spent in the department, in particular, Mr Suharsh Shah, Dr Hester Franks, Dr. Rachel Abbots, Mr Robb Moss, Dr Stewart Martin, and Mrs Julie Stanley.

I would also like to thank Dr David Wilson III, National Institute on Ageing, NIH, Baltimore, USA for his invaluable contribution in this thesis.

My parents and family have given me their unequivocal support throughout this testing time for which I am extremely grateful. Finally, I would like to thank my sponsor (Iraqi cultural office) for their, encouragement and support, all of which helped in no small part to the completion of this work.

## TABLE OF CONTENTS

Abstract.....	i
Acknowledgements.....	v
1. Introduction.....	2
1.1 DNA repair pathways and cancer.....	2
1.2 Base excision repair.....	5
1.2.1 Overview of BER pathway.....	5
1.2.2 BER Proteins .....	11
1.3 Human APE1 in BER.....	23
1.3.1 Formation and consequence of AP sites.....	23
1.3.2 APURINIC/APYRIMIDINIC (AP) ENDONUCLEASES .....	27
1.3.3 Human apurinic/apyrimidinic endonuclease (APE1) .....	28
1.3.4 Functions of APE1.....	31
1.4 Functional pre-clinical studies on APE1 .....	39
1.4.1 APE1 DNA repair activity is critical for cell viability .....	39
1.4.2 APE1 depletion hypersensitises cells to DNA base damage .....	40
1.4.3 APE1 overexpression protects cells from DNA damage and is implicated in treatment resistance .....	42
1.5 APE1 and human cancer.....	43
1.5.1 APE1 polymorphisms and cancer susceptibility .....	43
1.5.2 APE1 overexpression in human cancers.....	43
1.5.3 APE1 subcellular localisation in cancer .....	44
1.5.4 APE1 expression and localisation as marker of prognosis and treatment response .....	45
1.6 Synthetic lethality strategy .....	50
1.7 Combination therapy .....	52
1.7.1 APE1 is a promising anticancer drug target .....	53
1.8 Current status of APE1 repair domain inhibitors .....	53
1.8.1 Methoxyamine (MX).....	54
1.8.2 Lucanthone .....	54
1.8.3 CRT0044876 (7-Nitroindole-2-carboxylic acid) (CRT) .....	54
1.8.4 Arylstibonic acid compounds .....	55
1.8.5 Pharmacophore guided isolation of APE1 inhibitors .....	56
1.8.6 AR03.....	56
1.8.7 6-Hydroxy-DL-DOPA, Reactive Blue 2, and myricetin .....	58
1.9 Conclusion .....	59
Aims of the study.....	61
2. Material and methods .....	63
2.1 Enzymes, antibodies, chemicals and oligonucleotides .....	63
2.2 Potential small molecule inhibitors of APE1 .....	64
2.3 Molecular modelling.....	64
2.4 Virtual screening.....	67
2.4.1 APE1 active site localization .....	67
2.4.2 APE1 inhibitors template design .....	68
2.4.3 GOLD2.7 (Gene Optimization for Ligand Docking) .....	68
2.4.4 ROCS2.3.....	69
2.5 Biochemical screening.....	70
2.5.1 Fluorescence based AP-site cleavage assay .....	70
2.5.2 Screening and evaluation of potential APE1 inhibitors.....	72

2.5.3 Counter screening in endonuclease IV AP-site cleavage assay.....	73
2.5.4 Fluorescence quenching assay .....	74
2.5.5 Whole cell extract AP-site cleavage assay .....	75
2.6 Cell based investigation.....	76
2.6.1 Cell lines and culture media .....	76
2.6.2 CellTiter 96 <sup>®</sup> AQueous Non-Radioactive Cell Proliferation Assay (MTS assay).....	76
2.6.3 Growth Curve .....	78
2.6.4 Clonogenic survival assay .....	78
2.6.5 AP sites quantification assay (Aldehyde Reactive Probe).....	79
2.6.6 FACS analysis .....	81
2.6.7 Migration assay.....	82
2.7 APE1 knocked down studies .....	83
2.7.1 shRNA plasmid constructs and SurFECT transfection reagents .....	83
2.7.2 Transformation and purification of SureSilencing plasmid DNA ...	84
2.7.3 Large-scale preparation of plasmid DNA (QIAGEN, QIA prep <sup>®</sup> mini-prep protocol).....	85
2.7.4 Determination of DNA concentration .....	86
2.7.5 Restriction enzyme digestion.....	87
2.7.6 Selection of antibiotic resistance .....	87
2.7.7 Transfection of APE1 ShRNA plasmid.....	88
2.8 Western blot.....	89
2.8.1 Preparation of cell lysate .....	89
2.8.2 Cell lysate protein quantification (Bradford assay).....	89
2.8.3 Denaturing polyacrylamide gel electrophoresis .....	90
3. Molecular modelling.....	92
3.1 Introduction.....	92
3.2 Results .....	98
3.2.1. APE1 crystal structure selection and active site localization .....	98
3.2.2. Design of pharmacophore model.....	103
3.2.3. Pharmacophore guided similarity search analysis.....	106
3.2.4. Virtual docking studies of potential APE1 inhibitor hits.....	108
3.3 Discussion and conclusion.....	117
4. Biochemical screening.....	120
4.1. Introduction.....	120
4.2 Fluorescence based APE1 AP-site cleavage assay .....	123
4.3 Counter screenings.....	124
4.3.1 Fluorescence based endonuclease IV AP-site cleavage assay.....	124
4.3.2 Fluorescence quenching assay .....	125
4.4 Whole cell extract (WCE) AP-site cleavage assay.....	125
4.5 Results .....	126
4.5.1 Development of Fluorescence based AP-site cleavage assay.....	126
4.6.2 Optimization of fluorescence quenching assay (FQA).....	131
4.6.3 Optimization of Endonuclease IV AP-site cleavage assay .....	132
4.6.4 Identification of hits (table 4.2) .....	135
4.6.5 Measurement of IC <sub>50</sub> values for specific APE1 inhibitors .....	139
4.6.6 AP site cleavage using HeLa whole cell extracts .....	140
4.6.7 Kinetic analysis of P118 .....	142
4.6.8 AP-site cleavage assay using D148E polymeric variant of APE1	144

4.7 Discussion.....	146
5. Cell based investigations .....	149
5.1 Introduction.....	149
5.1.1 Alkylating agents .....	149
5.1.2 Doxorubicin .....	150
5.2 Results .....	151
5.2.1 Western blotting analysis.....	151
5.2.2 Cytotoxicity of APE1 inhibitors in cancer cell lines .....	152
5.2.3 AP site quantification .....	172
5.2.4 Fluorescence activated cell sorting (FACS) analysis .....	176
5.3 Discussion.....	178
APE1 expression was confirmed in all cancer cells. ....	178
6. APE1 Knock down studies .....	181
6.1 Introduction.....	181
6.2 Results .....	182
6.2.1 Transformation of BL21 (DE3) cells.....	182
6.2.2 Minimum effective dose determination.....	184
6.2.3 APE1 knock down in U89MG glioma cell line.....	185
6.2.5 Biological consequence of APE1 knock down in U89MG cells...	187
6.3 Discussion.....	190
7. Biochemical analyses of P118 analogues .....	192
7.1 Introduction.....	192
7.2 Results .....	193
7.2.1 Biochemical screening.....	193
7.3 Discussion.....	199
8. General discussion and conclusions .....	201
8.1 General discussion .....	201
8.2 Summary of key findings .....	208
8.3 Suggestions for future studies.....	210

**TABLE OF FIGURES**

FIGURE 1.1 ..... 3

FIGURE 1.2 ..... 9

FIGURE 1.3 ..... 24

FIGURE 1.4 ..... 27

FIGURE 1.5 ..... 30

FIGURE 1.6 ..... 37

FIGURE 1.7 ..... 57

FIGURE 2.1 ..... 66

FIGURE 2.2 ..... 72

FIGURE 2.3 ..... 84

FIGURE 3.1 ..... 100

FIGURE 3.2 ..... 102

FIGURE 3.3 ..... 104

FIGURE 3.4 ..... 105

FIGURE 3.5 ..... 106

FIGURE 3.6 ..... 108

FIGURE 3.7 ..... 110

FIGURE 3.8 ..... 111

FIGURE 4.1 ..... 128

FIGURE 4.2 ..... 129

FIGURE 4.3 ..... 130

FIGURE 4.4 ..... 131

FIGURE 4.5 ..... 132

FIGURE 4.6 ..... 133

FIGURE 4.7 ..... 134

FIGURE 4.8 ..... 137

FIGURE 4.9 ..... 138

FIGURE 4.10 ..... 140

FIGURE 4.11 ..... 143

FIGURE 4.12 ..... 145

FIGURE 5.1 ..... 151

FIGURE 5.2 ..... 152

FIGURE 5.3 ..... 155

FIGURE 5.4 ..... 157

FIGURE 5.5 ..... 157

FIGURE 5.6 ..... 158

FIGURE 5.7 ..... 158

FIGURE 5.8 ..... 159

FIGURE 5.9 ..... 160

FIGURE 5.10 ..... 161

FIGURE 5.11 ..... 161

FIGURE 5.12 ..... 163

FIGURE 5.13 ..... 164

FIGURE 5.14 ..... 166

FIGURE 5.15 ..... 167



FIGURE 5.16 .....	169
FIGURE 5.17 .....	170
FIGURE 5.18 .....	171
FIGURE 5.19 .....	172
FIGURE 5.20 .....	174
FIGURE 5.21 .....	175
FIGURE 5.22 .....	177

FIGURE 6. 1. ....	183
FIGURE 6.2 .....	185
FIGURE 6.3 .....	187
FIGURE 6.4 .....	188
FIGURE 6.5 .....	189
FIGURE 6.6 .....	189

FIGURE 7.1. ....	196
FIGURE 7.2 .....	198

## List of abbreviations

aa.....	Amino acid
AAG.....	Alkyl adenine glycosylase
AGT.....	alkylguanine DNA alkyltransferase
AP.....	Apurinic/Apyrimidinic
ATP.....	Adenosine 5'- triphosphate
BER.....	Base excision repair
Bp.....	Base pairs
BSA.....	Bovine serum albumin
cDNA.....	Complementary DNA
DMSO.....	Dimethylsulphoxide
DNA.....	Deoxyribonucleic acid
dNTP.....	Deoxy-nucleotide triphosphate
dRP.....	deoxy sugar phosphate
DSB.....	Double strand DNA break
DTT.....	Dithiothreitol
<i>E. coli</i> .....	<i>Escherichia coli</i>
EDTA.....	Ethylenediamine tetra-acetic acid
FBS.....	Foetal bovine serum
FEN1.....	Flap Endonuclease 1
FQA.....	Fluorescent quenching assay
g.....	Gram
g.....	Unit of centrifugal force
GOLD.....	Gene Optimisation for Ligand Docking
HEPES.....	9N- [2-Hydroxyethyl]piperazine-N'- [2-ethanesulphonicacid])
His•Tag.....	Hexa-histidine tag
HR.....	Homologus recomination
HRP.....	Horseradish peroxidase
IR.....	Ionizing radiation
kDa.....	Kilodalton
M.....	Molar
mM.....	Millimolar
MMR.....	DNA mismatch repair
μM.....	Micromolar
ml.....	Millilitre
μl.....	Microlitre
MMS.....	Methyl methane sulphonate
NER.....	nucleotide excision repair
NHEJ.....	Non homologous end joining
nM.....	Nanomolar
NTP.....	Nucleoside triphosphate
OD.....	Optical density (nm)
PAGE.....	Polyacrylamide gel electrophoresis
PARP-1.....	Poly(ADP-Ribose)Polymerase-1
PBSA.....	Phosphate buffered saline "A"
PCNA.....	Proliferating cell nuclear antigen
PNK.....	Polynucleotide kinase
PUA.....	Phospho α/β -unsaturated aldehyde
RFC.....	Replication Factor C

RNA.....	Ribonucleic acid
RNAse.....	Ribonuclease
ROCS.....	Rapid Overlay of Chemical Structure
ROS .....	Reactive oxygen species
Rpm.....	Revolutions per minute
SDS.....	Sodium dodecyl sulphate
SMUG1 .....	Single-strand selective monofunctional uracil DNA glycosylase1
SN.....	Nucleophilic substitution
SSA.....	Single-strand annealing
SSB.....	Single strand DNA break
ssDNA.....	Single-stranded DNA
TBE.....	Tris/borate/EDTA buffer
TDG .....	Thymine-DNA-glycosylase
THF .....	Tetrahydrofuran
TMZ.....	Temozolomide
Tris.....	Tris [hydroxymethyl]aminomethane
UDG.....	Uracil DNA glycosylase
UV.....	Ultra-Violet
VMD.....	Visual Molecular Dynamics
v/v.....	Volume for volume
WCE .....	Whole Cell Extract
WHO.....	World Health Organisation
w/v.....	Weight for volume
XRCC1.....	X-ray repair cross complementing protein 1

# ***Chapter 1***

## ***Introduction***

---

# **1. Introduction**

Cancer is a leading cause of mortality worldwide and accounts for about 13% of all deaths in 2004[1]. World Health Organisation (WHO) estimates that 84 million people will die from cancer between 2005 and 2015[2] with Lung, gastric, colorectal, hepatic and breast cancers accounting for more than 50% of cancer related deaths[2].

Chemotherapy and radiotherapy are important treatment modalities currently available to improve outcomes in patients with advanced tumours. The cytotoxicity of these agents is directly related to their ability to induce genomic DNA damage. However, the recognition of damage induced by these agents and the initiation of DNA repair are important mechanisms for therapeutic resistance which negatively impacts upon therapeutic efficacy [3].

## **1.1 DNA repair pathways and cancer**

Genomic DNA possesses an inherent instability and at risk of damage by endogenous (e.g. reactive oxygen species) and exogenous (UV, ionizing radiation and chemotherapeutic agents) DNA damaging agents. When left unrepaired, this damage could result in highly cytotoxic lesions or non-canonical base pairing during replication, leading to the propagation of potentially mutagenic lesions or induction of apoptosis. A number of DNA repair mechanisms have evolved to ensure genomic integrity can be preserved. In response to DNA damage normally cells respond by either (a) tolerance to damage (b) activation of DNA damage checkpoints and subsequent modulation of cell cycle progression to allow time for repair and to prevent transmission of damaged or incompletely replicated chromosomes; (c) initiation of DNA repair

and removal of damage; (d) transcriptional response that may be beneficial to the cell survival and (e) induction of apoptosis.

DNA damaging agents can induce a broad spectrum of DNA damaging lesions. Therefore, multiple DNA repair pathways exist in cells to repair these harmful damaging lesions. (Figure 1.1).

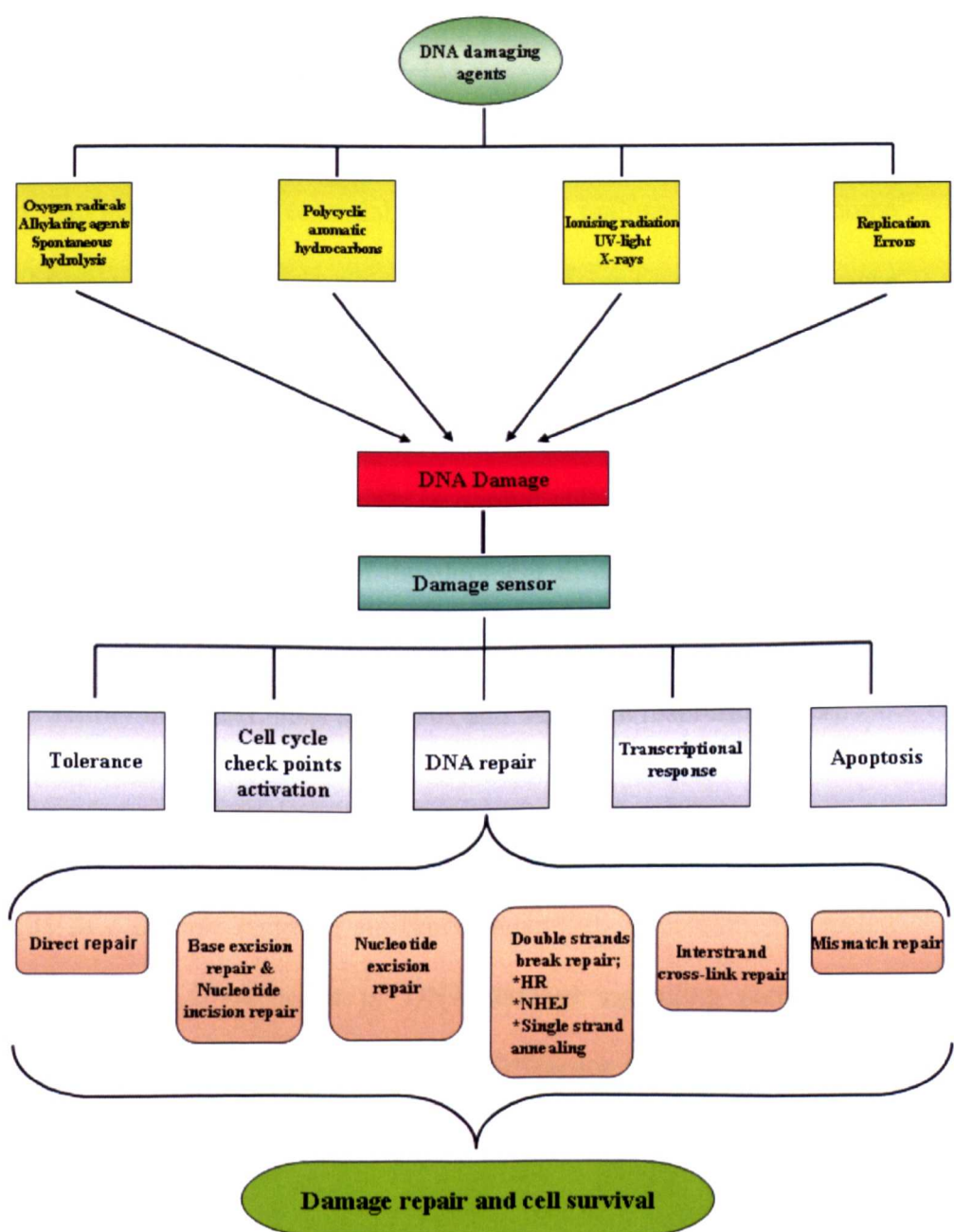


Figure 1.1 DNA damage responses in mammalian cells.

These pathways include: (a) direct repair of alkyl adducts by O6-

alkylguanine DNA alkyltransferase (AGT); (b) repair of mismatches and insertion/deletion loops by DNA mismatch repair (MMR); (c) repair of double-strand breaks by homologous recombination (HR), non-homologous end joining (NHEJ) and single-strand annealing (SSA); (d) repair of bulky DNA adducts by nucleotide excision repair (NER) (e) repair of cross-links by DNA inter-strand cross-link repair; (f) repair of base damage and single-strand breaks by base excision repair (BER) [4-11].

Several enzymes involved in DNA repair are conserved throughout evolution, suggesting their essential role in the maintenance of genome stability. Moreover, mutations in several of the DNA repair genes is the cause of cancer predisposing syndromes associated with inherent chromosome instability in man[12]. In addition, polymorphisms in DNA repair genes that confer suboptimal DNA repair capacity in normal cells may increase genomic instability and may increase risk of development of cancer to environmental carcinogens[13, 14]. Polymorphism of the DNA repair genes may also effect the natural history of cancer, alter prognosis and treatment response[15-19].

Pharmacological inhibition of DNA repair, has the potential to enhance cytotoxicity of a diverse range of anticancer agent[20]. Moreover, the recent use of inhibitors of DNA repair or DNA damage signalling pathways in synthetic lethality strategy exploiting genetic difference in cells is an exciting new treatment modality[21, 22].

In this thesis, I detail the work that I have done in targeting human Base Excision Repair (BER) for cancer therapy. The major human

apurinic/aprimidinic endonuclease (APE1), a key player in base excision repair (BER), was the focus of my research. The pioneering work from my group recently resulted in identification and characterization of first generation small molecule inhibitors of APE1[23]. The main aim of this project was to use the first generation APE1 inhibitor templates to design and identify novel, drug-like second generation of APE1 inhibitors.

In this chapter, I will provide an overview of the general features of BER in mammalian cells. A detailed description of individual components of BER, their interactions and the coordination of BER process in mammalian cells will be reviewed next. I will then focus on APE1, provide evidence as to why APE1 is a viable drug target and review studies on the development of APE1 inhibitors. Finally I will describe the aims and scope of my research work.

## **1.2 Base excision repair**

### **1.2.1 Overview of BER pathway**

BER is required for the accurate removal of bases that have been damaged by alkylation, oxidation and ring saturation as well as in handling deaminated bases and DNA single strand breaks (Table 1.1).

There are at least two sub-pathways in BER: the short-patch pathway and long-patch pathway (Figure 1.2). These sub-pathways differ from each other in the number of nucleotide incorporated during the repair process and in the subsets of enzymes involved. However, both pathways are initiated by a damage



specific DNA glycosylase, which recognize and excise the damaged base leaving an abasic site (apurinic/apyrimidinic, AP site). An AP endonuclease then hydrolyses the phosphodiester bond at the 5' end of the AP site. This results in a single strand break (SSB) with a 5' deoxy sugar phosphate (dRP) and a 3'-hydroxyl group. DNA polymerase  $\beta$  incorporates the first missing nucleotide to the 3'-end of the incised AP site. Normally, the reaction continues through the short-patch repair pathway (Figure 1.2) where Pol  $\beta$  removes the dRP residue by the process of  $\beta$ -elimination. DNA ligase III-XRCC1 heterodimer (or DNA ligase I) then completes the repair.

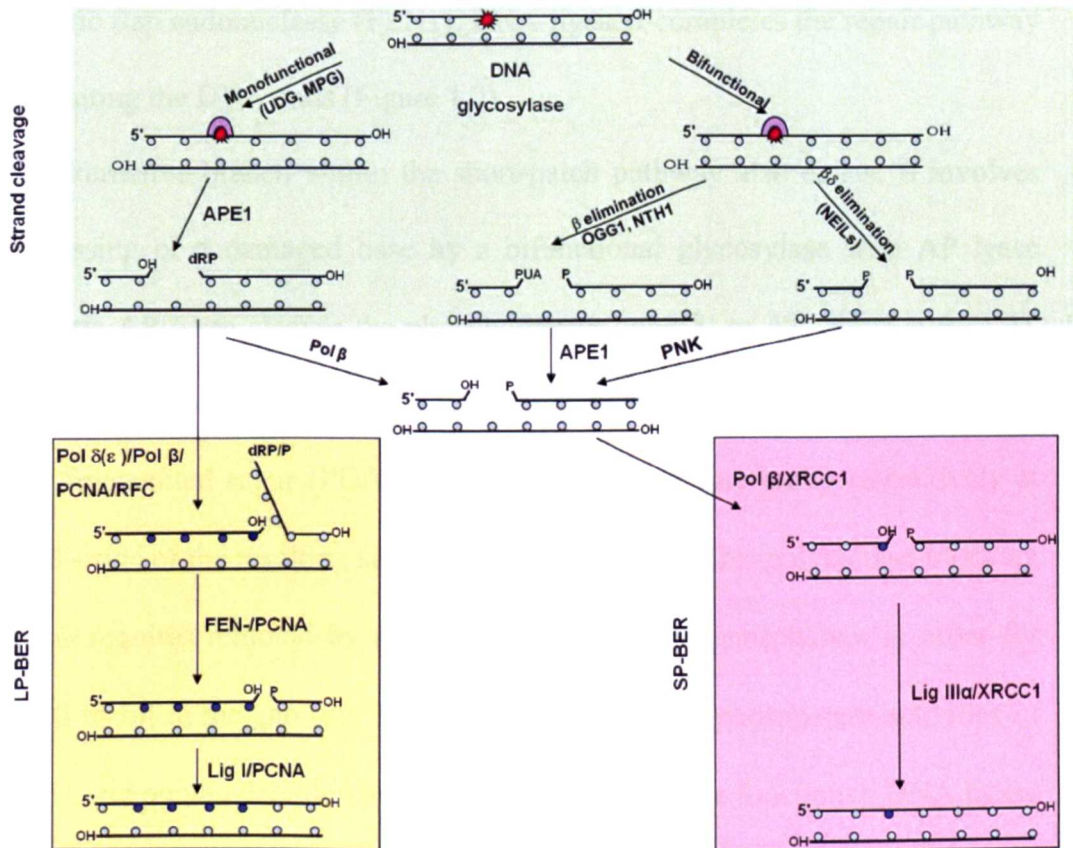
Table 1.1 A summary for base damages, glycosylase enzyme processing the damage, range of substrates and the BER subpathways that processing the damaged base.

Type of base damage	Glycosylase enzyme	Range of substrates	BER Sub-pathway
<u>Alkylation base damage</u> Usually DNA methylation damage. e.g damage induced by alkylating agents: MNU MNNG Temozolomide, Dacarbazine and many others ect.	N-alkylpurine-DNA-glycosylase	N-alkylpurines such as hypoxanthine, 1,N6-ethenoadenine, 7MeGua , and 3MeA [24].	SP-BER Or LP-BER
<u>Deaminated bases</u> Usually occur as a result of the spontaneous hydrolysis of the amine group fro the DNA bases.  It can also be produced by antimetabolates such as 5-Fluorouracil (5FU).	Nuclear Uracil DNA glycosylase UNG2	UNG2 removes the misincorporated uracil in the nascent DNA chain during replication[25].	SP-BER Or LP-BER
	SMUG1	SMUG1 acts on both single- and double-stranded DNA to remove U:G mismatches resulting from genome-wide hydrolytic deamination of cytosine[26]. SMUG 1 also acts on a subset of oxidized Uracil residues; 5-hydroxyuracil, 5-hydroxymethyl uracil and 5 formyluracil and it also removes 5-flourouracil residues [27, 28]. SMUG1 also catalyses the excision of oxidised pyrimidines such as 5-OH cytosine.	SP-BER Or LP-BER
	Thymine-DNA-glycosylase	Its range of substrates also includes ethenocytosine, 5-fluorouracil paired with a guanine or an adenine, 5-OH-U and 5 hydroxymethyluracil mispaired with guanine [29].	SP-BER Or LP-BER
	Methyl-CpG binding endonuclease 1.	It has preferential activity against methylated DNA and also recognizes thymine, uracil and 5-fluorouracil mispaired with guanine[30].	SP-BER Or LP-BER

Continuation of table 1.1

Type of base damage	Glycosylase enzyme	Range of substrates	BER Sub-pathway
<u><b>Oxidative base damage</b></u> Endogenous damage: such as ROS generated during normal metabolism. Exogenous damage e.g ionising radiation which generates ROS and chemotherapeutic agents such as bleomycin.	NEIL1 and NEIL2	NEIL1 and NEIL2 act on reactive oxygen species modified pyrimidines. NEIL1 also acts on ring open purines, namely formamidopyrimidines (Fapy-A and Fapy-G)[31, 32]. It is also active against thymine glycol. NEIL2 have preferential activity against cytosine derived lesions such as 5-OH uracil and 5-OH cytosine[32].	Alternative pathway bypassing APE1 and proceed through SP-BER Or LP-BER
	hNTH1	hNTH1 recognizes a wide range of substrates including thymine glycol, 5-OH cytosine, 5-OH uracil and other types of oxidized pyrimidines.	SP-BER Or LP-BER
	hOGG1	hOGG1 functions on oxidised purine residues such as 8-oxoguanine (8oxoG) and FapyG.	SP-BER Or LP-BER
	hMYH	hMYH main function is to remove Adenine that is misincorporated opposite 8oxoG in the template and hence preventing G:C→T:A transversions. It also excises 2-hydroxyadenine paired with G.	SP-BER Or LP-BER





**Figure 1.2 DNA base excision repair (BER).** BER is initiated by damage recognition and excision by monofunctional DNA glycosylases that excise the damaged base leaving abasic site (left side of green box). APE1 then cleave 5' to the abasic site leaving single strand break leaving 5' OH and 3' phosphate hanging at the single strand break. Bifunctional glycosylase can perform  $\beta$  or  $\beta/\delta$  elimination 3' to the abasic site leaving a strand break with  $\alpha/\beta$ -fragmented sugar derivative [phospho  $\alpha/\beta$ -unsaturated aldehyde (PUA)] or a phosphate group (P) respectively at the 3'-side and phosphate group (P) at 5' end (right side of green box). (PUA) is then excised by APE1 and (P) by polynucleotide kinase (PNK) leaving 3' OH group and 5' Phosphate group. The repair process continues by either short patch (SP-BER) (pink box) or long path (LP-BER) (yellow box).

If the 5'-sugar phosphate is resistant to  $\beta$ -elimination, then a longer fragment of DNA is synthesized and the repair process proceeds through the long patch pathway. In the long patch pathway, Replication Factor C (RF-C) loads proliferating cell nuclear antigen (PCNA) onto the DNA. PCNA acts as a DNA sliding clamp for DNA Pol  $\delta/\epsilon$  which performs DNA synthesis displacing the 5'-sugar phosphate as part of a flap. The flap is then removed by structure

specific flap endonuclease (FEN1). DNA ligase I completes the repair pathway by ligating the DNA ends (Figure 1.2).

An alternative branch within the short-patch pathway also exists. It involves processing of a damaged base by a bifunctional glycosylase with AP lyase activity. AP lyase cleaves the phosphodiester bond 3' to AP site (Figure 1.2). This cleavage of the AP site by  $\beta$  or  $\beta/\delta$  elimination reaction leaves either an  $\alpha/\beta$ -fragmented sugar (PUA) derivative or a phosphate group respectively at the 3'-side of the resulting strand break (Figure 1.2). This polymerase-blocking lesion requires removal by a phosphodiesterase and phosphatase in order for Pol  $\beta$  to fill in the gap (the 3'-phosphodiesterase and phosphatase activities of APE1 and polynucleotide kinase (PNK) performs these functions). DNA ligase III-XRCC1 heterodimer then completes the repair process. *In vitro* studies have shown that the rate limiting step in monofunctional glycosylase mediated short-patch BER is the removal of deoxyribonucleotide phosphate (dRP) i.e. dRP lyase, catalyzed by the amino-terminal domain of Pol  $\beta$ . However, for the bifunctional glycosylase mediated BER, APE1 was found to be rate limiting[4, 6, 33-37]. Although *in vitro* recognition systems have provided some insight, the mechanism of switching among multiple BER pathways is largely unknown[38].

## **1.2.2 BER Proteins**

### **1.2.2.1 DNA glycosylases**

BER is initiated by recognition and excision of a damaged base by a DNA glycosylase. DNA glycosylase hydrolyze the N-glycosylic bond between a damaged base and the sugar moiety thus releasing the free damaged base and giving rise to an AP site. DNA glycosylases are relatively small (~ 30-50kDa) monomeric proteins and belong to an extensive family of enzymes. They do not require cofactors for their activity. Some glycosylases show a very narrow substrate specificity, while others recognize a wide range of different base derivatives [33, 37, 39, 40].

DNA glycosylases have been broadly classified into monofunctional and bifunctional DNA glycosylases. The monofunctional DNA glycosylases operate by a base flipping mechanism in which the damaged base is flipped out from the DNA helix into the active site pocket of the enzyme. Hydrolytic cleavage of the N-glycosylic bond leads to the damaged base release and the formation of an AP site which is the substrate for an AP-endonuclease. The mechanism of action of monofunctional DNA glycosylase is not associated with the formation of covalent intermediates or phosphodiester backbone interruptions and hence an intact AP site is generated. On the other hand, bifunctional DNA glycosylases bind to the base lesion and catalyze the flipping of the damaged deoxyribonucleotide into the active site where a basic amino acid residue, generally a lysine or an N terminal proline, displaces the modified base by a nucleophilic reaction. A transient Schiff base intermediate is generated by the reaction between the C1 of deoxyribose sugar moiety and the

$\epsilon$ -NH<sub>2</sub> group of the lysine or proline. The covalent intermediate catalyzes the  $\beta$ -elimination or  $\beta/\delta$  elimination reactions at 3'-side of the AP site by an associated lyase activity generating a 3'  $\alpha,\beta$ -unsaturated aldehyde (PUA) or 3' phosphate respectively and a 5'-phosphate product. Gapped products are then further processed and fully repaired by the sequential action of a 3'-phosphodiesterase or phosphatase, DNA polymerase and DNA ligase (Figure 1.2). A detailed description of individual DNA glycosylases is beyond the scope of this thesis. However, a brief overview will be provided below.

#### **1.2.2.1.1 DNA glycosylases for alkylated bases**

Alkylating agents are commonly used in the treatment of cancer. They induce covalent modification for DNA bases. Alkylating agents react with both oxygen and nitrogen atoms of DNA bases with quite different efficiency although the nitrogen moieties of DNA bases are the main target. N7-methylguanine (7MeGua) and N3-methyladenine (3MeAde) are the primary DNA lesions accounting for 70–80% and 10–15% of the total DNA alkylation lesions respectively. 7MeGua appears to be harmless while 3MeAde is quite cytotoxic and can block DNA replication and transcription. N3-methylguanine and N7-methyladenine are also formed as minor products. Alkylation of oxygen moiety is induced to a significant extent by SN1-type alkylating agents (e.g. MNU, MNNG and others). O6-Methylguanine (O6-MG) and O4-methylthymine (O4-MA) lesions are highly mutagenic. SN2-type alkylating agents (e.g. MMS) induce a very limited alkylation of oxygen moieties[37, 41-43].

Of note in this context, direct repair mechanism is initiated by the O6-Methylguanine-DNA-methyltransferase (MGMT) protein which removes methyl group from O6 position of guanine (O6-MG) [formed by temozolomide, streptozotocin, procarbazine and dacarbazine], as well as O4-methyl thymine, O6-ethylguanine [formed by ethylnitrosourea and diethylnitrosamine and related compounds] and O6-chloroethylguanine adducts [formed by bis-(2-chloroethyl)-nitrosourea (BCNU) and 1-(2-chloroethyl)-3-cyclohexyl-1-nitrosourea. CCNU]. MGMT transfers the alkyl group from the target base to a cysteine residue within its active site and thereby inactivates itself in the process[5].

**N-alkylpurine-DNA-glycosylase (ANPG):** The alkylpurine-DNA-glycosylase, also known as alkyl adenine glycosylase (AAG), is the repairing enzyme for N-alkylpurines such as hypoxanthine and 1,N6-ethenoadenine. 7MeGua (7-methyl G) is considered potentially harmless as it does not interfere with DNA replication and it has no miscoding properties whereas 3MeAde (3-methyladenine) is both cytotoxic and mutagenic in mammalian cells [24].

#### **1.2.2.1.2 DNA glycosylases for deaminated bases**

Spontaneous deamination of DNA bases by hydrolytic reactions under physiological conditions can occur and result in highly mutagenic lesions such as uracil, hypoxanthine and xanthine in the DNA[44]. For example, the most frequently encountered deamination DNA product is spontaneous hydrolysis of



cytosine leading to the formation of uracil. This spontaneous deamination, if not repaired, can generate a promutagenic U:G mispair, which leads subsequently to GC > AT mutations. However, uracil can also occur in a U:A base pair by occasional incorporation of dUTP (an intermediate in the *de novo* biosynthesis pathway for TTP) instead of TTP, by replicative DNA polymerases. U:A base pairs are non-mutagenic.

**Uracil-DNA-glycosylases (UDG):** is a highly specific monofunctional DNA glycosylase that is conserved in evolution. In mammals, there are two uracil DNA glycosylases, UNG and SMUG1. There are two UNG uracil DNA glycosylases. The mitochondrial form (UNG1), and the nuclear form (UNG2). Both result from transcription of UNG gene by different promoters[45]. UNG2 removes the misincorporated uracil in the nascent DNA chain during replication, suggesting a main role in replication-associated BER[25]. UNG2 is also required to introduce DNA break necessary for class switching recombination in immunoglobulin gene diversification in lymphocytes [46]. SMUG1 has a similar activity to UNG and acts on both single- and double-stranded DNA. SMUG1 is active against uracil in U:G mismatches resulting from genome-wide hydrolytic deamination of cytosine *in vivo* [26]. It is also active against a subset of oxidized Uracil residues; 5-hydroxyuracil, 5-hydroxymethyl uracil and 5 formyluracil and it also removes 5-fluorouracil residues [27, 28]. SMUG1 also catalyses the excision of oxidised pyrimidines such as 5-OH cytosine.

**Thymine-DNA-glycosylase:** Human thymine-DNA-glycosylase

(TDG) is a monofunctional DNA glycosylase with broad substrates specificity. It has been shown to excise thymine and uracil from G/T and G/U mismatches. Its range of substrates also includes ethenocytosine which arise as a by-product of lipid peroxidation, 5-fluorouracil paired with a guanine or an adenine, 5-OH-U and 5 hydroxymethyluracil mispaired with guanine [29].

**Methyl-CpG binding endonuclease 1:** Methyl-CpG binding endonuclease 1 (MED1, MBD4) has preferential activity against methylated DNA and also recognizes thymine, uracil and 5-fluorouracil mispaired with guanine, preferentially at CpG sites[30].

#### **1.2.2.1.3 DNA glycosylases for oxidised bases**

Reactive oxygen species (ROS) are continuously generated during cellular aerobic metabolism as respiration by-products. They are responsible for the production of more than 50 products of purine/pyrimidine oxidation. ROS also produce DNA lesions through the radical attack on the C1' and C4' atoms of deoxyribose sugar moiety giving rise to oxidised abasic sites. Oxidation of C1 and C4 of the deoxyribose can generate DNA SSBs with 3'-phosphate and 3'-phosphoglycolate termini respectively. Some of these lesions are toxic whilst others are strongly mutagenic. Specific DNA glycosylases are involved in the recognition and removal of oxidised bases [47].

Oxidised base-specific DNA glycosylases were first discovered in *Escherichia coli* [endonuclease (Endo) III, Endo VIII, formamidopyrimidine-DNA glycosylase (Fpg/MutM), and MutY]. Human (functional) homologues

of these enzymes have now been identified.

**NEIL1 and NEIL2;** are bifunctional glycosylases with a broad range of substrate specificity. They belong to Nei/Fpg superfamilies and exhibit  $\beta$ ,  $\delta$  AP lyase activity. NEIL1 and NEIL2 act on reactive oxygen species modified pyrimidines. NEIL1 has also been shown to act on ring open purines, namely formamidopyrimidines (Fapy-A and Fapy-G)[31, 32]. NEIL1 is also active against thymine glycol formed by oxidation of thymine. On the other hand NEIL2 appears to have preferential activity against cytosine derived lesions such as 5-OH uracil and 5-OH cytosine[32]. NEILs have recently been shown to have high activity in excising base lesions from ss DNA and unrepaired damages in bubble DNA substrates suggesting their possible roles in base excision repair of oxidative damages during transcription and/ or replications. Additional human NEIL3 have also been identified with no glycosylases activity [48].

**hNTH1** is a bifunctional DNA glycosylase, with an associated  $\beta$  AP lyase activity. It belongs to Endo III superfamily. It recognizes a wide range of substrates including thymine glycol, 5-OH cytosine, 5-OH uracil and other types of oxidized pyrimidines.

**hOGG1** is a bifunctional DNA glycosylase with an associated  $\beta$  AP lyase activity. Structurally it belongs to the Endo III superfamily rather than the Endo VIII/Fpg family, but is nevertheless a “functional” homologue of Fpg. It functions on oxidised purine residues such as 8-oxoguanine (8oxoG) and FapyG.

**hMYH** is a monofunctional DNA glycosylases and a homologue of *E.*

*coli* MutY. hMYH main function is to remove A that is misincorporated opposite 8oxoG in the template, therefore, preventing G:C→T:A transversions. It also excises 2-hydroxyadenine paired with G.

### 1.2.2.2 DNA Polymerases in BER

DNA Polymerase  $\beta$  (Pol  $\beta$ ) is the primary DNA polymerase in base excision repair pathway. DNA Pol  $\beta$  is a 39 kDa protein consisting of two domains connected by a protease sensitive hinge region: the 8-kDa N-terminal domain is responsible for the 5'-dRP lyase activity through  $\beta$ -elimination. The N-terminal domain is also essential for DNA binding. The 31-kDa C terminal domain performs the nucleotidyltransferase function of Pol  $\beta$ . Although the DNA synthesis by Pol  $\beta$  is devoid of any intrinsic proofreading activity, it performs a moderately high fidelity DNA synthesis compared to other polymerases[49].

Mice nullizygous for the Pol  $\beta$  gene are non-viable and die early in embryogenesis. Histological examination of the embryos revealed defective neurogenesis, indicating that Pol  $\beta$  is vital for embryonic neural development. Embryonic fibroblast cell lines derived from these embryos are hypersensitive to the toxic effects of the methylating agent, MMS. The dRP lyase, rather than the polymerase activity of Pol  $\beta$  is required to revert MMS sensitivity [50]. In human tumours Pol  $\beta$  variation are frequently seen (30%) compared to surrounding normal tissue, implying that Pol  $\beta$  variation are involved in pathogenesis of tumours[51].

**Mammalian Pol  $\delta$**  is a 125kDa protein enzyme. It consists of four

subunits, (p125, p68, p50 and p12). These subunits are responsible of the polymerase activity and the 3'–5' exonuclease proofreading function. The low activity and processivity of Pol  $\delta$  is strongly stimulated by the auxiliary factor PCNA which interact with p50 subunit of the Pol  $\delta$ [52].

**Mammalian Pol  $\epsilon$**  consists of four subunits (p261, p59, p17 and p12) and interacts with PCNA. Pol  $\epsilon$  may be involved in the long-patch pathway of BER[53].

### **1.2.2.3 Replication Factor C (RFC)**

RFC is a heteropentameric protein complex composed of five subunits (RFC1, RFC4, RFC5, RFC2 and RFC3) respectively. Apart from its role in DNA repair (BER and NER), RFC plays a central role in chromosomal DNA replication and may have additional roles in cell cycle checkpoint control[54].

### **1.2.2.4 Proliferating cell nuclear antigen (PCNA)**

PCNA is a ring-shaped protein and consists of three identical subunits of 29kDa. These subunits are joined in head-tail arrangements forming a homotrimer. It forms a sliding clamp function on DNA by making a trimeric ring that encircles the DNA strand without any contact with it. At least 30 proteins are known to interact with PCNA including Pol  $\delta$ , Pol  $\epsilon$  and RFC that are involved in BER. PCNA is involved in several cellular processes including, DNA replication, repair and cell cycle control [55].

### 1.2.2.5 Flap Endonuclease 1 (FEN1)

FEN1 is a 40-kDa multifunctional,  $Mg^{2+}$ -dependent metallonuclease with structure-specific activity to cleave branched DNA structures with an overhanging, single-stranded 5' flap. It also has a 5'–3' exonuclease activity that removes mononucleotides at nicks and at gaps. FEN1 is highly conserved among different species and is essential for lagging-strand DNA replication by processing the 5' end of Okazaki fragments. The active-site structure of the enzyme suggests that DNA binding induces FEN1 to clamp onto the cleavage junction to form the productive complex. The enzyme also tracks along the flap from the 5'-end to the cleavage site. FEN1 activity is modulated by its interaction with PCNA through a conserved motif. PCNA enhances stability of FEN1 allowing for a higher cleavage activity, irrespective to the flap size. The interaction of FEN1 and PCNA is disrupted by p21, which bind competitively to PCNA displacing FEN1 from the replication fork and resulting in cell cycle arrest in response to DNA damage. Displacement of FEN1 from replication fork switches its function from DNA replication to DNA repair. In BER, FEN1 functions in long patch where it removes the dRP residue, along with several additional residues from the 5'-terminus. Mice homozygous for FEN1 mutation are embryonically lethal. Mice that are heterozygous for FEN1 mutation are viable and show a mild tumour predisposition phenotype. Moreover, *Fen1*<sup>–/–</sup> blastocysts exhibit hypersensitivity to ionizing radiation[56].

### 1.2.2.6 DNA Ligases

DNA nicks generated during DNA replication, recombination and repair need to be sealed in order to maintain genomic integrity. DNA ligation is accomplished through series of complex biochemical reactions and include enzyme adenylation and transfer of AMP moiety to the 5'-terminus at the site of a nick. Subsequently, the 5'-terminus is activated to attack the 3'-OH end in the final phosphoryl transfer step thereby sealing the nick [57]. Three mammalian ligase genes have been identified: LIG I, LIG III and LIG IV.

DNA ligase I, is the main replicative ligase of eukaryotes, encoded by the LIG I gene. It is involved in BER and other repair pathways. In BER, DNA ligase I directly interacts with Pol  $\beta$ . An association between DNA ligase I and PCNA has also been established[58].

LIG I interaction with Pol  $\beta$  and PCNA is mediated by its non catalytic N terminal domain. The human DNA ligase I activity is enhanced by PCNA which also enhanced its DNA binding ability to the ligation site[59]. *In vitro* studies from mammalian cell extracts defective in DNA ligase III-stabilizing factor XRCC1 demonstrated that XRCC1/ligase III complex is dispensable for long-patch repair, indicating that that the sealing step is performed by DNA ligase I [60].

The LIG III gene encodes several polypeptides that appear to have distinct cellular functions. An alternative splicing event results in two forms of DNA ligase III,  $\alpha$  and  $\beta$  that differ in their C-terminal domains [59]. The DNA ligase III $\alpha$  variants, but not DNA ligase III $\beta$ , forms a stable complex with the DNA repair protein XRCC1 [61]. This interaction occurs between a BRCT motif that resides within the unique C-terminus of DNA ligase III $\alpha$  and a

BRCT motif at the C-terminus of XRCC1. This interaction provides a physical link between this DNA ligase and Pol  $\beta$ . DNA ligase III $\alpha$  is primarily involved in the short-patch BER pathway [60].

LIG IV is a specialized ligase that is required for non-homologous end joining[62].

#### **1.2.2.7 X-ray cross complementing-1 (XRCC1)**

XRCC1, a 69.5 kDa protein interacts with Pol  $\beta$  and DNA ligase III $\alpha$  in BER [63, 64]. In addition, XRCC1 also interacts with APE1[65]. XRCC1 acts as a scaffolding and adapter protein. XRCC1 may be involved in the coordination of short-patch BER. The disruption of XRCC1 in mice leads to embryonic lethality [66]. In human, polymorphism in the XRCC1 gene may be related to cancer predisposition[67].

#### **1.2.2.8 Poly(ADP-Ribose)Polymerase-1 (PARP-1)**

PARP-1 is a DNA-binding enzyme, that gets activated upon encountering DNA strand breaks. Upon activation by strand breaks, PARP-1 undergoes homodimerization and catalyzes the cleavage of NAD<sup>+</sup> to ADP-ribose and nicotinamide. ADP-ribose is then used to synthesize poly(ADP-ribose) nucleic acid polymers that are covalently attached to acceptor proteins such as histones, transcription factors, topoisomerases, DNA ligases and polymerases [68]. However, the major target of poly(ADP-ribosyl)ation is PARP-1 itself. This Poly(ADP-ribosyl)ation not only alters the function of



target proteins, but also alters chromatin structure in a way that is essential for repair. In addition, decreased cellular NAD<sup>+</sup> levels alter the NAD/NADH ratio, redox state and deplete ATP, which is required for cellular metabolism [69].

PARP-1 automodification is strongly activated upon strand cleavage by APE1 [70]. This automodification promotes its interaction with several components of the BER including Pol  $\beta$ , XRCC1 and FEN-1. PARP-1 may be involved in the coordination of BER. In addition, PARP1 has also been shown to be involved in other DNA repair mechanisms including DNA double strand breaks repair such as non-homologous end joining repair (NHEJ)[71, 72].

Moreover, PARP-1 is also involved in several other cellular processes such as DNA replication, transcription, apoptosis, and genome stability [68, 73]. Although PARP-1 knockout is not embryonic lethal in mice, PARP-2 has overlapping function and knockout of both enzymes is lethal to the cells. The mice and the cells derived from PARP-1 knockout mice are highly sensitive to DNA damaging agents [74].

It has long been shown that PARP inhibition leads to persistence of single strand breaks, causing stalling of replication forks and formation of lethal double strand breaks[75]. PARP-1 is overexpressed in many human tumours[76-79] while its depletion potentiates the cytotoxicity of alkylating agents and ionizing radiation [80, 81]. Several potent and specific small molecule PARP inhibitors have been synthesized [82-84]. Blocking of PARP-1 by such inhibitors results in chemosensitisation and radiosensitisation[85]. The first clinical trial on PARP was started in 2003 with a potent tricyclic indole inhibitor (AGO14699) in combination with temozolomide [86]. Since then

several more PARP-1 inhibitors have entered clinical trials and showing promising results in combination with chemotherapeutic agents[87].

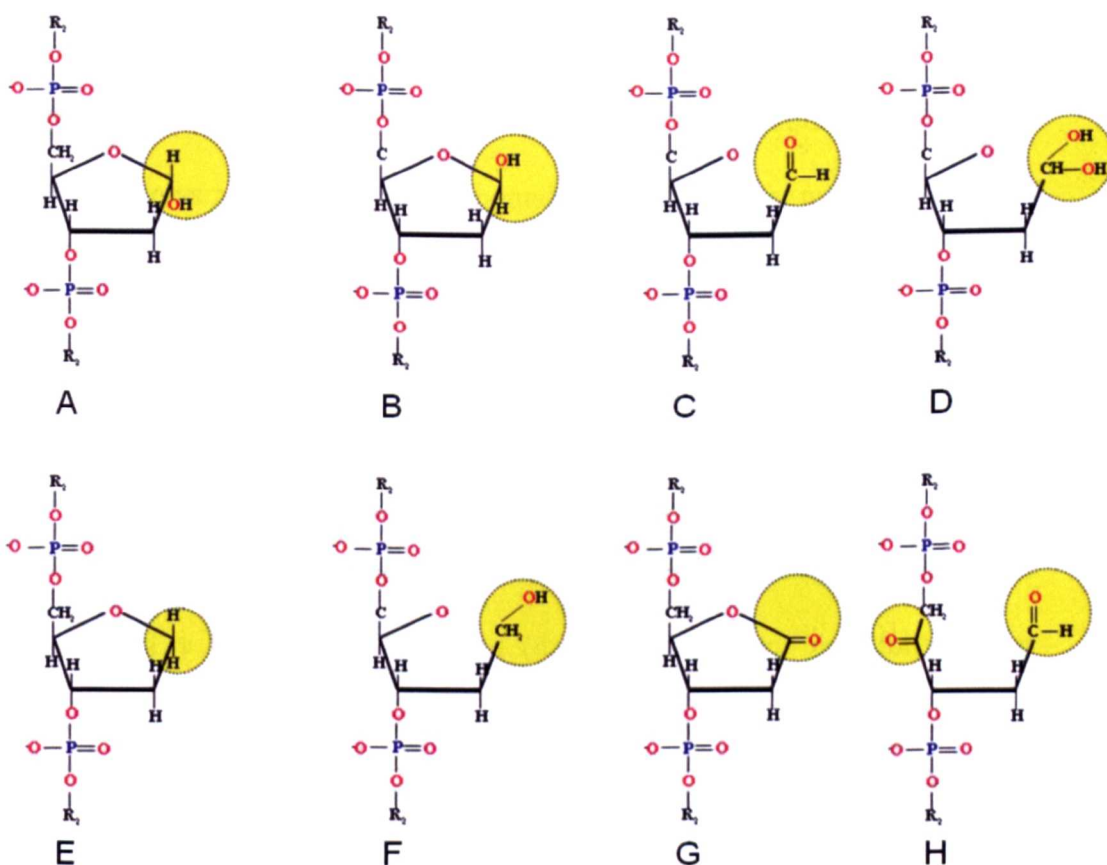
PARP inhibitors have shown particular promise in the setting of BRCA-deficient breast and ovarian cancers that have a dysfunctioning homologous recombination repair pathway. In these mutated cancer cells, blocking the second/rescue BER pathway with PARP inhibitors results in accumulation of DNA damages and cell death. Synthetic lethality is an important new therapeutic concept in cancer (discussed later in this chapter).

## **1.3 Human APE1 in BER**

### **1.3.1 Formation and consequence of AP sites**

Under physiological conditions spontaneous formation of AP sites can arise from the spontaneous hydrolysis of *N*- glycosyl bond and subsequent depurination. AP site formation occurs at a substantial rate and estimated to be responsible for around 10,000 AP sites generated per day in each human cell [88-90]. Moreover, DNA glycosylase activity in BER generates additional AP sites and adds more to this burden. In some studies it has been estimated that the steady-state level of AP lesions may be much higher, approaching 50,000 or more per cell[91, 92]. AP sites that are generated by DNA glycosylases as a repair intermediate are termed 'regular' AP sites. In addition, alkylating agents can also induce the release of bases, often by introducing base modifications that destabilize the N-glycosyl bond [90]. AP sites generated as a result of attack on the DNA sugar-phosphate backbone by ionizing radiation or by

oxidizing DNA damaging agents represent a different structural class from that of the 'regular' AP site. Here abstraction of proton from the deoxyribose sugar results in the formation of oxidised sugar AP site. Several sites on the deoxyribose skeleton are prone to this type of oxidative damage. In particular, the C-1', C-2' and C-4' positions are prone to such attack. Each agent generally produces only one form of oxidized AP site. For example Cu(II) phenanthroline selectively targets the C-1' position to generate 1' oxidized AP sites, whereas bleomycin, generates 4' oxidized AP site via attack on the C-4' position.



**Figure 1.3 Structure of various AP sites.** A=α- Hemiacetal, B = β- Hemiacetal, C = Aldehyde, D= Hydrated aldehyde, E = Tetrahydrofuran, F = Reduced AP site, G = 1'-Oxidized AP site, and H= 4'- Oxidized AP site. Yellow circle indicates the sites where the normal bases have been modified.

AP sites are obligatory intermediates in the pathway for repair of

alkylated and oxidized DNA bases[93]. The structures of various forms of AP sites are shown in (Figure 1.3). Spontaneously generated AP sites exist as an equilibrium mixture between four species: 99% as two hemiacetal enantiomers ( $\alpha$ - and  $\beta$ -2-deoxy-D-ribofuranose) and ~ 1% as ring-opened aldehyde and hydrated aldehyde forms[94]. The ring open type of AP site is a highly reactive variant, and is believed to be responsible for at least some of the biological effects of AP sites[90].

AP sites are cytotoxic and mutagenic. AP sites represent a major threat to the integrity and survival of the cells. Although the exact mechanism behind the cytotoxicity of AP sites is not completely clear, the cytotoxicity may be related to an ability to interfere with replication fork progression. The ring-opened AP site variant may be cytotoxic by virtue of an ability to react with nuclear proteins resulting in protein-bound DNA lesions that may also interfere with DNA replication. Upon encountering an AP site, DNA (and RNA) polymerases pause and dissociate, which leads to the formation of replicative chromosome strand break (or abortive, non-productive transcriptional events) which, when produced at high enough frequency, result in lethality or cellular dysfunction[94]. Furthermore, the cytotoxicity of AP sites may also be related to their ability to promote or inhibit (depending on their proximity to the cutting site) the DNA cleavage activity of topoisomerases[95], and/or to irreversibly trap topoisomerase-DNA covalent complex[96].

Several *in vitro* studies have shown that excessive production or impaired repairing of AP sites result in enhanced cell death. For example a severe depletion of APE1 by RNA interference in human cells leads to an accumulation of unrepaired AP sites, retards cell proliferation and activates

apoptosis [97]. Similarly, ANPG overexpression in CHO cells leads to enhanced sensitivity to the toxic and mutagenic effects of MMS [98]. It was proposed that abundant ANPG causes excessive formation of AP sites and this imbalance in BER induces cell death [98]. In addition, in mammalian cells, a methoxyamine (MX) bound AP site is not a substrate for APE1 and the relatively stable MX bound AP site enhances the cytotoxicity of alkylating agents[99].

Non-coding AP sites are also potentially mutagenic. It was shown previously that DNA and RNA polymerases, if they are able to bypass the AP lesion, they preferentially incorporate an adenine opposite the abasic site both *in vitro* and *in vivo*. This is referred to as the “A-rule”. Therefore, , it has been postulated that in *E. coli* the apurinic sites are responsible for the G:C → T:A transversions associated with SOS activation[94]. However, a precise eukaryotic mutagenic pattern has not yet been shown. Yeast lacking efficient AP site repair preferentially inserted guanine opposite the apurinic lesions which results in increased frequency of A:T to C:G transversions. In addition the stalling of transcription at abasic sites is highly mutagenic in yeast[100]. In mammalian cells, adenine, cytosine, thymine or guanine can be inserted opposite the abasic lesion. Translesion synthesis polymerases have been proposed to be involved in the induction of mutagenesis at AP sites[94].

Apurinic/apyrimidinic (AP) endonucleases are the critical enzymes involved in recognition and processing of AP sites in BER.

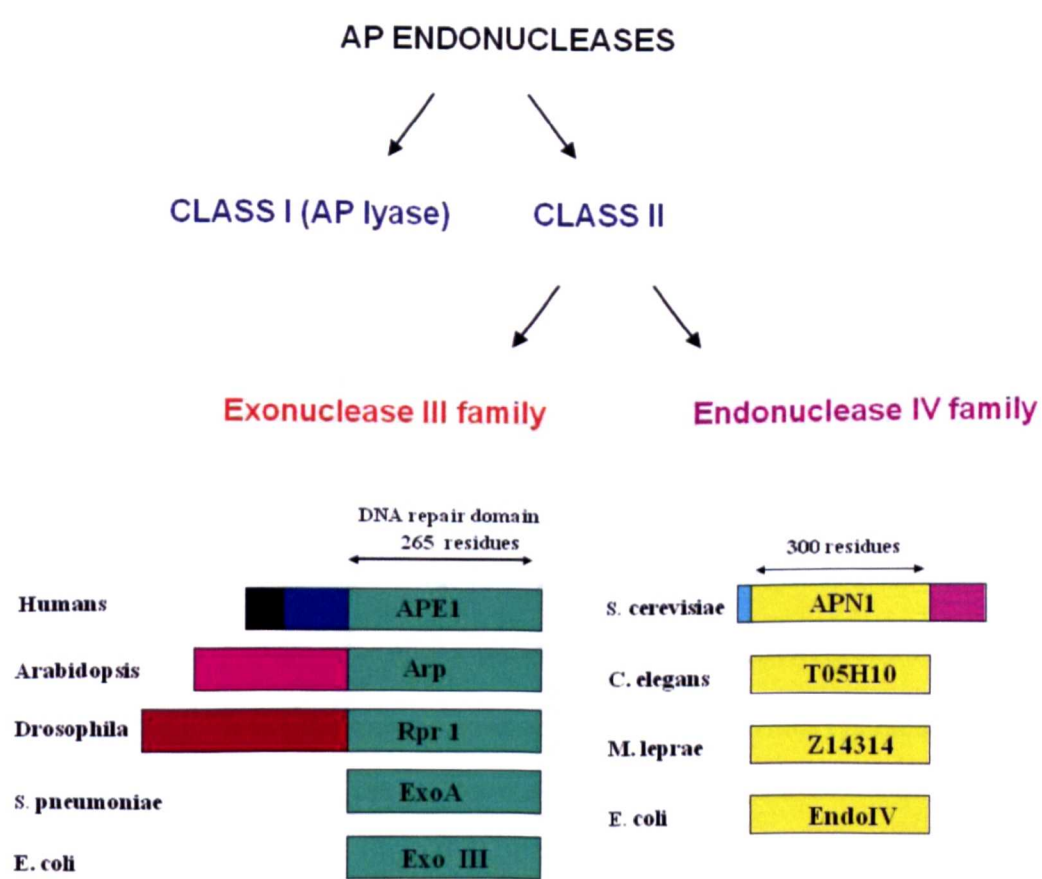
1.3.2

APURINIC/APYRIMIDINIC

(AP)

ENDONUCLEASES

AP endonuclease proteins can be broadly classified into two classes; Class I (AP Lyases), Class II (AP endonucleases). The class II AP endonucleases are further classified into two distinct families based on homology to the endonucleases in *E. coli*, namely, exonuclease III and endonuclease IV family. In *E. coli*, the major activity is encoded by the *xth* gene (exonuclease III) and a minor activity is contributed by the *nfo* gene (endonuclease IV) (Figure 1.4).



**Figure 1.4** Different family classes of AP endonucleases are shown here. AP Endonucleases are divided into two classes: Class I endonucleases are also called AP lyases. Class II is divided in to two families namely, exonuclease III and endonuclease IV family. Members within each family share structurally similar DNA repair domains.

The exonuclease III and the endonuclease IV families have structural and functional homologues in different species. Although they share similar enzymatic activity there is no structural homology between both families [101]. The exonuclease III homologues include exonuclease III (*E. coli*), APEX (mice), rAPE1 (rats), BAP1 (bovines), and APE1 (human). The endonuclease IV homologues include endonuclease IV (*E. coli*), APN1 (*S. cerevisiae*), T05H10 (*C. elegans*) Z14314 (*M. Leprae*) [102]. Studies on the X-ray crystal structure on AP endonucleases from bacteria and human cells has revealed that members of the exonuclease III [103, 104] and endonuclease IV [105] families are structurally unrelated, despite being able to catalyze similar endonuclease reactions yielding similar products.

The *E. coli* exonuclease III is a 265 amino acid protein [106] and a prototypical member of this family of AP endonucleases. The repair domain of Exonuclease III is highly conserved (Figure 1.4) [107]. Exonuclease III is a  $Mg^{2+}$  dependent AP endonuclease which has 3'-exonuclease, 3'-phosphatase, AP endonuclease, 3'-phosphodiesterase and RNase H activities [104].

The *E. coli* endonuclease IV is a  $Zn^{2+}$  dependent AP endonuclease that shares functional similarity to exonuclease III. Both enzymes possess AP endonuclease, 3' phosphatase and 3' phosphodiesterase activity [108]. However, endonuclease IV lacks the exonuclease and RNase H activities characteristic of exonuclease III (Figure 1.4) [108].

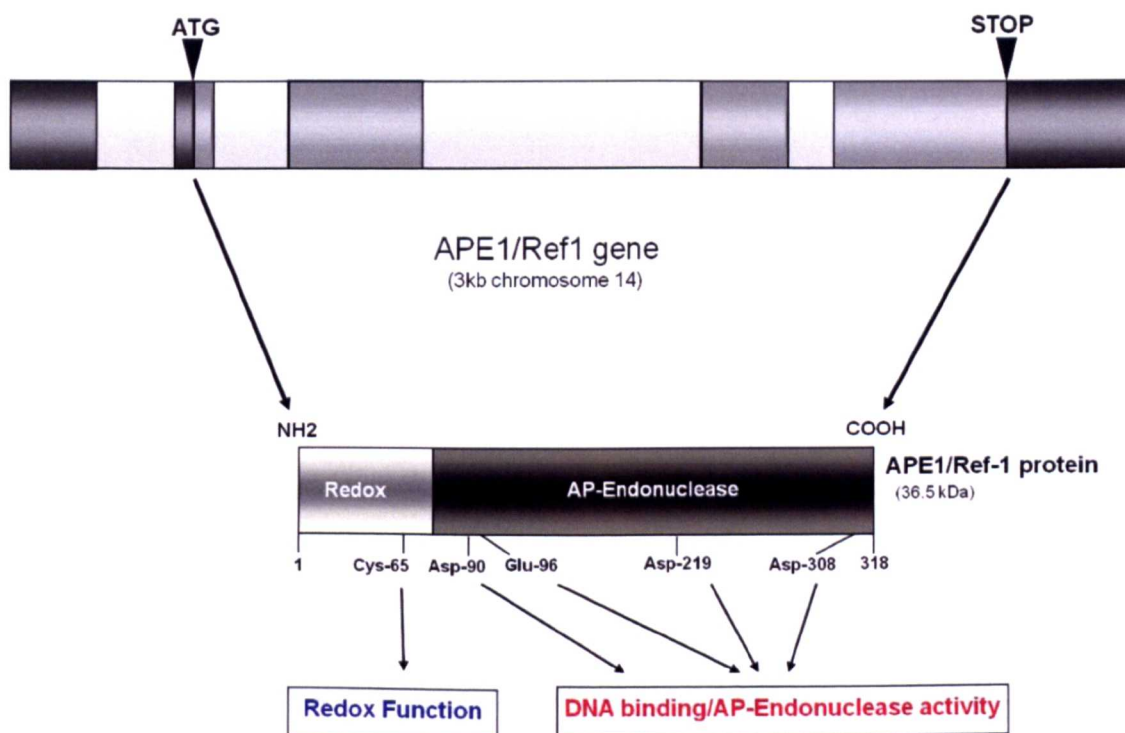
### **1.3.3 Human apurinic/apyrimidinic endonuclease (APE1)**


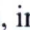

Human apurinic/apyrimidinic endonuclease (APE1/HAP1/Ref-1) is a multifunctional protein. The human APE1 gene (~ 2.6 kb in size) is located on

chromosome 14 q11.2-12 and consists of four introns and five exons (Figure 1.5). The human APE1 cDNA is about 1441 nucleotides in length and encompasses 205 nucleotides in the 5' non-translated region, 954 nucleotides in the coding region, and 216 nucleotides in 3' non translated region and poly(A). The coding region encodes a 318 amino acid protein with a molecular mass of approximately 36.5 kDa. APE1 is a globular  $\alpha/\beta$  protein that possesses both DNA repair activity and redox regulatory activity[102, 109, 110]. The C-terminal is responsible for the endonuclease activity and is essential for the DNA repair function of APE1[111]. The N-terminal domain is mainly responsible for the redox regulatory activity, by the amino acid Cysteine at 65 position.

The repair and redox functions of APE1 are completely independent from each other. This is evident by the observation that cys-ala65 mutation abolishes the redox function without affecting the repair function[112] whereas mutation of amino acids required for DNA repair activity, such as Histidine 309 (H309) and others[113], do not affect the redox function. While the DNA repair active site of APE1 has been clearly delineated requiring the amino acid residues between 61-80 of the N terminus and all the C-terminus[114], the redox domain is much less defined. The only Cys residue required for full redox function is Cys 65, which is located deep inside the APE1 protein[103]. The importance of Cys65 for the redox function was confirmed by a study in zebra fish AP endonuclease1 (zAPE1). In this study, point mutation of Thr58 to a Cys located at the same position of the Cys in the mammalian APE1, resulted in the acquisition of redox activity of the mutated protein[115].





**Figure 1.5 Structures of human APE1 gene and protein are shown here.** The gene encoding the 36.5 kDa APE/Ref-1 protein is about 3 kb in length and is located on chromosome 14. The 6 kDa N-terminal region of the APE1 protein, in particular Cys-65, is important for its redox activity. The repair activity of the protein is located in the C-terminus. Functional relevant amino acids are outlined in the structure of the APE1 protein. Mutational disruption of these amino acids results in loss of repair/redox function. , introns: , coding exons: , untranslated exons [116].

In addition to the redox regulatory function, the N-terminal domain also contains the nuclear localization sequence [117]. A study by systematic deletion analysis has showed that the first 7 residues and residues 7-18 can independently promote nuclear transport of APE1. Moreover, the subcellular distribution of APE1 protein may be regulated by both nuclear import and export signals [for example, the first 20 N-terminal residues interact with nuclear importins (Karyopherin  $\alpha$ 1 and 2)][118]. In addition, a recent study by Li *et al* has described an APE1 mitochondrial translocation sequence that include amino acids 289-318 in the C-terminal domain which is normally being masked by intact N-terminal domain. This sequence was identified by evaluating the interaction between APE1 and three purified translocase

receptors of mitochondrial outer membrane, using peptide array screening[119].

### **1.3.4 Functions of APE1**

#### **1.3.4.1 DNA repair function of APE1**

APE1 is a member of the highly conserved exonuclease III family of AP endonucleases, named after the *E. coli* homologue of APE1[101]. It accounts for over 95% of the total AP endonuclease activity in most cultured human cell lines[109, 110, 120, 121]. Upon encountering an abasic site in the DNA, the DNA repair domain hydrolytically cleaves the phosphodiester bonds 5' to the abasic site leaving a 3'-hydroxyl group and a 5'-deoxyribose phosphate group flanking the nucleotide gap. The subsequent repair process can be accomplished either in the short-patch or the long-patch pathway as discussed previously. Site directed mutagenesis analyses has revealed that APE1 repair function requires at least 10 evolutionarily conserved amino acids, D70, D90, E96, Y171, D210, N212, D219, D283, D308 and H309 (Figure 1.5)[122-127]. Beside AP site processing, APE1 protein performs additional roles in DNA repair [107]. In common with exonuclease III and endonuclease IV, APE1 exhibits a 3'-phosphodiesterase activity for removal of fragmented sugar moieties that are formed at the 3' end of DNA strand breaks induced by certain DNA damaging agents such as bleomycin and ionizing radiation[128]. APE1 enzyme also exhibits a weak 3'-phosphatase, 3'-5' exonuclease and RNaseH activity (i.e. the ability to degrade the RNA strand of an RNA-DNA hybrid

complex). The functional significance of these additional activities of APE1 is unknown and is an area of ongoing investigation[107]. All of these activities of APE1 apparently utilize a single active site in the DNA repair domain of APE1, which is the region of the protein that is conserved in exonuclease III. The 3'-5' exonuclease activity of APE1 may also be involved in the fidelity of repair synthesis by removing mispaired nucleotides[129-131]. In addition, the exonuclease activity of APE1 was shown to be involved in the removal of nucleoside analogues from the DNA and therefore, influence the pharmacological effects of the nucleoside analogue L-OddC (also known as troxacitabine) [132]. APE1 has a weak 3'-phosphatase activity that removes 3'-phosphate blocking groups, but is less efficient than polynucleotide kinase (PNK) in the repair of such lesions produced by bifunctional glycosylases such as NEIL1 and NEIL2[133, 134]. APE1 also plays a role in nucleotide incision pathway (NIR)[135] where APE1 initiates the repair process by creating a nick 5' to oxidatively damaged DNA leaving a 5' hydroxyl group and 3' deoxyribose sugar moiety carrying the oxidatively damaged base. Subsequently repair then progresses through the long patch pathway as described above. The substrates processed in NIR include alpha anomeric deoxynucleotides  $\alpha$ T,  $\alpha$ dA, and  $\alpha$ dC, DHT, 5 OH-uracil, me-FapyGua and 5-OH cytosine[11].

Structural studies of APE1 and its interaction with the AP site suggests a mechanism for AP site binding which involves the recognition of the deoxyribose moiety in an extrahelical conformation rather than the base opposite the AP site [103]. The efficiency of this reaction is limited by the rate

by which APE1 enzyme diffuse to damage site and the completion of which might be slowed down by the chemistry of resultant cleavage products[136]. The crystal structure suggests that APE1 has a preformed DNA binding interface which undergoes little conformational change upon AP-DNA complex formation and includes a hydrophobic pocket that accommodates the abasic sugar while excluding normal bases. However, a recent study, using the intrinsic tryptophan fluorescence indicated that upon encountering AP site, APE1 may undergo at least 4 conformational transitions[137].

#### **1.3.4.2 APE1's role in the co-ordination of BER**

Studies from reconstituted systems suggest that APE1 is involved in the coordination of BER by interacting either directly or indirectly with other BER factors. This coordination not only provides a defense mechanism against the accumulation of potentially toxic repair intermediates but also increases the overall efficiency of the repair process.

In reconstituted systems, APE1 interacts directly with MYH glycosylase and enhances the formation of efficient MYH·DNA complexes by decreasing the MYH·DNA substrate dissociation constant, resulting in 10-folds increasing its activity [138]. However, other glycosylases appear to interact indirectly with APE1, by competing for DNA binding sites. Alkyl Adenine Glycosylase (AAG) [139] Ogg1[140], Nth1 [141], Uracil DNA glycosylase [142] , and thymine DNA glycosylase [143] display product inhibition, binding tightly to their processed DNA products. This tight binding is thought to recruit APE1 to the damaged site and at the same time help to protect the AP sites or single-strand breaks until APE1 continues the repair process. APE1 displaces

the glycosylases from their substrate binding by its stronger association with the DNA[143].

Yeast two-hybrid and electrophoretic mobility shift assay suggest a direct interaction between DNA-bound APE1 and DNA polymerase  $\beta$  [144]. The presence of APE1 at the damage site enhances Pol  $\beta$  removal of 5' dRp by the lyase activity. This stimulation and consequent repair synthesis enhances APE1 endonuclease activity by removing, through DNA repair synthesis, the 3' terminus product inhibition of APE1[145]. In addition, XRCC1 which acts as a scaffold has also shown to bind directly to APE1 in yeast two-hybrid, far western, and affinity chromatography assays[65]. This interaction increases APE1 endonuclease activity, and 3'-phosphodiesterase activity. CHO cells Extracts defective in XRCC1 activity show a low APE1 endonuclease activity which could be rescued by the addition of XRCC1. A direct binding between APE1 and other factors such as PCNA, polymerases  $\delta$ , polymerase  $\epsilon$ , and FEN1 has also been demonstrated [146]. In addition APE1 stimulates flap cleavage activity of FEN1 and DNA ligase I activity by up to 10 folds, without affecting substrate specificity[147].

#### **1.3.4.3 APE1 interaction with other DNA repair factors**

Several studies suggest a possible role for the tumour suppressor p53 in BER. p53 binds directly to APE1[148] and stimulates BER, although the relationship of the binding and stimulation is unknown[149]. p53 also directly stimulates BER [150]. It was also shown that APE1 enhances specific DNA binding of p53 by promoting p53 tetramerization[151]. A recent study has

shown that APE1 subcellular distribution may be controlled by p53 through ubiquitination of APE1 N-terminal lysines [152]. APE1 also interacts directly with double-strand break repair proteins Ku 70/80[153] and a functional interaction with WRN helicase has also been demonstrated[154]. The synthesis of heat shock protein 70 (HSP70) is enhanced by stress induced by heat shock, oxidative insults, and ionizing radiation many of which also damage DNA. A direct interaction between HSP70 and APE1 has been demonstrated in which HSP70 stimulates APE1 activity[155].

#### **1.3.4.4 Redox regulation by APE1**

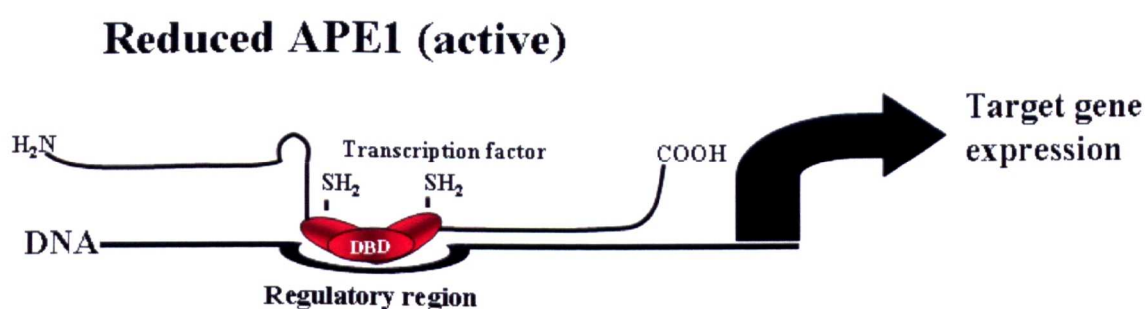
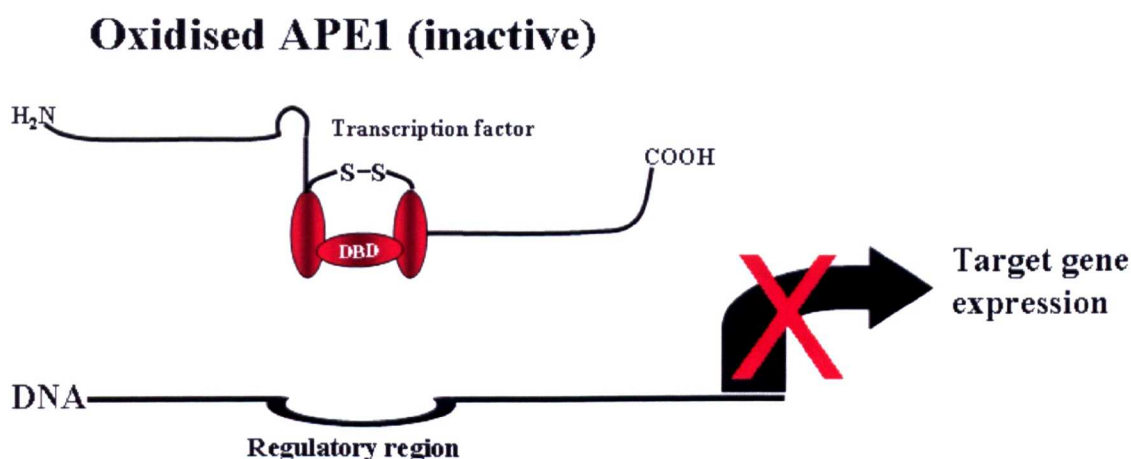
Normally the cells maintain a reduced intracellular environment in the face of a highly oxidizing external environment. An oxidized environment is very harmful for the cell because of the generation of the free radicals and subsequent lipid peroxidation, DNA cross link and formation of disulfide double bond within the protein.

APE1 represent a novel redox component of the signal transduction process that regulates the eukaryotic gene expression. The redox regulatory function of the APE1 is performed by the N-terminus and it is unrelated to the DNA repair function of APE1. APE1 accomplishes this function by monitoring the redox state of Cys residues present in the DNA-binding domains or within regulatory regions of transcription factors such as c-Jun and several others [111, 156-158] (Figure 1.6).

For proper binding to specific DNA target sequences, the transcription factors require that critical Cys residues are in a reduced state. Therefore, by maintaining these cysteines in the reduced state, APE1 provides a redox-

dependent mechanism for the regulation of target gene expression. The presence of a reduced Cys residue within the DNA binding domains of transcription factors is essential for binding to specific DNA targeting sequence which activates the transcription of several key genes essential for cell survival and in cancer promotion and progression[102, 158].

APE1 contains two cysteine residues located within the redox-active domain (Cys65 and Cys93). Many studies showed that Cys65 was essential for redox activity of APE1. In addition, it was also proposed that Cys93 could regulate the redox activity of APE1 through its interaction with Cys65. Oxidized APE1 protein may contain a disulfide bridge between Cys65 and Cys93 and the disruption of this interaction is essential to expose the sulfhydryl group of the active site cysteine residue[159]. Further studies have demonstrated that Cys65 is the essential residue for the redox function of APE1. Mutation of Cys65 abolish the redox function of APE1 while maintaining a normal DNA repair activity[112]. The cysteine residues may be reduced by thioredoxin that interacts with the redox domain of APE1 [160, 161].



**Figure 1.6 Molecular model showing the redox regulation function of the N-terminal domain of APE1.** APE1 exerts a transcriptional coactivator function inside the cells. For proper binding to specific DNA target sequences, the transcription factors require that critical Cys residues in the DNA binding domain (DBD) in a reduced state. APE1 provides a redox-dependent mechanism of regulation by maintaining these cysteines in a reduced state.

Several transcription factors have been shown to be activated by APE1 through the redox activation mechanism including AP-1, NF- $\kappa$ B, CREB, ATF, HIF-1, HLF, NF-Y, P53, MYB, PAX, and PEBP2. These transcription factors play crucial roles in cell growth, differentiation and stress response [162]. A recent report indicated a possible important role of the redox domain and not the DNA repair domain of the APE1 in the normal embryonic haematopoiesis development [163].



### **1.3.4.5 Acetylation-mediated gene regulation function of APE1**

Another important function of APE1 protein is its role as transacting factor, in which it monitors the target gene expression in a  $\text{Ca}^{2+}$  dependant manner. APE1 was first identified as a trans-acting factor involved in  $\text{Ca}^{2+}$ - dependent repression of the parathyroid hormone (PTH) gene where an increase in  $\text{Ca}^{2+}$  due to elevated PTH level triggers down-regulation of the PTH gene. In this gene regulatory function, APE1 was found to be a component of protein complexes that bind to a negative calcium responsive element (nCaRe-A and nCaRe-B) that is found at the PTH promoter [164]. Similarly APE1 was also later found to regulate the human renin gene, via  $\text{Ca}^{2+}$ -dependent down-regulation of the human rennin gene [165]. Moreover, it is possible that the negative calcium response elements may also be present in other genes [166]. Further studies indicated that acetylation of APE1 at Lys-6 or Lys-7 by the histone acetyltransferase (HAT) p300 enhances APE1 binding to nCaRe-B element[167]. Acetylation of APE1 as a post-translational modification may stimulate the co-repressor activity of APE1 as suggested by the interaction of APE1 with HDAC (histone deacetylases) that deacetylate histones, leading to chromatin recondensation and inhibition of transcription[167] as well as APE1 acetylation might even impact its role in BER by regulating APE1 catalytic activity at abasic sites and its interaction with other BER factors[168].

In two recent studies, acetylation of APE1 has been shown to be involved in early growth response (Egr-1) mediated activation of phosphoinositol phosphatase and tensin homologue (PTEN) expression. In addition acetylated APE1 stably interacts with YB-1 protein and enhances its binding to Y-box element that results in activation of MDR gene expression[169, 170]. These

findings suggest further roles for APE1 in regulation of genes expression. In one recent study APE1 down-regulation sensitized MDR overexpressing tumours to cisplatin and doxorubicin[171]. APE1 was also shown to interact with RNA transcription factor II on the MDR1 promoter factor in association with the P300 cofactor. This indicates the importance of acetylated APE1 on the transcription regulated drug resistance[171].

## **1.4 Functional pre-clinical studies on APE1**

### **1.4.1 APE1 DNA repair activity is critical for cell viability**

APE1 is essential for viability and survival of cells. Three groups independently demonstrated that knockdown of APEX in mice cause a post-implantation embryonic lethality between days E5 and E9 [172-174]. Although these studies demonstrate that APE1 is essential for early embryonic development, it was difficult to address the biological significance and contributions of each of the three different functions of APE1 (namely, DNA repair, redox activation and acetylation-mediated gene regulation) to embryonic lethality in mice. Recent data from several groups has suggested that the DNA repair function of APE1 may be crucial for cell survival. In one study by Fung et al, down-regulation of APE1 using an siRNA approach was shown to correlate with AP sites accumulation and induction of apoptosis with reduced cell proliferation. In that study, expression of yeast Apn1 (that lacks redox regulatory activity but has intact DNA repair function) in APE1 knocked-out cells reversed some of the deleterious effects [97]. Another study by Ordway et al, showed that mice homozygous for APE1 mutation at

Cys64Ala and hence lack redox activity are viable and survive normally without obvious phenotype [175]. Izumi et al. established APE1 nullizygous MEF (mouse embryonic fibroblast) cells expressing floxed human APE1 transgene. They could demonstrate that cell survival required DNA repair function and acetylation-mediated gene regulation functions of APE1[176]. Although homozygous deletion of the APEX is embryonically lethal in mice [172, 173], APEX<sup>-/+</sup> heterozygous mice are viable and are hypersensitive to oxidative stress [174].

#### **1.4.2 APE1 depletion hypersensitises cells to DNA base damage (table 1.2)**

While induction of apoptosis in response to APE1 downregulation has been confirmed in numerous cell types and *in vivo* in rats and mice [102, 177], the response to knockdown may vary between cell types. In ovarian cancer cells, APE1 knockdown causes S phase prolongation rather than apoptosis, manifested in tumour xenografts as a reduced growth rate associated with impaired glucose metabolism that is suggestive of reduced cellular proliferation[178]. Heterozygosity for APE1 in mice is associated with hypersensitivity to oxidative stress[174]. HeLa cells transfected with anti-sense APE1 RNA were sensitive to killing by MMS, H<sub>2</sub>O<sub>2</sub> as well as menadione and paraquat which induce oxidative DNA damages [157]. Similar antisense approaches in lung cancer and human glioma cell lines resulted in increased sensitivity to ionising radiation, MMS, temozolomide and nitrosurea [179, 180]. Rat glioma cells transfected with antisense RNA for rAPE also showed

increased sensitivity to MMS and  $H_2O_2$  [181]. Moreover, in human myeloid leukaemia cell lines and murine cell lines, down-regulation of APE1 has been correlated to apoptosis[102, 177]. Similarly, APE1 down-regulation using siRNA was associated with enhanced cytotoxicity and induction of apoptosis to alkylating agents,  $H_2O_2$  and other DNA damaging agents in osteosarcoma[182]. In another study, siRNA-mediated APE1 depletion led to an accumulation of AP sites, reduced cell proliferation and induced apoptosis in the absence of any other treatments[97]. Xiang et. al. showed that APE1 knockdown using siRNA approach validated by decreased mRNA expression resulted in significant decrease in growth of pancreatic cancer cells and increased in apoptotic rate and sensitisation to cell killing by gemcitabine[183]. Wang et. al. showed that down-regulation of APE1 using siRNA approach sensitise non small cell lung cancer cells (NSCLC) to cisplatin[184].

### **1.4.3 APE1 overexpression protects cells from DNA damage and is implicated in treatment resistance (table 1.2)**

Upregulation of APE1 has a protective effect against agents causing DNA damage. In AP endonuclease-mutant *E. coli* and Apn1-deficient yeast, transfection of hAPE1 restored resistance to the effects of DNA damaging agents [109, 120, 185]. Co-expression of hAPE1 as a chimeric protein with MGMT conferred resistance to hydrogen peroxide and MMS in AP endonuclease-deficient *E. coli*. In HeLa cells overexpression of the chimeric protein had a similar protective effect [186]. Overexpression of APE1 in human teratocarcinoma cells[187] in melanocytes[188] and in ependymoma [189] conferred resistance of radiation and chemotherapy.

Upregulation of APE1 can be induced by chemotherapy agents, contributing to treatment resistance. In non small cell lung cancer cells, cisplatin treatment induces a dose-dependent increase in APE1 expression. When APE1 is downregulated using antisense methods, cisplatin cytotoxicity is significantly increased [184] suggesting that combining inhibitors of APE1 with chemotherapeutic agents may overcome treatment resistance.

## **1.5 APE1 and human cancer**

### **1.5.1 APE1 polymorphisms and cancer susceptibility**

Polymorphic APE1 variants have been reported and correlated to cancer susceptibility. In an analysis of seven APE1 polymorphisms, namely (Leu104Arg, Glu126Asp, Asp148Glu, Arg237Ala, Gly241Arg, Asp283Ala, and Gly306Ala,) reduced repair activity was noted in four (Leu104Arg, Glu126Asp, Arg237Ala, and Asp283Ala) [190]. In a study by Lu et al. a Thr141Gly promoter polymorphism was associated with reduced levels of APE1 mRNA in blood and lung tissue, possibly due to reduced affinity for Oct-1 transcription factor, thought to be activated by DNA damage. Homozygosity for the Gly allele was associated with a 40% reduction in lung cancer risk [191]. Asp148Glu, a variant which exhibits normal repair activity, is associated with an increased risk of cancer development [192], including melanoma [193], pancreatic [194], cervical [195] and lung cancer susceptibility [196]. The Asp148Glu variant may also be associated with hypersensitivity to ionising radiation [197], although it has also been demonstrated to have a protective effect against acute radiation toxicity reactions in normal skin [198]. Further studies are required to elucidate how APE1 polymorphisms might impact response to treatment.

### **1.5.2 APE1 overexpression in human cancers**

APE1 expression is cell cycle dependent, with highest levels seen during early and middle S-phase [199]. Immunohistochemical analysis of many human

cancers has demonstrated elevated levels of APE1 (table 1.1). For example, APE1 protein expression is increased in human gliomas, and pancreatic cancer and is positively correlated with AP endonuclease activity [200, 201]. AP endonuclease activity was also found to be positively correlated with tumour grade, and with the fraction of S-phase cells, suggesting that APE1 activity is related to level of proliferation [200]. APE1 is also elevated in prostate cancer, with immunohistochemical staining levels increasing from low in benign prostatic hypertrophy to intense in prostatic carcinoma [202].

### **1.5.3 APE1 subcellular localisation in cancer**

APE1 expression and subcellular localisation demonstrates complex and heterogenous patterns that vary between tissue types (table1.1). Nuclear localisation is common, and is thought to reflect functions in DNA repair. Cytoplasmic localisation is commonly seen in cell types exhibiting rapid metabolic or proliferative rates, particularly when under high oxidative stress. Cytoplasmic localisation is predominantly within the mitochondria and endoplasmic reticulum, in keeping with the role of mitochondria in cellular response to oxidative stress, and may relate to APE1's role in mitochondrial DNA repair and redox regulation of transcription factors [158]. In non-small cell lung cancer, APE1 dysregulation is common, with upregulation in the cytoplasm contributing to global overexpression and associated with increased superoxide production and lipid peroxidation [203].

Alterations in subcellular distribution of APE1 compared to normal tissue have been seen in a number of human tumours. In normal colorectal mucosa, the less differentiated cells in the lower part of the crypt show nuclear staining

whereas, the more differentiated superficial mucosal epithelium shows predominantly cytoplasmic staining. In colorectal adenomas and carcinomas there is a complete disruption for this staining pattern. The nuclear restricted pattern is lost and they display both nuclear and cytoplasmic localization with a predominance of the latter [204]. Increased cytoplasmic staining is also seen in thyroid [205], hepatocellular [206], epithelial ovarian [207] and prostate carcinomas [202]. In contrast, melanomas display an increased level of APE1 expression which is predominantly localised to the nucleus, compared to cytoplasmic staining in normal skin [188]. Increased levels of APE1 expression with nuclear-specific localisation are also seen in cervical carcinomas [208], bladder cancers [209], rhabdomyosarcomas [210], and squamous cell head and neck cancers [211]. Some tumour types have shown variance of APE1 localisation between studies. There is consensus regarding elevated levels of APE1 in non-small cell lung cancer, but different groups have found predominantly cytoplasmic [184] or nuclear [212, 213] localisation.

#### **1.5.4 APE1 expression and localisation as marker of prognosis and treatment response (table1.2)**

Alterations in APE1 expression may be of prognostic significance. In non-small cell lung cancer, elevated APE1 expression is an independent poor prognostic factor, associated with reduced disease-free and overall survival [212]. Similarly, elevated APE1 is suggestive of poor prognosis in medulloblastoma [214], ovarian, gastro-oesophageal and pancreatobiliary cancers [215]. Alterations in APE1 localisation may also be of prognostic



significance. Breast cancers display heterogenous localisation, compared to predominantly nuclear distribution in normal breast tissue. Localisation appears to be correlated to patient outcomes, with nuclear localisation being associated with better prognostic features such as differentiation, reduced angiogenesis and negative lymph node status [216, 217]. Similar prognostic correlations are also seen in osteosarcoma [182], where cytoplasmic staining is associated with poor survival outcomes. Conversely, in ovarian and pancreatobiliary cancers, nuclear APE1 expression is associated with aggressive tumour biology and poor overall survival [215].

Table 1.2 Summary of APE1 expression and preclinical and clinical data in human tumours

Tumour site	APE1 expression	Pre-clinical findings	Clinical findings
Breast	Nuclear in normal Mixed localization in ductal carcinoma <i>in situ</i> [216].		Nuclear expression associated with negative lymph node status, low angiogenesis [216, 217]
Cervical	Overexpression with nuclear localization [208].	Anti-sense inhibition sensitise HeLa cells to killing by MMS, H <sub>2</sub> O <sub>2</sub> , menadione and paraquat [157] Overexpression conferred resistance against alkylating agents in HeLa cells [186]	Increased expression associated with radioresistance[218] Cytoplasmic expression associated with poor survival [219]
Colon	Predominantly cytoplasmic [204].	siRNA inhibition sensitises LOVO cells and xenografts to ionising radiation (IR)[220]	
Germ cell	Overexpression with nuclear localization [187].	Overexpression confers bleomycin resistance [187]	Overexpression of APE1 promote resistance to radiation in pediatric ependyoma and is a predictive marker of resistance to radiotherapy[189]
Gastro-oesophageal	Mixed or nuclear expression [215].		Nuclear expression associated with poor survival Cytoplasmic expression associated with differentiation [215]
Glio-blastoma	APE1 overexpression [200].	Upregulation by oxidative stress associated with resistance to MMS, temozolomide, and IR[200] Antisense down-regulation sensitises cells to temozolomide[180] siRNA, CRT0044876 and lucanthone sensitise cells to IR[221]	
Head & neck	Overexpression with nuclear, cytoplasmic, or mixed localization[211].		Overexpression associated with earlier relapse, reduced survival [211] Nuclear localization associated with nodal positivity, treatment resistance [211]

Continuation of table 1.2

Tumour site	APE1 expression	Pre-clinical findings	Clinical findings
Hepatocellular	Predominantly cytoplasmic[206].		Cytoplasmic expression associated with poor survival [206] Cytoplasmic expression associated with increase risk of relapse following liver transplants[222]
Leukaemia		Down regulation of APE1 by using retinoic acid/DMSO (granulocytic) or phorbol 12-myristate 13-acetate in HL-60 myeloid leukemia cell line enhanced apoptosis[177]	
Lung	Overexpression with mixed localization (nuclear in normal tissue)[203, 212].	Antisense down-regulation sensitises cells to nitrosurea[179] APE1 upregulated by cisplatin treatment siRNA inhibition reduces cell growth and induces apoptosis of non small cell lung cancer (NSCLC) [184].	Asp148Glu associated with sensitivity to IR, improved response to chemo-radiotherapy [197] Low expression associated with cisplatin sensitivity, improved survival[184] Overexpression associated with chemoresistance[184] APE1 expression is associated with reduced disease-free and overall survival [212].
Medullo-blastoma	Predominantly nuclear Increased in expression in women, younger patients [214].	siRNA inhibition sensitises cells to carmustine and temozolomide [214]	Overexpression associated with early relapse[214]
Melanoma	Predominantly nuclear [188].	Overexpression protected melanoma cells from cisplatin and H <sub>2</sub> O <sub>2</sub> [188]	
Osteo-sarcoma	Overexpression [182].	Reduced HO5 cell viability following antisense depletion Antisense down-regulation sensitises cells to MMS, H2O2, thiotepa, etoposide, IR [182]	Overexpression associated with poor survival [182]

Continuation of table 1.2

Tumour site	APE1 expression	Pre-clinical findings	Clinical findings
Ovarian	Nuclear/cytoplasmic [207].	siRNA inhibition reduces SKOV-3x growth [178]	Nuclear expression associated with poor survival[215]
Pancreatico-biliary	Nuclear localization [215]. Overexpression[201].	APE1 upregulated by gemcitabine treatment Antisense down-regulation sensitises cell to gemcitabine [223] siRNA inhibition resulted in significant decrease in growth in pancreatic cancer and increase in apoptotic rate with sensitisation to cell killing by gemcitabine [183] siRNA inhibition resulted in growth inhibition, increased apoptosis, and altered cell cycle progression[201]	Absence of cytoplasmic staining associated with high risk features[215]
Prostate	Increasing overexpression from benign prostatic hypertrophy to prostatic intraepithelial neoplasia to cancer[202]		
Rhabdomyosarcomas	Overexpression with nuclear localization [210]		
Thyroid	Predominantly cytoplasmic[205]		

## 1.6 Synthetic lethality strategy

The early promise of PARP inhibitors suggested the potential of BER proteins as therapeutic targets [224, 225]. PARP inhibitors have shown particular promise in the setting of BRCA-deficient breast cancers, indicating an important therapeutic concept that may be applicable to inhibitors of APE1. Synthetic lethality utilizes the inter-gene relationships where the loss of function of either of two related genes is non-lethal, but the loss of function of both causes cell death. This offers the potential to specifically target cancer cells through inhibition of a gene known to be in a synthetic lethal relationship with a mutated tumour suppressor gene [226]. BRCA-1 and -2 have long been identified as tumour suppressors, being mutated in an inherited cancer predisposition that increases susceptibility to breast and ovarian tumours [227]. Both gene products have a role in the homologous recombination (HR) DNA repair pathway, which repairs double strand DNA breaks (DSBs) [228]. A degree of redundancy exists between the BER and HR pathways, allowing cells to compensate for the loss of one pathway. The BER enzyme PARP1, which binds to single strand DNA breaks and recruits other repair proteins, can be successfully targeted for inhibition, leading to failure of the BER pathway, replication fork stalling, and acquisition of double strand breaks. In normal cells, these double strand breaks are repaired via HR. However, in BRCA-deficient cells loss of effective HR leads to DSB persistence and cell death. As heterozygosity at a BRCA allele is associated with effective HR, PARP inhibition specifically targets only tumour cells with acquired BRCA<sup>-/-</sup> homozygosity [21, 22]. PARP inhibitors demonstrated favourable efficacy and



limited toxicity in BRCA-related breast and ovarian cancers in phase I and II trials [226] and currently phase III trials are underway.

Other potential synthetic lethal relationships in PARP inhibition are currently being explored. 'BRCAness' refers to a subset of breast cancers, including 'triple negative' (oestrogen-, progesterone- and HER2-negative) and 'basal phenotype' cancers, that possess molecular and histopathological similarity to BRCA-deficient tumours, that may successfully be targeted by PARP inhibition [229, 230]. There is also developing interest in PTEN (phosphatase and tensin homolog), which is mutated in many sporadic cancers and, like BRCA mutations, causes a defect in homologous recombination [231, 232].

Recent evidence suggests that other BER factors may also be targeted by a synthetic lethality approach. Mismatch repair (MMR) is responsible for the repair of DNA damage occurring during replication, and shares a degree of overlap with BER function. For example, 8-oxoguanine base lesions, which are induced by metabolic ROS and can cause mutagenic GC→TA transversions if unrepaired, may be processed by both BER and MMR. Mutations in the mismatch repair (MMR) genes *MLH1* or *MSH2* are implicated in human non-polyposis carcinoma coli (HNPCC) and some sporadic colorectal cancers. siRNA inhibition of the BER constituent DNA polymerase  $\beta/\gamma$  is selectively lethal in *MLH1/MSH2* mutant cell lines, suggesting a synthetic lethality relationship. Given the potential for BER inhibitors as a synthetic lethality target, it remains to be established if additional factors such as APE1 may have a role in this capacity[233].

## 1.7 Combination therapy

Chemotherapeutic agents and ionizing radiation are the main therapeutic modalities currently available for treatment of cancer. The cytotoxic effects of these agents are directly related to their ability to induce DNA damage. The ability of cancer cells to recognise and repair DNA damage contributes significantly to therapeutic resistance. Therefore, pharmacological inhibition of DNA repair pathways has been explored as a useful strategy to enhance sensitivity for chemotherapy and radiotherapy and to reverse drug resistance. Different agents have shown excellent results in preclinical studies in combination with radiation or chemotherapy. BER is centrally involved in processing base damage induced by alkylating agents and ionising radiation. One of the mostly studied enzyme target is PARP-1 protein which protect the single strands intermediates during the BER [68]. Preclinical studies have shown that the presence of PARP inhibitors potentiated the cytotoxicity of temozolomide by 1.5 - 4 fold in lung, colon, ovary, and breast cancer cell lines [234]. Similar results were obtained in glioma and human colonic adenocarcinoma xenograph models, where the combination of PARP inhibitors and temozolomide resulted in marked decrease in cancer cell growth compared to temozolomide alone[235]. Early phase clinical trials on PARP-1 inhibitors showed promising results in combination with chemotherapeutic agents such as temozolomide [86, 87].

### **1.7.1 APE1 is a promising anticancer drug target**

APE1 is a critical protein in BER. In pre-clinical studies APE1 depletion reduces cell viability and sensitises cells to DNA damaging agents. Overexpression of APE1 confers resistance to DNA damaging agents. In human studies APE1 expression has predictive and/or prognostic significance in patients. Given the successful paradigm of PARP inhibitors and the pre-clinical and clinical evidence about APE1s' roles in cancer, APE1 became a tempting enzyme to target for cancer therapy.

## **1.8 Current status of APE1 repair domain inhibitors (Figure 1.7)**

Preclinical and clinical studies described above confirm that modulation of BER resulted in enhanced sensitivity to DNA base damaging agents. Therefore, inhibition of various DNA repair proteins is a logical target to combat therapeutic resistance and to increase sensitivity of cancer cells to conventional therapy. APE1 is a key enzyme in BER and is centrally involved in the initiation and coordination of BER. In addition, APE1 plays additional roles in BER and DNA strand break repair. Therefore APE1 is considered as logical target for drug design in cancer therapy. Over the past few years several APE1 inhibitors have been described and in the following section I will provide an overview of these APE1 inhibitors in development.



### **1.8.1 Methoxyamine (MX)**

Methoxyamine is an alkoxyamine derivative and blocks the APE1 cleavage activity by binding irreversibly to the AP site[236]. It is an indirect inhibitor of APE1 since it blocks APE1 from processing cytotoxic AP sites. Methoxyamine potentiates the cytotoxicity of base damaging agents such as Temozolomide (TMZ) *in vitro* and tumour xenograft [237-239]. It also potentiates radiotherapy cytotoxicity in combination with the potent radiosensitiser 5-iodo-2'-deoxyuridine[240]. Methoxyamine has undergone phase I clinical trials in combination with pemetrexed and temozolomide in patients with advanced refractory cancer [241, 242].

### **1.8.2 Lucanthone**

Lucanthone is a topoisomerase II inhibitor (Figure 1.7) [243, 244]. It was later shown to have a direct APE1 inhibitory activity and to induce a dose dependant AP sites accumulation in cells[245]. Lucanthone treatment in cell culture induces an increase in abasic site accumulation[246] and potentiates the cytotoxic effects of MMS and temozolomide[245]. Clinically, lucanthone treatment accelerates regression of brain metastases following whole brain radiotherapy[247]. However, it is unclear whether this effect is mediated via APE1 inhibition, or due to lucanthone's effect on topoisomerase[248].

### **1.8.3 CRT0044876 (7-Nitroindole-2-carboxylic acid) (CRT)**

CRT0044876 was identified by our group, using a high-throughput screen of a 5000 drug like chemical library (Figure 1.7). It specifically blocks AP

endonuclease, 3' phosphatase, 3' phosphodiesterase and 3'-5' exonuclease activities of APE1 enzyme at low micromolar concentrations ( $IC_{50}= 3 \mu M$ ). At a relatively non toxic concentration, CRT0044876 potentiated the cytotoxicity of a number of DNA base damaging agents such as methyl methanesulfonate (MMS), TMZ,  $H_2O_2$  and Zeocin (which intercalates between DNA strands and induces DNA strand breaks) in HT1080 human fibrosarcoma cell cells[23]. This effect was not replicated when the DNA damaging agents used induced damage repaired by mechanisms other than BER, suggesting BER-specific inhibition[23]. It also enhances cell death of glioma cell lines treated with radiation, though not as much as Lucanthone [221]. CRT0044876-induced BER inhibition has been reproduced elsewhere[249, 250] including cytotoxicity potentiation with ionising radiation[251], although another group were not able to replicate the results [248].

Because of the poor drug like properties, including its water solubility and membrane permeability as well as the presence of nitro-aromatic feature CRT0044876 is not druggable. Although providing proof of principle, it is clear that further work will have to be done before a genuine lead APE1 inhibitor can emerge.

#### **1.8.4 Arylstibonic acid compounds**

Seiple et al. have identified the potential of arylstibonic acids as APE1 inhibitors [252]. Arylstibonic acids ability to block APE1 cleavage activity may be caused by their arylstibonic core that mimic the phosphonate derivative. The investigators felt that this pharmacophore is not suitable for further development [253]. Although arylstibonic acids have very low  $IC_{50}$

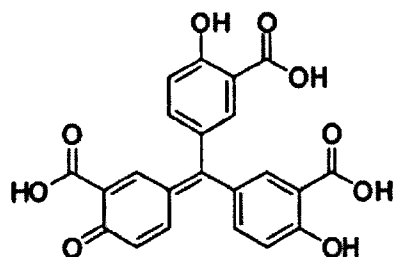
against APE1 *in vitro*, they did not show any cellular activity. This may be related to poor transmembrane transport and cellular uptake [252].

### **1.8.5 Pharmacophore guided isolation of APE1 inhibitors**

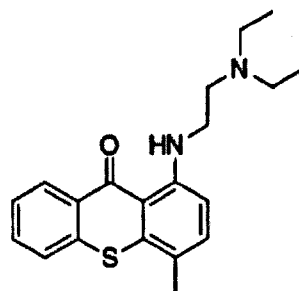
Using *in silico* pharmacophore models-based screening, Zawahir et al performed a virtual screening of a 365,000 small molecule chemical library and identified 21 potent and specific inhibitors [254]. They share common features of carboxylate groups arranged around a hydrophobic core, bearing structural similarity to the 3'- and 5'- deoxyribosephosphate groups on abasic DNA[254].

### **1.8.6 AR03**

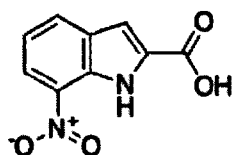
Using a high throughput screening of 60,000 chemical library, Bapat *et al* were able to isolate four potential APE1 inhibitor, named AR01, AR02, AR03 and AR06 all of them have an  $IC_{50} < 10 \mu M$ [255]. Of these inhibitors, AR03 was further screened using a radiolabelled assay and a human whole cell extract assay and was shown to have partial specificity against APE1, It potentiates the cytotoxicity of MMS and TMZ in SF767 glioblastoma cell line. AR03 showed a high intrinsic toxicity with  $LD_{50}$  around  $1 \mu M$ [253].



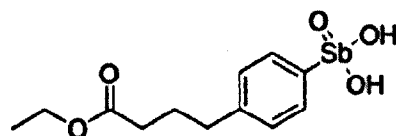
Aurintricarboxylic Acid (0.055  $\mu\text{M}$ )



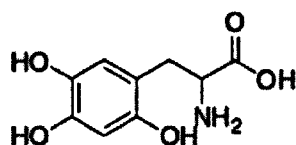
Lucanthone (100  $\mu\text{M}$ )



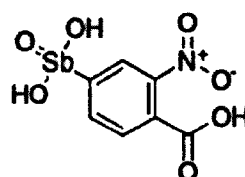
CRT0044876 (3.0  $\mu\text{M}$ )



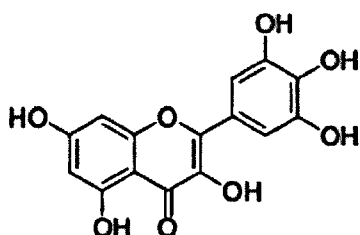
NSC-13793 (0.017  $\mu\text{M}$ )



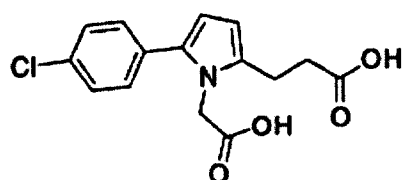
6-hydroxy-DL DOPA (0.11  $\mu\text{M}$ )



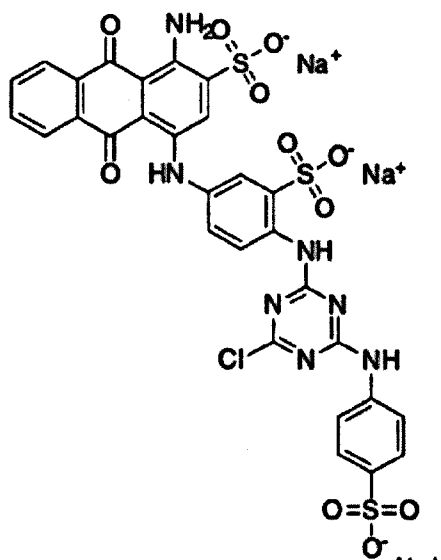
NSC-13755 (0.004  $\mu\text{M}$ )



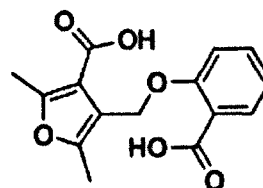
Myricetin (0.32  $\mu\text{M}$ )



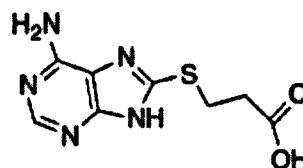
Compound 1 (4  $\mu\text{M}$ )



Reactive Blue 2 (0.25  $\mu\text{M}$ )



Compound 17 (6  $\mu\text{M}$ )



Compound 21 (20  $\mu\text{M}$ )

Figure 1.7 Chemical structures of different APE1 inhibitors described up to the time of where this thesis was written. (Read the text for more details)

### 1.8.7 6-Hydroxy-DL-DOPA, Reactive Blue 2, and myricetin

A recent work by Simeonov *et al* has isolated several specific APE1 inhibitors using a high throughput fluorescence screening of a commercially available pharmacologically active library of 1280 chemical compounds representing 56 pharmacological classes [256]. Hits identified by the primary screening were then counter screened for the ability to inhibit Endonuclease IV and tested further for their APE1 inhibition on HeLa whole cell extracts. Three inhibitors were identified using this approach (6-OH-DL-DOPA, Reactive blue, and myricetin). The inhibitors were able to potentiate the cytotoxicity of MMS in HeLa cell lines[253].

It was evident that current APE1 inhibitors do not have promising pharmaceutical properties. However these APE1 inhibitors represent important guides for future attempts to design, test and to isolate drug-like APE1 inhibitors. The apparent tendency of the above inhibitors to share common features, like their relative small sizes, aromatic hydrophobic cores with a negative ionisable group (mostly carboxylate group) establish a reasonable guideline for what future potential inhibitor skeletons should include. Moreover, the appropriate use of *in silico* approach that utilizes these common features together with the study of APE1 active site morphology would likely facilitate the design and subsequent identification of APE1 inhibitors with more selectivity and drug-like properties.

## 1.9 Conclusion

Genomic integrity is constantly challenged by damage inflicted from a variety of endogenous and exogenous sources, including spontaneous deamination, reactive oxygen species, ionising radiation, ultraviolet light and chemical agents. Highly conserved pathways of DNA repair have evolved to maintain stability within the genome. Base excision repair (BER) processes and repairs damage to individual bases induced by alkylation, oxidation or ring saturation. Human apurinic/apyrimidinic endonuclease 1 (APE1) is a critical BER enzyme that recognises and processes the site of excised base damage (an 'abasic' site). APE1 is of considerable interest as a potential predictive and prognostic biomarker in cancer. Polymorphisms causing variable APE1 activity may alter cancer susceptibility and treatment response. APE1 expression is upregulated in response to treatment with DNA damaging agents such as chemotherapy and ionising radiation, and is frequently associated with resistance to treatment and poor prognostic outcomes in patients.

Overexpression of APE1 is induced by DNA damaging agents and is associated with treatment resistance. Constitutional or engineered down-regulation of APE1 confers sensitivity to treatment, and can overcome chemoresistance. Preclinical and clinical studies have confirmed that APE1 is an emerging therapeutic target in cancer. A number of inhibitors of the APE1 DNA repair domain are currently under development. These inhibitors show promise *in vitro* in their ability to potentiate the actions of agents causing alkylating or oxidation damage. However development of these inhibitors is at

a very early stage and isolation of clinically-relevant compounds is an important and expanding area of research.

## **Aims of the study**

- 1) Identify drug-like patentable second generation APE1 inhibitor hits for drug development.
- 2) Virtual screening approach to design APE1 inhibitors that can achieve APE1 inhibition with desirable pharmacological properties.
- 3) Using the pre-optimized screening strategy to identify candidate APE1 inhibitors.
- 4) Examining the ability of APE1 inhibitors to potentiate the cytotoxicity of the base damaging agents in a panel of cancer cell lines.
- 5) Structure based analysis and hit series selection.
- 6) To evaluate biological consequences of APE1 depletion using shRNA in cancer cell lines.



## ***Chapter 2***

### ***Material and methods***

---

## 2. Material and methods

### 2.1 Enzymes, antibodies, chemicals and oligonucleotides

Human APE1 and *E. coli* endonuclease IV were obtained from New England Biolabs, USA. D148E APE1 polymorphic variant protein was a gift from Dr David Wilson III, National Institute on Ageing, NIH, Baltimore, USA. *Pst* I restriction enzyme was obtained from New England Biolabs, USA. The rabbit polyclonal anti-APE1 (IgG fraction) and mouse anti  $\beta$  Actin primary antibodies were obtained from Novus Biologicals Ltd, Newmarket Suffolk, UK. Infrared dye labelled, IRDye 800CW Donkey Anti-Rabbit IgG (H+L) and IRDye 680CW Donkey Anti-Mouse IgG (H+L), secondary antibodies were obtained from LI-COR Bioscience Ltd, Cambridge, UK.

Dimethyl sulfoxide (DMSO), Methyl methanesulphonate (MMS) and Mitomycin C were purchased from Sigma-Aldrich. Doxorubicin was obtained from Pharmacy, City Hospital, Nottingham, UK. Temozolomide was a gift from Dr Tracey Bradshaw, University of Nottingham. Stock solutions of potential APE1 inhibitors were dissolved in DMSO. MMS, mitomycin C, temozolomide were dissolved in PBS. All stock solutions were maintained at 4 °C.

Oligonucleotides, 5' F-  
GCCCCXGGGGACGTACGATATCCCGCTCC 3' and 3' Q-  
CGGGGGCCCCCTGCATGCTATAGGGCGAGG 5' [where F = Fluorescein, Q = Dabcyl and X is Tetrahydrofuran (abasic site)] were custom made by Eurogentec Ltd.

## **2.2 Potential small molecule inhibitors of APE1**

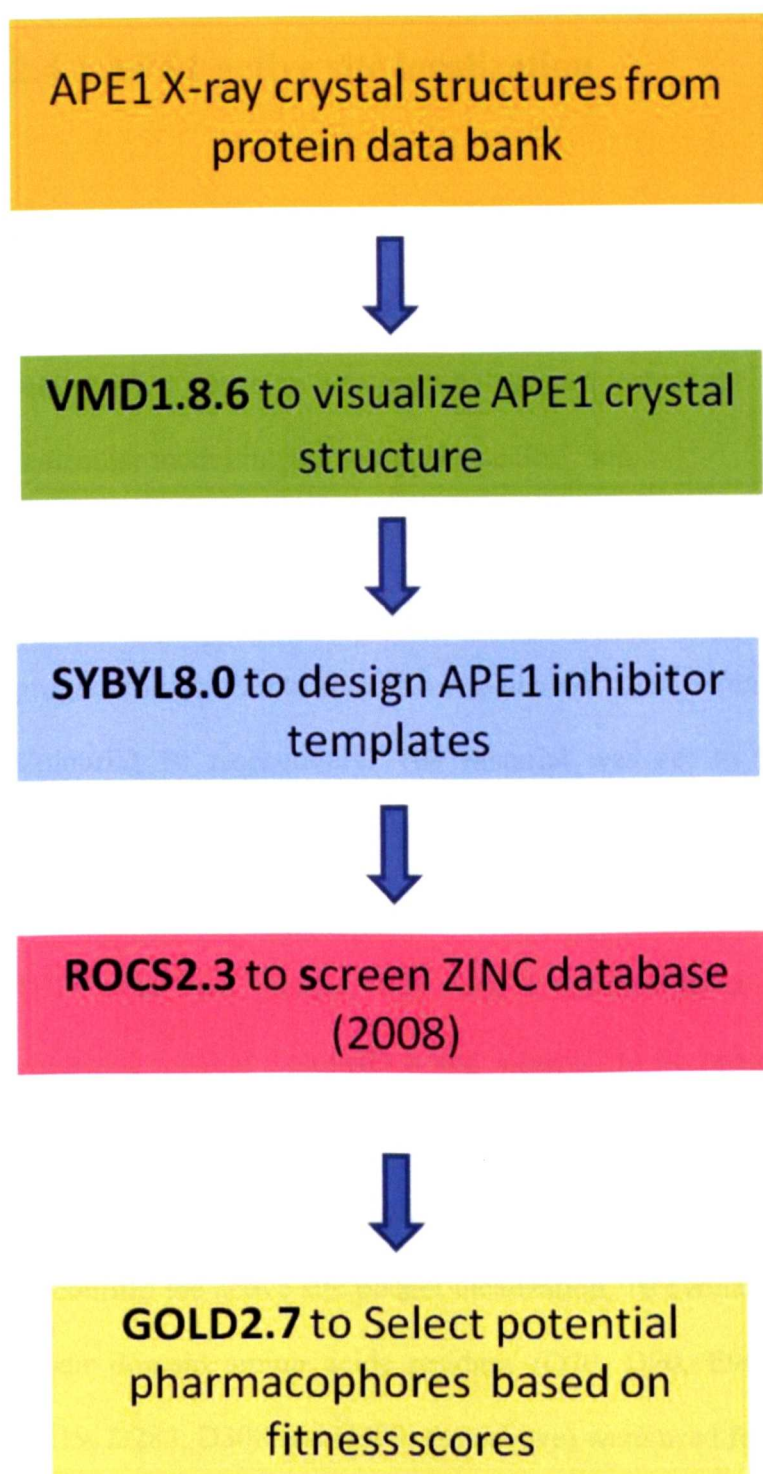
A total of 160 compounds were investigated in this project. Compounds were purchased from Maybridge Chemicals (Tintagel, UK), ChemBridge corporation (CA, USA), ASINEX intelligent chemistry (Laan van Vredenoord, Netherlands), Life Chemicals (Braunschweig, Germany), Enamine Ltd (Kiev, Ukraine), Specs Chemicals (Delft, Netherlands), ChemDiv Inc. (CA, USA), Ukrorgsynthesis Ltd (Kiev, Ukraine) and Sigma-Aldrich. All compounds were dissolved into 10 mM in 100% DMSO stock solutions.

## **2.3 Molecular modelling (Figure 2.1)**

The modelling work was conducted at the molecular modelling lab, Centre of Biomolecular Science, School of Pharmacy, University of Nottingham. This work was supervised by Dr Charlie Laughton, Reader in Molecular Recognition, School of Pharmacy, University of Nottingham.

- Publicly available coordinates of the high resolution crystal structure of APE1, namely 1BIX was downloaded from the protein data bank website <http://www.pdb.org/pdb/home/home.do>.
- Commercially available chemically diverse ZINC 2008 database was obtained online from <http://zinc.docking.org/>.
- VMD1.8.6 (visual molecular dynamic), a program for displaying, animating, and analyzing large biomolecular systems such as proteins using 3-D graphics and built-in scripting[257], was obtained from theoretical and computational biophysics group, University of Illinois, USA.

- SYBYL8.0, a general molecular modelling programme that provides a computational tool kit for molecular design and analysis which was obtained from Tripos A Certara <sup>TM</sup> Company, Missouri, USA.
- GOLD2.7 (Gene Optimisation for Ligand Docking) a package of programmes for structure visualisation and manipulation was obtained from Cambridge Crystallographic Data Centre, Cambridge, UK.
- ROCS2.3 (Rapid Overlay of Chemical Structures) a powerful shape similarity and comparison application used for conducting virtual screening to identify potentially active compounds that are similar to a known lead compound or template[258] was obtained from OpenEye scientific software®, New Mexico, USA.



**Figure 2.1 Molecular modelling approach used to shortlist potential APE1 inhibitors.** Modelling was conducted using a UNIX supercomputer system at the Centre for Biomolecular Sciences, School of Pharmacy, University of Nottingham, UK.

## 2.4 Virtual screening (Figure 2.1)

### 2.4.1 APE1 active site localization

The chosen APE1 structure (1bix) [103] was downloaded from the protein data bank (PDB) and the  $\text{Sm}^{3+}$  ion located at the active site was replaced manually with  $\text{Ni}^{2+}$ . This step was essential since most of the programmes used for molecular modelling do not recognise  $\text{Sm}^{3+}$  ion.

VMD 1.8.6 was used to visualize APE1 with its active site as below; The APE1 \*.pdb file was uploaded to VMD 1.8.6. The graphic option in the programme was set to (the *drawing method* and *colouring method*) Surf and ColourID 10 respectively. The material was set to be transparent. These selections enabled viewing the protein in 3 dimensions and facilitated the localization of the APE1 active site. A new superimposed representation of 1BIX was then created, this time I selected to *drawing method* VDW, *colouring method* ColourID 0 and *material* to be opaque and fine tuned the protein selection to include only  $\text{Sm}^{3+}$  ion (serial number 2192 in the protein). Although this ion is known to be localized at the active site of APE1, however, to confirm the active site pocket localization, 10 evolutionally conserved DNA repair domain amino acids residues (D70, D90, E96, Y171, D210, N212, D219, D283, D308 and H309) (see above) were used for localization. This was performed by choosing the analysis option in the programme to localize these amino acids. Subsequently, the APE1 active site was localized and the shape of the active site pocket was viewed.

## **2.4.2 APE1 inhibitors template design**

Sybyl8.0 was used to build new template pharmacophores designed to fill the APE1 hydrophobic active site pocket. The programme was run in the following steps;

- Using Sketch Molecule Menu, GRID was selected to ease the sketching of the template.
- The template was then energy minimised and stored in \*.mol<sub>2</sub> format.

## **2.4.3 GOLD2.7 (Gene Optimization for Ligand Docking)**

The templates, and the potential hits from the ZINC database (see below) were docked onto the APE1 active site using GOLD2.7. GOLD2.7 was used to calculate the docking pose of the binding mode of chemical structures onto the APE1 active site pocket using different scoring functions.

The programme was run as below:-

- APE1 protein was uploaded onto the programme.
- H<sub>2</sub>O molecules situated in the active site pocket were removed to prevent their interference with docking interaction between APE1 protein and the selected ligand.
- To identify the active site pocket for GOLD2.7, the Ni<sup>2+</sup> atom within the protein active site was selected and GOLD2.7 was set to automatically detect the active site cavity within a radius of 11°A of Ni<sup>2+</sup> atom.
- The ligand was then uploaded onto GOLD2.7.

- The scoring function was later set to be either ChemScore or GoldScore.
- GOLD2.7 was set to perform 100 docking runs and the output was set to retain only the top pose based on the scoring functions discussed below.

## 2.4.4 ROCS2.3

ROCS2.3 was utilized to perform similarity searching in the ZINC 2008 database. The chemical hits identified were ranked based on shape and chemical similarity to the originally designed template. The programme was run as described below.

The parameters were set as follows :-

- 1- **query file:** (template or a chemical compound).
- 2- **database:** (ZINC 2008 database).
- 3- **prefix:** to designate a name for the output file.
- 4- **besthits:** to limit the results to include the top scoring hits.
- 5- **oformat:** to assign a format for the output file,(\*.sdf format).
- 6- **pvmconf:** to distribute the ROCS search to include different processors of the supercomputer in the modelling lab.

An example of a command to search for M1 template based similarity hits from the ZINC data base is given below.

```
*ROCS -query M1.sdf -dbase ZINC_Purchasable_druglike_database -  
besthits 500 -oformat *.sdf -pvmconf pvm.
```



(This command implies that ROCS will use M1 template file to search ZINC purchasable drug-like data file based on shape fit and chemical alignment, keeping the top 500 hits and also that output file is saved in \*.sdf format.)

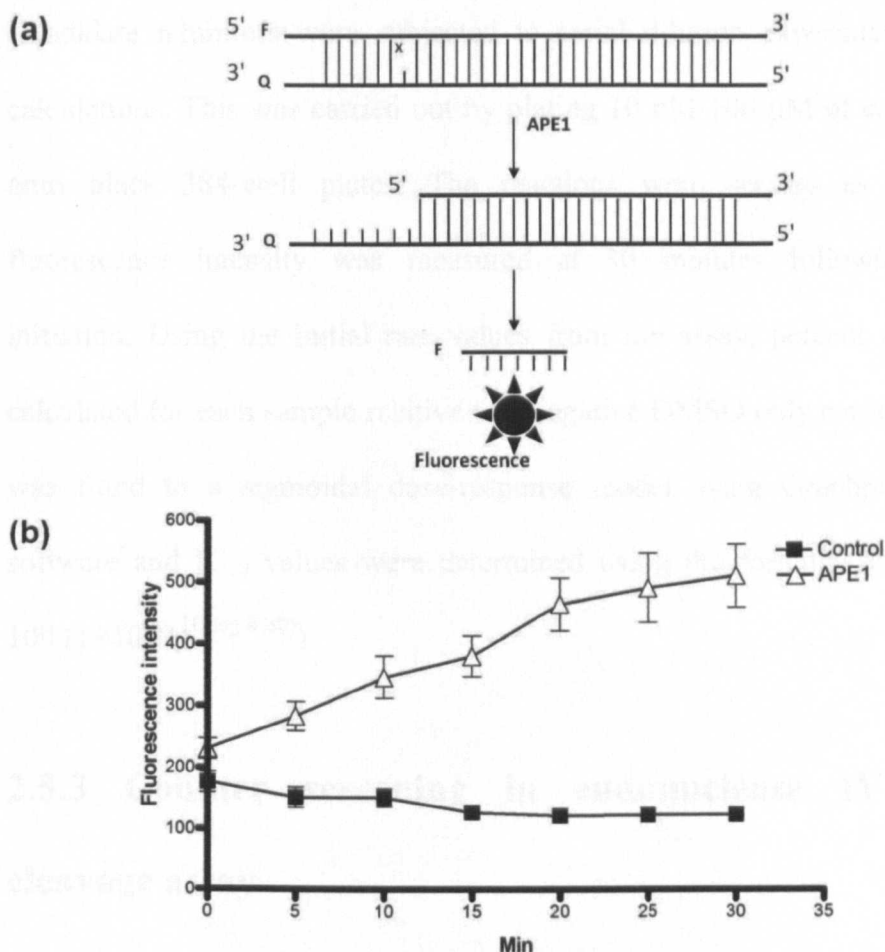
## **2.5 Biochemical screening**

### **2.5.1 Fluorescence based AP-site cleavage assay (Figure 2.2)**

The assay was performed as described previously with some modifications [23]. APE1 (50 nM ) (New England Biolabs) was incubated in a buffer system consisting of 50 mM Tris-HCl, pH 8.0, 1 mM MgCl<sub>2</sub>, 50 mM NaCl, 2 mM DTT at 37 °C for 10 minutes. The total volume of the enzyme and the buffer system was 30 µl.

5' F-GCCCCCXGGGGACGTACGATATCCCGCTCC 3' and its complementary Q labelled oligonucleotide 3' Q-CGGGGGCCCCCTGCATGCTATAGGGCGAGG 5' were annealed in a buffer system containing 100 µM Tris-HCl, 50 mM NaCl and 1 µM EDTA by mixing equal volumes of 250 µM from each oligonucleotide. The mixture was then heated at 95 °C for 5 minutes and allowed to cool slowly to room temperature. AP site cleavage was initiated by addition of 10 µl of the annealed substrate (25 nM) to the reaction mixture in black 384-well plate in a 40 µl total reaction. The Fluorescence readings were taken at 5 minute intervals during 30 minute incubation at 37 °C using an Envision® Multilabel reader from Perkins Elmer with a 495 nM excitation and a 512 nM emission filter. Upon encountering the APE1 endonuclease activity the DNA is cleaved at the abasic site at position 7 from the 5' end and a 6-mer fluorescein-containing

product will dissociate from its complement by thermal melting. Subsequently, the quenching effect of the 3' dabcyI (which absorbs fluorescein fluorescence when in close proximity) is lost, and APE1 activity is measured indirectly as an increase in fluorescence signal. Similar assays were generated for monitoring the AP endonuclease activity of endonuclease IV using a buffering system containing 10 mM HEPES-KOH, pH 7.4, 100 mM KCl and 60 ng of endonuclease IV (New England Biolabs). The final DMSO concentration was maintained at 1.2% in all assays.



**Figure 2.2 Primary screening.** (a) Fluorescence based APE1 AP-site cleavage assay is shown here. If the DNA is cleaved at the abasic site at position 7 from the 5' end by APE1, the 6-mer fluorescein-containing product will dissociate from its complement by thermal melting. As a result, the quenching effect of the 3' dabcyl (which absorbs fluorescein fluorescence when in close proximity) is lost, and APE1 activity is measured indirectly as an increase in fluorescence signal (b) A typical increase in fluorescence in response to APE1 cleavage is shown here. For detailed protocol see Materials and Methods section.

## 2.5.2 Screening and evaluation of potential APE1 inhibitors

To investigate the ability of a candidate inhibitor to block APE1 endonuclease activity, APE1 was incubated with the candidate inhibitors at 100  $\mu\text{M}$  (final DMSO concentration 1.2%) prior to initiating the AP-site cleavage assay described in the previous section. The candidates that showed more than 90% inhibition of APE1 activity were then investigated further for  $\text{IC}_{50}$  calculations.

Candidate inhibitors were subjected to serial dilution experiments for IC<sub>50</sub> calculations. This was carried out by plating 10 nM-100 µM of each inhibitor onto black 384-well plates. The reactions were set up as before and fluorescence intensity was measured at 30 minutes following reaction initiation. Using the initial rate values from the assay, percent activity was calculated for each sample relative to a negative DMSO only control. The data was fitted to a sigmoidal dose-response model using Graphpad Prism3.0 software and IC<sub>50</sub> values were determined using the formula: % Activity =  $100/(1+10^{(\log [I]-\log IC_{50})})$ .

### **2.5.3 Counter screening in endonuclease IV AP-site cleavage assay**

The basic principle of this assay was very similar to the AP-site cleavage assay discussed previously. Endonuclease IV rather than APE1 was used in the assay under different buffering conditions.

In this assay, endonuclease IV (60 nM ) (Trevigen, Abingdon, UK) was incubated in a buffer system consisting of 10 mM HEPES-KOH, pH 7.4, and 100 mM KCl at 37 °C for 10 minutes. The total volume of the enzyme and the buffer system was 20 µl. The final DMSO concentration was maintained at 1.2% in all assays.

The endonuclease IV AP site cleavage was initiated by addition of 10 µl of 25 nM of the annealed DNA substrate (see above) to the reaction mixture in black 384-well plate in a 40 µl total reaction. The fluorescence readings were taken at 5 minute intervals during 30 minute incubation at 37 °C using an Envision®

Multilabel reader from Perkins Elmer with a 495 nM excitation and a 512 nM emission filter.

100  $\mu$ M of the candidate APE1 inhibitors were incubated with endonuclease IV. Any inhibitor that showed more than 25% inhibition to Endonuclease IV cleavage activity was considered as a non specific inhibitor.

#### **2.5.4 Fluorescence quenching assay**

To exclude the possibility that a given compound might possess intrinsic quenching activity, fluorescence quenching assays were performed. Briefly, the oligonucleotides 5'-F-oligonucleotide (see above) and 3'CGGGGGCCCCCTGCATGCTATAGGGCGAGG-5' were annealed as described previously. The double stranded oligonucleotide (5 nM) was incubated with 100  $\mu$ M of a potential APE1 inhibitor in a buffer consisting of 50  $\mu$ M Tris-HCl, pH 8.0, 1 mM MgCl<sub>2</sub>, 50 mM NaCl, and 2 mM DTT at 37 °C for 30 minutes. Fluorescence intensity was measured every 5minutes. Any hits that showed a decrease of more than 50% in the fluorescence intensity were considered as quenchers and discarded from further analyses.

APE1 inhibitors isolated above were sent to Dr Wilson's laboratory at NIH, USA. for screening in a whole cell extract assay.

### **2.5.5 Whole cell extract AP-site cleavage assay**

This work was done in collaboration with Dr David Wilson III at NIH, USA. Briefly HeLa cells – maintained in DMEM with 10% fetal bovine serum and 1% penicillin-streptomycin were harvested, washed with 1X PBS and the pellet was resuspended in cold 222 mM KCl plus protease inhibitors (0.5 mM PMSF, 1 µg/ml each of Leupepetin and Pepstatin A), incubated on ice for 30 minutes. Then the cell lysate was clarified by centrifugation at 12 000 X g for 15 minutes at 4°C. The protein concentration was determined using the Bio-Rad Bradford reagent, and aliquots were stored at -80 °C. AP endonuclease activity assays using 18mer radiolabelled oligonucleotide substrates, 18FNMR 5'-GTCACCGTGXTACGACTC-3' and 18GNMR 5'-GAGTCGTAGCACGGTGAC-3' (Trilink Biotechnologies Inc., San Diego, CA, USA and Midland certified reagent company, respectively) were performed. In brief, potential APE1 inhibitors were incubated at 100 µM concentrations with 30 ng of HeLa WCE at room temperature for 15 minutes in incision buffer consisting of 50 mM Tris-HCl pH 8, 1 mM MgCl<sub>2</sub>, 50 mM NaCl, and 2 mM DTT. Following the incubation, 0.5 pmol <sup>32</sup>P-radiolabeled tetrahydrofuran (THF)-containing 18mer double-stranded DNA substrate was added. Incision reactions were then carried out immediately at 37 °C for 5 minutes in a final volume of 10 µl after which the reaction was terminated by the addition of an equal volume of stop buffer (0.05% bromophenol blue and xylene cynol, 20 mM EDTA, 95% formamide) followed by denaturation of samples at 95 °C for 10 minutes. The radiolabeled substrate and product were

separated on a standard polyacrylamide denaturing gel and quantified by phosphorimager analysis.

## **2.6 Cell based investigation**

### **2.6.1 Cell lines and culture media**

MeWo (melanoma), SK-Mel30 (melanoma), and PANC1 (pancreatic) cancer cell lines were grown in RPMI culture medium. U89MG glioma cancer cell line was grown in DMEM culture medium. Culture media were supplemented with penicillin 0.06 g/l, streptomycin 0.1 g/l pH 7.0, 10% foetal bovine serum (FBS, PAA Laboratories Inc., Yeovil, UK). HUVEC cell line was grown in Endothelial Cell Growth Medium supplemented with 2% FBS (Clonogenic<sup>®</sup>, Verviers, Belgium). Only cultures with a plating efficiency of over 70% were used for the analysis.

### **2.6.2 CellTiter 96<sup>®</sup> AQueous Non-Radioactive Cell Proliferation Assay (MTS assay)**

MTS assay (Promega) is a calorimetric assay for determining the number of viable cells. It is frequently used in cytotoxicity and chemosensitivity assays. MTS assay system consists of solutions of a tetrazolium compound (3-(4,5-dimethylthiazol-2-yl)-5-(3-carboxymethoxyphenyl)-2-(4-sulfophenyl)-2H tetrazolium; MTS) and an electron coupling reagent (phenazine methosulfate; PMS). MTS is bio-reduced by cells into a formazan compound that is soluble in tissue culture medium.

The conversion of MTS into formazan is accomplished by dehydrogenase enzymes that are only found in metabolically active cells. The absorbance of the formazan at 490 nm is then measured directly from 96-well assay plates using a universal plate reader FLUOstar OPTIMA from BMG LABTECH Ltd., Aylesbury, UK. The quantity of formazan product as measured by the amount of 490 nm absorbance is directly proportional to the number of viable cells in culture.

To evaluate the intrinsic cytotoxicity and to evaluate the potentiation of cytotoxicity of alkylating agents, the MTS assay was performed according to manufacturer recommendations. 2000 cells per well were seeded into a 96-well plate. For intrinsic cytotoxicity assessments cells were incubated with varying concentrations of APE1 inhibitors and the MTS assay was performed on day 5. For potentiation experiments cells were pre-incubated overnight with a non toxic concentration of APE1 inhibitors and then an increasing concentration of a base damaging agents (MMS or Temozolomide) or doxorubicin (negative control) was added and MTS assay was performed on day 5. For HUVEC cells, 5  $\mu$ l of 2% type2 gelatine (Sigma-Aldrich) was added to the wells and the plates were pre-incubated for 20 min at 37°C before seeding of cells. The total volume was maintained at 200 $\mu$ l per well in all assays. On day 5, 20  $\mu$ l of the reagent mixture consisting of 50  $\mu$ l PMS and 1ml MTS was added to each well (a ratio of 1:10 MTS to total well volume) and the plate was incubated for 4 hours at 37 °C before reading the absorbance at 490 nm. All assays were performed in triplicates for each APE1 inhibitor and GI<sub>50</sub> were calculated for each compound.



### **2.6.3 Growth Curve**

Tissue culture flasks (T25, FALCON®) were seeded with  $10^5$  cells and maintained in media containing three different doses of APE1 inhibitor ( $GI_{10}$ ,  $GI_{25}$  and  $GI_{50}$  that has been identified by the MTS assay). A negative control was incubated with media. Cells were maintained in a humidified incubator at 37°C in an atmosphere of 5% CO<sub>2</sub> and 95% air. Cells were counted on days 1, 2, 3 and 4. Fold increase in cell number was calculated compared to day 1.

### **2.6.4 Clonogenic survival assay**

Tissue culture plates (FALCON®) were seeded with 300 cells per well, and the cells were maintained in a humidified incubator at 37°C in an atmosphere of 5% CO<sub>2</sub> and 95% air for 10-14 days. The medium was later aspirated, and the cells were incubated at room temperature in 3 ml of fixing solution [(75% (v/v) methanol, 25% (v/v) acetic acid)] for 30 minutes. The fixing solution was then poured off and the cells were stained with crystal violet (1 mg/ml in distilled water) for 4 hours at room temperature. The stain was poured off and the plates were washed in running water to remove excess stain, before being left to air-dry overnight. Blue stained visible colonies with  $\geq 50$  cells were counted by eye using a colony counter (Stuart Scientific, UK).

To evaluate the toxicity profile of APE1 inhibitors cell cultures at approximately 80% confluence were trypsinized, and 300 cells were seeded per plate and allowed to adhere over 1 hour. Increasing concentrations (5  $\mu$ M- 20  $\mu$ M) of APE1 inhibitor were added to the medium, and the plates were

incubated. Visible colonies were counted after 10-14 days incubation as discussed previously.

To evaluate the potentiation of the cytotoxicity of DNA damaging agents by APE1 inhibitors, 300 cells were plated with or without APE1 inhibitor and allowed to adhere to the plate for 1 hour. This was followed by exposure to the DNA damaging agent MMS for 1 hour. The medium was then removed, plates were then washed with PBS and culture medium with or without APE1 inhibitor was added and incubated for 10-14 days. Analysis of colony formation and counting was performed as described above. All experiments were performed in triplicates. The final concentration of DMSO was maintained to less than 1% in all experiments (note: APE1 inhibitors were dissolved in this solvent).

### **2.6.5 AP sites quantification assay (Aldehyde Reactive Probe)**

Aldehyde reactive probe (ARP) reagent, (N'-aminooxymethylcarbonylhydrazin o-D-biotin) reacts specifically with the aldehyde group that is present in ring open form of AP sites. This reaction allows detection and quantification of AP sites. After treating genomic DNA containing AP sites with ARP reagent, the AP sites are 'tagged' with biotin residues. AP sites are then quantified using an avidin-biotin assay followed by a calorimetric detection of peroxidase conjugated to the avidin.

The ARP site assay was performed according to manufacturer protocol. Sub-confluent cells were exposed to MMS with or without APE1 inhibitor. The cells were then trypsinized at various time points and centrifuged at 1000 rpm

for 5 minutes. Genomic DNA was extracted from a pellet of  $1 \times 10^6$  cells using the guanidine/detergent lysis method. Briefly, 0.5 mls of DNAzol<sup>®</sup> (Helena Biosciences) was added to the pellet and the cell lysate was passed gently several times through a pipette. The resultant viscous supernatant was transferred into eppendorf tubes and centrifuged at 13,000rpm for 10 minutes at room temperature. The viscous supernatant was then transferred to a fresh tube and 0.25mls of 100% ethanol was added to the lysate to precipitate the DNA. The tubes were gently inverted 5-8 times at room temperature for 1-3 minutes. The tubes were then centrifuged at 7000 rpm for 5 minutes, and the 100% ethanol was discarded. The DNA was washed by adding 0.4 mls of 75% ethanol and the tubes were re-centrifuged for another 5 minutes. 75% ethanol was then discarded and the DNA was then solubilised in TE buffer pH 8.0, and its concentration was quantified using a GeneQuant *pro* spectrophotometer from Biochrom Ltd, Cambridge, UK. All DNA samples were equalized to a concentration of 100  $\mu\text{g/ml}$ .

The AP site quantification was performed using the aldehyde reactive probe assay kit and based on the protocol provided by the manufacturer (BioVision Research product, CA, USA). 5  $\mu\text{l}$  of purified genomic DNA solution (100  $\mu\text{g/ml}$ ) was mixed with 5 $\mu\text{l}$  of 10 mM ARP solution in a 1.5 ml eppendorf tube and the mixture was incubated at 37°C for 1 hour to tag the DNA AP site. 88  $\mu\text{l}$  of TE buffer and 2  $\mu\text{l}$  of Glycogen were added to the reaction solution. The samples were mixed well and 0.3 ml of 100% ethanol was added and incubated at -20 °C for 10 minutes. The reaction solution was then centrifuged at 14000 rpm for 10 minutes to precipitate the AP site tagged DNA. The ARP labelled DNA was then washed with 70% ethanol and quickly

spun to remove traces of ethanol from the DNA. The samples were then dissolved in 1 ml TE buffer so that the AP-DNA tagged concentration is 0.5 µg/ml. Meanwhile the ARP-DNA standards were prepared to generate 0, 8, 16, 24, 32 and 48 abasic sites/10<sup>5</sup> bp in microcentrifuge tubes. 60 µl of each of the above ARP-DNA and ARP-labelled DNA samples were added into a 96-well plate provided by manufacturer. To ensure accurate measurements three wells were used per sample. 100 µl of DNA binding solution was added to both samples and standards, and the plate was sealed and incubated overnight at room temperature to allow binding of the tagged –DNA on to plate surface. Next day the DNA binding solution was discarded and the wells were washed 5 times with 250 µl of washing buffer. 100 µl of horseradish peroxidase (HRP) was added to each well and the plate was incubated for 1 hour. The HRP was later discarded and the wells were washed 5 times with 250 µl of washing buffer. Finally 100 µl of HRP developer was added to each well and the plate was incubated for 1 hour at 37 °C. Absorbance of O.D. 650 was then measured using FLUOstar OPTIMA from BMG LABTECH Ltd., Aylesbury, UK. The data obtained from the standard ARP-DNA solution was used to construct a calibration curve. The ARP numbers represented AP sites per 10<sup>5</sup> bp in the genomic DNA samples. The number the AP sites were measured in samples treated with APE1 inhibitor and untreated control.

### **2.6.6 FACS analysis**

The cells were grown to sub-confluence in T25 tissue culture flasks and harvested by trypsinization and centrifugation (1000 rpm for 5 minutes). The cell pellets were fixed in 70% ethanol in PBS. The samples were then placed at

4°C for at least 12 hours to allow fixation. The samples were stored under these conditions until required for FACS analyses. Prior to FACS analysis, 70% ethanol fixed cells were harvested by centrifugation (1000 rpm for 5 minutes) and the pellet was resuspended in PBS containing propidium iodide (4 µg/ml) and DNase-free RNase A (10 µg/ml). After incubation at 37°C for 30 minutes the samples were analysed by flow cytometry using Cytomics F500 machine (Beckman Coulter, Fullerton, CA, USA) with a 488 nm laser. Red fluorescence (DNA) was collected for 20,000 cells for each sample. Data was analysed using FlowJo7.6.1 software.

### **2.6.7 Migration assay**

APE1 inhibitors were evaluated in migration assays. The assay was performed as below. On day 1 of the experiment, two parallel lines were drawn on the back of 6-well plate, using a marker pen. Each well was seeded with  $1 \times 10^6$  cells so that they would become confluent next day. The cells were maintained in a humidified incubator at 37°C in an atmosphere of 5% CO<sub>2</sub> and 95% air. On day 2 the media was removed, cells were washed with PBS and then fresh media with different concentration of APE1 inhibitor was added (0µM, 10µM and 20µM). The plate was then incubated overnight in the humidified incubator at 37°C in an atmosphere of 5% CO<sub>2</sub>. On day 3 of the experiment the media containing the inhibitor was removed and cells were washed with PBS. A wound perpendicular to the drawn lines was scratched using a p20 pipette tip, then the cells were washed twice with PBS and a fresh media containing 10 µg/ml mitomycin C was added to each well. Addition of mitomycin C was to

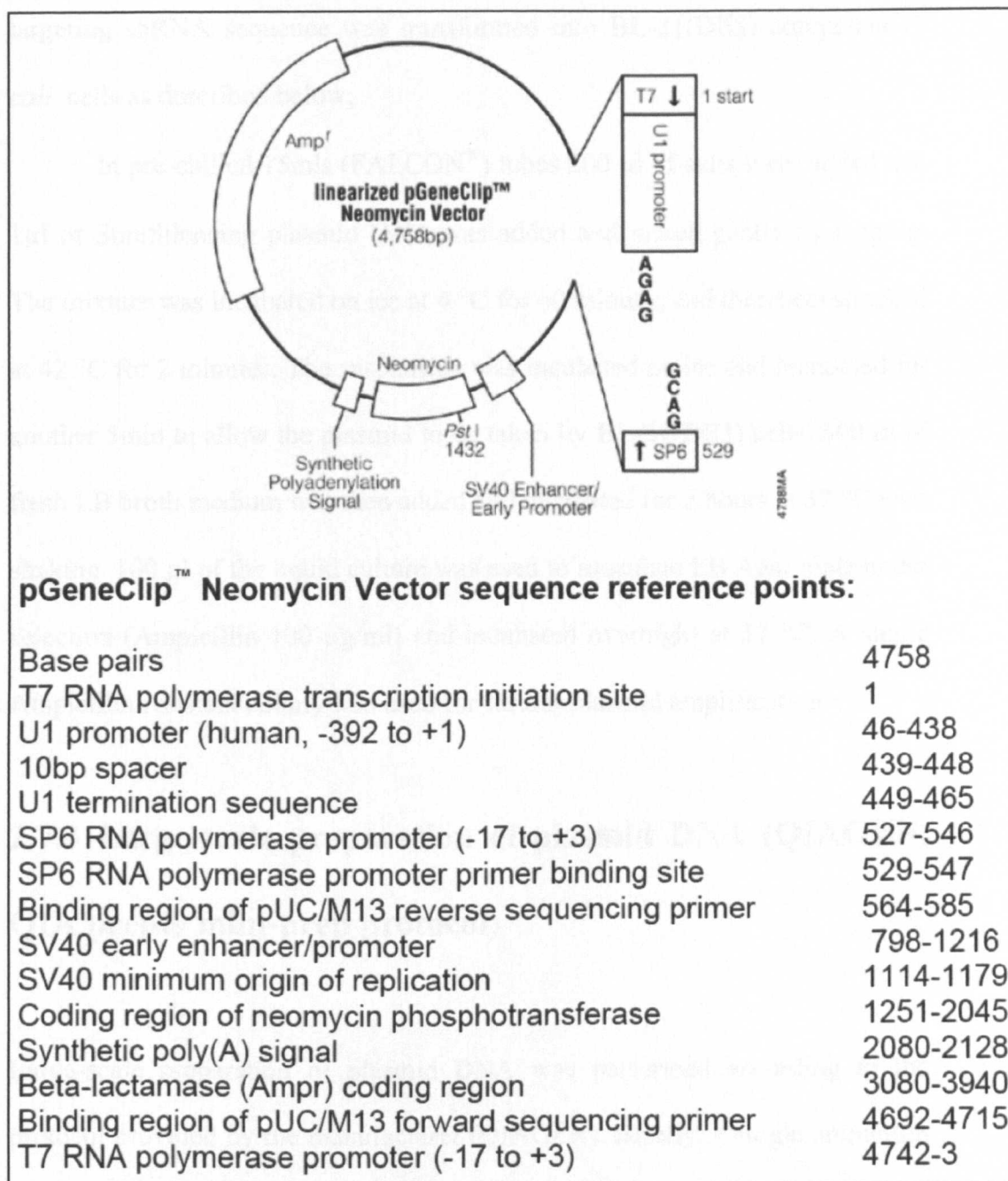
allow measurement of the wound healing induced by cell migration rather than cell proliferation. Serial photographic pictures were taken to the wounds using a photographic microscope (Nikon TS-100) on time points 0 hour, 2 hour, 4 hour, 6 hour, 8 hour, 16 hour, 24 hour, 36 hour and 48 hour.

The pictures were analysed, using imageJ analytical software (<http://rsbweb.nih.gov/ij/download.html>). The surface area of the wound was measured and the percentage of healing was calculated relative to the wound area at time “0”.

## **2.7 APE1 knocked down studies**

### **2.7.1 shRNA plasmid constructs and SurFECT transfection reagents**

shRNA plasmids designed to specifically knock down the expression of human APE1 gene by RNA interference under antibiotic selection (SureSilencing™, Catalog # KH02201) were purchased from SABioscience, MD USA, together with one control plasmid. Each plasmid contains shRNA under control of U1 promoter with neomycin gene for the selection of stably transfected cells (Figure 2.3). SureFECT™ Transfection Reagent (SABioscience, MD, USA) which is a high-efficiency, low-toxicity solution for the reverse transfection of a wide variety of cultured mammalian cells was used to transfect shRNA plasmid into cancer cell lines as described below.



**Figure 2.3 SureSilencing™ shRNA APE1 Plasmid.** The vector contains a short hairpin RNA, or shRNA, under control of the U1 promoter and the neomycin, resistance gene an (<http://www.sabiosciences.com/Manual/shRNA.pdf>).

## 2.7.2 Transformation and purification of SureSilencing plasmid DNA

To amplify plasmids and to produce high quality plasmid ready for transfection, pGeneClip™ Neomycin vector (promega®) carrying the APE1

targeting shRNA sequence was transformed into BL-21(DE3) competent *E. coli* cells as described below;

In pre-chilled 15mls (FALCON®) tubes 200 µl of cells were added and 1µl of SureSilencing plasmid DNA was added and mixed gently by tapping. The mixture was incubated on ice at 4 °C for 60 minutes and then heat shocked at 42 °C for 2 minutes. The suspension was incubated on ice and incubated for another 5min to allow the plasmid to be taken by BL-21(DE3) cells. 800 µl of fresh LB broth medium was then added and incubated for 2 hours at 37 °C with shaking. 100 µl of the liquid culture was used to inoculate LB Agar plate under selection (Ampicillin 100 µg/ml) and incubated overnight at 37 °C. A single Ampicillin resistant colony was used for further plasmid amplification.

### **2.7.3 Large-scale preparation of plasmid DNA (QIAGEN, QIA prep® mini-prep protocol)**

Large-scale preparation of plasmid DNA was performed according to the protocol provided by the manufacturer (QIAGEN). Briefly, a single ampicillin resistant colony was picked and inoculated into 5 ml LB broth under selection and grown up for 8 hours at 37 °C with shaking. After the incubation, 250 µl of liquid culture was inoculated into 200 mls of LB broth under selection in a 2 litre flask and incubated overnight at 37 °C with shaking. The culture was then transferred into 50 mls tube and the bacterial growth was harvested by centrifugation at 4000 rpm. The process was repeated until 200 mls of LB broth was centrifuged. The harvested bacteria were then resuspended in 10 mls of Buffer P1 (containing RNase A). Then 10 mls of buffer P2 was added and



the tube was shaken vigorously and incubated at room temperature for 5 minutes. After incubation, 10 mls of pre-chilled buffer P3 was added and the tube was inverted 5-6 times and the cell lysate was transferred directly to QIAfilter cartridge and incubated at room temperature for 10 minutes. Meanwhile, QIAGEN-tip 500 was equilibrated by adding 10 mls of QBT buffer until it drained completely through the QIAGEN-tip 500. Following the 10 minutes incubation, a plunger was inserted into QIAfilter cartridge, and clear lysate was passed into QIAGEN-tip 500. Once all the lysate drained from the QIAGEN-tip, the tip was washed twice with 30 mls of QC buffer, and transferred into 50 ml clean tube. 15 mls of QF buffer was then added to the tip and DNA was eluted and collected into the clean 50 ml tube. To precipitate DNA, 10.5 mls of isopropanol (at room temperature) was added to the eluted DNA mixed rapidly and centrifuged at 4000 rpm for 30 minutes. Following centrifugation the precipitated DNA was transferred to 1.5 mls eppendorf tube. The DNA was washed by adding 1 ml of 70% ethanol and centrifuged for 10 minutes at 14000 rpm. Ethanol was then discarded, and the tube was then re-centrifuged for 1 minute without closing the lid, to allow the ethanol to dry. Finally the DNA was eluted by adding 500 µl of TE buffer, pH 8.0 and the sample was left on bench overnight to allow the DNA to dissolve completely prior to quantification, and then it was stored at -20 °C.

#### **2.7.4 Determination of DNA concentration**

The DNA concentration was determined by diluting the sample (1:100) and measuring the absorption ( $OD_{260}$ ) with a GeneQuant *pro* spectrophotometer from Biochrom Ltd, Cambridge, UK. It was assumed that

an  $OD_{260} = 1$  was equivalent to 50  $\mu\text{g/ml}$  of double stranded DNA and 33 $\mu\text{g/ml}$  of single stranded DNA.

### **2.7.5 Restriction enzyme digestion**

In order to verify that the amplified shRNA contained plasmid, a restriction digestion of the amplified plasmid was performed. 1  $\mu\text{l}$  of plasmid DNA isolated by MaxiPrep was digested at 37 °C for 2-4 hours using 100U of *pst* I restriction enzyme in NEBuffer 3 (100 mM NaCl 50 mM Tris-HCl 10 mM  $\text{MgCl}_2$  1 mM Dithiothreitol and pH 7.9 at 25 °C) and bovine serum albumin (BSA), in a total reaction volume of 20  $\mu\text{l}$ . The sample was then loaded onto a 0.8% agarose gel (with ethidium bromide 0.03  $\text{ng}/\mu\text{l}$ ). The DNA was electrophoresed at a constant current of 80 mA for 1 hour and imaged under UV transillumination.

### **2.7.6 Selection of antibiotic resistance**

The minimum concentration of neomycin needed to kill untransfected cells, also called effective concentration, depends on type of cell line, rate of growth, and state of confluence during growth. Therefore a dose response curve for neomycin was generated as described below.

Cancer cells were seeded onto 12-well tissue culture plates at 10% confluence and incubated in fresh media containing an increasing dose of neomycin (0, 100, 200, 400, 600, 800, and 1000  $\mu\text{g/ml}$ ). The plates were then maintained in a humidified incubator at 37 °C in an atmosphere of 5%  $\text{CO}_2$  and 95% air. The media was replaced every 2 days with appropriate neomycin

concentration. The minimum concentration of neomycin that kills all the cells is the effective concentration used for subsequent selection.

### **2.7.7 Transfection of APE1 ShRNA plasmid**

Mammalian cell transfection experiments were performed according to the protocol provided by the manufacturer.

100  $\mu$ l of Opti-MEM™ I Reduced-Serum Medium (Gibco) was added to a 24-well tissue culture plate. 0.4  $\mu$ g of APE1 shRNA plasmid was then added. The mixture was mixed by gently shaking the plate. 3  $\mu$ l of SureFECT (that is 7.5  $\mu$ l of SureFECT per  $\mu$ g of plasmid) was added and again mixed gently. The plate was then incubated at room temperature for 20 minutes. Mammalian cell line to be transfected (U89MG) was prepared for transfection. The cells were washed twice in Dulbecco's PBS without Calcium and Magnesium, trypsinized and harvested by centrifugation at 1000 rpm for 5 minutes.

The cells were then counted by haemocytometer, centrifuged and suspended ( $1 \times 10^6$  cells per well) in fresh DMEM medium [containing 10% fetal bovine serum and 1% Non essential amino acids (NEAA)]. 500  $\mu$ l of cell suspension was added into the wells containing the SureFECT-plasmid complexes. The suspension was mixed gently by rocking the plate back and forth and the cells were then incubated at 37 °C in a CO<sub>2</sub> incubator for 48 hours. Following incubation, the cells were harvested by passaging and transferred to a 6-well tissue culture plate and seeded at 10% confluence. Media containing neomycin (at the effective concentration) was added, and the cells were maintained in humidified incubator at 37 °C and 5% CO<sub>2</sub> for 6-7 days week. The media with neomycin was replaced every 72 hours.

## **2.8 Western blot**

### **2.8.1 Preparation of cell lysate**

70-80% confluent cells were washed with PBS, trypsinised and counted using haemocytometer. The cells were then resuspended in a fresh media at a concentration of  $10^6$  cells per ml. 1 ml of cell suspension was pipetted into 1.5 ml eppendorf tube and washed ones with PBS and lysed using 100  $\mu$ l of RIPA buffer (20 mM Tris, 150 mM NaCl, 1% Nonidet p-40, 0.5% sodium deoxycholate, 1 mM EDTA, 0.1% SDS) containing 1  $\mu$ l of protease inhibitor (Sigma-Aldrich) and 1  $\mu$ l of phosphatase inhibitor cocktail 1 and 2 (Sigma-Aldrich). The lysate was then incubated overnight at 4 °C and then centrifuged at 13000 rpm for 20 minutes at 4 °C. The supernatant was then stored at -20 °C.

### **2.8.2 Cell lysate protein quantification (Bradford assay)**

The concentration of cell lysate protein was determined using the BioRad coomassie assay with BSA as a standard. Briefly, 10 $\mu$ l of protein were mixed with 250  $\mu$ l diluted and filtered assay solution in 96-well plate. Subsequently, OD<sub>595</sub> was determined within 1 hour using FLUOstar OPTIMA from BMG LABTECH Ltd., Aylesbury, UK.

### **2.8.3 Denaturing polyacrylamide gel electrophoresis**

20 µg of protein samples were mixed with an equal volume of sample loading buffer (1x 50 mM Tris-HCl, pH 6.8, 10%(v/v) glycerol, 2% (w/v) SDS, 0.01% (w/v) bromophenol blue, 1% (v/v) β-mercaptoethanol) and denatured at 98 ° C for 5 minutes before loading onto SDS-polyacrylamide gels. 10-15% Tris-HCl pre-poured 'Criterion' gels (Bio-Rad) were run in SDS electrophoresis buffer (25 mM Tris-HCl, pH 8.3, 190 mM glycine, 0.1% (w/v) SDS) at a constant voltage of 200 V, using 'Criterion' (Bio-Rad) gel equipment. Proteins were transferred to a nitrocellulose membrane for western blot analysis. Electroblotting was performed at 25V for 90 minutes in transfer buffer [20% (v/v) methanol, 50 mM Tris-HCl, 380 mM glycine]. The membrane was then blocked by incubation with PBST (PBS, 0.05% Tween 20) containing BSA/milk for 60 minutes with swirling. Then the membranes were incubated with primary antibody at 4 °C overnight. [Rabbit polyclonal APE-1 antibody, Novus Biologicals Inc, Littleton, CO 1:250 dilution and mouse monoclonal β-Actin (Abcam) 1:5000 dilution] and infrared dye labeled polyclonal secondary antibody (Li-cor) (IRDye 800CW Donkey Anti-Rabbit IgG (H+L) and IRDye 680CW Donkey Anti-Mouse IgG (H+L) in the dilution of 1:15000 for 60 minutes. Protein expression was determined by scanning the membranes on Licor-Odyssey's Scanner from LI-COR Bioscience Ltd, Cambridge, UK, at the pre-defined intensity fluorescence channel (700 nm and 800 nm).

## ***Chapter 3***

### ***Molecular Modelling***

---

## **3. Molecular modelling**

### **3.1 Introduction**

Drug design is an iterative process that begins with the identification of a compound that displays an interesting biological profile and culminates in the optimisation of both the biological activity profile and the chemical synthesis of the newly identified compound. Recent advances in the development of mathematical models that describe chemical phenomena and the development of more intuitive programme interfaces together with the rapidly progressing computer technology has allowed the use of virtual approaches to study the structural properties of compounds. In addition, it has allowed developing and testing hypotheses and correlates to observed biological activities and utilizes these correlations to predict properties and activities of new chemical entities. Molecular modelling is now an industry-standard approach for drug design and discovery.

The biological activity of a given chemical (a ligand or a drug) is the result of its binding to a pocket of another molecule (the receptor). The receptor is usually a protein. Geometric and chemical complementarity of ligand-receptor binding is essential for potential drug activity. In drug discovery, the biological activity of a given ligand is highly dependent on the three dimensional placement of specific functional groups (the pharmacophore) into the active site of target protein. A variety of molecular modelling softwares are now available for both academic and industrial use that allow drug discovery researchers generate and present molecular data to facilitate the drug discovery process.

Molecular modelling studies generally utilize two distinct strategies for drug design. The first strategy is *the direct drug design* approach. Here the 3D structure of the target protein is known from X-ray crystallographic data and the active site can then be utilized to design primary pharmacophores. This is usually followed by a series of docking experiments and to predict binding strength between ligand and target protein.

The second approach is the indirect design of pharmacophore by analysing the structural feature of known active or sometimes inactive molecules that are complementary to the active site protein. In my PhD project I utilized both the direct and indirect approaches to identify potential APE1 inhibitors. APE1 protein structure can be obtained from the protein data bank. The active site of APE1 can be precisely localized and allowed me to directly design potential inhibitors for APE1 repair domain. Moreover the existence of previously characterised specific APE1 inhibitors was a useful starting point for identifying more specific and drug-like pharmacophores. By analysing the shape of active site pocket of APE1 as well as the chemical structure of existing inhibitors, I was able to predict the most suitable template for APE1 inhibition.

Molecular modelling softwares, such as VMD1.8.6, SYBYL8.0, GOLD2.7 and ROCS2.3 were used to achieve these goals. In this introduction I will give an overview of each programme specification and its importance for my virtual screening work.

The first step in virtual screening and drug design is the visualisation of target protein using software programmes to display molecules as ball and stick



models, surface display or space filling display model. The active site is localized and then used for structure based design studies.

VMD1.8.6 software was used to display, animate, and analyze APE1 in this project [257]. VMD1.8.6 was developed by Theoretical and computational Biophysics Group, University of Illinois, USA in 1992 and first released in 1995. A Microsoft windows platform version was released in 1999 and since then a regular updates have been released to improve graphical simulation. VMD1.8.6 includes tools for working with volumetric data, protein sequence analysis and arbitrary graphics which makes it ideal for analysing target protein structures and localising their active sites.

SYBYL8.0, is a computational tool kit from Tripos<sup>TM</sup> available for molecular design and analysis. This software allows building dynamic models of compounds and visualisation of geometry. SYBYL8.0 is also a powerful tool for new lead design as well as optimisation of existing lead series. SYBYL8.0 also allows other life science experiments such as modelling a protein structure by introduction of mutation in its amino acids sequence.

The process of utilising computer programmes to perform ligand-protein interactions and to test their fitness both geometrically and energetically into the binding site of a protein is called molecular docking. The computational docking of small molecules into the structures of macromolecular targets and “scoring” of their potential complementarity is a widely used approach in hit identification and lead optimization in the drug discovery process [259]. The computerised docking studies aim accurate structural modelling and prediction of biological activity. However, the intermolecular interaction is complex and influenced by hydrophobic,

dispersion, Van der Waals, hydrogen bonding, electrostatic, metal ion binding interactions. Docking is a multistep process that begins with the application of the docking algorithms that pose small molecules into the active site of target protein. The algorithms are complemented by *scoring functions* that are designed to predict the biological activity through the evaluation of interactions between compounds and target protein.

One of the key aspects of molecular modelling is the calculation of energy of conformations and interactions. In the context of docking, energy evaluations are usually carried out with the help of a scoring function. A large number of current scoring functions are based on forcefields that were initially designed to simulate the function of proteins. A forcefield is simply an empirical fit to the potential energy surface in which the protein exists and is obtained by establishing a model with a combination of bonded terms (bond distances, bond angles, torsional angles, etc.) and non-bonded terms (Van der Waals and electrostatic). The relative contributions of these terms are adjusted for the different types of atoms in the simulated molecule by adjusting a series of parameters. Some scoring functions used in molecular docking have been adapted to include terms such as solvation and entropy.

Most of the docking methods used in academic and industrial research all assume a rigid protein. GOLD2.7 is one of the docking programmes which is able to conduct a rigid protein docking study, with an additional option of selecting partial protein flexibility, including protein side chain and backbone flexibility for up to ten user-defined residues.

GOLD2.7 programme is provided as part of the GOLD Suite and designed to calculate the docking modes of small molecules onto protein binding sites. In

addition GOLD2.7 allows visualisation of docking results. GOLD2.7 offers a choice of scoring functions, GoldScore, ChemScore, ASP (Astex Statistical Potential), PLP (Piecewise Linear Potential). GoldScore and ChemScore are the most widely used scoring function in docking experiments.

The GoldScore fitness function is made up of four components: a) Protein-ligand hydrogen bond energy (*external H-bond*), b) Protein-ligand Van der Waals (vdw) energy (*external vdw*), c) Ligand internal vdw energy (*internal vdw*), d) Ligand torsional strain energy (*internal torsion*) and a fifth optional component, e) Ligand intramolecular hydrogen bond energy (*internal H-bond*). The fitness score is taken as the negative of the sum of the component energy terms, so that larger fitness scores are better. The GoldScore fitness function has been optimised for the prediction of ligand binding positions rather than the prediction of binding affinities although some correlation with the latter has been found.

ChemScore fitness function was derived empirically from a set of 82 protein-ligand complexes for which measured binding affinities were available. It estimates the total free energy change that occurs on ligand binding as follows:

**Equation1**

$$\Delta G_{\text{binding}} = \Delta G_0 + \Delta G_{\text{hbond}} + \Delta G_{\text{metal}} + \Delta G_{\text{lipo}} + \Delta G_{\text{rot}}$$

Each component of this equation is the product of a term dependent on the magnitude of a particular physical contribution to free energy (e.g. hydrogen bonding) and a scale factor determined by regression.

#### Equation2

$$\Delta G_0 = V_0, \Delta G_{hbond} = V_1 P_{hbond}, \Delta G_{metal} = V_2 P_{metal}, \Delta G_{lipo} = V_3 P_{lipo}$$

$$\Delta G_{rot} = V_4 P_{rot}.$$

The  $V$  terms are the regression coefficients and the  $P$  terms represent the various types of physical contributions to binding. The final ChemScore value was obtained by adding in a clash penalty and internal torsion terms, which militate against close contacts in docking and poor internal conformations. Covalent and constraint scores may also be included. The final ChemScore is the results of

#### Equation3

$$\Delta G_{binding} + P_{clash} + c_{internal} P_{internal} + (c_{covalent} P_{covalent} + P_{constraint}).$$

ROCS2.3 (Rapid Overlay of Chemical Structure) is a powerful virtual screening tool designed for fast shape comparison application. ROCS2.3 can rapidly identify potentially active compounds with a similar shape to a known hit/lead compound. ROCS2.3 is based on the principle that molecules have similar shape if their volumes overlay well and any volume mismatch is a measure of dissimilarity. It uses a smooth Gaussian function to represent the molecular volume, so it is possible to routinely minimize to the best global match. ROCS2.3 allows screening of entire multiconformer corporate collections in a single day using a single processor. The alignment and fitness of the query molecule used for similarity search to a given chemical hits can be expressed as a shape fitness score called Tanimoto score. Moreover, ROCS2.3 provides an option to use a chemical alignment as well as a shape alignment to assess a similarity between the two molecules, the query molecule and the hits

molecule. This is called combo score, which is used by default in ROCS2.3 for scoring of similarity.

The previous identification of CRT0044876 as specific small molecule inhibitor of APE1 in our laboratory as well as the availability of APE1 3D crystal structure in the protein data bank was my starting point for the virtual screening strategy in the current project.

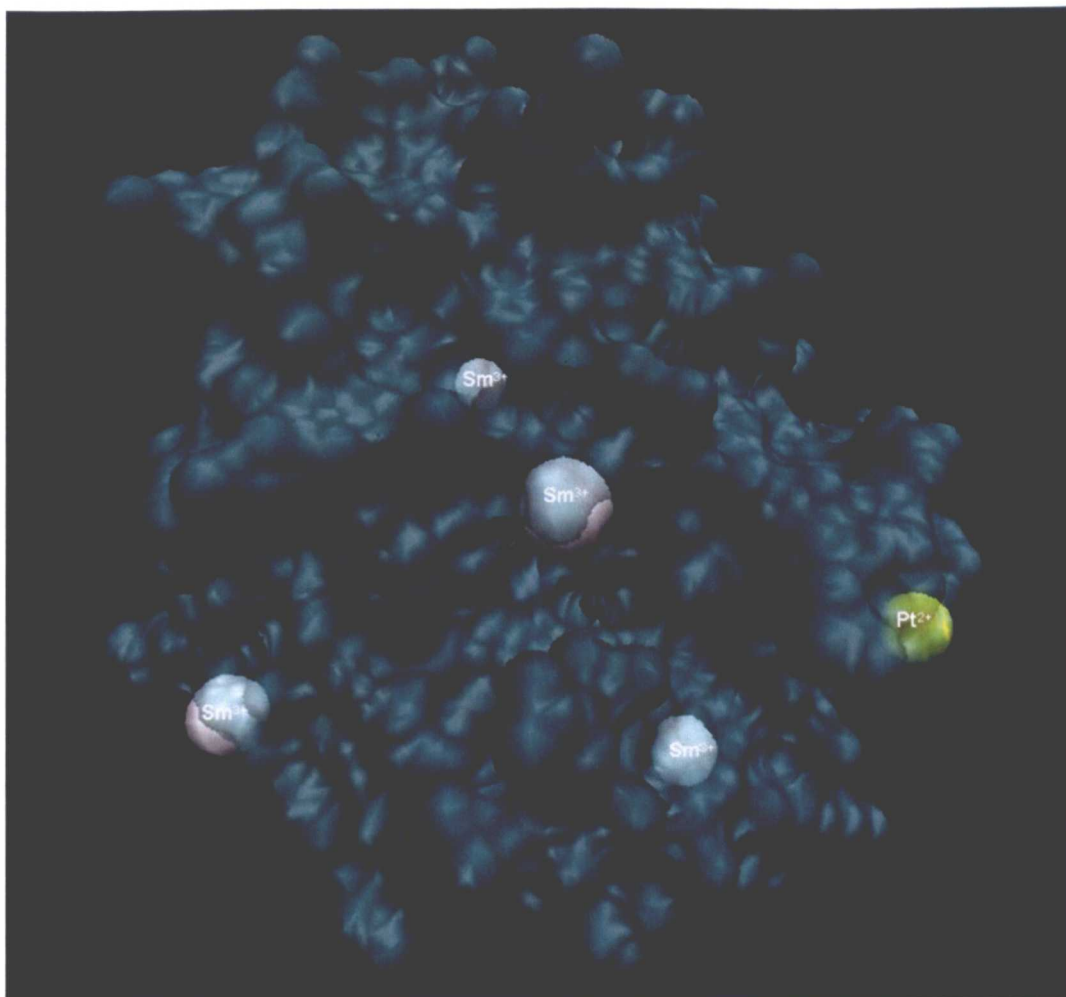
## **3.2 Results**

### **3.2.1. APE1 crystal structure selection and active site localization**

There were seven publicly available coordinates of crystal structure of the APE1 protein at the time of initiation of this project. APE1 crystals had been generated either alone or in complex with DNA. The crystals available include **1DE8, 1DE9, 1DEW, 1HD7, 1BIX, 1E9N and 2ISI**. As molecular modelling requires precise definition of the ligand binding site in the target protein, an APE1 protein crystal with moderate to high resolution with open binding site not bound to DNA substrate was essential to provide a clear view to the hydrophobic active site pocket.

As **1DE8, 1DE9, 1DEW and 2ISI** were bound to DNA, they were excluded from further analysis [260, 261]. **1HD7** was crystallised at low pH and does not represent APE1 shape under physiological condition [262]. Therefore **1HD7** was also excluded from further analysis. **1E9N** was crystallised at neutral pH, but it has two  $\text{Pb}^{2+}$  ions at its active site[262]. This was not considered to be ideal for molecular modelling and hence excluded from further analysis.

1BIX is a relatively high resolution crystal structure of APE1 and the protein has been crystallised unbound to a DNA substrate at a relatively neutral pH. 1BIX has 4 metal ions in its structure namely three samarium ions ( $\text{Sm}^{3+}$ ) and one platinum ion ( $\text{Pt}^{2+}$ ) (see Figure 3.1). 1BIX was chosen for molecular modelling in this study.



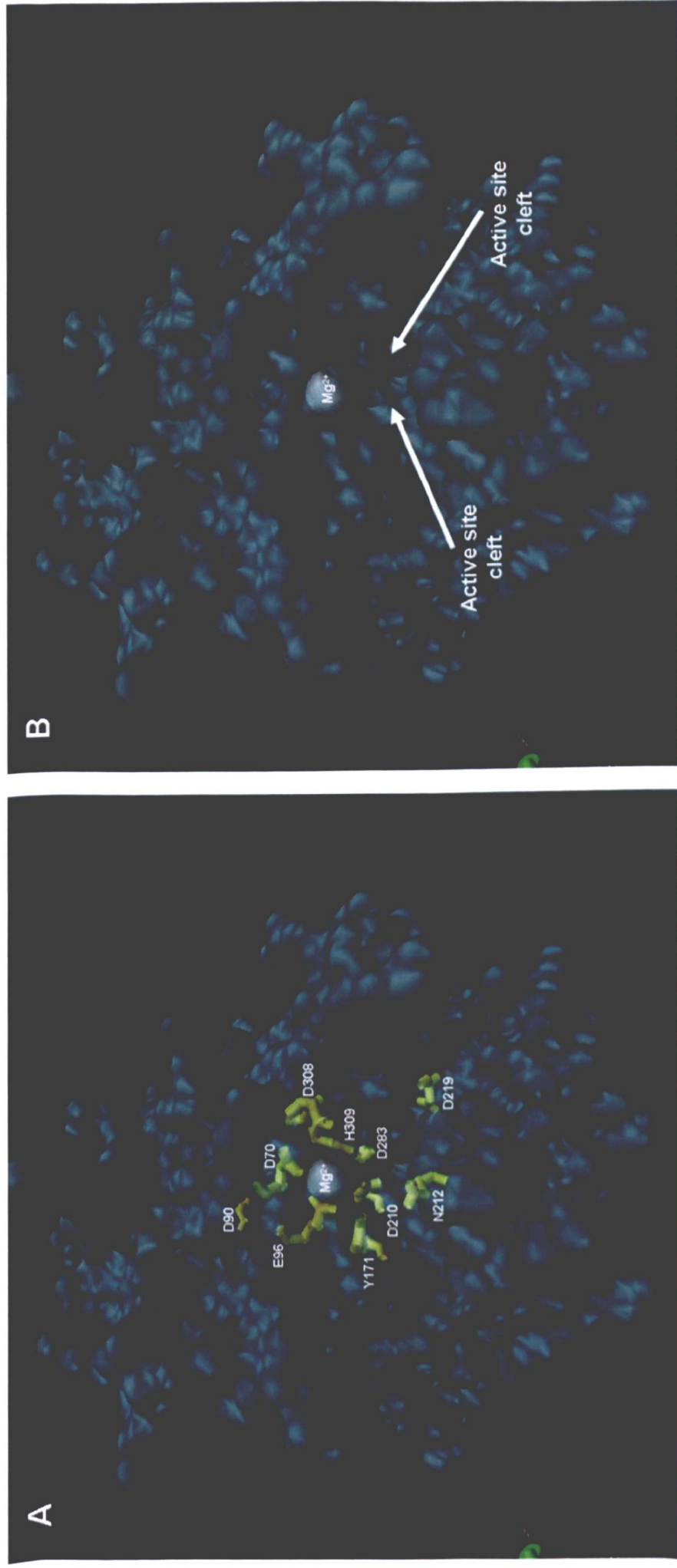
**Figure 3.1 Molecular modelling.** 3D simulation of the crystal structure of APE1 showing the metal ions present in 1BIX \*.pdb file. The four white spheres represent the Samarium ions ( $\text{Sm}^{3+}$ ) while the yellow sphere represents the platinum ion ( $\text{Pt}^{2+}$ ).

1BIX crystal structure was downloaded from the protein data bank website <http://www.pdb.org/pdb/home/home.do>. and the file was saved in \*.pdb file format. As most of the modelling programmes do not recognise  $\text{Sm}^{3+}$  ion and consider it as a dummy atom (i.e. unidentified atom that behave neutral and does not participate in any virtual interaction), \*.pdb file format of 1BIX was modified so that  $\text{Sm}^{3+}$  was replaced with  $\text{Mg}^{2+}$  and  $\text{Ni}^{2+}$  wherever necessary. These modified \*.pdb files were then used in molecular modelling.

The next step was to locate different APE1 domains in 3D space and specify our domain of interest namely, the DNA repair domain. VMD1.8.6 was used to

localize the DNA repair domain. The previously reported ten critical amino acid residues that are essential for the AP endonuclease activity of APE1 (D70, D90, E96, Y171, D210, N212, D219, D283, D308, and H309) were located to identify the DNA repair domain of APE1 (Figure 3.2 A) [122-127]. This localization identified a well-defined deep V-shaped active site cleft with a  $Mg^{2+}$  ion at its 'elbow' (Figure 3.2 B).

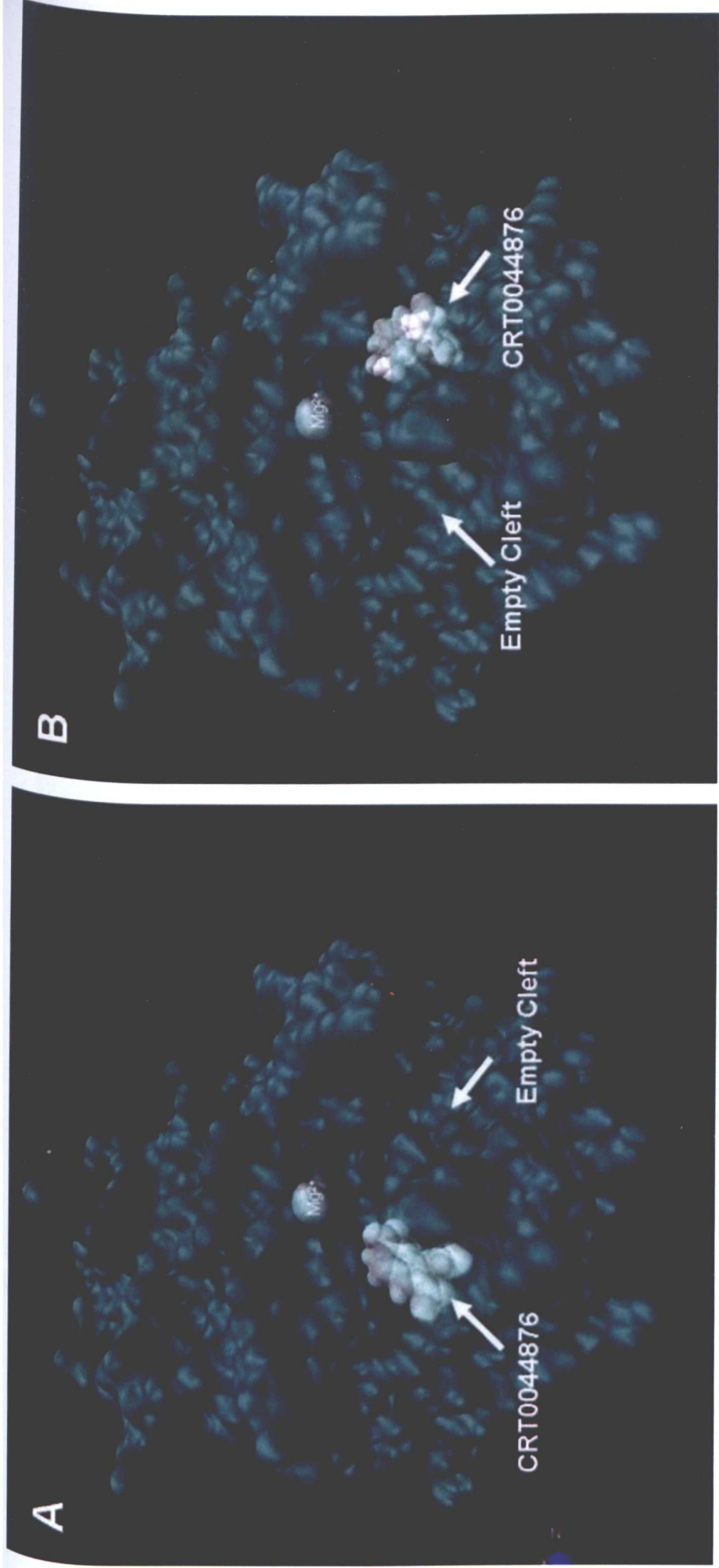




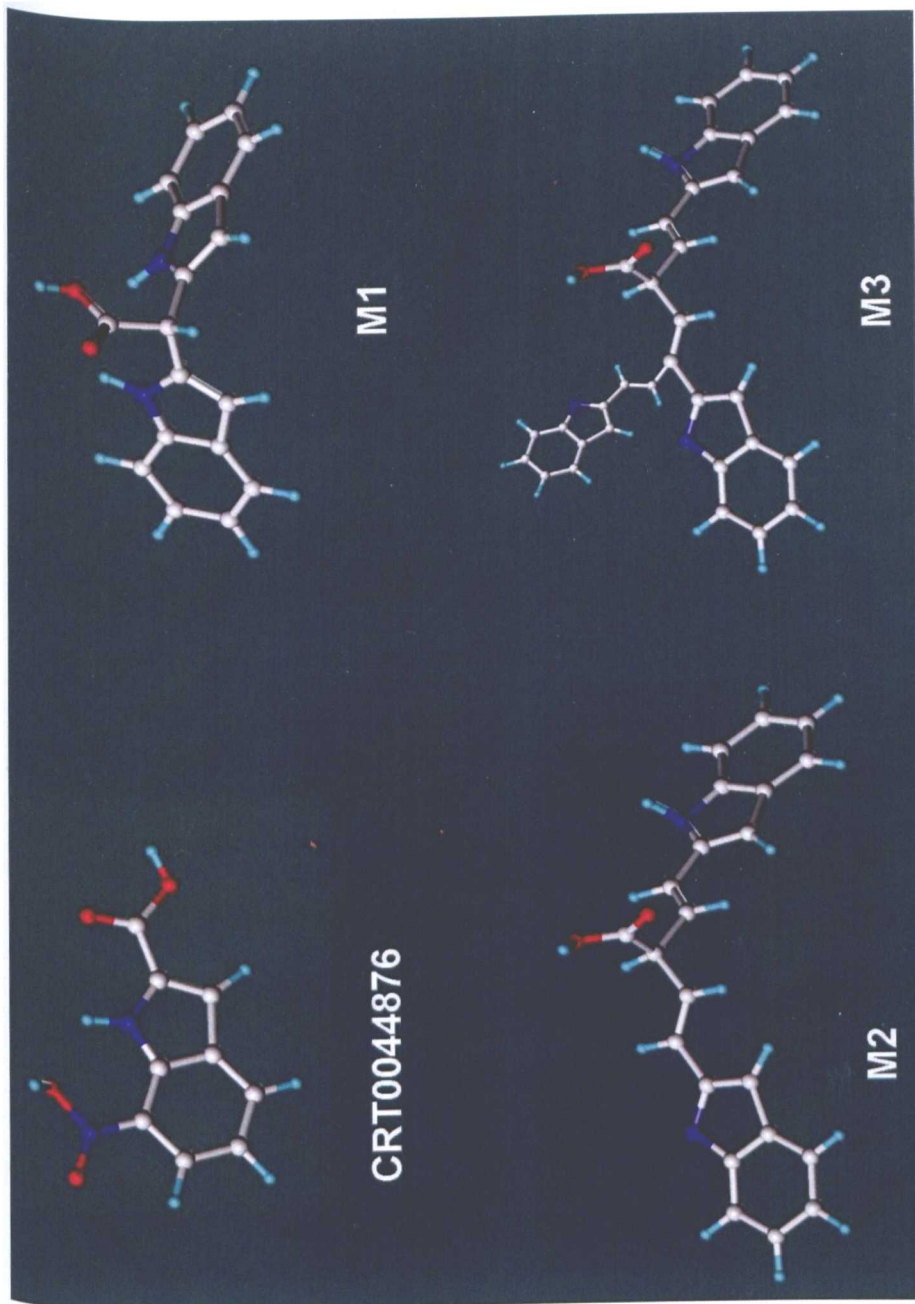
**Figure 3.2 Molecular modelling.** 3D simulation of the crystal structure of APE1 protein. (A) shows 10 critical amino acids essential for AP endonuclease activity, surrounding the  $Mg^{2+}$  ion. (B) The white arrows indicate the two clefts of the hydrophobic active site.

### 3.2.2. Design of pharmacophore model

VMD1.86 was used to conduct manual docking of the first generation APE1 inhibitor, CRT0044876, onto the active site cleft of the APE1 protein [23]. CRT0044876 was visualised to be able to dock very neatly on either sides of the V shaped hydrophobic cleft (Figure 3.3). To design promising pharmacophores models, CRT0044876 template was utilized to generate potential chemotypes that are able to fit the active site model as shown in figure 3.4 and figure 3.5. Three prototypical scaffolds named M1, M2 and M3 were built using SYBYL8.0. The templates have indole carboxylic acid as the primary building block and represent structures with shape complementarity to the active site of APE1. M1 Template features a central tetrahedral centre bearing a potential  $Mg^{2+}$ -interacting carboxylate group plus two heteroaromatic branches that have dimensions and relative orientations designed to fit snugly into the active site groove. M2 template bears similar features and the heteroaromatic substituents were extended to increase interaction with amino acids residues. M3 template was designed to bear an additional heteroaromatic side chain that can access a subsidiary cleft in the ligand-binding groove (Figures 3.4). Docking studies of M1, M2 and M3 templates by GOLD 2.7 revealed a near complete filling of the active site clefts ensuring the desired shape complementarity of the templates to the active site of APE1 (Figure 3.5).

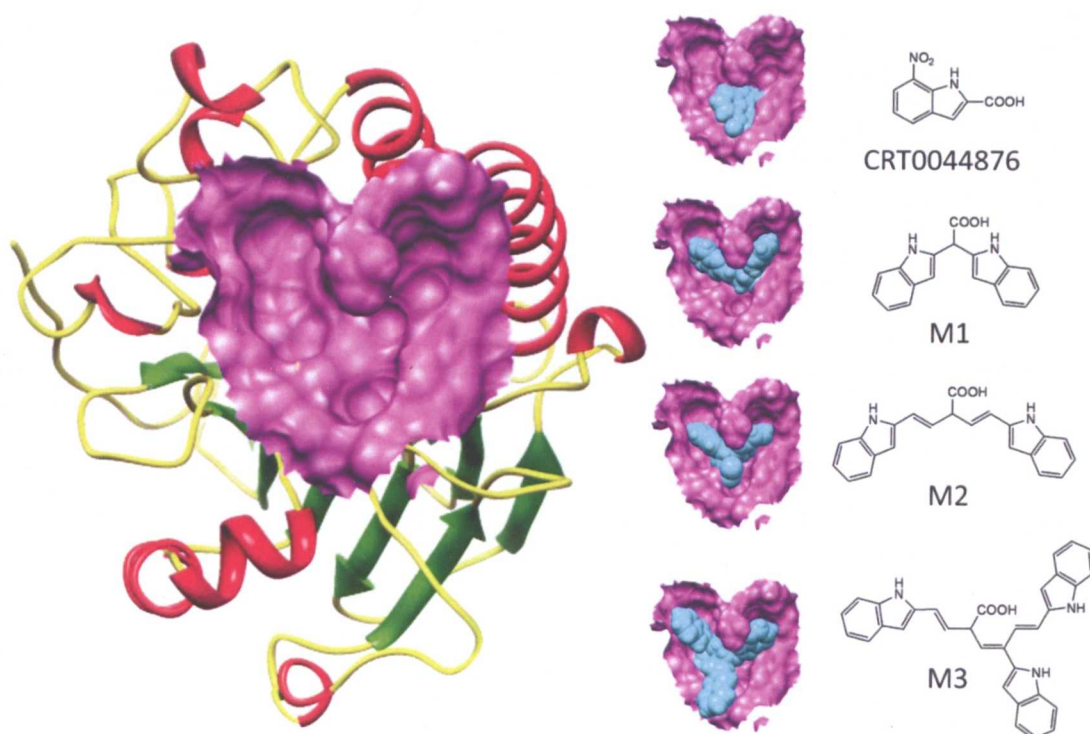


**Figure 3.3 Molecular modelling.** 3D simulation of the crystal structure of APE1 protein. The APE1 inhibitor, CRT0044876, represented by the white 3D block docks either onto the left side of the active site cleft (A) or onto right side of the active site cleft (B). The empty cleft in both configurations is indicated by the white arrow.



**Figure 3.4 Molecular modelling.** SYBY8.0 generated 3D shape of CRT0044876 together with three designed pharmacophore templates. M1, M2, and M3 were three prototypical scaffolds built using SYBYL8.0. They have indole carboxylic acid as the primary building block and represent structures with shape complementarity to the active site of APE1. M1 and M2 template bears similar features and only differ in the length of heteroaromatic substituents extended to increase interaction with amino acids residues. M3 template was designed to bear an additional heteroaromatic side chain that can access a subsidiary cleft in the ligand-binding groove.





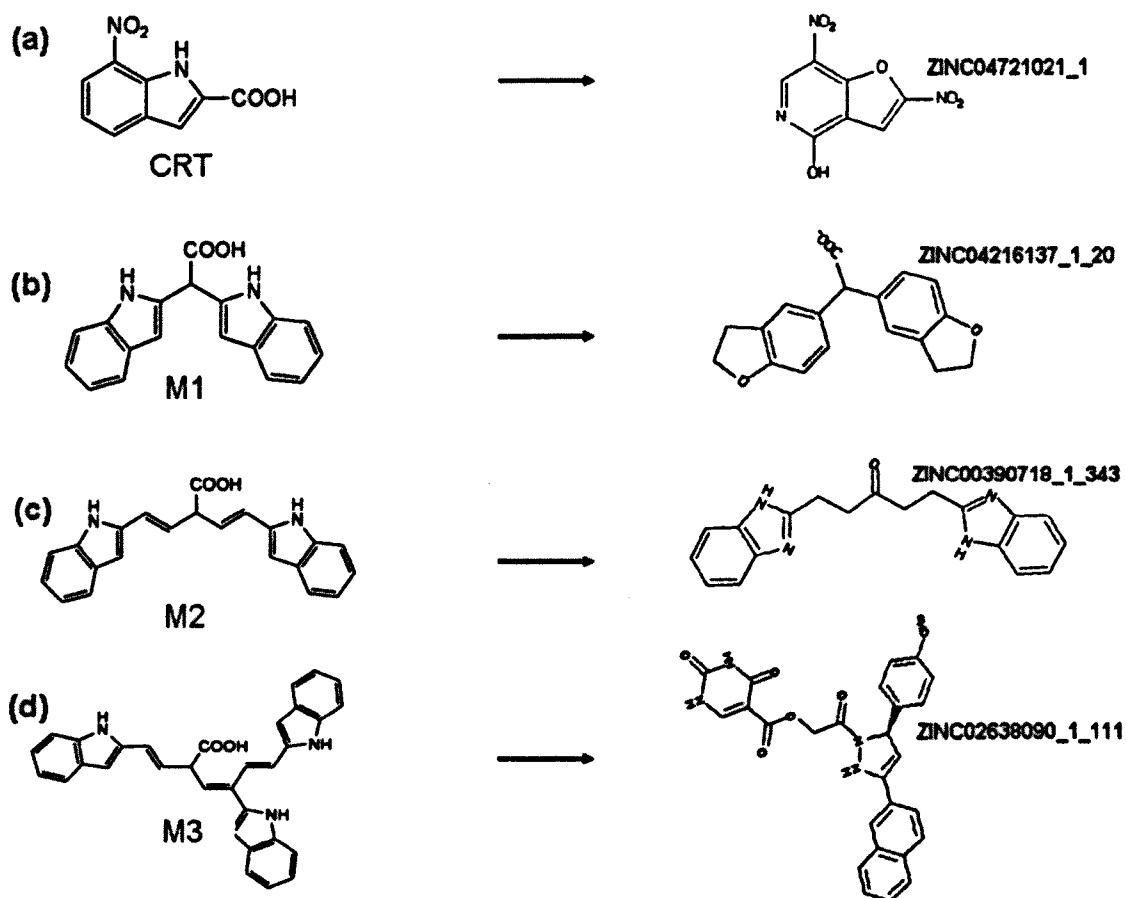
**Figure 3.5 Molecular modelling.** 3D simulation of the crystal structure of APE1 protein. (B) The 3D structure of APE1 repair domain in pink showing the deep binding pocket active site. (B). The designed molecules M1, M2 and M3 docked into hydrophobic active site. The two clefts of the active site are filled by the M1, M2 and M3 butterfly shaped templates, with the structure of each template aligned in parallel with its docked 3D block.

### 3.2.3. Pharmacophore guided similarity search analysis

M1, M2 and M3 templates were used to conduct a virtual similarity search of the ZINC 2008 database (<http://zinc.docking.org/>). The ZINC 2008 database is a library of 2549387 commercially available drug-like chemical structures. This database was downloaded and saved in 3D file format. A rapid structure-based similarity search using ROCS2.3 (OpenEye Scientific) was performed in a computational costly process where the 3D pharmacophore models of M1, M2, M3 templates and the CRT0044876 templates were queried. The search was based on shape and chemical similarity. The programme was set to

retrieve the best 500 hits that match the templates shape and chemistry and set a cut-off point for shape similarity (which is represented by the Tanimoto score described previously) as follows; 0.75 for CRT00876, M1 and M2 and 0.6 for M3. Setting a cut-off value for shape similarity was important to direct ROCS2.3 to focus on the shape similarity search and to a lesser extent chemical similarity (represented by Color Scale). Therefore, the search was directed to mine the ZINC database for chemical compound similar in shape to the templates. This results in structural hits that have chemical similarity to the templates. This was important to ensure that hits will maintain shape complementarity to APE1 active site clefts. The hits in each template were scored according to their shape similarity (Tanimoto Score) and chemical similarity (Color Scale). The summation of the two scores called ComboScore was used to rank these hits [range from most similar to least similar]. The data is presented in tables 3.1, 3.2, 3.3 and 3.4 and in Figure 3.6.

CRT0044876 template retrieved 359 hits M1, M2 and M3 templates retrieved 373, 459 and 488 hits respectively (tables 3.1, 3.2, 3.3 and 3.4). A total number of 1679 hits were identified (0.066% of the total of Zinc database) and is a highly selective collection of potential pharmacophores. The conformations of these 1679 compounds were then subjected to further virtual screening by docking against the active site of the APE1 model as described below.



**Figure 3.6** The chemical structure of the templates used for ROCS2.3 similarity search analyses are shown here. The left panel shows the templates CRT (CRT0044976), M1, M2 and M3 respectively. The right panel side shows the top hits obtained from the ZINC data base for each corresponding template. The strong shape and chemical similarity is evident from comparing the two corresponding structures.

### 3.2.4. Virtual docking studies of potential APE1 inhibitor hits

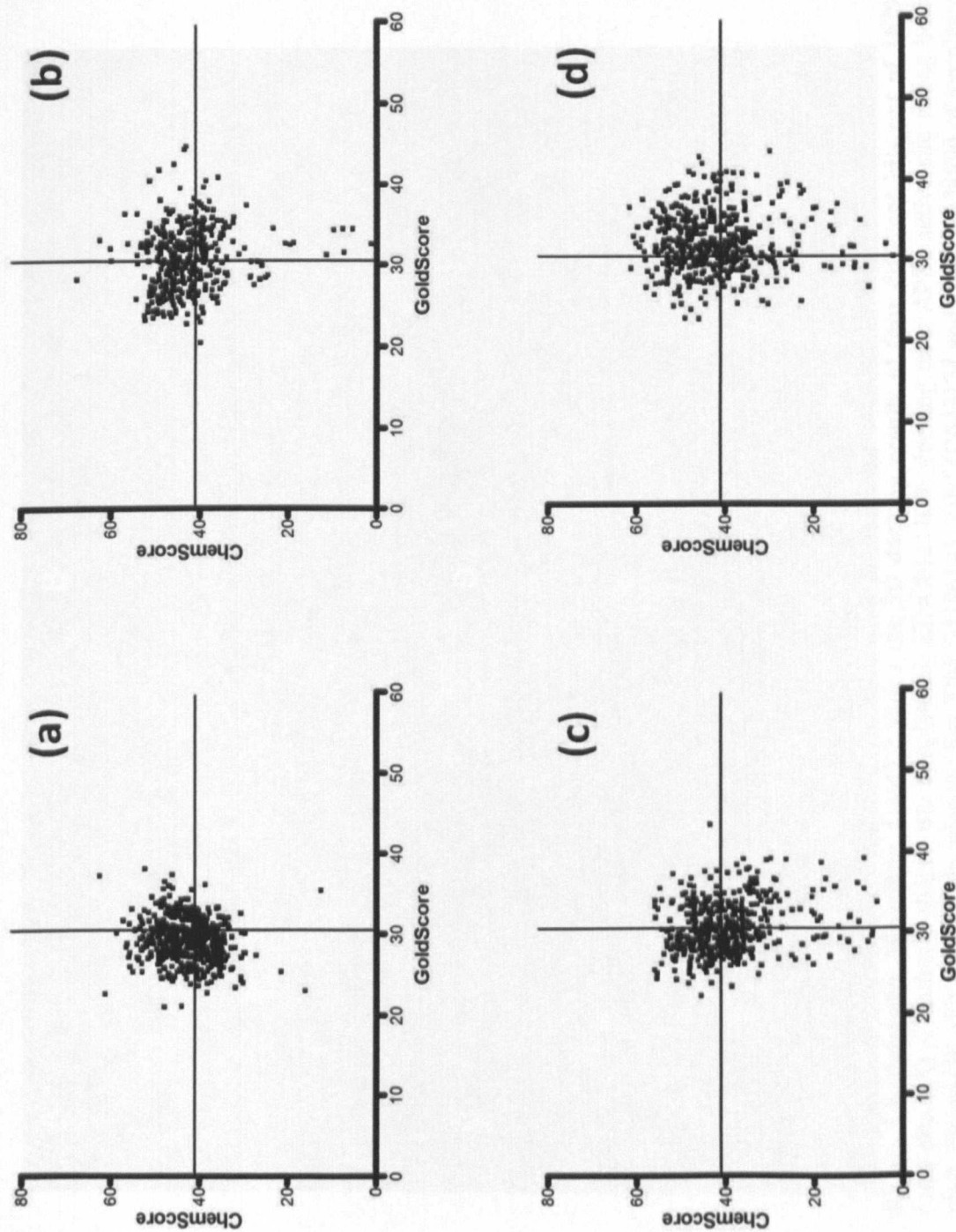
To validate the binding affinity of 1679 potential hits a computationally costly process of virtual docking using GOLD2.7 programme was performed [263]. A 3D pharmacophore file format was used to conduct docking and the programme was set to perform 100 runs per hit. Assessment of the binding affinity of hits onto the active site of APE1 was made by using ChemScore and GoldScore functions described previously. The programme was set to keep the top score out of 100 runs per each scoring function. The top score was taken as

the best binding affinity for a given hit. Plotting the results of GoldScore against ChemScore for each template hits showed a significant similarity in the scoring patterns as demonstrated in figure 3.7.

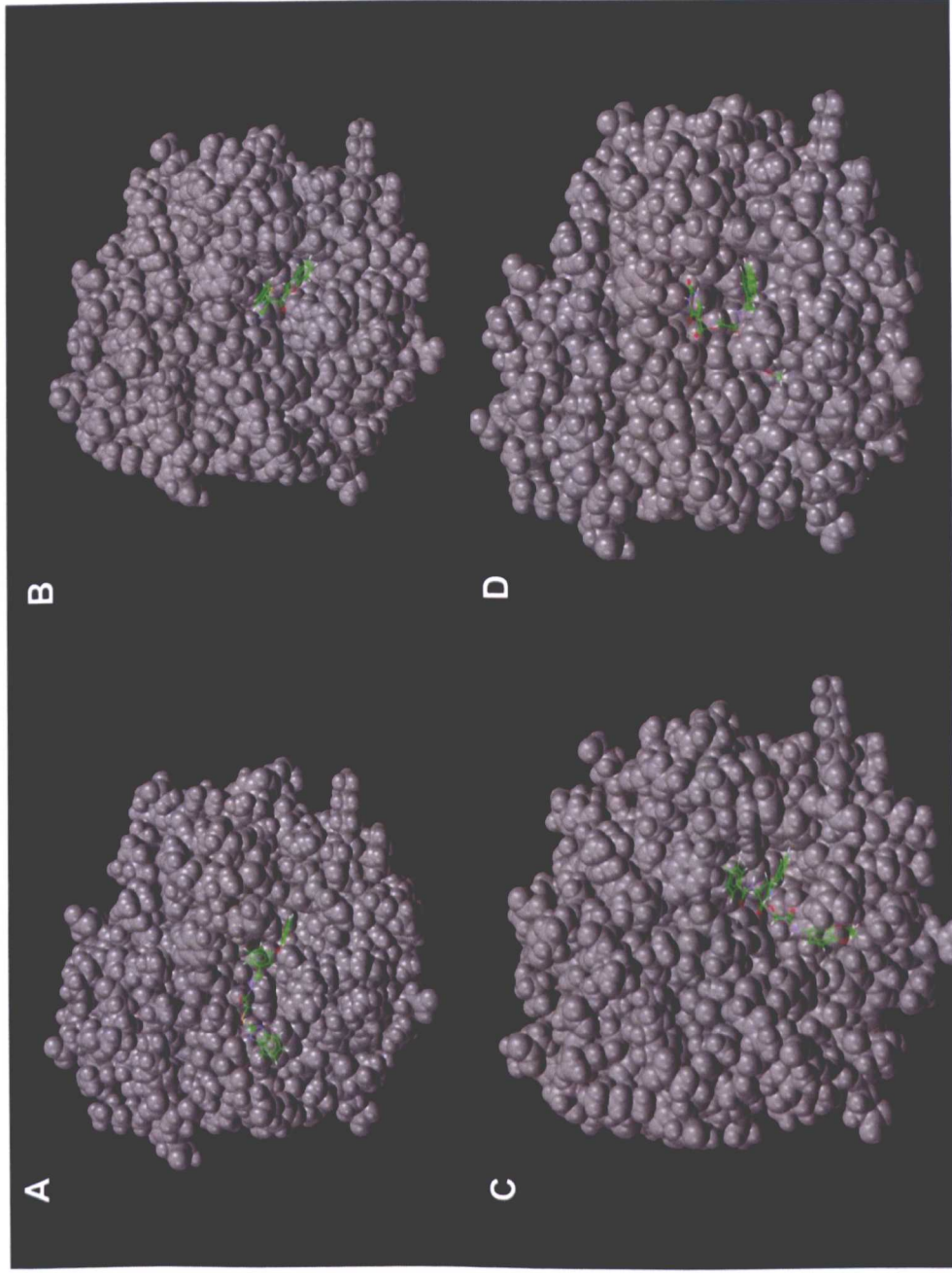
The scores were then imported into Microsoft Excel and results were as shown in table 3.5. A consensus score was generated by taking the sum of the ChemScore and GoldScore. The hits with the best consensus score were predicted to be potentially promising biochemical inhibitors of APE1 (Figure 3.8).

Therefore we chose top 25% of hits from the consensus plot for future biochemical analysis. A collection of 420 hits were shortlisted and examined by Professor Peter Fischer, Professor of Medicinal Chemistry, School of Pharmacy, University of Nottingham. 250 (of the 420 hits) with drug-like chemical characteristics were selected for biochemical analysis described in the next chapter.





**Figure 3.7** A diagram showing plotting of GoldScore against the ChemoScore of the four template hits: Graphs were divided into four quadrants. The right upper quadrant represent hits with high Goldscore and ChemoScore. (a) CRT template, (b) M1 template, (c) M2 template and (d) M3 template hits.



**Figure 3.8 Molecular Modelling, Gold2.7 shows the 3D docking results of four different hits out of 1679 total hits. (A) A butterfly shaped M2 template hit ZINC01211006 docking onto APE1 active site filling both cleft. Figure (B), (C), and (D) showing the hits ZINC03196143, ZINC02649134 and ZINC02638090 of templates M1, M3 and M3 respectively docking onto APE1 active site cleft.**

**Table 3.1** ROCS similarity search results for CRT0044876 template hits. 359 hits were retrieved and ranked by their shape similarity score (Tanimoto score). Color Scale indicates chemical similarity. Combination of shape and chemical similarity scores is termed Comboscore. The table shows the top and the last 10 hits.

Ligand Name	Shape Query	Rank	Shape Tanimoto	Color Scale	ComboScore
ZINC00156165_1	CRT0044876	1	0.996	0.858	1.854
ZINC04721021_1	CRT0044876	2	0.974	0.87	1.843
ZINC04228179_1	CRT0044876	3	0.959	0.864	1.823
ZINC00066138_1	CRT0044876	4	0.97	0.795	1.765
ZINC02537107_1_1	CRT0044876	5	0.888	0.866	1.754
ZINC02506905_1	CRT0044876	6	0.946	0.795	1.741
ZINC00156176_1_5	CRT0044876	7	0.945	0.795	1.74
ZINC02532865_1	CRT0044876	8	0.945	0.795	1.74
ZINC00191086_1	CRT0044876	9	0.935	0.796	1.731
ZINC00503439_1	CRT0044876	10	0.928	0.799	1.726
.....	.....	.....	.....	.....	.....
ZINC00091306_1_1	CRT0044876	350	0.855	0.666	1.521
ZINC01386944_1	CRT0044876	351	0.914	0.608	1.521
ZINC00281814_1_81	CRT0044876	352	0.791	0.73	1.521
ZINC02582696_1	CRT0044876	353	0.901	0.62	1.521
ZINC02454565_1	CRT0044876	354	0.9	0.621	1.521
ZINC02537081_1	CRT0044876	355	0.775	0.746	1.521
ZINC01677069_1_1	CRT0044876	356	0.866	0.655	1.52
ZINC03123543_1_0	CRT0044876	357	0.932	0.588	1.52
ZINC04128051_1	CRT0044876	358	0.926	0.595	1.52
ZINC04218937_1_4	CRT0044876	359	0.88	0.64	1.52

**Table 3.2** ROCS similarity search results for M1 template hits. 373 hits were retrieved and ranked by their shape similarity score (Tanimoto score). The table shows the top and the last 10 hits

Ligand Name	Shape Query	Rank	Shape Tanimoto	Color Scale	ComboScore
ZINC03214778_1_8	M1	1	0.866	0.703	1.569
ZINC04216137_1_20	M1	2	0.92	0.648	1.568
ZINC00035513_1_66	M1	3	0.861	0.688	1.549
ZINC00189065_1_3	M1	4	0.832	0.744	1.576
ZINC04118500_1_36	M1	5	0.864	0.71	1.575
ZINC00189078_1_23	M1	6	0.843	0.727	1.569
ZINC06751147_1_32	M1	7	0.906	0.656	1.562
ZINC03299013_1_27	M1	8	0.868	0.692	1.56
ZINC04228062_1_37	M1	9	0.858	0.693	1.551
ZINC02461387_1_12	M1	10	0.864	0.639	1.503
.....	.....	.....	.....	.....	.....
ZINC02367226_1_18	M1	364	0.869	0.487	1.356
ZINC02641767_1_19	M1	365	0.852	0.503	1.356
ZINC04197488_1_15	M1	366	0.798	0.558	1.356
ZINC04801896_1_75	M1	367	0.828	0.527	1.356
ZINC06590518_1_63	M1	368	0.76	0.596	1.356
ZINC02206972_1_4	M1	369	0.837	0.518	1.355
ZINC02310517_1_72	M1	370	0.788	0.567	1.355
ZINC05175229_1_11	M1	371	0.778	0.577	1.355
ZINC00151167_1_19	M1	372	0.846	0.509	1.355
ZINC00122728_1_88	M1	373	0.761	0.594	1.355

**Table 3.3** ROCS similarity search results for M2 template hits. 459 hits were retrieved and ranked by their shape similarity score (Tanimoto score). The table shows the top and the last 10 hits

Ligand Name	Shape Query	Rank	Shape Tanimoto	Color Scale	ComboScore
ZINC00390718_1_343	M2	1	0.93	0.69	1.62
ZINC00638464_1_36	M2	2	0.887	0.731	1.617
ZINC03313631_1_307	M2	3	0.9	0.691	1.591
ZINC00189065_1_3	M2	4	0.832	0.744	1.576
ZINC04118500_1_367	M2	5	0.864	0.71	1.575
ZINC00189078_1_23	M2	6	0.843	0.727	1.569
ZINC06751147_1_32	M2	7	0.906	0.656	1.562
ZINC03299013_1_279	M2	8	0.868	0.692	1.56
ZINC04228062_1_376	M2	9	0.858	0.693	1.551
ZINC02461387_1_127	M2	10	0.864	0.639	1.503
.....	...	.....	.....	.....	.....
ZINC03501112_1_34	M2	451	0.8	0.537	1.338
ZINC06657644_1_99	M2	452	0.802	0.535	1.337
ZINC05253459_1_361	M2	453	0.817	0.52	1.337
ZINC04103196_1_332	M2	454	0.788	0.549	1.337
ZINC00902601_1_64	M2	455	0.811	0.526	1.337
ZINC05171030_1_39	M2	456	0.757	0.58	1.337
ZINC02596979_1_164	M2	457	0.8	0.537	1.337
ZINC04018001_1_314	M2	458	0.857	0.48	1.337
ZINC01059333_1_83	M2	459	0.809	0.528	1.337

**Table 3.4** ROCS similarity search results for M3 template hits. 488 hits were retrieved and ranked by their shape similarity score (Tanimoto score). The table shows the top and the last 10 hits

Ligand Name	Shape Query	Rank	Shape Tanimoto	Color Scale	ComboScore
ZINC04939776_1_302	M3	1	0.632	0.415	1.047
ZINC01667467_1_54	M3	2	0.6	0.444	1.045
ZINC01102617_1_368	M3	3	0.614	0.42	1.035
ZINC04144071_1_16	M3	4	0.606	0.414	1.019
ZINC04314951_1_167	M3	5	0.613	0.402	1.015
ZINC02821288_1_236	M3	6	0.626	0.378	1.004
ZINC06316005_1_304	M3	7	0.607	0.396	1.003
ZINC06657717_1_343	M3	8	0.62	0.376	0.996
ZINC02649158_1_201	M3	9	0.726	0.265	0.991
ZINC02638090_1_111	M3	10	0.673	0.315	0.989
.....	...	...	.....	.....	.....
ZINC01454922_1_371	M3	480	0.646	0.244	0.89
ZINC03484557_1_16	M3	481	0.601	0.289	0.89
ZINC04583876_1_12	M3	482	0.614	0.276	0.89
ZINC01022216_1_265	M3	483	0.605	0.285	0.89
ZINC04678280_1_108	M3	484	0.602	0.288	0.89
ZINC01333367_1_290	M3	485	0.618	0.272	0.89
ZINC03332146_1_386	M3	486	0.607	0.283	0.89
ZINC03428897_1_25	M3	487	0.646	0.244	0.89
ZINC04777243_1_281	M3	488	0.601	0.288	0.89

**Table 3.5** Gold docking results of 1679 hits onto APE1 active site cleft. GoldScore and ChemScore were used to measure the binding affinities. The Summation of the two scores was termed Consensus score. The table shows the top 40 and the last 10 hits.

Rank	Ligand	GoldScore	ChemScore	Consensus Score
1	'ZINC05225031 1'	62.43	37.23	99.66
2	'ZINC01215578 1 393'	61.55	36.57	98.12
3	'ZINC00780173 1 152'	58.55	37.52	96.07
4	'ZINC01229958 1 12'	67.63	28.25	95.88
5	'ZINC05628180 1 62'	59.62	34.12	93.74
6	'ZINC02073144 1 48'	60.59	32.98	93.57
7	'ZINC03196143 1 44'	56.87	36.41	93.28
8	'ZINC03356675 1 186'	56.29	36.06	92.35
9	'ZINC06740382 1 23'	60.09	32.11	92.2
10	'ZINC06141145 1 329'	57.82	34.34	92.16
11	'ZINC06150767 1 313'	59.99	32.14	92.13
12	'ZINC05216611 1 245'	53.33	38.6	91.93
13	'ZINC01357069 1 309'	54.85	37.01	91.86
14	'ZINC05234891 1 140'	51.33	40.5	91.83
15	'ZINC04195895 1 341'	57.43	34.13	91.56
16	'ZINC02030125 1 267'	56.86	34.55	91.41
17	'ZINC00904848 1 220'	52.57	38.82	91.39
18	'ZINC06061053 1 168'	58.66	32.56	91.22
19	'ZINC04492943 1 172'	55.64	35.44	91.08
20	'ZINC05938287 1 354'	54.2	36.85	91.05
21	'ZINC02641767 1 19'	49.2	41.83	91.03
22	'ZINC02721718 1 340'	59.27	31.69	90.96
23	'ZINC01032476 1 33'	54.2	36.4	90.6
24	'ZINC00929241 1 192'	51.21	39.36	90.57
25	'ZINC04023605 1 16'	59.87	30.55	90.42
26	'ZINC02492440 1'	52.19	38.07	90.26
27	'ZINC01102617 1 368'	61.21	29	90.21
28	'ZINC02624389 1 237'	0.07	34.98	35.05
29	'ZINC00938318 1 248'	7.6	26.73	34.33
30	'ZINC05062899 1 328'	1.25	32.63	33.88
31	'ZINC03404599 1 395'	2.03	30.47	32.5
32	'ZINC04118499 1 358'	-5.99	34.82	28.83
33	'ZINC04872743 1 79'	-11.72	28.54	16.82
34	'ZINC00236768 1 149'	-18.12	32.7	14.58
35	'ZINC00236781 1 148'	-23.38	35.92	12.54
36	'ZINC06701391 1 388'	-18.36	29.9	11.54
37	'ZINC02254324 1 75'	-26.62	35.31	8.69
38	'ZINC04672982 1 328'	-26.97	31	4.03
39	'ZINC03269861 1 137'	-24.42	27.58	3.16
40	'ZINC03269866 1 194'	-22.37	25.29	2.92
.....	.....	.....	.....	.....
1673	'ZINC04118554 1 344'	-43.34	31.28	-12.06
1674	'ZINC04118498 1 98'	-50.49	34.73	-15.76
1675	'ZINC03251742 1 304'	-48	30.91	-17.09
1676	'ZINC00843594 1 139'	-53.89	28.08	-25.81
1677	'ZINC03889391 1 44'	-65.01	35.59	-29.42
1678	'ZINC00843580 1 69'	-58.84	26.14	-32.7
1679	'ZINC00841532 1 25'	-89.19	32.92	-56.27

### 3.3 Discussion and conclusion

The process of identification and development of a novel drug is complex. The high cost of research and human clinical trials made the drug discovery process potentially expensive. To minimize cost and to accelerate drug discovery, the current approach in modern drug discovery is to initiate investigation using virtual screening strategies based on computationally simulated ligand-protein interactions. The aim of this screening is to evaluate orientation of the ligands relative to the protein. In addition, virtual screening aims to achieve a scoring function that measure how strongly a given ligand will interact with the target protein. Moreover, virtual screening allows screening of a large chemical library, even chemicals that have not yet been synthesised. Therefore virtual screening reduces the initial number of compounds that will undergo primary biochemical screening and subsequently reducing the total cost of the drug discovery process.

Almost all the APE1 inhibitors identified to date were isolated by direct screening of chemical libraries that includes several thousands of chemical compounds [253]. However, none of the inhibitors described to date showed pharmacological properties optimal for therapeutic application [253]. A recent study by Zawahir et al. utilized a virtual strategy to design a set of pharmacological models based on the unique interaction between APE1 active site with the abasic DNA. These templates used for identification of APE1 inhibitors from a 365000 chemical library. However the biological efficiency of these inhibitors was not fully evaluated [254].



In the current PhD project, an industry standard virtual screening approach was adopted to develop novel drug-like chemotypes. The architecture of the active site of APE1 in the absence and presence of bound abasic DNA indicates that there is little or no remodelling of the active site upon substrate binding, a feature that is suitable for a virtual screen [103, 104]. The structural feature of APE1 was exploited to develop an enhanced virtual screening strategy and I identified several novel small molecule inhibitors for further drug development. Three new pharmacophore templates were designed *in silico* (M1, M2 and M3) and a total of 1679 virtual hits with similarities to the templates were identified (CRT template = 359, M1 template = 373, M2 template = 459 and M3 template = 488). These hits were designed to achieve maximum geometrical and chemical complementarity to APE1 active site. The structures of these hits show that they have relatively small size and comprise an aromatic hydrophobic core. In addition, they tend to have a negative ionisable group mostly carboxylate similar to CRT0044876. The top 25% hits, i.e., a collection of 420 compounds were shortlisted based on their APE1 binding affinity. 250 chemical were then selected based on structural and pharmacological features for biochemical analysis described in the next chapter.

## ***Chapter 4***

### ***Biochemical screening***

---

## 4. Biochemical screening

### 4.1. Introduction

Modulation of base excision repair (BER) has the potential to enhance the cytotoxicity of several DNA damaging agents used in cancer therapy. APE1 is a key protein in BER. Several biochemical, preclinical and clinical studies have confirmed that APE1 is an attractive target for anti-cancer drug development.

In chapter 3, I described the virtual screening approach to isolate potential APE1 inhibitors. Using molecular modelling softwares three templates M1, M2, and M3 were designed. These templates and the CRT0044876 template were used to search a large chemical library. This approach made it possible to screen a large drug-like chemical library. Although virtual screening reduces costs and enhances the efficiency of drug discovery process, biochemical screening is an essential step to directly evaluate the ability of the ligand to alter protein function *in vitro*. This primary screening could identify genuine APE1 inhibitors. Therefore, compounds selected from virtual screening were tested in a series of biochemical assay. The main aim was to identify specific and potent APE1 inhibitors.

420 compounds identified from virtual screening were initially shortlisted. These chemicals were then examined by Professor Peter Fischer, Professor of Medicinal Chemistry, School of Pharmacy, University of Nottingham. 250 compounds were selected for the biochemical screening. The compounds were selected based on structural novelty and drug-like properties. 147 out of 250 selected were commercially available and therefore underwent

detailed analysis. A list of compounds analysed in this study is shown in table

4.1.

**Table 4.1** List of chemical library compounds used for Fluorescence based AP-site cleavage assay.

ZINC database 2008 Code	Vendor	Supplier code	Lab Code	Template
ZINC00040219	ChemBridge	5140421	P1	CRT
ZINC00177196	ChemBridge	5926401	P2	CRT
ZINC00193042	ChemBridge	5210777	P3	CRT
ZINC01211006	ChemBridge	5771747	P4	M3
ZINC01821694	ChemBridge	6623906	P5	CRT
ZINC02537038	ChemBridge	8929409	P6	CRT
ZINC02580950	AstaTech	59587	P7	CRT
ZINC03001624	ChemBridge	5253606	P8	CRT
ZINC04362893	ChemBridge	9031355	P9	CRT
ZINC05003907	ChemBridge	5556647	P10	CRT
ZINC05049941	ChemBridge	7926856	P11	CRT
ZINC06702569	ChemBridge	9021992	P12	CRT
ZINC04128392	Sigma-Aldrich	556890	P13	CRT
ZINC04798293	Alfa-Aesar	43899	P14	CRT
ZINC01661333	Alfa-Aesar	B25627	P15	CRT
ZINC05225031	Alfa-Aesar	A18548	P16	CRT
ZINC04253599	Apollo Scientific	OR6746	P17	CRT
ZINC02168694	LOPAC1280	H8759	P18	CRT
ZINC03130439	Sigma-aldrich	S235997	P19	CRT
ZINC02156420	Sigma-aldrich	S688916	P20	CRT
ZINC0081085	Maybridge	RH00720	P21	CRT
ZINC0083028	Maybridge	RH01182	P22	CRT
ZINC01554037	alfa chemicals	A13445	P23	CRT
ZINC00156841	alfa chemicals	A11018	P24	CRT
ZINC00156671	alfa chemicals	B22645	P25	CRT
ZINC02027393	alfa chemicals	A10278	P26	CRT
ZINC06467621	alfa chemicals	B25307	P27	CRT
ZINC01753102	alfa chemicals	B21074	P28	CRT
ZINC00156343	alfa chemicals	L12750	P29	CRT
ZINC04977184	www.ukrorgsynth.com	PB-90178380	P30	M2
ZINC00127379	Enamine	T0513-9472	P31	CRT
ZINC03498135	Enamine	T5842095	P32	CRT
ZINC01641182	Enamine	T0501-9967	P33	CRT
ZINC03196143	Enamine	T5871233	P34	M1
ZINC00056465	Enamine	T5883874	P35	CRT
ZINC00193177	ChemBridge	5211687	P36	CRT
ZINC01077004	ChemBridge	7909184	P37	M3
ZINC00479857	ChemBridge	7822043	P38	CRT
ZINC01109314	ChemBridge	7726917	P39	M3
ZINC00206678	ChemBridge	7701580	P40	M1
ZINC00308590	ChemBridge	6435543	P41	M1
ZINC00275159	ChemBridge	5212613	P42	CRT
ZINC01218405	ChemBridge	6122609	P43	CRT
ZINC00345355	ChemBridge	6131881	P44	CRT
ZINC00168069	ChemBridge	6630522	P45	CRT
ZINC01215578	ChemBridge	6082170	P46	M3
ZINC01234763	ChemBridge	5107319	P47	CRT
ZINC01834823	ChemBridge	5624394	P48	CRT
ZINC02197289	ChemBridge	5269953	P49	CRT
ZINC00216961	ChemDiv	6228-0723	P50	CRT
ZINC01577022	Life Chemicals	F0378-0062	P51	CRT
ZINC02484656	ChemBridge	5119306	P52	CRT
ZINC01693409	ChemBridge	5252868	P53	CRT
ZINC01576969	ChemBridge	5252882	P54	CRT
ZINC01881604	ChemBridge	5550054	P55	CRT

ZINC01783481	ChemBridge	5631104	P56	CRT
ZINC02446376	ChemBridge	5816568	P57	CRT
ZINC02593383	ChemBridge	7743810	P58	CRT
ZINC02709237	ChemBridge	7987841	P59	M1
ZINC02012856	Specs	AP-770/42745275	P60	CRT
ZINC04289696	Specs	AG-690/12090344	P61	M2
ZINC00345371	Specs	AE-562/12222005	P62	CRT
ZINC00651236	Specs	AK-968/41171453	P63	M3
ZINC00345373	Specs	AE-562/12222011	P64	CRT
ZINC01102617	TimTec	ST051641	P65	M3
ZINC04482340	TimTec	ST4037676	P66	CRT
ZINC13658636	Maybridge	HTS09008	P67	M1
ZINC15924031	Maybridge	SPB07800	P68	M1
ZINC05003653	ChemBridge	5109356	P69	M2
ZINC04755154	ChemBridge	5122037	P70	CRT
ZINC04012812	ChemBridge	5153927	P71	CRT
ZINC08656548	ChemBridge	5474011	P72	M2
ZINC02903501	ChemBridge	5572732	P73	M3
ZINC05926194	ChemBridge	5574725	P74	CRT
ZINC01783481	ChemBridge	5631104	P75	CRT
ZINC04469351	ChemBridge	5479114	P76	CRT
ZINC05017790	ChemBridge	5670158	P77	M3
ZINC05730977	ChemBridge	6327080	P78	M1
ZINC04717421	ChemBridge	7932719	P79	CRT
ZINC06747323	ChemBridge	9068997	P80	CRT
ZINC02875831	ChemBridge	7955265	P81	M2
ZINC02732054	ChemBridge	8928371	P82	CRT
ZINC04294570	ChemBridge	8928374	P83	CRT
ZINC02732020	ChemBridge	8928490	P84	CRT
ZINC04163878	ChemBridge	8882832	P85	CRT
ZINC02661072	Enamine	T5252878	P86	M2
ZINC03263338	Enamine	T0510-5174	P87	M3
ZINC03434925	Enamine	T5330235	P88	M3
ZINC05415907	Enamine	T0510-5395	P89	M2
ZINC06787264	Enamine	T5373986	P90	M1
ZINC03257904	Enamine	T0511-5029	P91	M3
ZINC13147800	Enamine	T5415905	P92	M2
ZINC03277194	Enamine	T5210153	P93	M3
ZINC04061877	Enamine	T5434491	P94	M2
ZINC02649134	Enamine	T5227191	P95	M3
ZINC02638090	Enamine	T5234908	P96	M3
ZINC09367024	Enamine	T5717818	P97	M2
ZINC01357069	Asinex	ASN05673042	P98	M3
ZINC00780173	Asinex	BAS04209407	P99	M3
ZINC00929241	Asinex	ASN03270465	P100	M3
ZINC00904848	Asinex	ASN03988707	P101	M3
ZINC02073144	Asinex	BAS01516436	P102	M3
ZINC04195895	Asinex	BAS00675915	P103	M3
ZINC02030125	Asinex	BAS01279511	P104	M3
ZINC01405478	KeyOrganics	12N-326S	P105	M2
ZINC04025249	KeyOrganics	JS-1302	P106	M2
ZINC00919531	Asinex	ASN04196885	P107	M3
ZINC04061877	Asinex	BAS07396170	P108	M2
ZINC00189065	ChemBridge	5147377	P109	M1
ZINC00035512	ChemBridge	5219225	P110	M1
ZINC01029672	ChemBridge	5618929	P111	M2
ZINC03877685	ChemBridge	5694123	P112	M2
ZINC00102630	ChemBridge	5848776	P113	M1
ZINC04653992	ChemBridge	8884964	P114	M1
ZINC02925395	ChemDiv	K292-1334	P115	M3
ZINC02975647	ChemDiv	K284-5645	P116	M3
ZINC02721681	ChemDiv	C176-0119	P117	M3
ZINC02721656	ChemDiv	C176-0087	P118	M3
ZINC04061877	ChemDiv	7287-0980	P119	M2
ZINC00517811	ChemDiv	7602-0979	P120	M1
ZINC03655023	ChemDiv	C071-0291	P121	M3
ZINC06150773	UkrOrgSynthesis	PB20177232	P122	M3

ZINC06428067	UkrOrgSynthesis	PB-04511045	P123	M2
ZINC01354011	UkrOrgSynthesis	PB228048608	P124	M3
ZINC08685966	UkrOrgSynthesis	PB-90362471	P125	M2
ZINC02322284	UkrOrgSynthesis	PB-90122293	P126	M3
ZINC06428375	Enamine-REAL	ZT-5787893	P127	M2
ZINC05781327	Enamine-REAL	ZU-8667769	P128	M2
ZINC05754351	Enamine-REAL	ZU-8116949	P129	M3
ZINC03239779	Enamine-REAL	ZT-0067825	P130	M3
ZINC03240290	Enamine-REAL	ZT-0144444	P131	M3
ZINC04959904	Enamine-REAL	ZS1136441	P132	M3
ZINC06428148	Enamine-REAL	ZU-8256558	P133	M2
ZINC00622770	Life Chemicals	F0790-0053	P134	M3
ZINC02721656	Life Chemicals	F0586-0116	P135	M3
ZINC02721681	Life Chemicals	F0586-0162	P136	M3
ZINC04248413	Life Chemicals	F1837-0024	P137	M3
ZINC04583861	Life Chemicals	F2617-0316	P138	M3
ZINC04583882	Life Chemicals	F2617-0616	P139	M3
ZINC04583893	Life Chemicals	F2617-0796	P140	M3
ZINC04583965	Life Chemicals	F2617-1636	P141	M3
ZINC04289694	Specs	AG-690/12090337	P142	M3
ZINC04180015	Specs	AK-918/12392039	P143	M3
ZINC04115900	Specs	AG-690/40721859	P144	M3
ZINC03877685	Specs	AG-690/12090297	P145	M3
ZINC00186360	ChemDiv	3253-0243	P146	M3
ZINC00186724	Asinex	BAS01808853	P147	M3

## 4.2 Fluorescence based APE1 AP-site cleavage assay

The fluorescence-based APE1 AP-site cleavage assay is based on the principle of ‘proximal quenching’ also known as ‘collisional quenching’. A 30 mer oligonucleotide (5' F-GCCCCCXGGGGACGTACGATATCCCGCTCC 3') was custom made to contain an abasic site analogue (tetrahydrofuran ring; ‘X’) at the seventh position and was 5' labelled with fluorescein (‘F’). This was annealed with its complementary 30 mer oligonucleotide that was 3' labelled with Dabcyl (‘Q’) (3' Q-CGGGGGCCCCCTGCATGCTATAGGGCGAGG 5'). In its native state, Dabcyl which is in close proximity to fluorescein quenches the fluorescence emitted by Fluorescein. However, in the presence of AP Endonuclease activity the oligonucleotide is cleaved 5' to the abasic site, and the 6 mer, fluorescein-containing single stranded oligonucleotide is free to

melt into solution at 37°C. As a result the quenching effect of the 3' Dabcyl molecule in the complementary strand is lost, and APE1 activity is measured as an increase in fluorescence signal (Figure 2.2). The absence of fluorescence emission in the assay containing a screening compound would indicate a potential APE1 inhibitor. This assay was optimised and adapted to a 384-well format. Hits identified from this primary screening were then taken to counter screening assays.

## **4.3 Counter screenings**

### **4.3.1 Fluorescence based endonuclease IV AP-site cleavage assay**

Hits isolated from the primary screening using APE1 enzyme were counter screened against endonuclease IV. Endonuclease IV is a  $\text{Zn}^{2+}$ -dependent AP endonuclease that has functional similarity to APE1, but has a structurally distinct active site although both enzymes share AP endonuclease, 3' phosphatase and 3' phosphodiesterase activities [108]. Therefore a specific inhibitor that blocks endonuclease activity of APE1 should not have any inhibitory activity against endonuclease IV. A fluorescent based endonuclease IV AP-site cleavage assay was developed. The assay was optimized and buffering conditions were as provided by the supplier of the endonuclease IV (TREVIGEN<sup>®</sup>).

### 4.3.2 Fluorescence quenching assay

Compounds were then investigated for the possibility that they might possess intrinsic quenching activity. This was developed to exclude false positive results. The oligonucleotides 5' F-GCCCCXGGGGACGTACGATATCCCGCTCC 3' and 3'CGGGGGCCCCCTGCATGCTATAGGGCGAGG-5' were annealed as described previously. The double stranded oligonucleotide (5 nM) was incubated with 100  $\mu$ M of potential APE1 inhibitor in a buffer consisting of 50  $\mu$ M Tris-HCl, pH 8.0, 1 mM MgCl<sub>2</sub>, 50 mM NaCl, and 2 mM DTT at 37 °C for 30 minutes. Fluorescence intensity was measured every 5 minutes. Compounds that caused more than 50% decrease in the fluorescence emission were considered as quenchers and excluded from further analyses.

### 4.4 Whole cell extract (WCE) AP-site cleavage assay

To further confirm AP-site cleavage inhibition *in vitro*, a whole cell extract based screening was conducted. This work was performed in collaboration with Dr David Wilson III, Laboratory of Molecular Gerontology, Biomedical Research Centre, National Institute on Ageing, NIH, Baltimore, USA.

In the WCE assay 100  $\mu$ M of a given inhibitor was incubated in the presence of 30 ng of HeLa WCE at room temperature for 15 minutes in an incision buffer containing 50 mM Tris-HCl pH 8.0, 1 mM MgCl<sub>2</sub>, 50 mM NaCl, and 2 mM DTT. After incubation, 0.5 pmol <sup>32</sup>P-radiolabeled THF-containing 18 mer double-stranded DNA substrate was added to the reaction mixture. The mixture



was then incubated for 5 minutes at 37 °C and the reaction was terminated by the addition of stop buffer (0.05% bromophenol blue and xylene cynol, 20 mM EDTA, 95% formamide) followed by denaturation of samples at 95 °C for 10 minutes. The radiolabelled substrate and product were separated on a standard polyacrylamide denaturing gel and quantified by phosphorimager analysis.

## **4.5 Results**

### **4.5.1 Development of Fluorescence based AP-site cleavage assay**

#### **4.5.1.1 Optimisation**

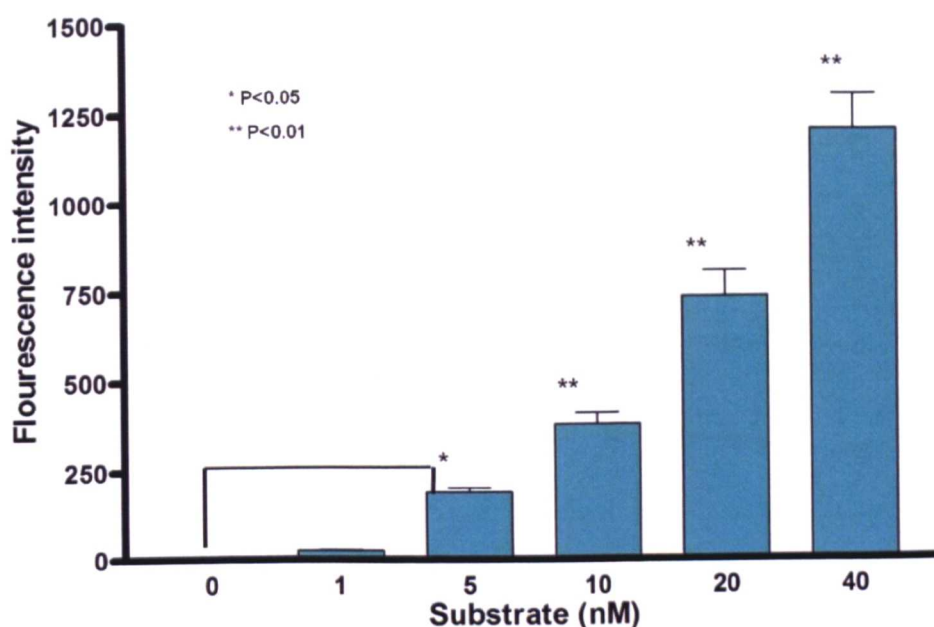
A valid screening assay needs to be optimised to generate robust data. Therefore several component of the assay had to be optimised prior to screening of compounds. These included:

- **Optimisation of concentration of oligonucleotide substrate:**  
Minimum concentration of oligonucleotide required for measurement of fluorescence emission signal was identified. In its native state the oligonucleotide DNA substrate emit fluorescence signal that can be detected by the multi- plate reader machine even in the presence of Dabcyl quenching. This signal is directly related to the amount of DNA substrate included in the assay. The minimum concentration of the DNA substrate that resulted in significant difference in fluorescence signal emission compared to the background signal was considered as the optimal concentration.

- **APE1 concentration:** Once the DNA substrate was optimised, the minimum concentration of APE1 (or) endonuclease IV required for efficient AP-site cleavage and fluorescence emission was estimated.
- **Incubation time:** The time needed to complete the assay was another variable that needed to be taken in consideration. The minimum incubation time that results in significant increase in fluorescence emission for a given concentrations of APE1 and DNA substrate was estimated.
- **Buffering condition:** The buffer used consists of 50 mM Tris-HCl (PH 8.0), 1 mM MgCl<sub>2</sub>, 50 mM NaCl and 2 mM dithiothreitol (DTT). As Mg<sup>2+</sup> is essential for AP-site cleavage activity, I used the pre-optimised Mg<sup>2+</sup> concentration for the assay [23].

#### 4.5.1.1.1 DNA substrate

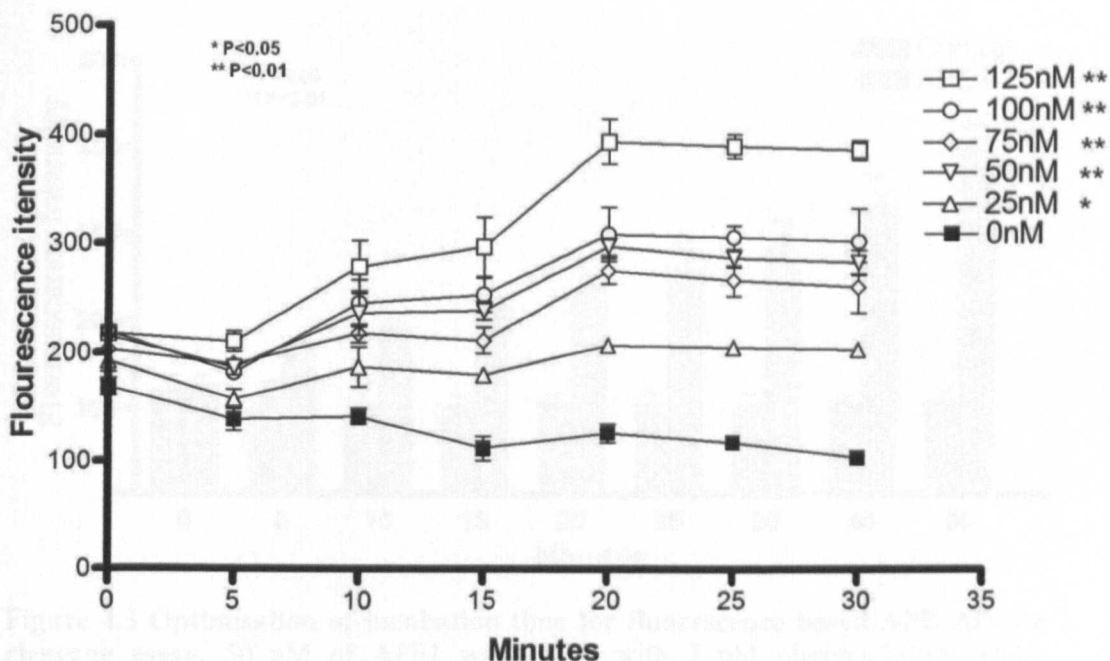
Serial dilution of the annealed double stranded DNA substrate stock solution was made. The fluorescence emission of reaction mixtures containing substrates at concentrations 1, 5, 10, 20 and 40 nM was performed (Figure 4.1). 5 nM was identified as the minimum substrate concentration that will give a significant fluorescence signal compared to background signal measurement (P <0.05).



**Figure 4. 1 Optimisation of oligonucleotide DNA substrate concentrations for AP-site cleavage assay.** A histogram showing fluorescence emission at different DNA substrate concentrations. 5 nM of DNA substrate was the lowest substrate concentration that gave a significant fluorescence signal compared to background signal. This concentration was therefore used in the subsequent assays. All experiments were performed in triplicates and the results represent the Mean  $\pm$  S.E.

#### 4.5.1.1.2 APE1 protein concentration

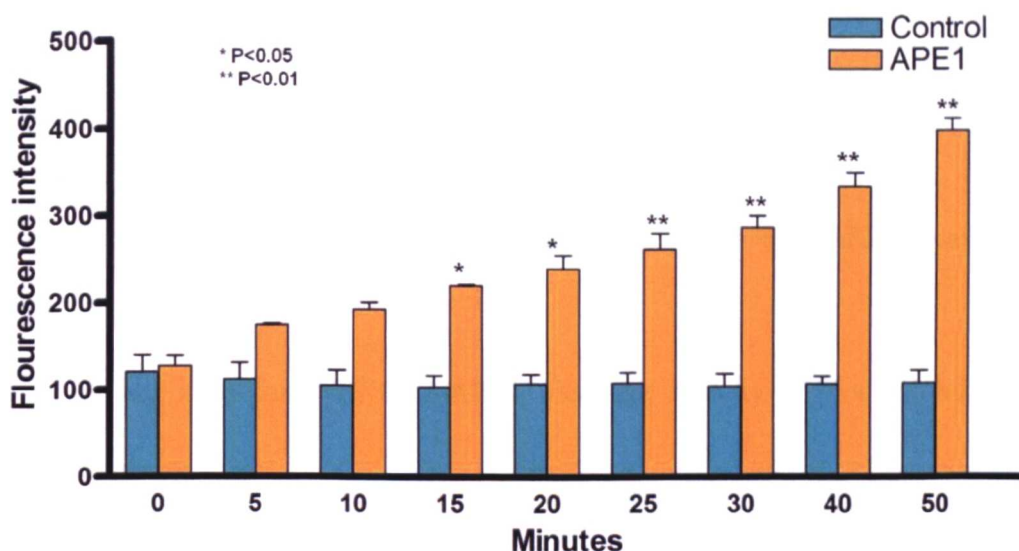
APE1 was quantified using NanoDrop 2000c spectrophotometer (Thermo Scientific). The stock protein concentration was 5  $\mu$ M. Serial dilutions of the protein stock was made and mixed with 5 nM of substrate to give a final concentration of 25, 50, 75, 100 and 125 nM of APE1 protein. Protein and substrates were incubated in the buffering condition mentioned above at 37  $^{\circ}$ C for a total time of 30 minutes. Serial measurement of the Fluorescence emission was detected every 5 minutes. A concentration of 50 nM was the minimum APE1 concentration required to produce a significant increase in fluorescence emission compared to negative control at 30 minutes ( $P < 0.01$ ) (Figure 4.2).



**Figure 4.2 Optimisation of APE1 concentration for fluorescence based APE1 AP-site cleavage assay.** Increasing amounts of APE1 was mixed with 5 nM oligonucleotide DNA substrate under buffering condition described in the Materials and Methods. A concentration dependent rise in fluorescence indicated AP-site cleavage activity by APE1. 50 nM of APE1 enzyme was able to give a highly significant increase in fluorescence signals after 30 minutes incubation with DNA substrate ( $P<0.01$ ). All experiments were performed in triplicates and the results represent the Mean  $\pm$  S.E.

#### 4.5.1.1.3 Incubation time

Although 30 minutes in previous studies seemed optimum, I tested further incubation time as follow: 5, 10, 15, 20, 25, 30, 35, 40, 45 and 50 minutes. As shown in figure 4.4 fluorescence emission at 30 minutes was judged to be acceptable although emission at 50 minutes was more compared to 30 minutes. As an efficient assay not only has to be robust but also has to be time efficient, I decided to run the assay with incubation time at 30 minutes (Figure 4.3).



**Figure 4.3 Optimisation of incubation time for fluorescence based APE AP-site cleavage assay.** 50 nM of APE1 was mixed with 5 nM oligonucleotide DNA substrates under buffering condition described in the Materials and Methods. Serial measurements of fluorescence intensity were taken every 5 minutes intervals for 50 minutes incubation time. 30 minutes incubation resulted in a highly significant ( $P<0.01$ ) increase in fluorescence signals compared to a negative control. All experiments were performed in triplicates and the results represent the Mean  $\pm$  S.E.

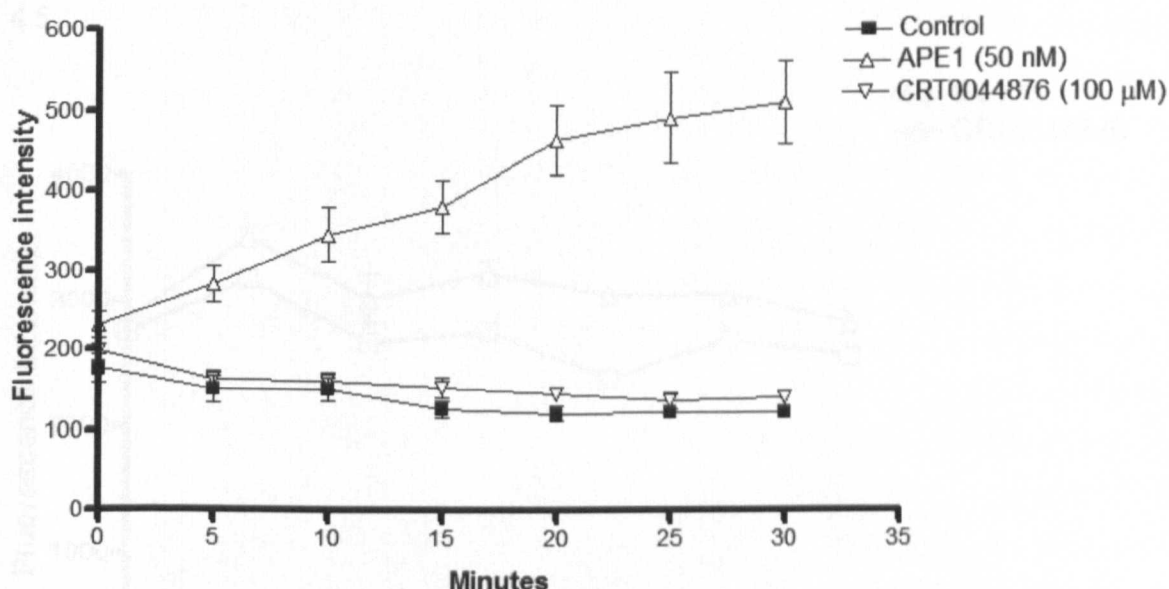
#### 4.5.1.1.4 Positive control

As a final validation of the AP-site cleavage assay 100  $\mu$ M CRT0044876, a specific APE1 inhibitor was used as positive control to confirm APE1 inhibition in the cleavage assay. Figure 4.4 shows a typical result for CRT0044876 (100  $\mu$ M). The percentage of APE1 inhibition was calculated as the percentage of net fluorescence signal measured in the presence of inhibitor relative to net fluorescence signal in absence of inhibitors. A complete inhibition of fluorescence emission confirms the inhibition of APE1 activity in the assay system.

Hits screened in the AP-site cleavage assay were classified according to the percentage inhibition of APE1 activity into five groups:

- Non inhibitor: were the APE1 retains 100% of its cleavage activity.

- Mild inhibitor: the inhibitor blocked <25% of APE1 cleavage activity.
- Moderate inhibitors: the inhibitor blocked 25-50% of APE1 cleavage activity.
- Strong inhibitor: the inhibitors blocked 50.1% - 75% of APE1 cleavage activity.
- Potent inhibitor: >75% of APE1 cleavage activity is blocked by the inhibitor.



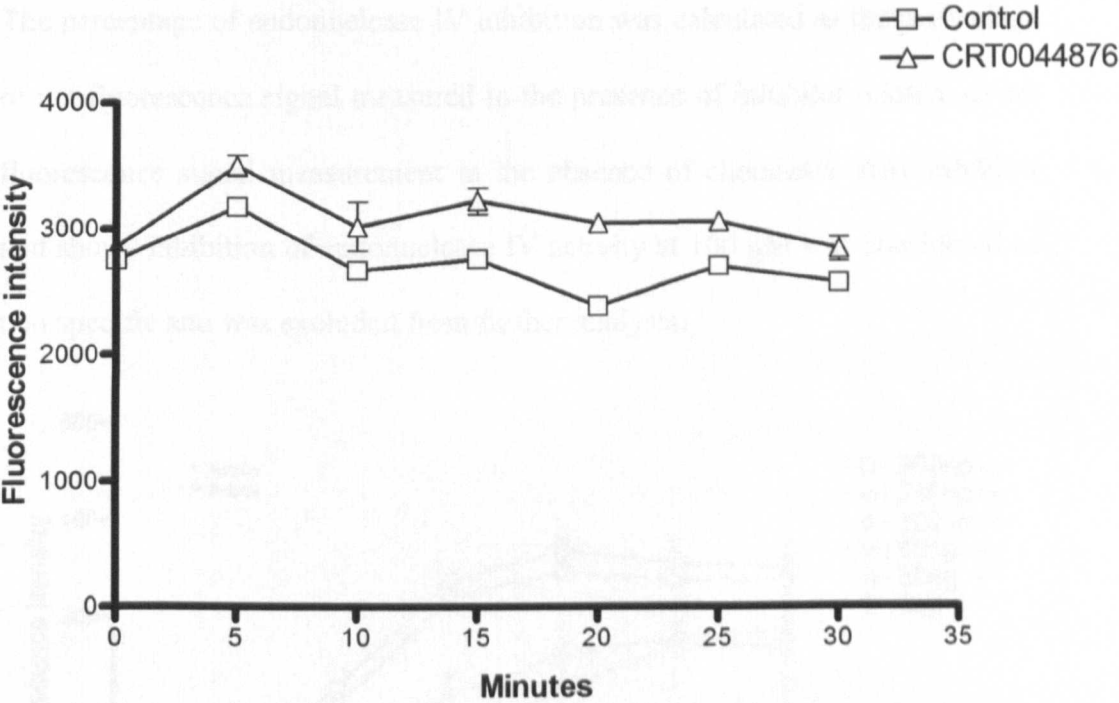
**Figure 4.4 Fluorescence based APE1 AP-site cleavage assay.** 100 μM of CRT0044876 was used as a positive control and incubated with 50 nM of APE1 and 5 nM DNA oligonucleotide substrate under the pre-optimised buffering condition. CRT0044876 demonstrates inhibition of APE1 activity in the fluorescence assay. All experiments were performed in triplicates and the results represent the Mean ± S.E.

#### 4.6.2 Optimization of fluorescence quenching assay (FQA)

To exclude the possibility that inhibitors may be quenchers of fluorescence emitted by the fluorescein tagged oligonucleotide substrate, a fluorescence quenching assay was developed. In this assay the 5' F-GCCCCXGGGGACGTACGATATCCCGCTCC 3' and



3'CGGGGGCCCCCTGCATGCTATAGGGCGAGG-5' were annealed to generate the substrate. 5 nM of this DNA substrate was incubated with 100  $\mu$ M of potential inhibitor under similar buffering conditions as the AP-site cleavage assay. Serial measurements of fluorescence intensity were taken every 5 minutes intervals for a total of 30 minutes. An inhibitor was considered as a quencher if it caused a decrease in Fluorescence intensity by >50%. CRT0044876 was used to validate this assay and the result is shown in figure 4.5

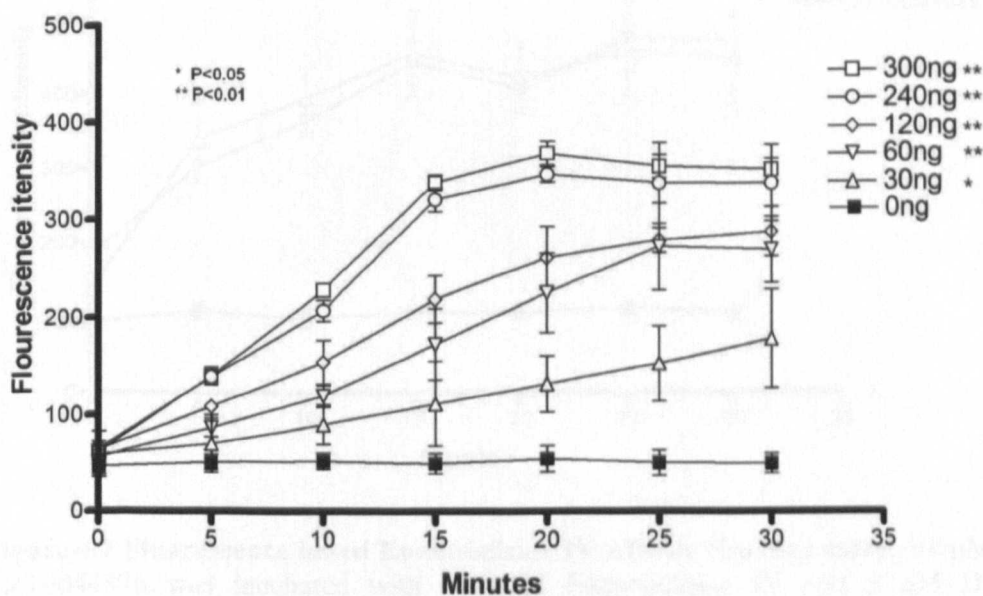


**Figure 4.5 Fluorescence quenching assay.** 100 $\mu$ M of CRT0044876 was incubated with 5 nM oligonucleotide DNA substrate for 30 minutes. CRT0044876 did not show any quenching effect on the substrate fluorescence signal. All experiments were performed in triplicates and the results represent the Mean  $\pm$  S.E.

### 4.6.3 Optimization of Endonuclease IV AP-site cleavage assay

Potential hits that blocks APE1 and are non-quenchers were then counter screened against endonuclease IV. The substrate concentration and inhibition time were set as before and the minimum concentration of endonuclease IV required was optimised. Endonuclease IV was purchased from Trivigen™ and its concentration was quantified using the NanoDrop 2000c spectrophotometer. The concentration of endonuclease IV was found to be 6 µg/ml. The buffer system was as supplied by the manufacturer and it consisted of 10 mM HEPES-KOH, pH 7.4, 100 mM KCl.

The percentage of endonuclease IV inhibition was calculated as the percentage of net fluorescence signal measured in the presence of inhibitor relative to net fluorescence signal measurement in the absence of chemicals. Any inhibitor that shows inhibition of endonuclease IV activity at 100 µM was considered as non specific and was excluded from further analysis.

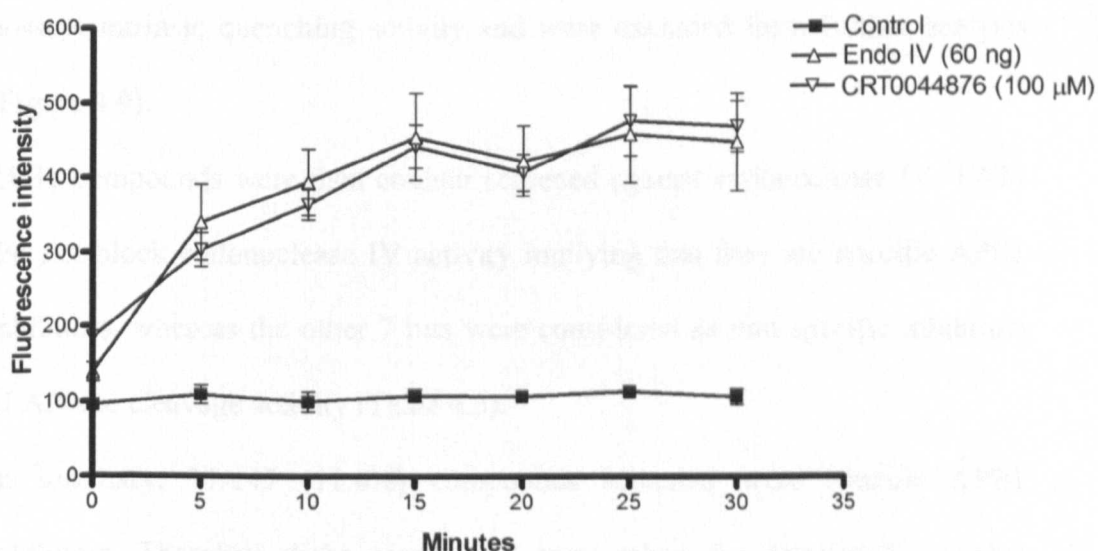


**Figure 4.6 Fluorescence based endonuclease IV AP-site cleavage assay.** Increasing concentrations of endonuclease IV were mixed with 5 nM oligonucleotide substrate under conditions described above. A concentration dependent rise in fluorescence indicated AP site cleavage activity was seen. 60ng of Endonuclease IV resulted in a highly significant increase in fluorescence signal compared to negative control ( $P<0.01$ ). This concentration was used in the subsequent counter screening of chemical library. All experiments were performed in triplicates and the results represent the Mean  $\pm$  S.E.



Different concentrations of endonuclease IV were used to run AP-site cleavage assay (Figure 4.6). It was evident that at 60 ng, endonuclease IV activity resulted in a significant increase in fluorescence emission compared to negative control ( $P < 0.01$ ).

A typical counter screening was set as follow: 100  $\mu$ M of the potential inhibitor was incubated with 60 ng of endonuclease IV and 5 nM of DNA substrate in a buffering condition consisting of 10 mM HEPES-KOH, pH 7.4, 100 mM KCl at 37 °C for 30 minutes. Serial measurements of fluorescence emission were taken every 5 minutes for a total of 30 minutes. Figure 4.7 shows a typical result for testing CRT0044876 tested at 100  $\mu$ M in the endonuclease IV AP-site cleavage assay. As CRT0044876 is a specific inhibitor of APE1, it does not block endonuclease IV activity.



**Figure 4.7 Fluorescence based Endonuclease IV AP-site cleavage assay.** 100 $\mu$ M of CRT0044876 was incubated with 60ng of Endonuclease IV and 5 nM DNA oligonucleotide substrate under the optimised buffering condition. CRT0044876 did not inhibit endonuclease IV activity in this fluorescence based assay suggesting that it is a specific APE1 inhibitor. All experiments were performed in triplicates and the results represent the Mean  $\pm$  S.E.

#### **4.6.4 Identification of hits (table 4.2)**

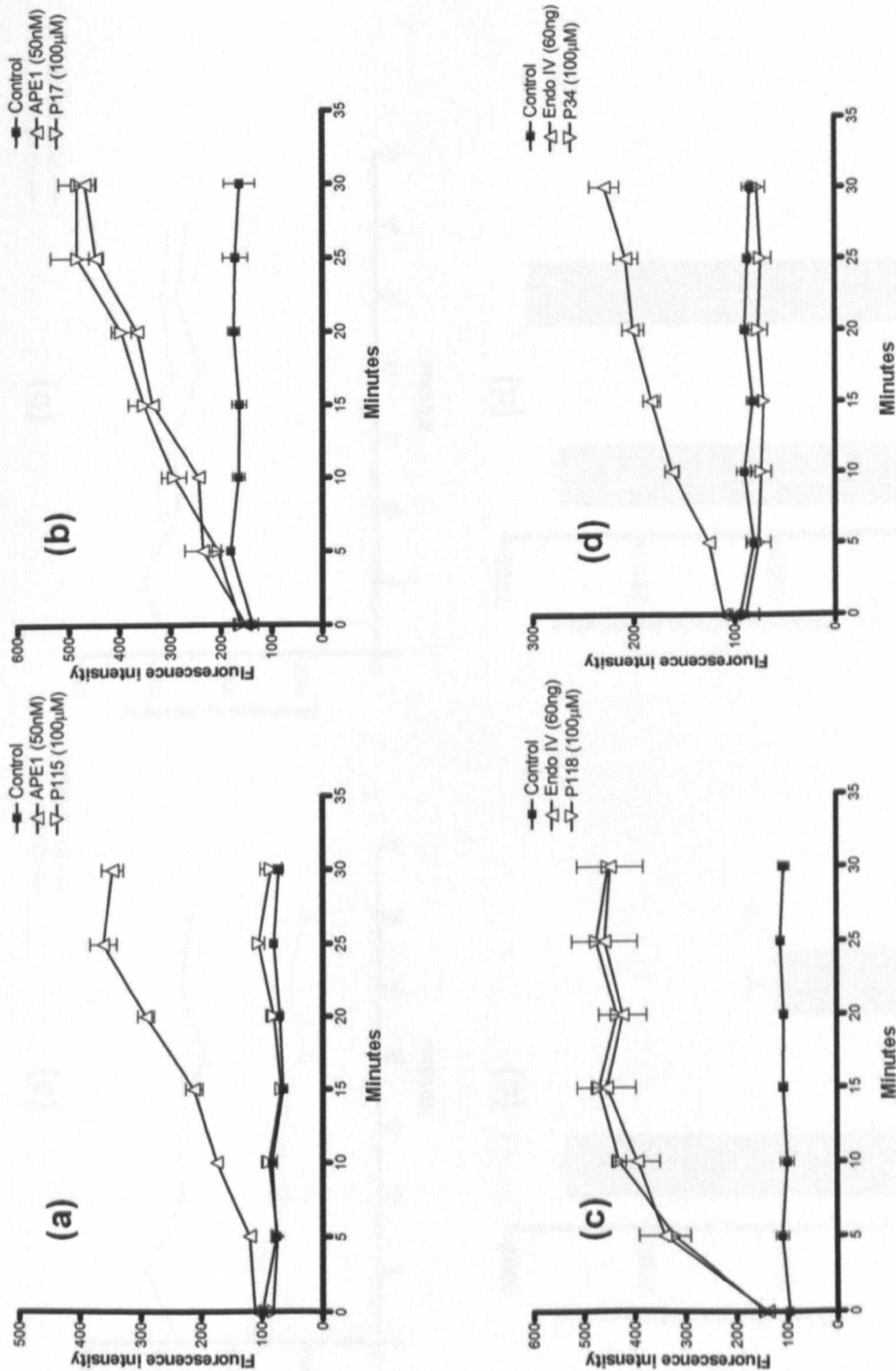
The fluorescence based assays were performed in a 384-well format. Initial screen of 147 compounds were performed at 100  $\mu$ M in triplicate. Figure 4.9 shows typical read outs for potential APE1 inhibitors. P115 completely blocked APE1 mediated AP-site cleavage activity (Figure 4.8 a) whereas P17 did not inhibit APE1 mediated AP-site cleavage activity (Figure 4.8 b). Although P118 showed potent inhibition of APE1 it did not inhibit endonuclease IV activity (Figure 4.8 c) implying that P118 is specific inhibitor of APE1. P34 on the other hand not only inhibited APE1 but also endonuclease IV (Figure 4.8 d). P34 is likely to be a non-specific inhibitor or DNA binder. 31/147 compounds screened were potent APE1 inhibitors. These hits were therefore further tested for intrinsic quenching activity. 7/31 were shown to possess intrinsic quenching activity and were excluded from further analysis (Figure 4.9).

24/31 compounds were then counter screened against endonuclease IV. 17/24 did not block endonuclease IV activity implying that they are specific APE1 inhibitors, whereas the other 7 hits were considered as non specific inhibitors of AP-site cleavage activity (Table 4.3).

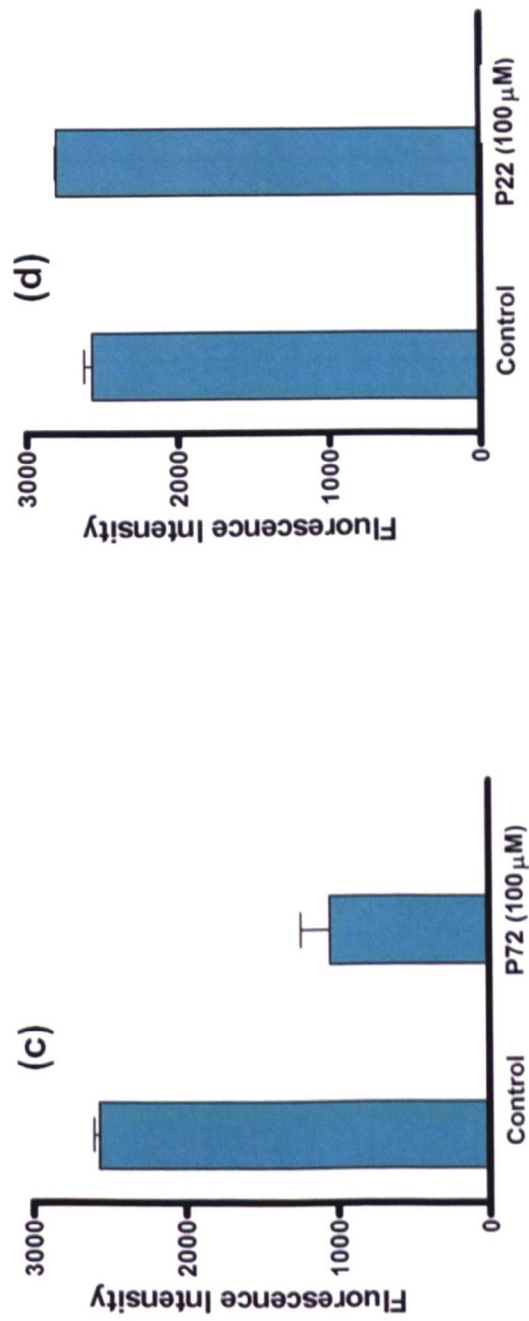
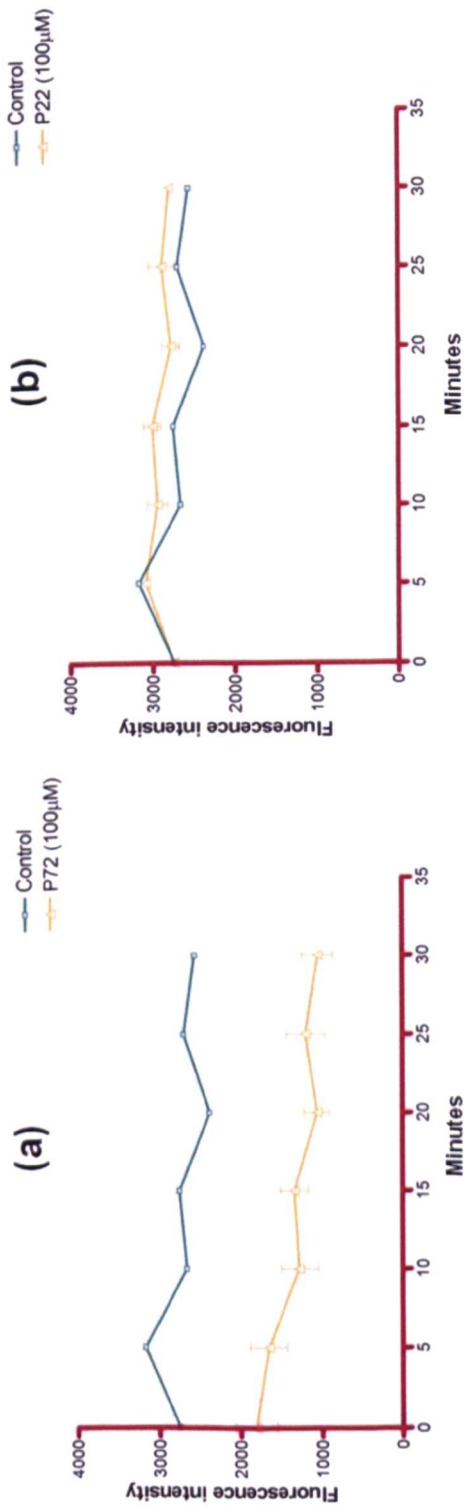
In summary, 17/147 (11.6%) compounds screened were specific APE1 inhibitors. Therefore these compounds were taken for detailed IC<sub>50</sub> value estimation.

**Table 4.2** Summary of Fluorescence based APE1 AP-site cleavage assay (n=147 compounds).

Template	Non Inhibitor	Mild inhibitor	Moderate inhibitor	Strong Inhibitor	Potent inhibitor	Total number	percentage
CRT0044876	38	11	11	3	2	65	44.2%
M1	5	1	0	4	3	13	8.8%
M2	6	0	4	3	7	20	14.3%
M3	10	2	13	5	19	49	32.7%
Total Number	59	14	28	15	31	147	
Percentage	40.1%	9.5%	19.1%	10.2%	21.1%		100%



**Figure 4.8 Fluorescence based AP-site cleavage assay.** Figures 4.9 (a) and (b) show the screening results of compounds P115 and P17 against APE1. P115 showed a potent inhibition of APE1 activity, whereas P17 did not show any inhibition against APE1. Figure 4.9 (c) and (d) show results of Counter screening of compound P118 and P34 respectively against endonuclease IV. While P118 did not exhibit any inhibition function against endonuclease IV, P34 demonstrated a complete inhibition for endonuclease IV suggesting that it is a non specific inhibitor. All experiments were performed in triplicates and the results represent the Mean  $\pm$  S.E.



**Figure 4.9 Fluorescence quenching assay.** Figure 4.10 (a) and (b) shows FQA of two potent hits (P72 and P22) identified by APE1 AP-site cleavage assay. Figure 4.10 (c) and (d) are histograms of fluorescence emission at 30 minutes incubation time point for P72 and P22. P72 showed more than 75% reduction in fluorescence suggesting that this compound is a quencher. While P22 did not show any reduction in the fluorescence emission. All experiments were performed in triplicates and the results represent the Mean  $\pm$  S.E.

**Table 4.3** Summary of counter screening and IC<sub>50</sub> estimation of APE1 inhibitors. N.A means the result is not available as the compound was excluded from counter screening.

Compound ID	Fluorescence quenching assay	Endonuclease IV inhibition	APE1 IC <sub>50</sub>
P4	-	-	400 nM
P22	-	-	10 µM
P30	-	-	4 µM
P34	-	+	N.A
p46	-	-	25 µM
P65	-	-	1.6 µM
P69	-	+	N.A
P72	+	N.A	N.A
P88	-	+	N.A
P89	+	N.A	N.A
P91	-	+	N.A
P93	-	-	3 µM
P95	-	-	500 nM
P96	-	-	500 nM
P97	-	+	N.A
P101	+	N.A	N.A
P102	+	N.A	N.A
P103	+	N.A	N.A
P107	-	+	N.A
P111	-	-	3µM
P113	+	N.A	N.A
P115	-	-	20.5 µM
P116	-	-	15 µM
P117	-	+	N.A
P118	-	-	11 µM
P124	+	N.A	N.A
P125	-	-	3 µM
P126	-	-	15 µM
P128	-	-	16 µM
P133	-	-	3 µM
P147	-	-	50 nM

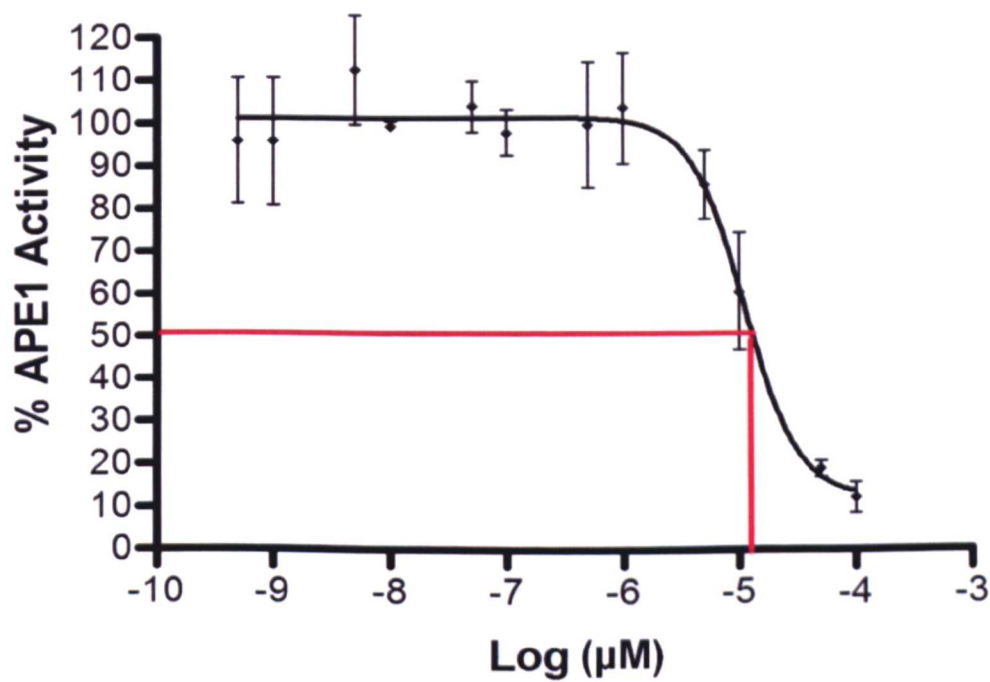
#### 4.6.5 Measurement of IC<sub>50</sub> values for specific APE1 inhibitors

Specific APE1 inhibitors were taken for IC<sub>50</sub> value estimation. IC<sub>50</sub> is defined as the concentration of a compound that results in a 50% reduction in activity of the target protein of interest.

Serial dilutions were set up at 5 nM – 100 µM. The percentage of inhibition for



each concentration was calculated by taking the net fluorescence signal of the reaction containing the inhibitor relative to signal detected from reactions containing no inhibitor. The results were then analysed using prism3.0 Graphpad software. A non-linear regression analysis was used to fit a Hill curve on the data points using sigmoid dose-response. Figure 4.10 shows a typical IC<sub>50</sub> measurement of an APE1 inhibitor (P118) The IC<sub>50</sub> values ranged from 50 nM to 25  $\mu$ M (table 4.3).



**Figure 4.10 Measurement of P118 IC<sub>50</sub> using Prism3.0 software.** P118 IC<sub>50</sub> was found to be 11.6  $\mu$ M. All experiments were performed in triplicates and the results represent the Mean  $\pm$  S.E.

#### 4.6.6 AP site cleavage using HeLa whole cell extracts

Specific and potent APE1 inhibitors isolated from the fluorescence based assays were then screened further using HeLa WCE in a radiolabelled oligonucleotide assay. All potent specific APE1 Inhibitors (n=17) were tested

in the HeLa whole cell AP-site cleavage assay and results are summarised in table 4.4.

**Table 4.4** AP-site cleavage assay using HeLa WCE.

<b>Inhibitor</b>	<b>Percentage cleavage activity</b>	<b>St Error</b>	<b>Template</b>
P111	2.8	0.9	M2
P96	4.7	1.1	M3
P118	7.6	0.8	M3
P147	10.2	1.2	M3
P126	13.0	2	M3
P128	18.5	1.5	M2
P133	30.6	1.9	M2
P116	32.7	2.3	M3
P115	39.8	4	M3
P95	46.9	3	M3
P46	50.7	3.1	M3
P4	55.6	3.2	M3
P22	57.5	3.3	CRT
P125	61.1	4	M2
P30	80.7	5.8	M2
P65	108.1	7.2	M3
P93	112.2	7.4	M3

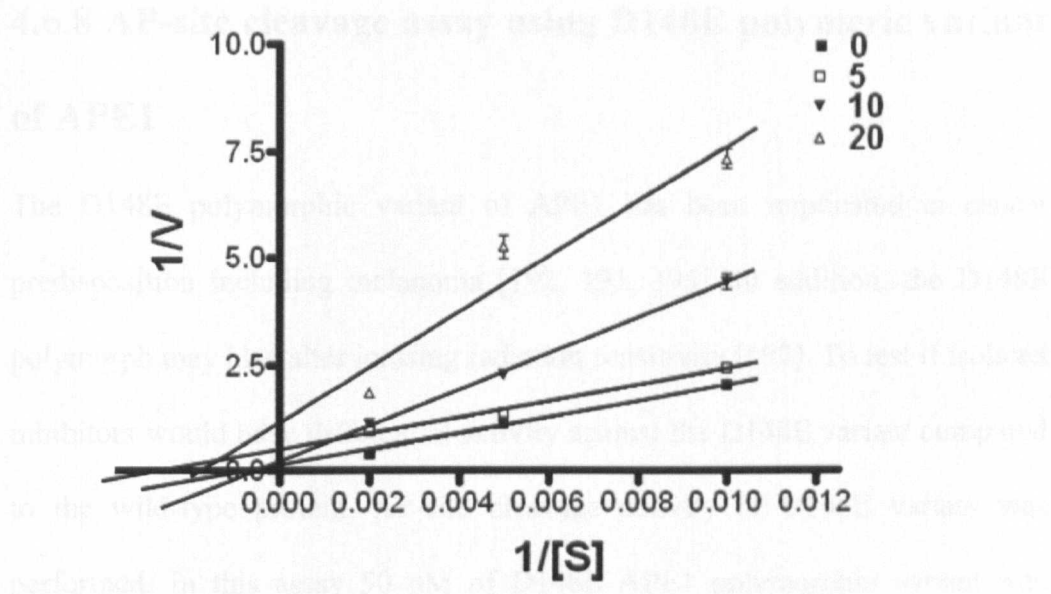
6/17 (P111, P96, P118, P147, P126 and P128) showed more than 80% inhibition of AP site cleavage in WCE implying that they are highly specific and potent inhibitors. While 2/17 (P65 and P93) did not block AP site cleavage activity using WCE. 9/17 (P133, P116, P115, P95, P46, P4, P22, P125, and P30) exhibited mild to moderate inhibition (20-80% inhibition).



#### 4.6.7 Kinetic analysis of P118

To evaluate mechanism of action of APE1 inhibitor, kinetic analysis was performed. P118, a candidate inhibitor was taken for exploratory kinetics analysis.

50 nM of APE1 protein was incubated at room temperature for 30 minutes without or with P118 (5  $\mu$ M, 10  $\mu$ M and 20  $\mu$ M). DNA substrate was then added to a final concentration of 100 nM, 200 nM and 500 nM (in 40  $\mu$ l final volume), and enzyme activity was allowed to proceed for 30 minutes at 37 °C. The percentage APE1 cleavage activity at various concentrations was calculated as the relative net fluorescence signal in the presence of inhibitor to compare to reactions without inhibitor. Lineweaver-Burk plots and kinetic parameters ( $k_{cat}$  and  $K_M$ ) were determined from 8 independent data points. The results showed that  $K_M$  and  $k_{cat}$  decreased at each inhibitor concentration (compared to no inhibitor) and the  $k_{cat}/K_M$  decreased at increasing inhibitor concentration (Figure 4.11).



	$K_M$ (nM)	$k_{cat}$ (min <sup>-1</sup> )	$k_{cat}/K_M$
No Inhibitor	3166	8022	2.5
5 $\mu$ M	375	994	2.7
10 $\mu$ M	1554	1880	1.2
20 $\mu$ M	600	457	0.76

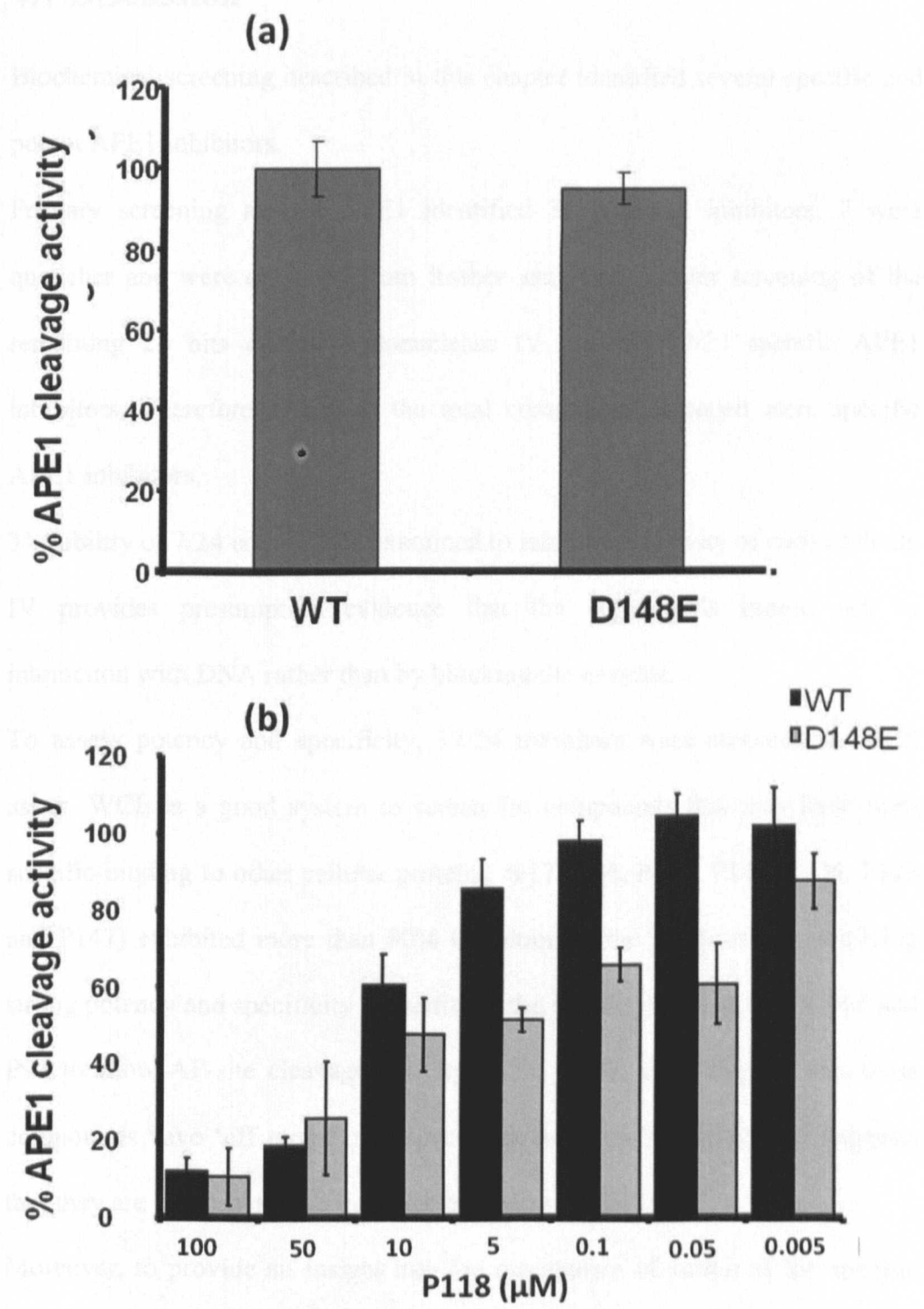
**Figure 4.11 Kinetics analysis of P118.** Shown are the Lineweaver-Burk plots and kinetic parameters determined from 8 independent data points (note: error bars are in some cases too small to see). The APE1 inhibitor was tested at three dose levels (5 $\mu$ M, 10 $\mu$ M, 20 $\mu$ M) and oligonucleotide substrate was evaluated at 3 different concentrations (100 nM, 200 nM and 500 nM). The reaction was performed as described in methods.  $K_M$ ,  $k_{cat}$  decreased at each inhibitor concentration (compared to no inhibitor and the  $k_{cat}/K_M$  decreased at increasing inhibitor concentration. The data is consistent with uncompetitive inhibition.

The data is consistent with the conclusion that P118 is uncompetitively inhibiting APE1 enzyme. However, the possibility that P118 operates as a weak uncompetitive inhibitor (meaning it binds the protein-DNA substrate complex) cannot be excluded, as a reproducibly lower  $K_M$  in the presence of the P118 is observed, though this is unlikely.

#### **4.6.8 AP-site cleavage assay using D148E polymeric variant of APE1**

The D148E polymorphic variant of APE1 has been implicated in cancer predisposition including melanoma [192, 193, 195]. In addition, the D148E polymorph may also alter ionising radiation sensitivity [197]. To test if isolated inhibitors would have differential activity against the D148E variant compared to the wild-type protein, AP-site cleavage activity of D148E variant was performed. In this assay 50 nM of D148E APE1 polymorphic variant was incubated in a buffer system of 50 mM Tris-HCl, pH 8.0, 1 mM MgCl<sub>2</sub>, 50 mM NaCl, 2 mM DTT at 37 °C, and 5 nM of DNA substrate with and without the presence of P118. The incubation time was set to 30 minutes.

Although the AP-site cleavage activity of D148E variant was similar to that of the wild type (Figure 4.12 a), consistent with a previous report [190], figure 4.12 b demonstrates that for P118, the IC<sub>50</sub> for APE1 inhibition was significantly reduced (by 50.5%) for the D148E protein (5.56 µM) compared to wild type (11.6 µM).



**Figure 4.12 Testing AP-site cleavage activity in wild-type and D148 polymorph.** (a) The figure shows that AP-site cleavage activity was similar in both wild-type and the D148E polymorph. (b) D148E was more sensitive to inhibition by P118 compared with wild type. All experiments were performed in triplicates and the results represent the Mean  $\pm$  S.E.

## 4.7 Discussion

Biochemical screening described in this chapter identified several specific and potent APE1 inhibitors.

Primary screening against APE1 identified 31 potential inhibitors. 7 were quencher and were excluded from further analysis. Counter screening of the remaining 24 hits against endonuclease IV isolated 17/24 specific APE1 inhibitors. Therefore 11.5% of the total compounds screened were specific APE1 inhibitors.

The ability of 7/24 compounds examined to inhibit the activity of endonuclease IV provides presumptive evidence that the compounds indeed act by interaction with DNA rather than by blocking the enzyme.

To assess potency and specificity, 17/24 inhibitors were screened in WCE assay. WCE is a good system to screen for compounds that may have non-specific binding to other cellular proteins. 6/17 (P96, P111, P118, P126, P128 and P147) exhibited more than 80% inhibition in the WCE assays, implying strong potency and specificity. In addition, the inability of compounds P65 and P93 to show AP-site cleavage activity in the WCE assay implies that these compounds have 'off target' non-specific protein-binding effect and suggests that they are unlikely to be a good development candidates.

Moreover, to provide an insight into the mechanism of action of the specific inhibitors on APE1 protein, a kinetic analysis was conducted using P118. Kinetic analysis has shown a decreased  $K_M$ ,  $k_{cat}$  (compared with no inhibitor) and decreased the  $k_{cat} / K_M$  implying uncompetitive inhibition. Future co-crystallization experiments in the presence of DNA are likely to provide further information regarding the exact mechanism of action of this compound.

D148E variant of APE1 was more sensitive to inhibition by P118. This provides evidence that APE1 inhibitors may be more effective in blocking the endonuclease activity of the D148E polymorphic variant, a common polymorph associated with cancer predisposition, compared with the wild type.

## ***Chapter 5***

### ***Cell based investigations***

---

## **5. Cell based investigations**

### **5.1 Introduction**

As discussed in chapter 3 and chapter 4, using virtual screening and biochemical screening I isolated several specific and potent inhibitors of APE1. Six specific APE1 inhibitors (P96, P111, P118, P125, P126, P128 and P147) were taken for detailed cell based analyses.

Preclinical studies discussed in chapter 1 demonstrate that APE1 depletion enhance cellular sensitivity to a wide range of DNA base damaging agents. The DNA base excision repair (BER) pathway is critically involved in the repair of bases that have been damaged by alkylating agents such as temozolomide that is routinely used for the treatment of patients with advanced melanoma and glioma [12]. In addition, BER may also be involved in the repair of damage induced by nucleoside analogues (such as gemcitabine) that are commonly used in patients with pancreatic cancer [223].

The ability of the isolated APE1 inhibitors to potentiate chemotherapy cytotoxicity was tested in MTS and clonogenic survival assays. The assays were undertaken in a panel of human cancer cell lines: MeWo (Melanoma), SK-Mel30 (Melanoma), U89MG (Glioma) and PANC1 (Pancreatic) cancer cell lines. All experiments were performed in triplicates.

#### **5.1.1 Alkylating agents**

Alkylating agents are highly reactive electrophilic compounds that interact chemically with nucleophilic centres in organic macromolecules such



as DNA. Alkylating agents are broadly classified into; mono-functional and bi-functional alkylating agents.

**Monofunctional alkylating agents** include methyl methane sulfonate (MMS), temozolomide, dacarbazine, procarbazine and others. These agents have single reactive group (such as methyl or other alkyl groups) and interact covalently with single nucleophilic centres in the DNA. Such reactive sites are present in all four bases, but they are attacked with different affinities and specificities. Most reactive sites are in the ring nitrogen atoms, in particular N7 of guanine (N7mG) and N3 of adenine (N3mA). Moreover, alkylation can also occur at the less nucleophilic oxygen atom such as O6 position of guanine (O6mG). O6mG is predominantly carcinogenic because of its miscoding properties and is processed by *o*<sup>6</sup>-alkylG-DNA alkyltransferase (MGMT) that directly repairs O6mG the damage in single step. N7mG is the most common lesion but is relatively non-toxic. N3mA is a more minor lesion but is highly cytotoxic because it blocks DNA replication. N7mG and N3mA are repaired by the BER machinery [41, 42, 264].

**Bifunctional alkylating agents** such as (BCNU [1,3-bis(2-chloroethyl)-1-nitrosoureas], cyclophosphamide, mitomycin C, mechlorethamine hydrochloride (nitrogen mustard), busulfan (methane sulfonic acid esters) and others induce labile alkylated bases and more complex lesions including intra- or inter-strand crosslinks[41].

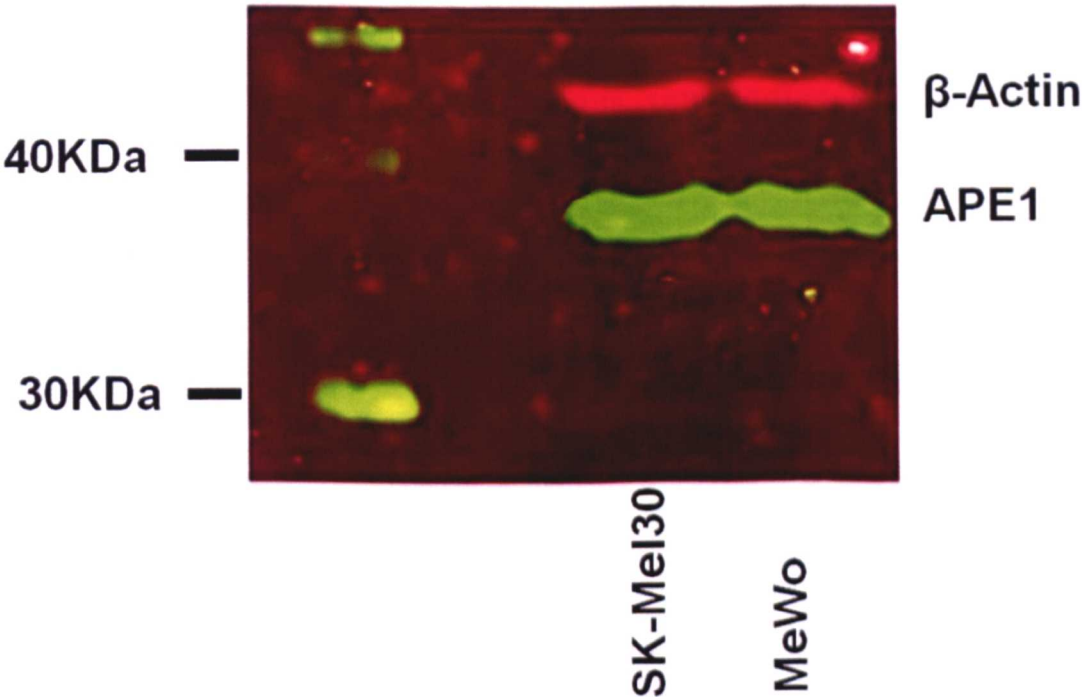
**5.1.2 Doxorubicin** is an anthracycline antibiotic that is commonly used in the treatment of solid tumours such as breast cancer. Doxorubicin intercalate in between DNA base pairs leading to DNA cross linking and interfere with DNA

unwinding, strands separation and helicase activity. As a result doxorubicin blocks DNA transcription and replication. In addition doxorubicin also was shown to inhibits topoisomerase II activity and it can also induce apoptosis [265]. Since DNA damage induced by doxorubicin is not repaired by BER, it was used as a negative control for cytotoxicity analysis.

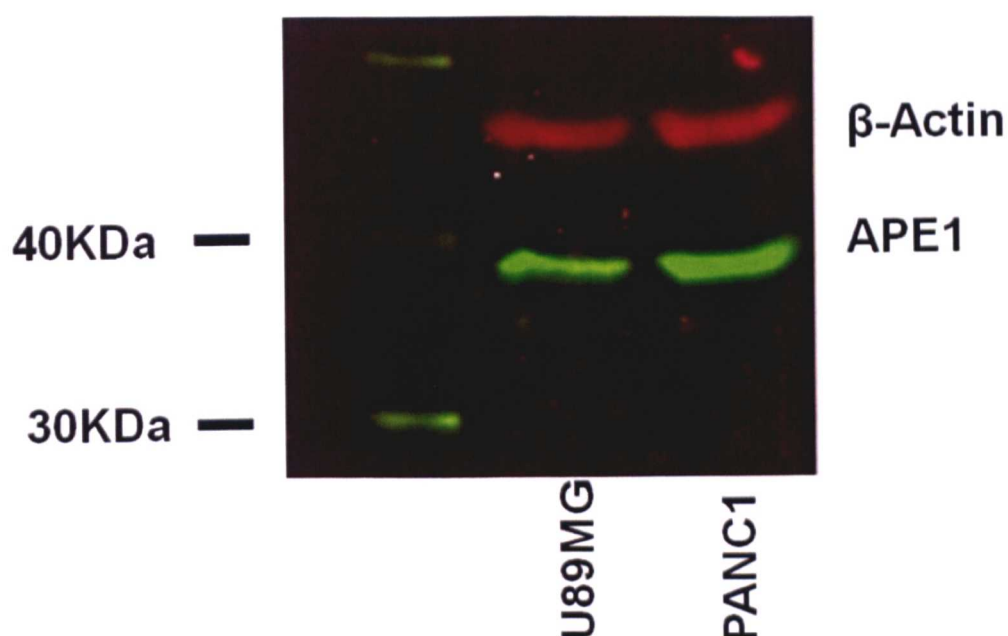
## 5.2 Results

### 5.2.1 Western blotting analysis

SK-Mel30, MeWo, U89MG and PANC1 cancer cell lines were initially tested for APE1 expression. Western blotting analysis showed robust APE1 expressions in these cell lines (Figure 5.1 and 5.2).



**Figure 5.1 Western blotting.** APE1 expression in, SK-Mel30 and MeWo melanoma cancer cell lines is shown here. APE1 (36.5 KDa) is highlighted in green.  $\beta$ -Actin (red) is shown as a loading control.



**Figure 5.2 Western blotting.** APE1 expression in U89MG (Glioma) and PANC1 (pancreatic) cancer cell lines is shown here. APE1 (36.5 KDa) is highlighted in green.  $\beta$ -Actin (red) is shown as a loading control.

## 5.2.2 Cytotoxicity of APE1 inhibitors in cancer cell lines

### 5.2.2.1 CellTiter 96® AQueous Non-Radioactive Cell Proliferation Assay (MTS)

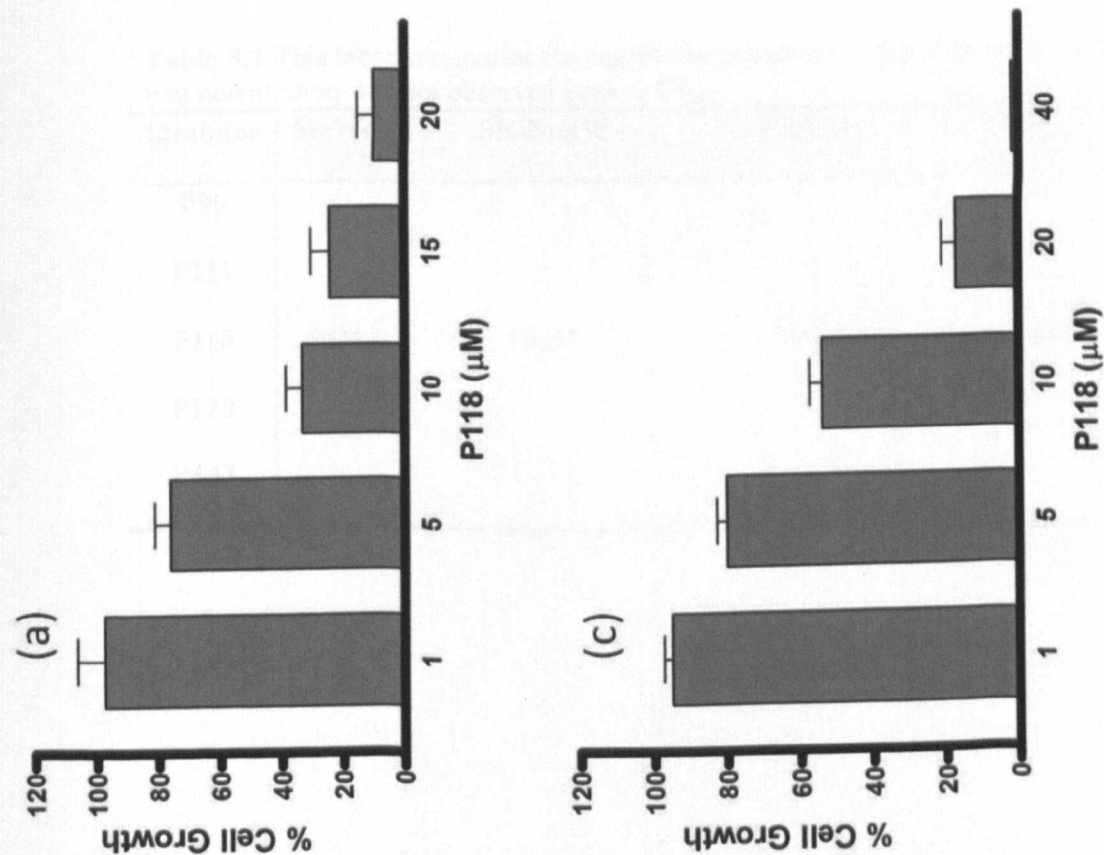
#### 5.2.2.1.1 Intrinsic cytotoxicity of APE1 inhibitors

To investigate biological consequences of APE1 inhibitors MTS cell proliferation assay was initially undertaken. At the time of conducting this research P125 and P126 were not commercially available and the previous stocks were not sufficient to pursue the cell based investigations and therefore were excluded. P96, P111, P118, P128 and P147 were tested for their intrinsic toxicity at different concentrations.  $GI_{50}$  (the concentration needed to reduce the growth

of treated cells to half that of untreated cells) were calculated from these studies. Table 5.1 summarizes the results in MeWo, SK-Mel30, PANC1 and U89MG cancer cell lines. P96, P111 and P147 consistently showed a  $GI_{50}$  of more than 40  $\mu M$  in all the four cancer cell lines tested. P128 showed a considerable difference in  $GI_{50}$  [8  $\mu M$  for SK-Mel30 to around 35-40  $\mu M$  to other cancer cell lines]. P118 exhibited a  $GI_{50}$  of 8-18  $\mu M$  which is comparable to its  $IC_{50}$  (11.6  $\mu M$ ) measured in the biochemical assays. Figures 5.3 a, b, c and d show examples of dose dependant inhibition of cellular proliferation by P118 in cancer cell lines.

**Table 5.1** GI<sub>50</sub> of APE1 inhibitors in four different cancer cell lines.

Inhibitor	Biochemical IC <sub>50</sub>	MeWo	SK-Mel30	U89MG	PANC1
P96	0.5 μM	48 μM	44 μM	>60 μM	>60 μM
P111	3 μM	>60 μM	>60 μM	>60 μM	>60 μM
P118	11 μM	8 μM	18 μM	15 μM	12 μM
P128	16 μM	38 μM	8 μM	40 μM	35 μM
P147	50 nM	>40 μM	>40 μM	>40 μM	>40 μM



**Figure 5.3 MTS assay showing cytotoxicity profile of P118.** Cells were exposed to different concentrations of P118 (a) MeWo cell line was very sensitive to P118 with relatively low  $GI_{50}$  around 8 $\mu$ M. (b) P118 was less toxic to SK-Mel30 cell line and  $GI_{50}$  was around 18 $\mu$ M. (c) PANC1 showed a  $GI_{50}$  around 12 $\mu$ M (d) U89MG showed a  $GI_{50}$  around 15 $\mu$ M. All experiments were performed in triplicates and the results represent the Mean  $\pm$  S.E.

### 5.2.2.1.2 Potentiation of cytotoxicity of base damaging agents by APE1 inhibitors

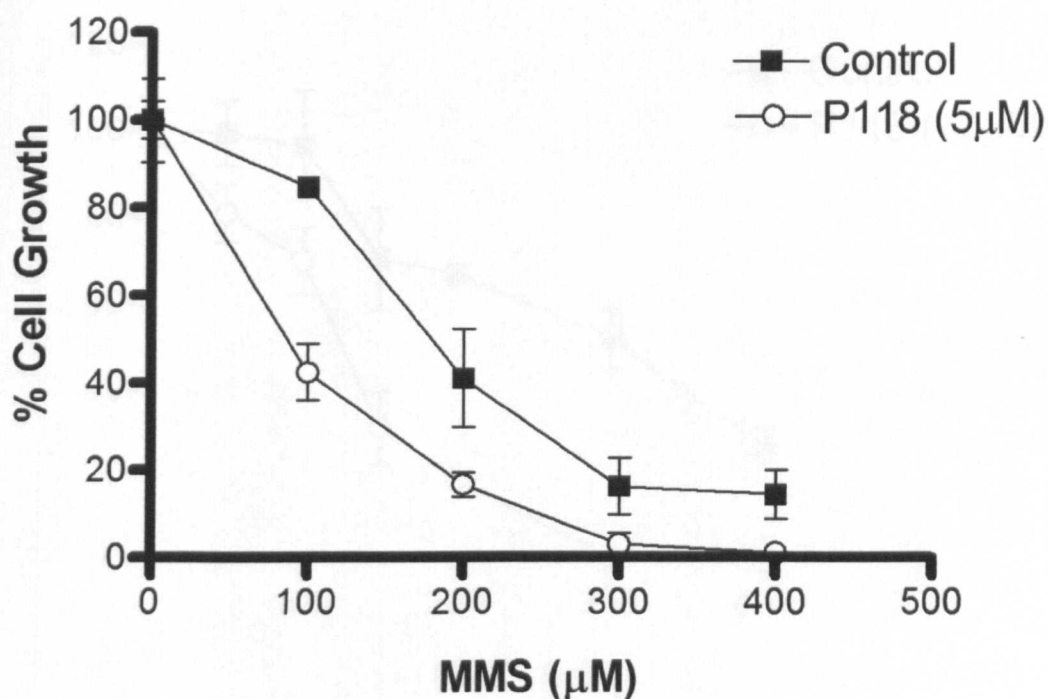
The ability of P96, P111, P118, P128 and P147 to potentiate the cytotoxicity of DNA base damaging agents was tested. APE1 inhibitors were tested well below  $GI_{50}$ . Monofunctional alkylating MMS was used in these studies.

Table 5.2 summarizes the results for all inhibitors. P118 demonstrated consistent ability to potentiate MMS cytotoxicity in all the four cancer cell lines (see also Figures 5.4, 5.5, 5.6 and 5.7). Unlike P118, compound P96, P111, P128 and P147 did not show any potentiation of cytotoxicity of MMS. Figure 5.8 shows results of P96, P111, P128 and P147 potentiation experiments in SK-Mel30 cancer cell line.

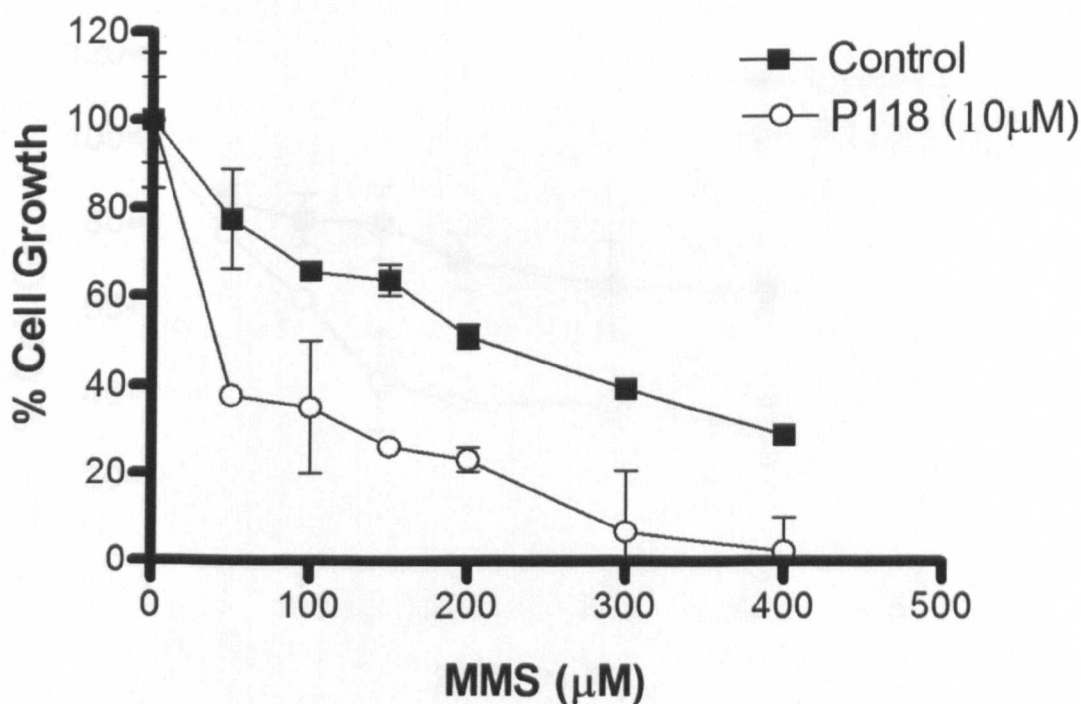
**Table 5.2** This table summaries the results for potentiation experiments. (–) indicates that potentiation was not observed even at  $GI_{50}$

Inhibitor	MeWo	SK-Mel30	U89MG	PANC1
P96	–	–	–	–
P111	–	–	–	–
P118	5 $\mu$ M	10 $\mu$ M	10 $\mu$ M	10 $\mu$ M
P128	–	–	–	–
P147	–	–	–	–



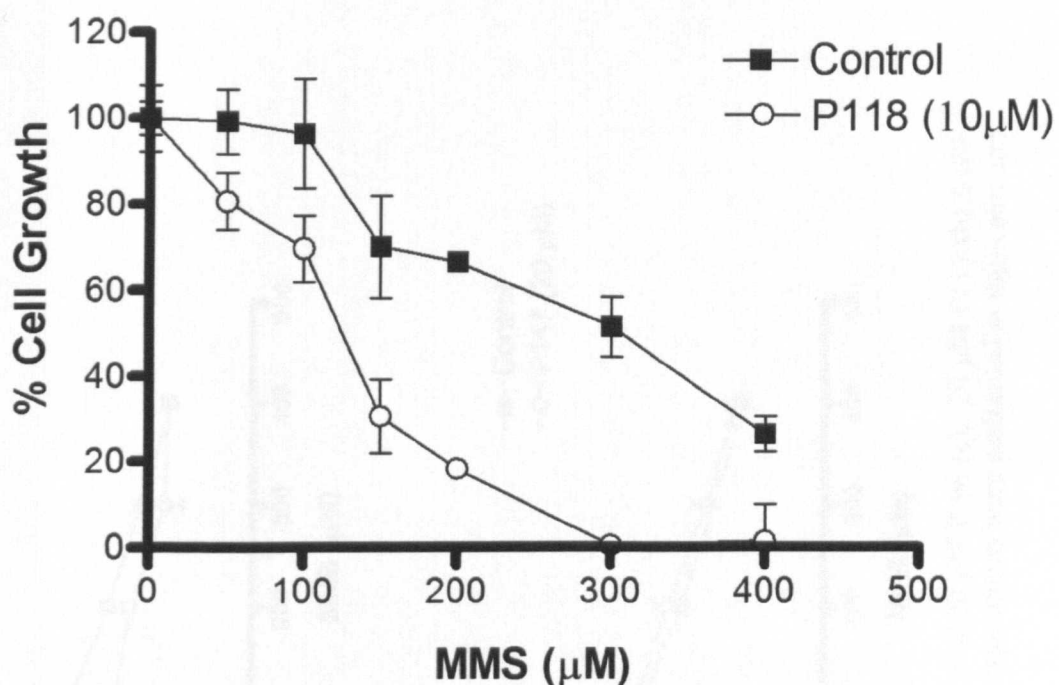


**Figure 5.4 MTS assay in MeWo cells.** P118 (5 μM) significantly potentiated the cytotoxicity of MMS in MeWo cell line. All experiments were performed in triplicates and the results represent the Mean ± S.E.

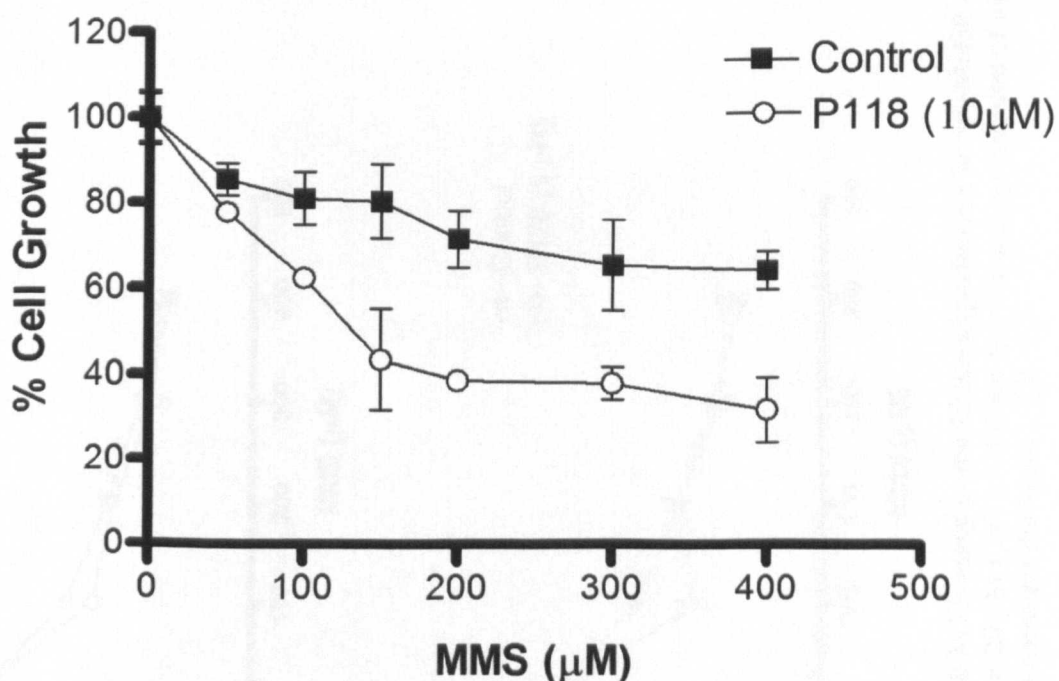


**Figure 5.5 MTS assay in SK-Mel30 cells.** P118 (10 μM) significantly potentiated the cytotoxicity of MMS in SK-Mel30 cell line. All experiments were performed in triplicates and the results represent the Mean ± S.E.

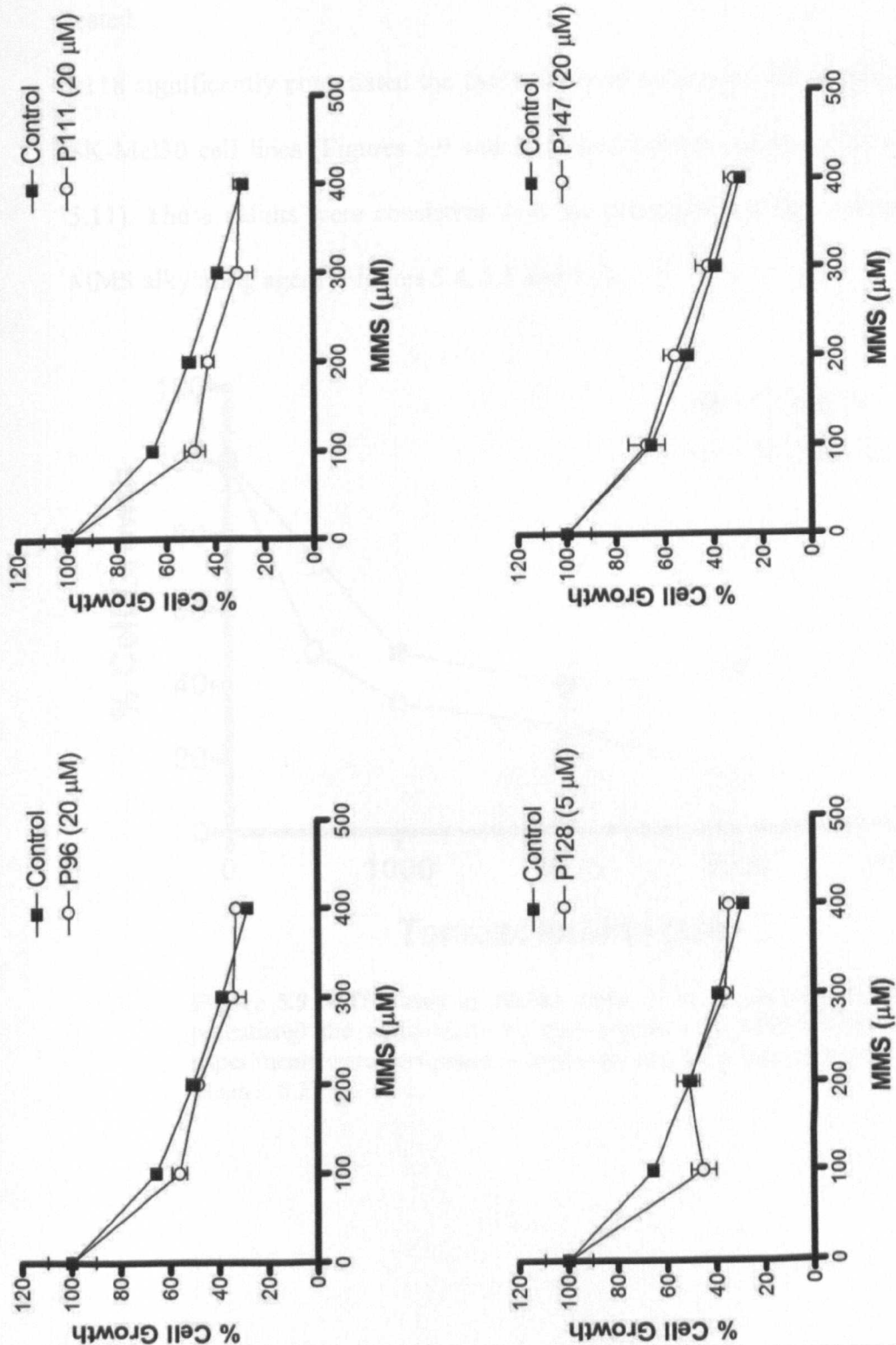




**Figure 5.6 MTS assay in PANC1 cells.** P118 (10 μM) significantly potentiated the cytotoxicity of MMS in PANC1 cell line. All experiments were performed in triplicates and the results represent the Mean  $\pm$  S.E.



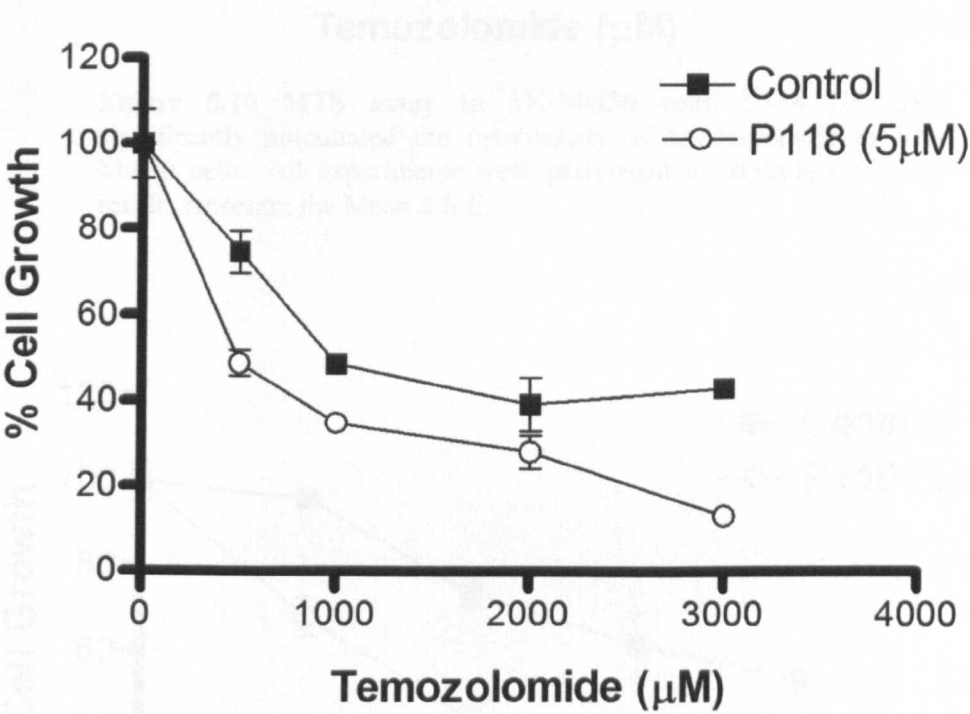
**Figure 5.7 MTS assay in U89MG cells.** P118 (10 μM) significantly potentiated the cytotoxicity of MMS in U89MG cell line. All experiments were performed in triplicates and the results represent the Mean  $\pm$  S.E.



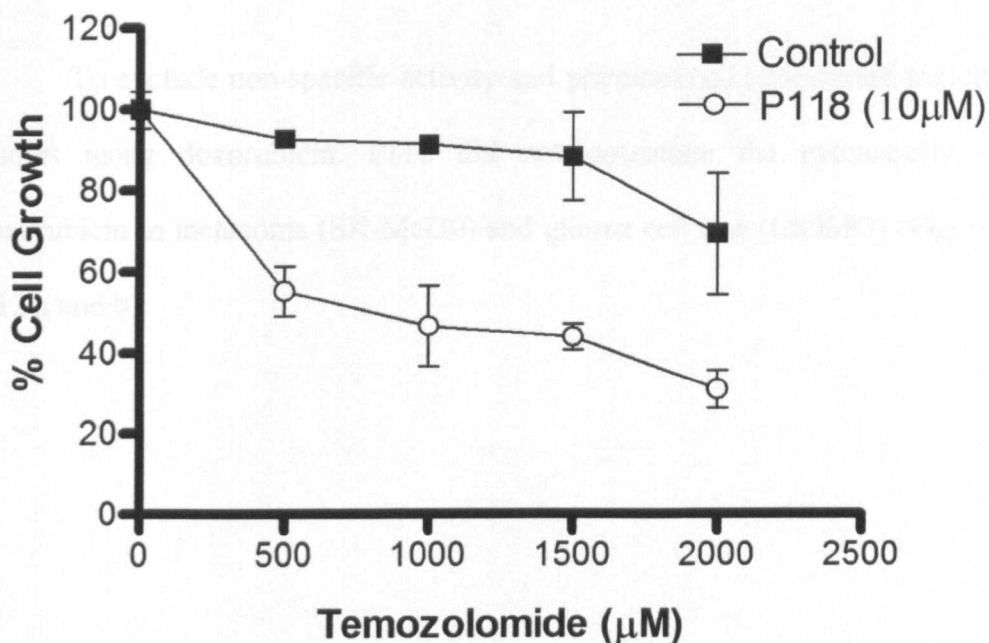
**Figure 5.8 MTS assay potentiation experiments in SK-Mel30 cell line.** The presence of 20  $\mu$ M P 96 (a), 20  $\mu$ M P111 (b) 5  $\mu$ M P128 (c) or 20  $\mu$ M P147 (d) did not result in any potentiation of MMS cytotoxicity. All experiments were performed in triplicates and the results represent the Mean  $\pm$  S.E.

As P118 showed promising cytotoxicity potentiation in all the cell lines tested, it was chosen for further analysis. The ability of P118 to potentiate the cytotoxicity of temozolomide, a clinically relevant alkylating agent was then tested.

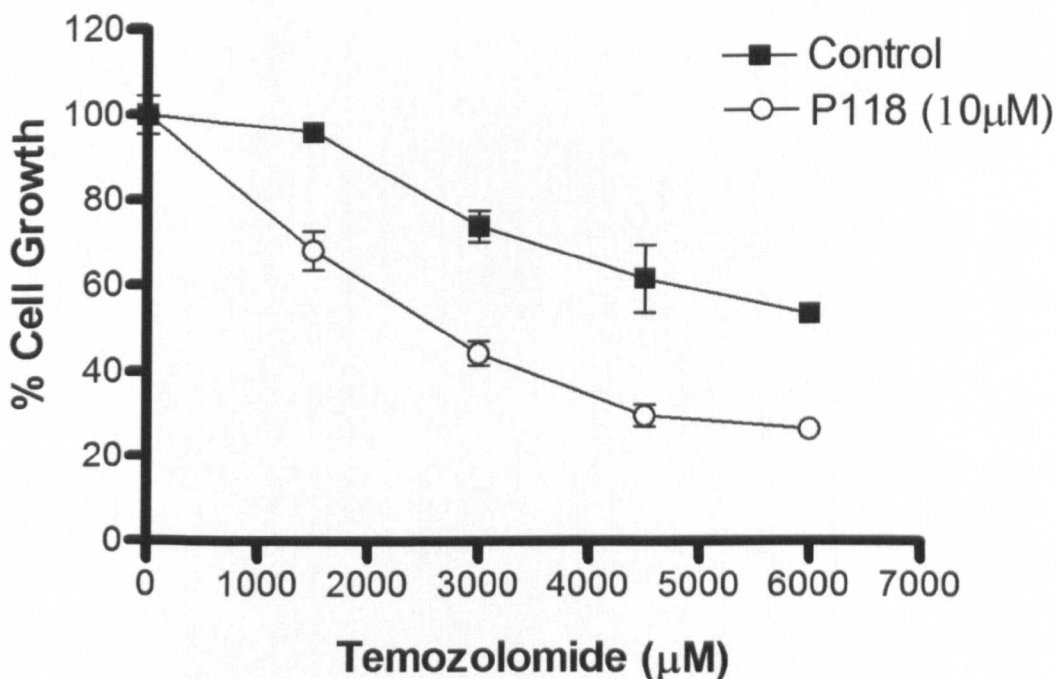
P118 significantly potentiated the cytotoxicity of temozolomide in MeWo and SK-Mel30 cell lines (Figures 5.9 and 5.10) and U89MG glioma cells (Figure 5.11). These results were consistent with the potentiation effect noticed with MMS alkylating agent (Figures 5.4, 5.5 and 5.7).



**Figure 5.9 MTS assay in MeWo cells.** P118 (5 μM) significantly potentiated the cytotoxicity of temozolomide in MeWo cells. All experiments were performed in triplicates and the results represent the Mean ± S.E.

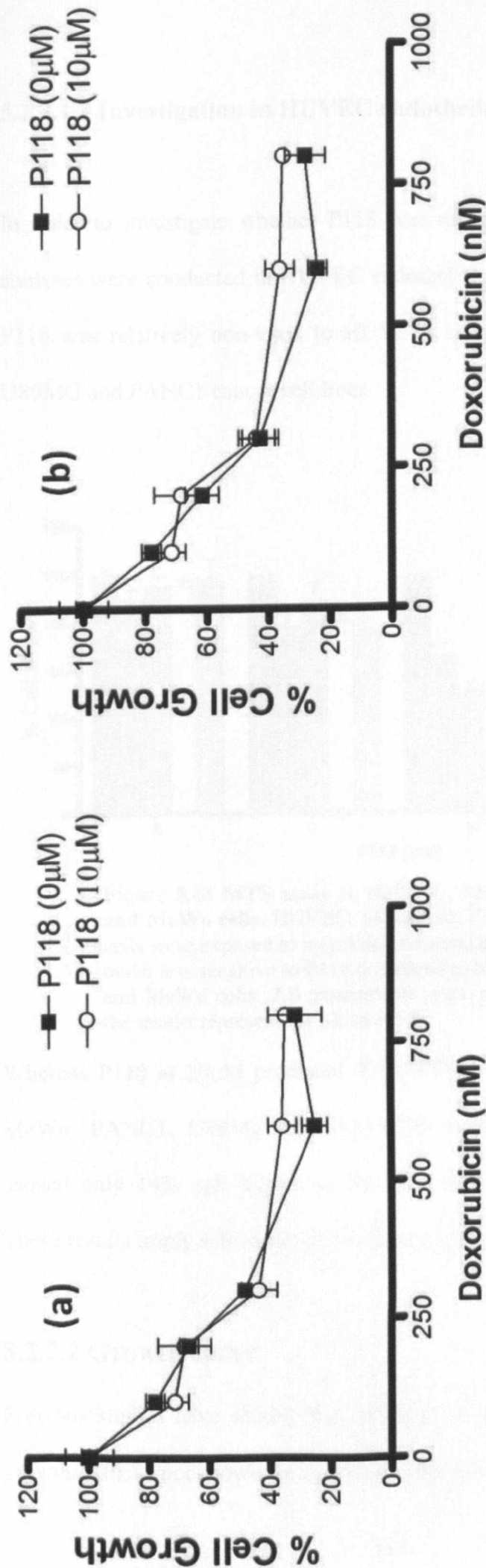


**Figure 5.10 MTS assay in SK-Mel30 cells.** P118 (10 μM) significantly potentiated the cytotoxicity of temozolomide in SK-Mel30 cells. All experiments were performed in triplicates and the results represent the Mean ± S.E.



**Figure 5.11 MTS assay in U89MG cells.** P118 (10 μM) significantly potentiated the cytotoxicity of temozolomide in U89MG cells. All experiments were performed in triplicates and the results represent the Mean ± S.E.

To exclude non-specific activity and potentiation, I conducted toxicity studies using doxorubicin. P118 did not potentiate the cytotoxicity of doxorubicin in melanoma (SK-Mel30) and glioma cell line (U89MG) (Figures 5.12 a and b).

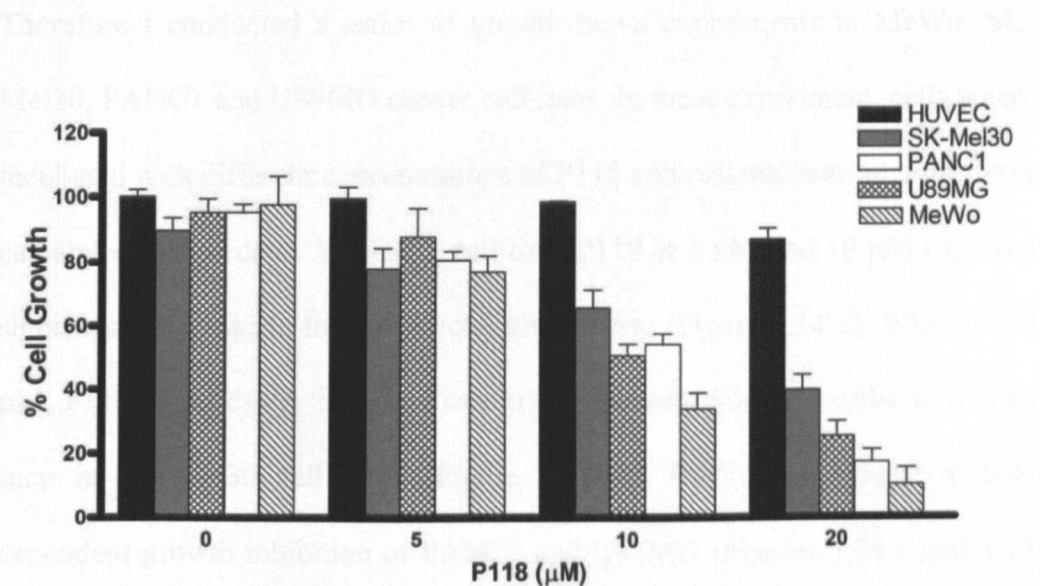


**Figure 5.12. MTS assay P118 Potentiation experiment with doxorubicin.** (a) In SK-Mel30 cell line the presence of 10  $\mu$ M of P118 did not potentiate the cytotoxicity of doxorubicin. Similar results were seen in U90MG (b) where the presence of 10  $\mu$ M of P118 did not potentiate the cytotoxicity of doxorubicin. All experiments were performed in triplicates and the results represent the Mean  $\pm$  S.E.



5.2.2.1.3 Investigation in HUVEC endothelial cells

In order to investigate whether P118 was toxic to noncancer cells, toxicity analyses were conducted in HUVEC endothelial cells. Figure 5.13 shows that P118 was relatively non-toxic to HUVECs compared to MeWo, SK-Mel30, U89MG and PANC1 cancer cell lines.



**Figure 5.13 MTS assay in HUVEC, SK-Mel30, PANC1, U89MG and MeWo cells.** HUVEC, SK-Mel30, PANC1, U89MG and MeWo cells were exposed to increasing concentrations of P118. HUVEC was much less sensitive to P118 compared to SK-Mel30, PANC1, U89MG and MeWo cells. All experiments were performed in triplicates and the results represent the Mean  $\pm$  S.E.

Whereas P118 at 20μM produced 90%, 83%, 75% and 60% cell killing in MeWo, PANC1, U89Mg and SK-Mel30 cancer cell lines respectively, it caused only 14% cell killing in HUVEC cell normal endothelial cell line. These results imply selectivity of P118 on cancer cells (Figure 5.13).

5.2.2.2 Growth curve

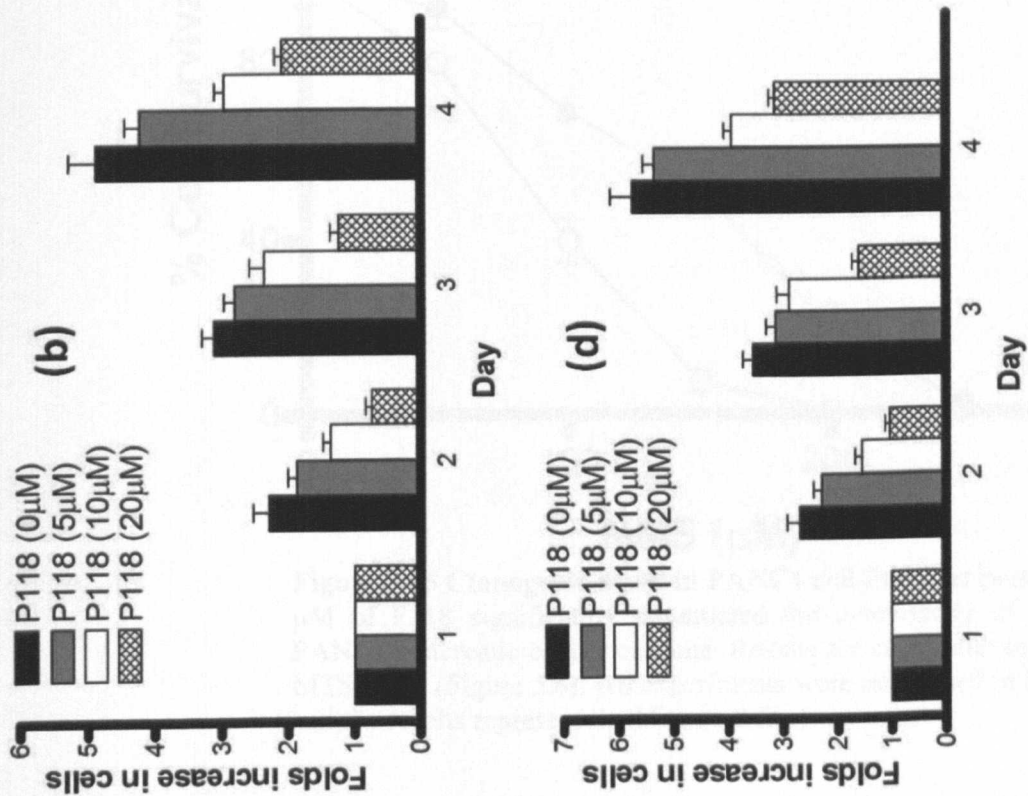
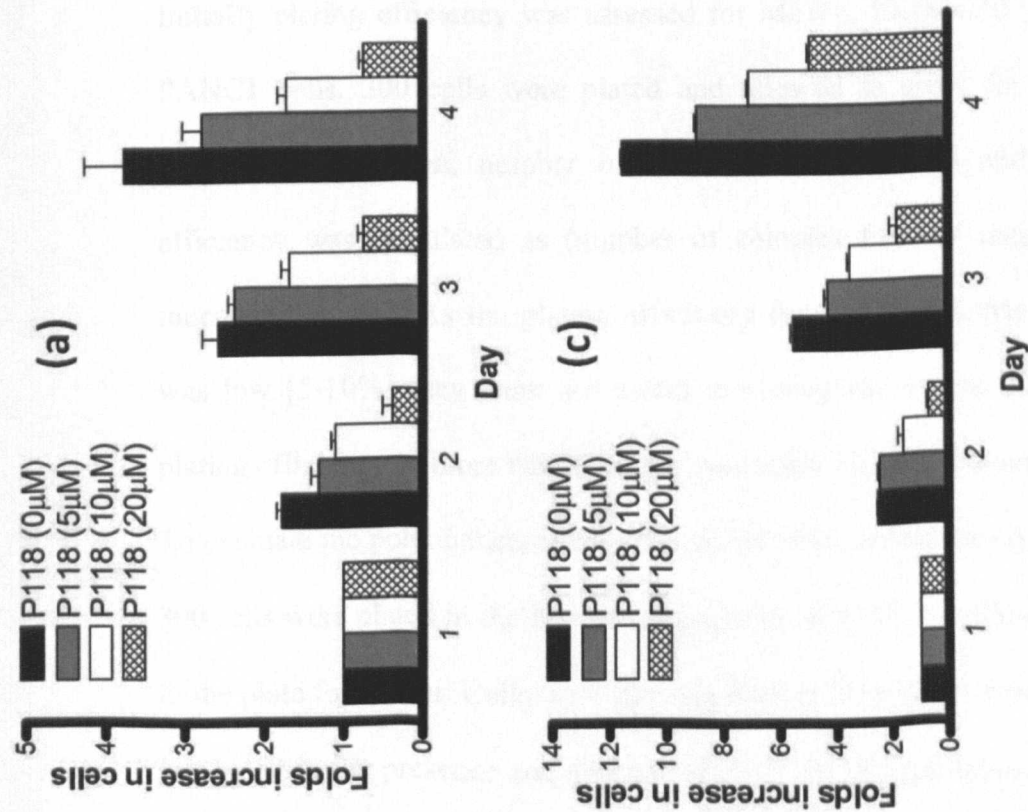
Previous studies have shown that APE1 plays a vital role in controlling cell growth. APE1 knockdown using siRNA results in a significant decrease in cell

growth with increased apoptosis in cancer cell lines [178, 183, 201]. Moreover, a recent study by Vascotto et al has shown that APE1 down-regulation by siRNA can have a direct impact on cell growth interfering with RNA quality control mechanism [266]. Blocking APE1 repair activity by chemical inhibitor was also shown to block cell growth and proliferation in glioblastoma cells [255].

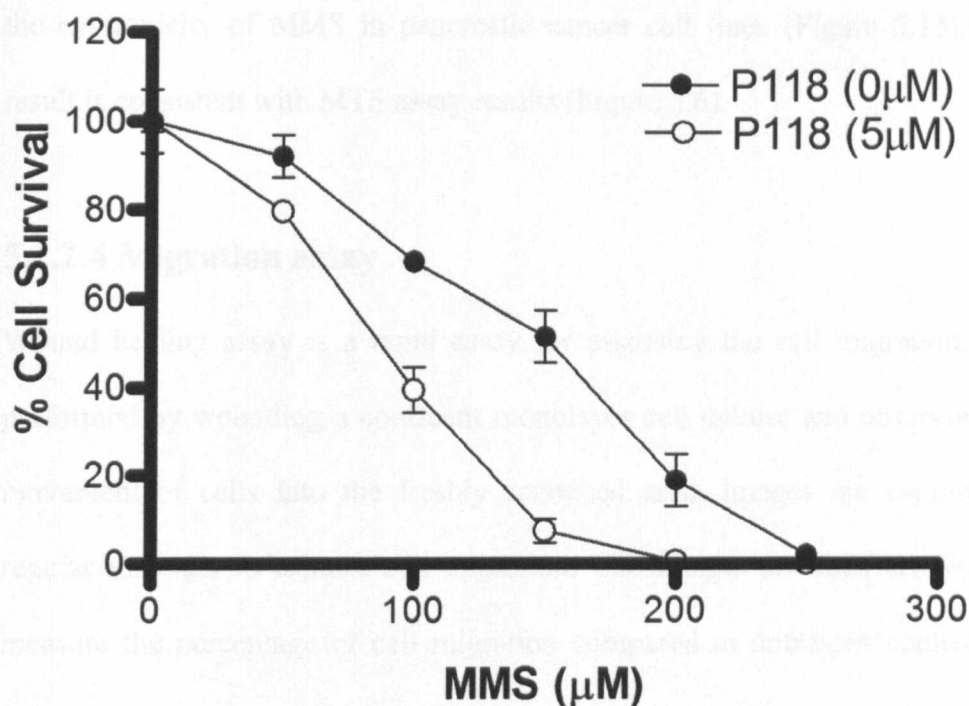
Therefore I conducted a series of growth curve experiments in MeWo, SK-Mel30, PANC1 and U89MG cancer cell lines. In these experiment, cells where incubated with different concentrations of P118 and cell duplication times were calculated over 4 days. In MeWo cell line, P118 at 5  $\mu$ M and 10  $\mu$ M caused a significant decrease in the cancer cell growth rate (Figure 5.14 a). While at 20  $\mu$ M, P118 significantly impaired cancer cell growth. Similar results were also seen in SK-Mel30 cell lines (Figure 5.14 b). P118 also showed a dose dependent growth inhibition of PANC1 and U89MG (Figures 5.14 c and 5.14 d).

Results obtained from the growth curve experiments imply that P118 interferes with cancer cell growth and is consistent with results obtained in MTS assays.





**Figure 5.14 Histograms showing the growth curve in MeWo, SK-Mel30, PANC1 and U89MG cancer cell lines in the presence of P118.**  $10^5$  cells were seeded into T25 tissue culture flasks and cell number was monitored over the next 4 days incubation. The folds increase in cell number compared to day 1 was measured. A dose-dependent decrease in cell growth was demonstrated in (a) MeWo (b) SK-Mel30 (c) PANC1 and (d) U89MG cells. All experiments were performed in triplicates and the results represent the Mean  $\pm$  S.E.



**Figure 5.15 Clonogenic assay in PANC1 cell line.** The presence of 5  $\mu$ M of P118 significantly potentiated the cytotoxicity of MMS in PANC1 pancreatic cancer cell line. Results are consistent with that of MTS assay (Figure 5.6). All experiments were performed in triplicates and the results represent the Mean  $\pm$  S.E.

### 5.2.2.3 Clonogenic survival assay

Initially plating efficiency was assessed for MeWo, SK-Mel30, U89MG and PANC1 cells. 300 cells were plated and allowed to grow for 10-14 days. Following incubation, number of colonies were counted and the plating efficiency was calculated as (number of colonies formed/ number of cells inoculated)  $\times$  100. As the plating efficiency for MeWo, SK-Mel30, U89MG was low [5-10%] they were not tested in clonogenic assays. PANC1 had a plating efficiency of more than 60% and was taken for potentiation experiment. To evaluate the potentiation of cytotoxicity of DNA damaging agents by P118, 300 cells were plated in the absence or presence of P118 and allowed to adhere to the plate for 1 hour. Cells were then exposed to MMS for 1 hour. Cells were incubated in the presence and absence of P118. P118 significantly potentiated

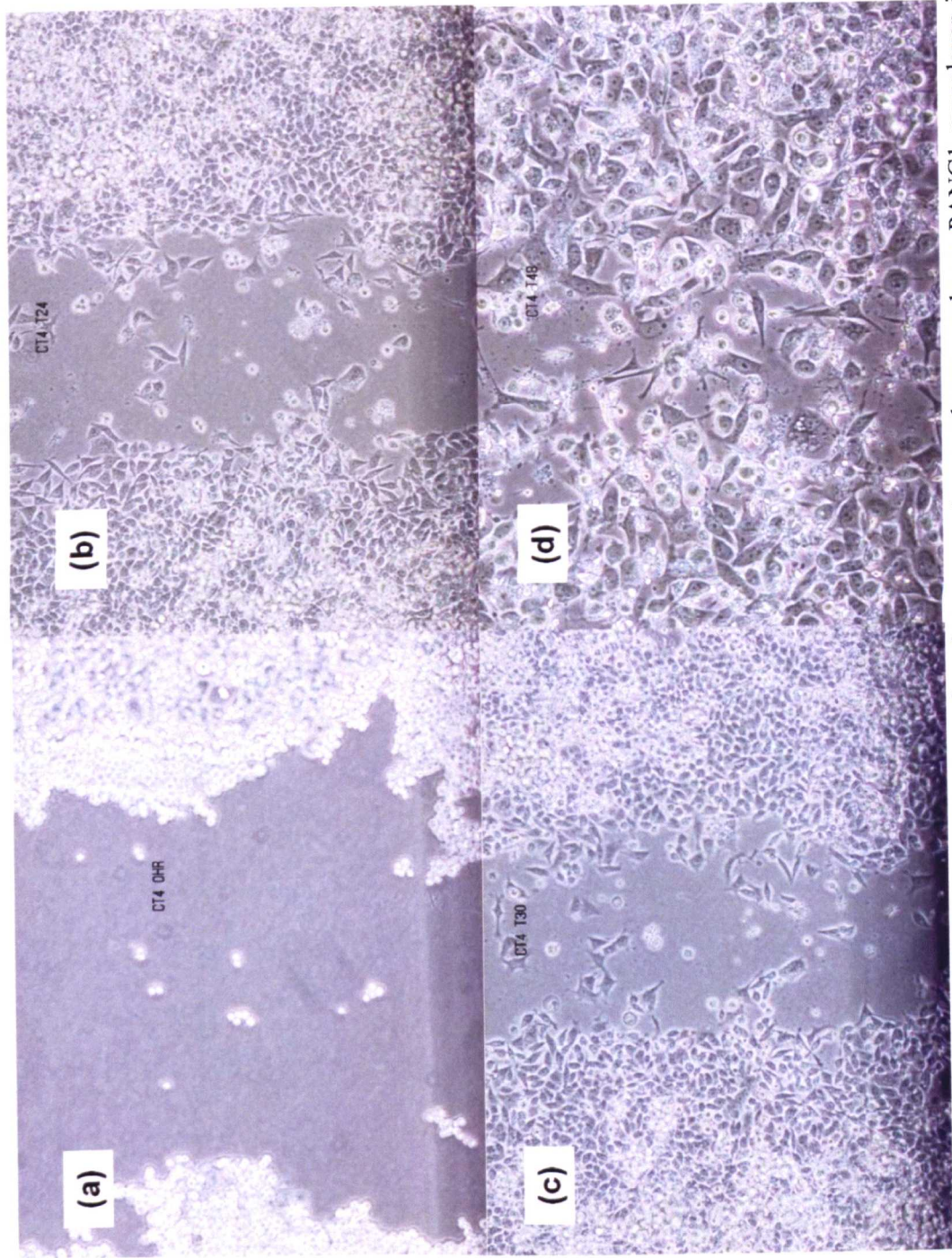
the cytotoxicity of MMS in pancreatic cancer cell lines (Figure 5.15). This result is consistent with MTS assay results (Figure 5.6).

#### **5.2.2.4 Migration assay**

Wound healing assay is a rapid assay for assessing the cell migration. It is performed by wounding a confluent monolayer cell culture and observing the movement of cells into the freshly scratched area. Images are captured at regular intervals to capture cell migration. The images are then analysed to measure the percentage of cell migration compared to untreated control cell line.

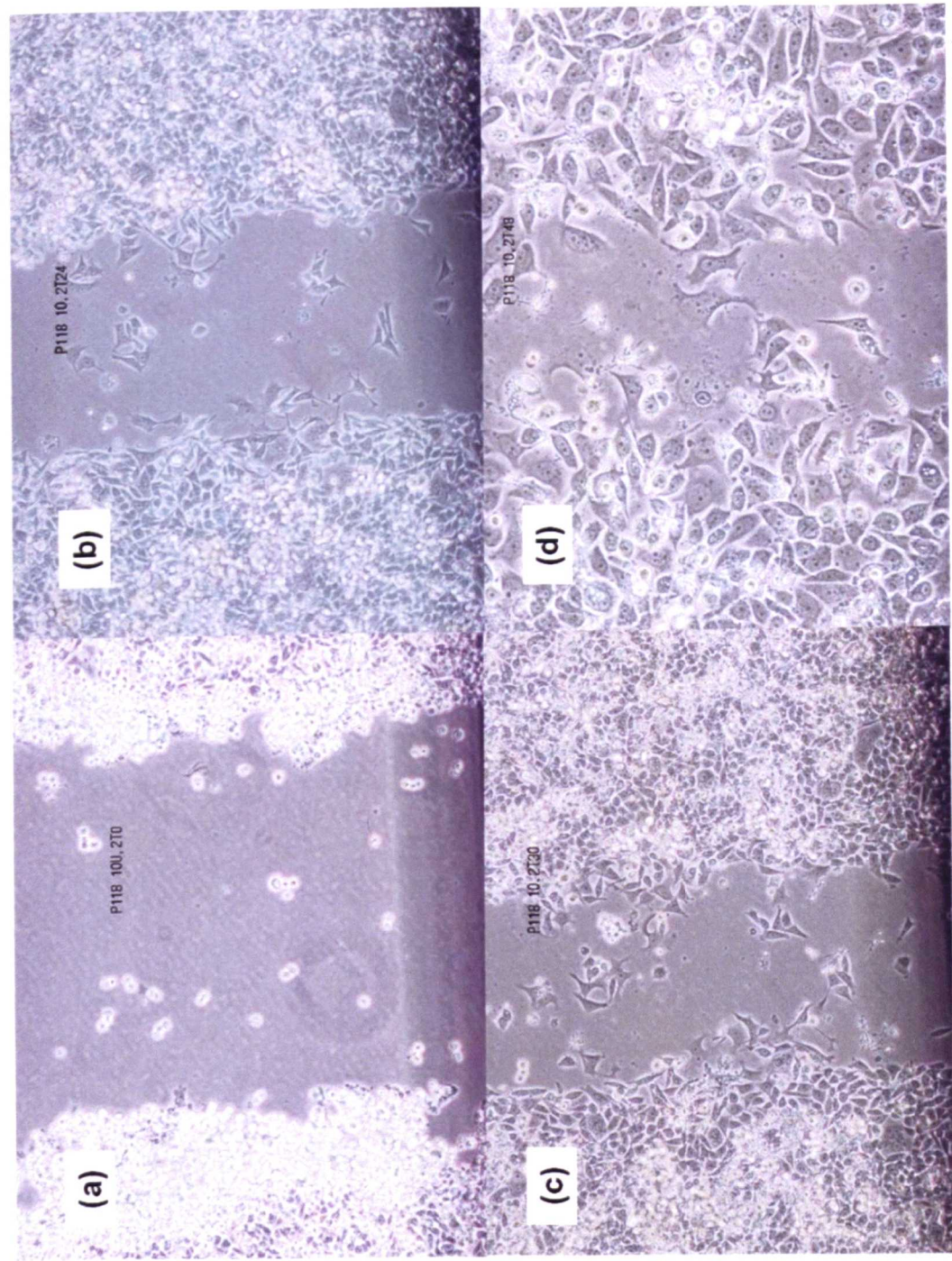
PANC1 cell line monolayers were exposed to two different concentrations of P118 (10 $\mu$ M and 20 $\mu$ M) and a wound was induced. Analysis of images taken over 48 hours showed a significant dose dependant reduction in PANC1 cell migration. At 20 $\mu$ M a significant reduction was seen compared to 10 $\mu$ M (Figures 5.16, 5.17, 5.18 and 5.19). Trials to study the migration assay in SK-Mel30, MeWo (Melanoma) and U89MG (Glioma) cancer cell lines were not successful because of the difficulty to induce wounds on monolayer cell culture of these cancer cell lines.





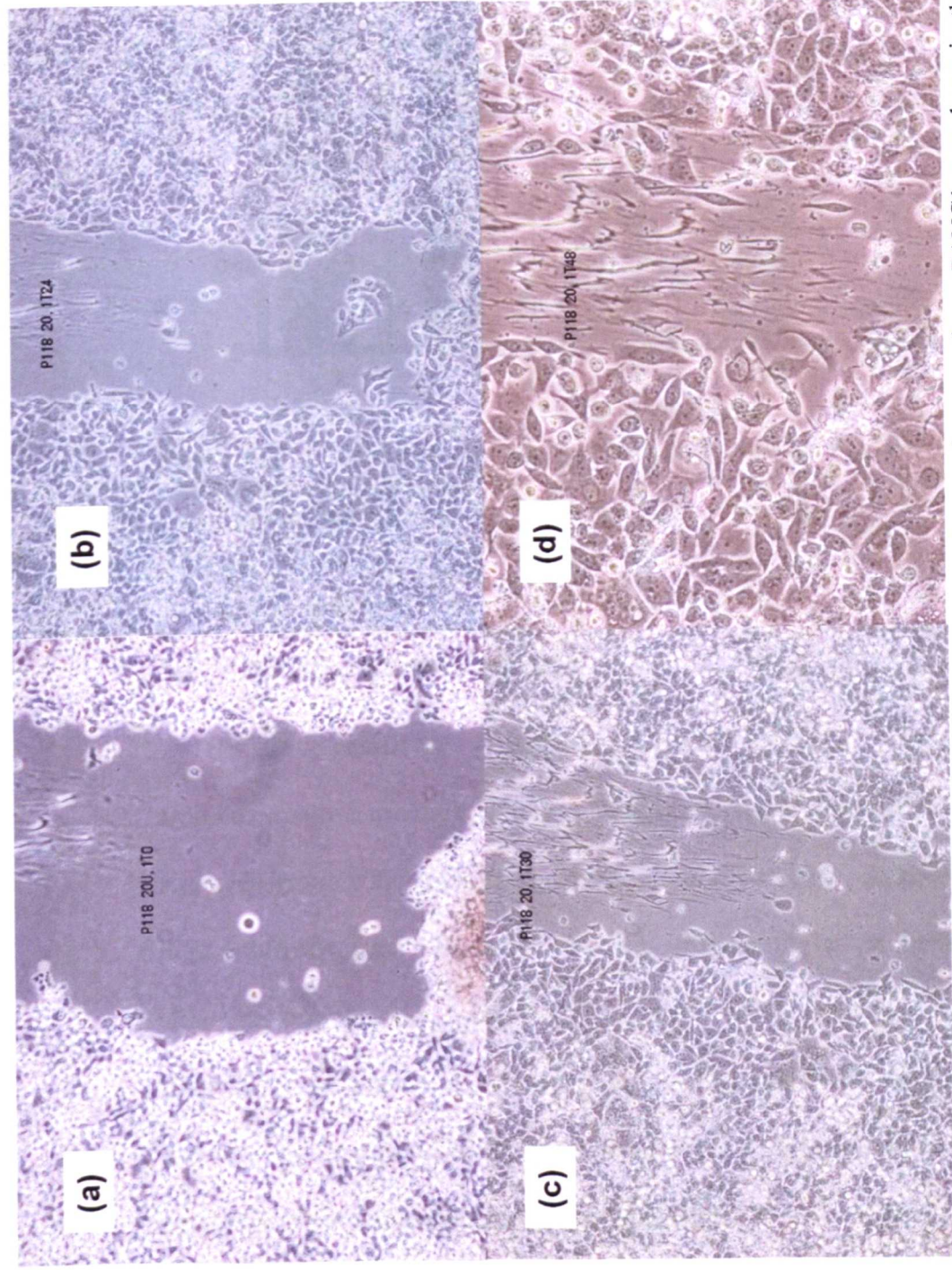
**Figure 5.16 Microscopic pictures showing migration assay.** A wound was made on PANC1 monolayer in absence of P118 and imaged at varying time points: 0 hours (a) 24 hours (b) 30 hours (c) and 48 hours (d).



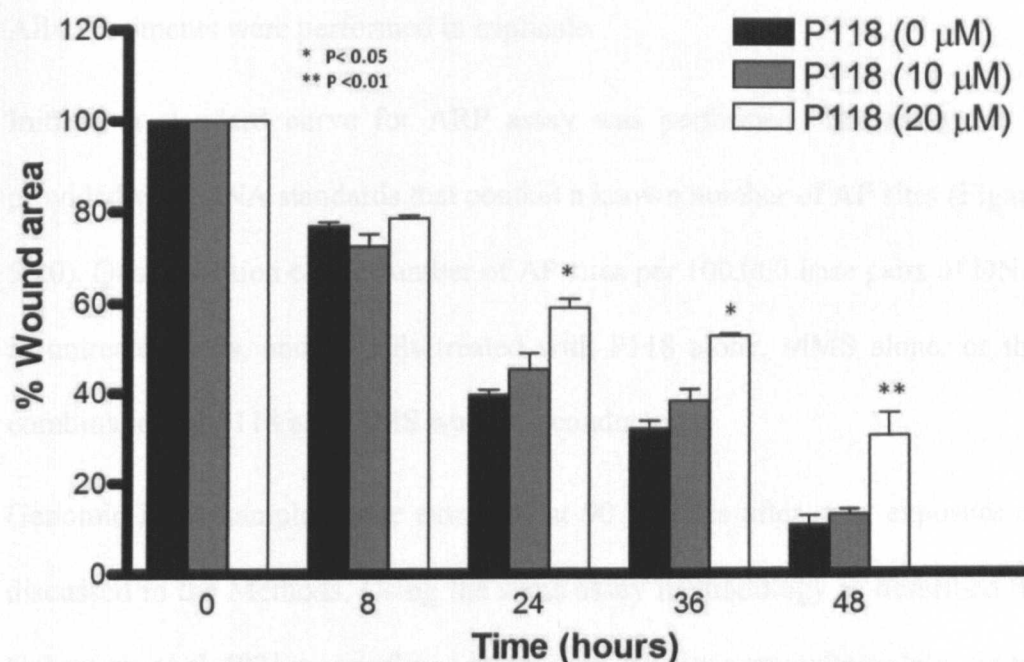


**Figure 5.17 Microscopic pictures showing migration assay.** A wound was made on PANC1 monolayer in the presence of 10  $\mu$ M P118 and imaged at varying time points: 0 hours (a) 24 hours (b) 30 hours (c) and 48 hours (d).





**Figure 5.18 Microscopic pictures showing migration assay.** A wound was made on PANC1 monolayer in the presence of 20  $\mu$ M P118 and imaged at varying time points: 0 hours (a) 24 hours (b) 30 hours (c) and 48 hours (d).



**Figure 5.19** A histogram showing percentage wound area in PANC1 cells in a migration assay. The presence of 20μM of P118 results in a significant decrease in wound healing in PANC1 cells.

### 5.2.3 AP site quantification

The aldehyde reactive probe (ARP) reagent (N'-aminooxymethylcarbonylhydrazino-D-biotin) reacts specifically with the aldehyde group which is in the open ring form of AP sites. This reaction makes it possible to detect DNA modifications that result in the formation of an aldehyde group. In this assay treating genomic DNA containing AP sites with the ARP reagent leads to AP sites being tagged with biotin residues. AP sites can then be quantified using avidin-biotin assay followed by a calorimetric detection of peroxidase conjugated to the avidin.

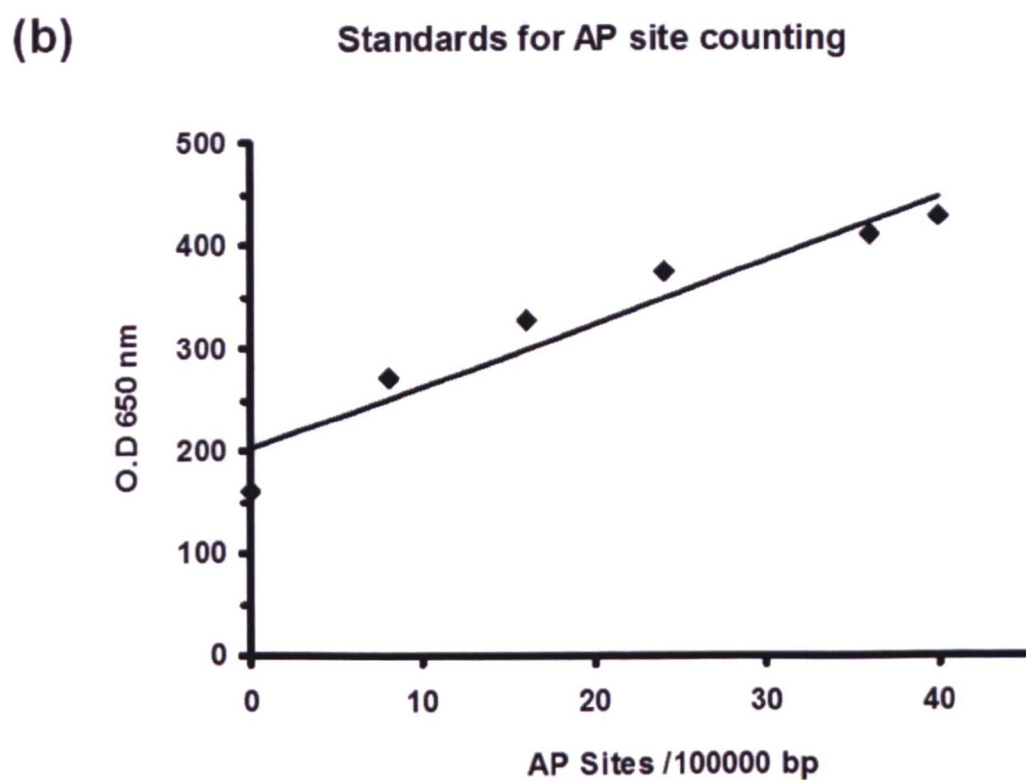
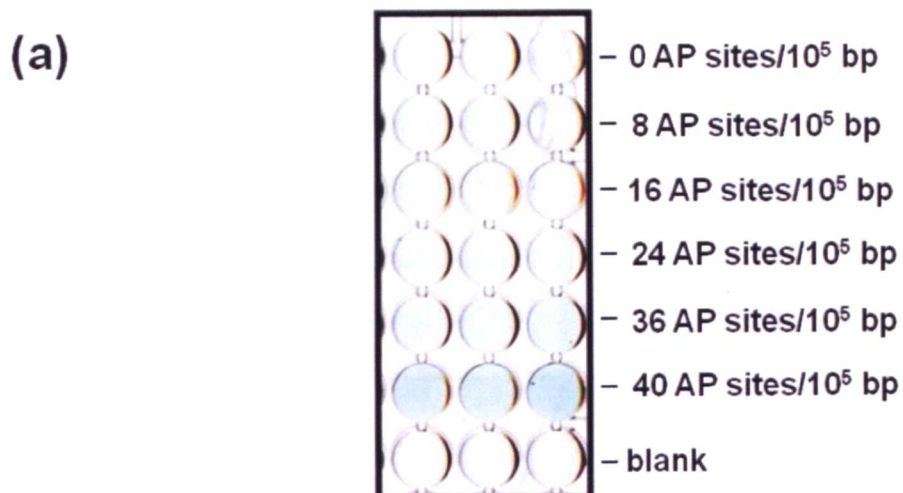
Fung et al. showed that APE1 down-regulation by RNA interference lead to an accumulation of AP sites in the genomic DNA as assessed by the ARP assay [97]. Therefore ARP assay was performed in U89MG and SK-Mel30 cells

exposed to MMS in the presence or absence of specific APE1 inhibitor (P118). All experiments were performed in triplicate.

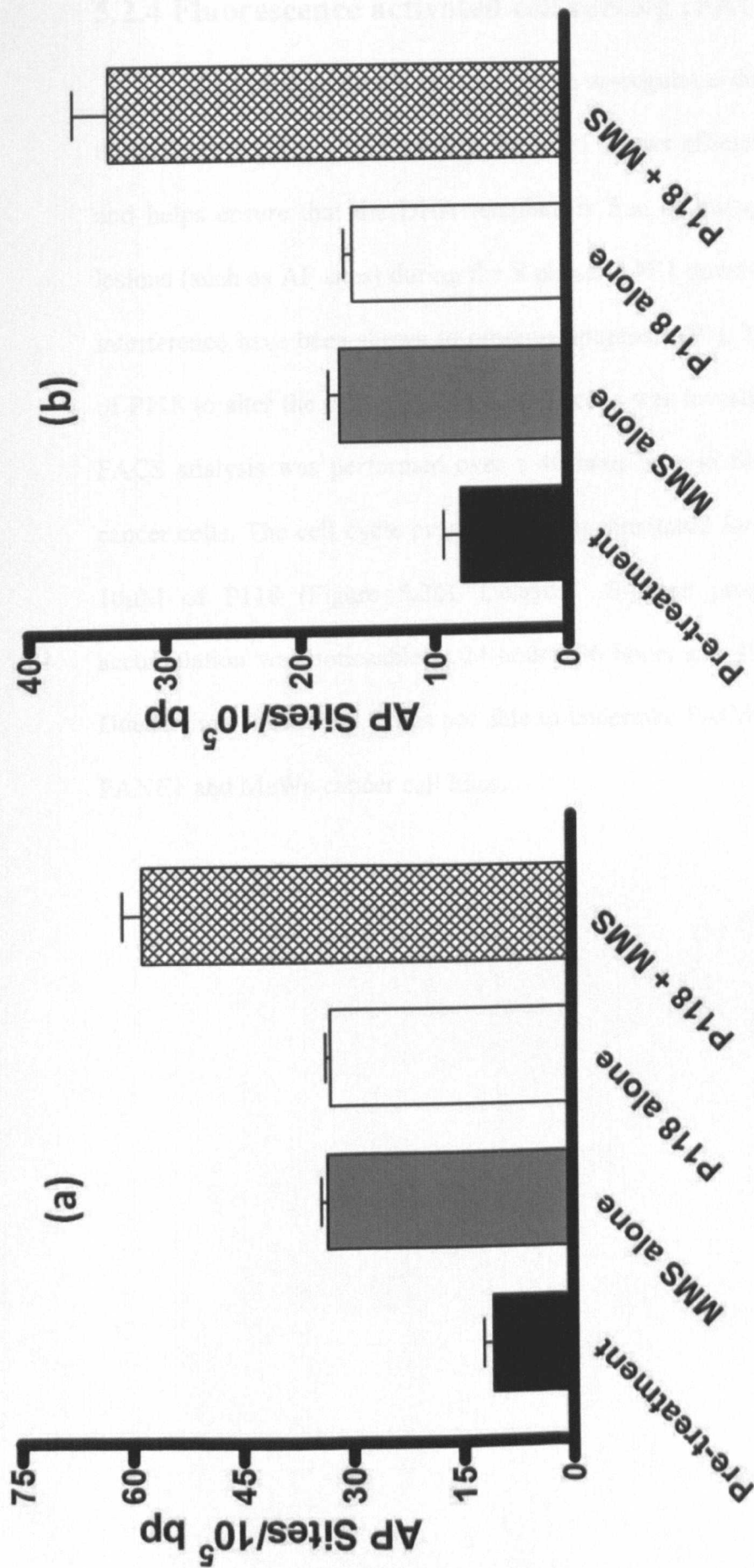
Initially a standard curve for ARP assay was performed. The assay kit is provided with DNA standards that contain a known number of AP sites (Figure 5.20). Quantification of the number of AP sites per 100,000 base pairs of DNA in untreated cells, and in cells treated with P118 alone, MMS alone, or the combination of P118 and MMS was then conducted.

Genomic DNA samples were extracted at 90 minutes after drug exposure as discussed in the Methods. Using the same assay methodology as described by Nakamura et al. [92], a significant increase in AP site accumulation was found in U89MG and SK-mel30 cancer cell lines treated with P118 alone. As expected, MMS also caused an elevation in the level of AP sites. The combination of MMS and P118 led to a further increase in AP site levels. This data confirms that P118 inhibit APE1 activity *in vivo* (Figure 5.21 a and 5.21 b).





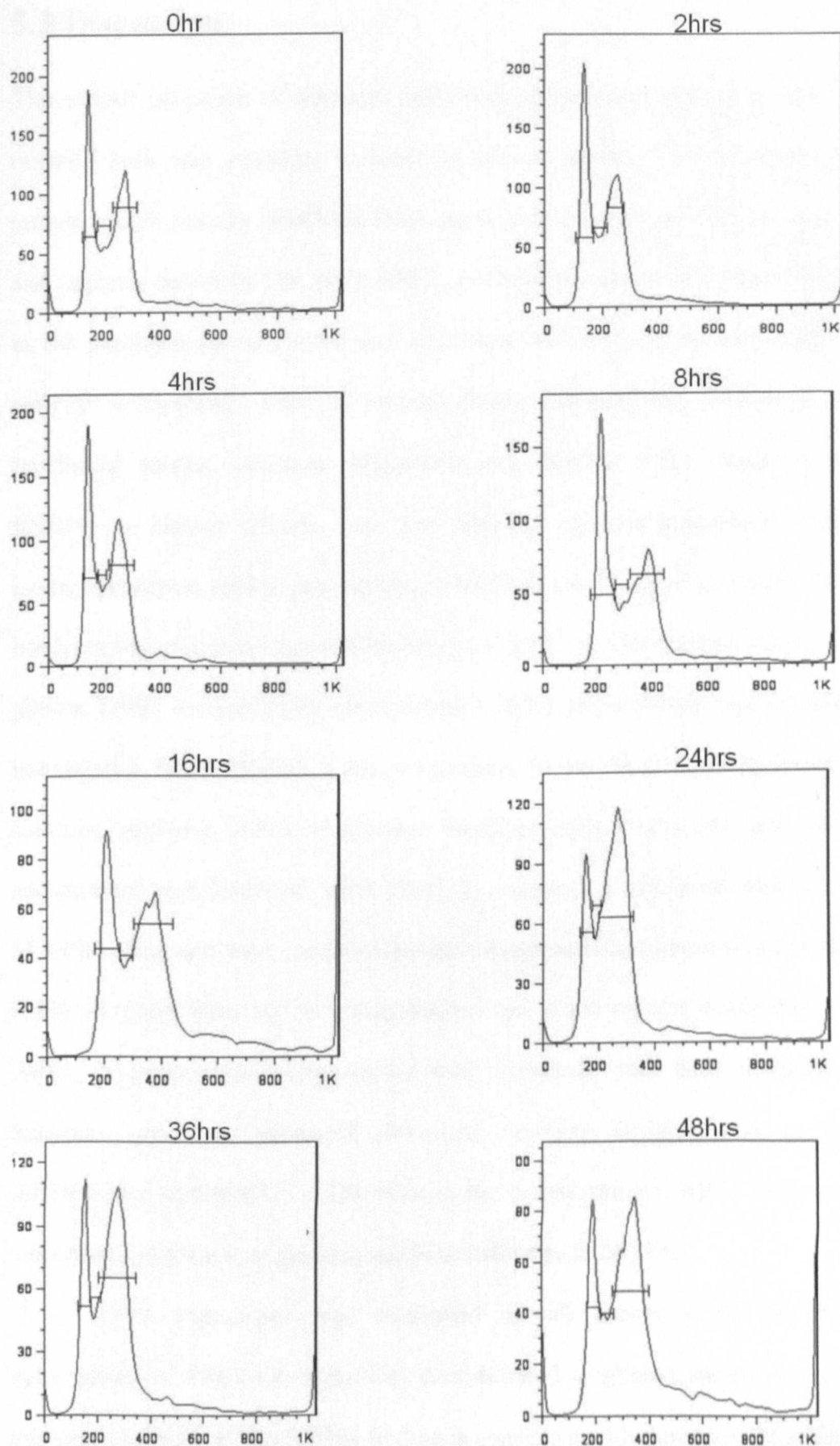
**Figure 5.20 Optimization of AP site quantification assay.** Colorimetric assay for DNA substrates with a known number of AP sites is shown here (a) and the data are represented by x-y plot (b).



**Figure 5.21. AP sites quantification assay.** Histograms show results of cells treated with P118 alone, MMS alone and combination of P118 and MMS in (a) U89MG Glioma (b) SK-Mel30. A small, but statistically significant, increase in AP site accumulation was found in cells treated with P118 alone. As expected, MMS also caused an elevation in the level of AP sites. However, the combination of MMS and P118 led to a further increase in AP site levels, consistent with the notion that P118 was able to inhibit APE1 activity *in vivo*. All experiments were performed in triplicates and the results represent the Mean  $\pm$  S.E.

#### **5.2.4 Fluorescence activated cell sorting (FACS) analysis**

APE1 protein level was shown to be up-regulated during the S-phase of the cell cycle [199]. This increase in APE1 allows efficient DNA replication and helps ensure that the DNA template is free of mutagenic and blocking lesions (such as AP sites) during the S phase. APE1 down-regulation by RNA interference have been shown to promote apoptosis [97]. Therefore the ability of P118 to alter the cell cycle response in cells was investigated. In this assay FACS analysis was performed over a 48 hour time in SK-Mel30 melanoma cancer cells. The cell cycle progression was monitored for the cell exposed to 10 $\mu$ M of P118 (Figure 5.22). Delayed S-phase progression and G2M accumulation was noticeable at 24 hours, 36 hours and 48 hours time points. Due to time constraints, I was not able to undertake FACS studies in U89MG, PANC1 and MeWo cancer cell lines.



**Figure 5.22** FACS analysis of SK-Mel30 cell line exposed to 10  $\mu$ M P118. The presence of P118 altered S-phase progression and led to G2M accumulation in SK-Mel30 cells and was evident at time points between 24 hours and 48 hours.

### 5.3 Discussion

The overall prognosis of advanced melanoma, glioma and pancreatic cancer remains poor and strategies to improve tumour response to chemotherapy remain a high priority. Blocking DNA repair may enhance cell kill in cancer and improve outcomes [20, 267]. APE1, a critical protein in BER, is involved in the pathogenesis of glioma and melanoma. Elevated AP endonuclease 1 activity is frequently seen in human glioma tumours[200]. Moreover in preclinical studies, antisense oligonucleotides directed APE1 depletion in SNB19, a human glioma cell line lacking O(6)-methylguanine-DNA-methyltransferase, lead to potentiation of MMS and temozolomide cytotoxicity implying that pharmacological modulation of APE1 is a promising strategy in glioma [180]. A recent study has demonstrated that microphthalmia-associated transcription factor (MiTF), a key transcription factor for melanocyte lineage survival, regulates APE1 expression. MiTF-positive melanoma cell lines accumulated high levels of APE1 [268]. In a separate study, down-regulation of APE1 using antisense constructs promoted apoptosis in melanoma cell lines [188]. A recent study by our group showed that a sub-cellular localization of APE1 in pancreatobiliary cancer was correlated with poor prognostic features such as perineural invasion, vascular invasion and poorly differentiated tumours[215]. Therefore in the current project, APE1 inhibitors were tested in glioma, melanoma and pancreatic cancer cell lines.

APE1 expression was confirmed in all cancer cells. Intrinsic cytotoxicity of APE1 inhibitors was demonstrated in glioma, melanoma and pancreatic cancer cell lines. This finding is consistent with the observation that APE1 down-regulation in cancer cell lines promotes apoptosis, although non-

specific toxicity at higher doses of these inhibitors cannot be excluded [188]. Interestingly, P118 was relatively non-toxic to HUVEC cells implying selectivity to cancer cells. P118 was shown to potentiate the cytotoxicity of DNA base damaging agents such as MMS and temozolomide. P118 did not potentiate the cytotoxicity of doxorubicin implying that APE1 inhibitors potentiate chemotherapy that only induce base damage and repaired through BER and not by other pathways. P118 delayed cell growth consistent with previous studies where APE1 knock down decreased cell growth rate[97, 183]. P118 also caused a significant inhibition of pancreatic cancer cell migration. P118 led to accumulation of AP sites confirming target inhibition. Accumulation of AP sites was seen with P118 alone or in combination with MMS. This accumulation of AP sites results in delay of S- phase progression and leads to G2-M accumulation.

## ***Chapter 6***

### ***APE1 Knock down studies***

---

## **6. APE1 Knock down studies**

### **6.1 Introduction**

In chapter 5 it was shown the APE1 inhibition by P118 potentiated the cytotoxicity of DNA base damaging agents. The cytotoxicity of P118 was associated with AP site accumulation in cells and resulted in S/G2M cell cycle arrest. Moreover, P118 also inhibited cellular proliferation as well as cell migration.

To complement studies using small molecule APE1 inhibitors and to provide additional validation that APE1 depletion results in cytotoxicity potentiation, I conducted APE1 knock down studies using shRNA technology.

The aim was to generate a stable APE1 knocked down glioma cell line and to study the biological consequences of APE1 depletion.

shRNA Plasmids were purchased from SABiosciences, QIAGEN Company, Frederick, MD, USA (table 6.1). These shRNA plasmids were designed by the manufacturer to knock down the expression of APE1 genes by RNA interference. The plasmid vectors express a short hairpin RNA, or shRNA, under control of the U1 promoter and the neomycin resistance gene (Figure 2.3). Neomycin resistance permits selection of stably transfected cells.

To generate a large quantity of plasmid ready for transfection into cancer cells I initially amplified the plasmid in BL21(DE3) competent bacteria as described below in methods.



**Table 6.1** A table showing the SureSilencing™ shRNA kit components.

Component	Specification	Quantity
shRNA	SureSilencing™ shRNA vector	Four
NC	Negative Control shRNA* vector	One

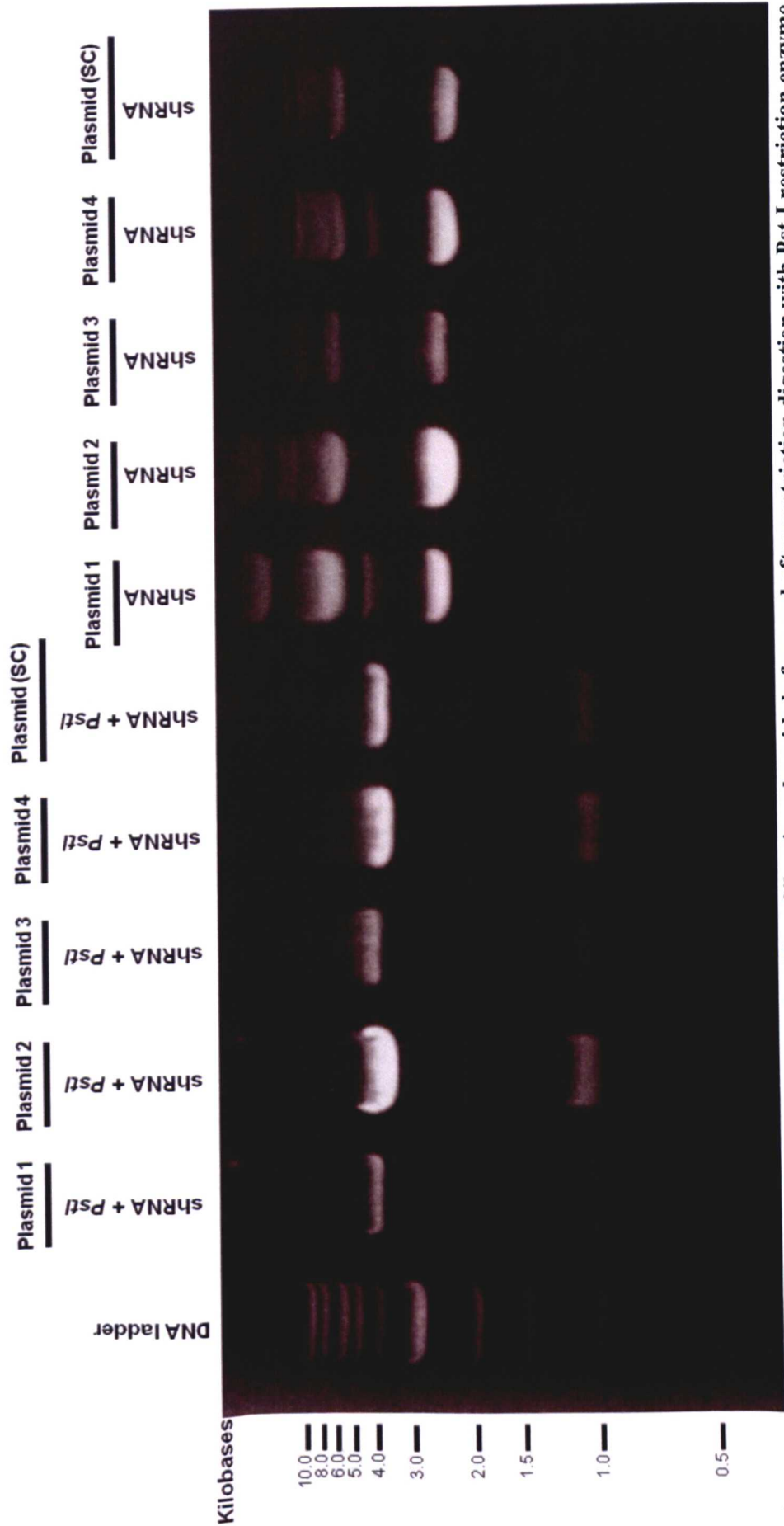
## 6.2 Results

### 6.2.1 Transformation of BL21 (DE3) cells

The plasmids vectors carrying the APE1 shRNA knockdown sequence and the scramble shRNA control were transformed into BL21(DE3) cells. The transformation of these plasmid vectors were accomplished as follow:

Competent cells were incubated with plasmid DNA initially at 4 °C for 60 minutes and then heat shocked at 42 °C for 90 seconds. This procedure facilitates the entry of the plasmid into the cell. Cells were then plated in agar plates containing ampicillin for bacterial selection. The presence of ampicillin resistant colonies would indicate successful transformation. To confirm successful transfection the plasmids were extracted from ampicillin resistant colonies using a maxiprep protocol (described in materials and methods). Isolated plasmids were then restriction digested with *Pst* I. *Pst* I generates two bands of DNA containing 3827 and 991 base pairs respectively that can be visualised in agarose gel electrophoresis (1%) (Figure 6.1).

The plasmid DNA was quantified by spectrophotometer (as described in material and methods) and 0.40 µg of plasmid DNA was used in each transfection experiments.

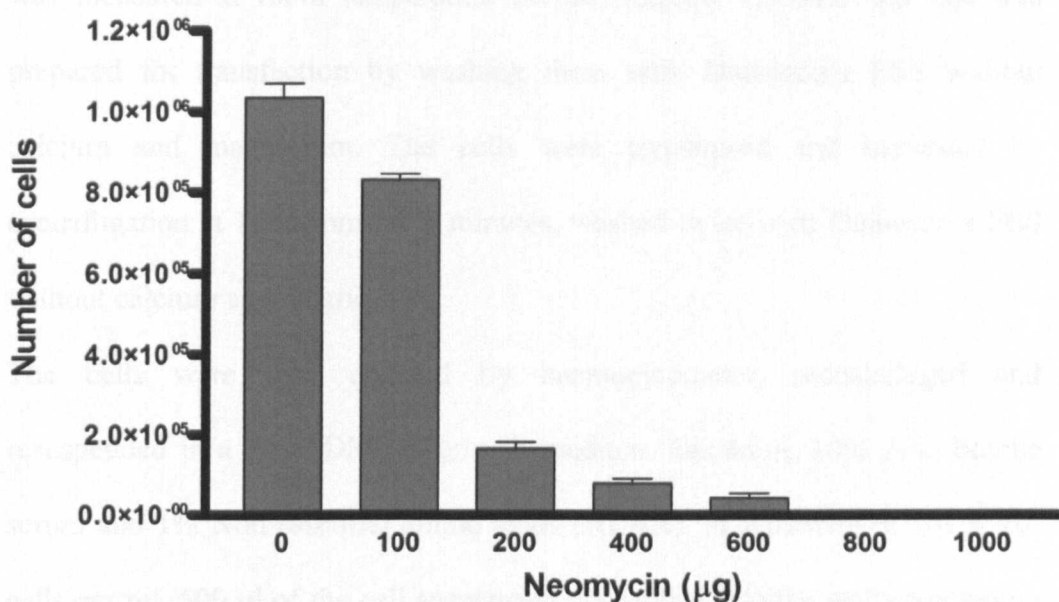


**Figure 6.1 Gel electrophoresis showing bands of SureSilencing plasmids before and after restriction digestion with Pst I restriction enzyme.** Four APE1 knocked down shRNA plasmids [named plasmid 1, 2, 3, and Plasmid 4] together with negative control plasmid with scrambled sequence (Plasmid (SC)) were extracted and digested using *Pst*I and run in parallel with undigested plasmid. Lane 1 corresponds to the DNA ladder, lanes 2-6 corresponds to plasmids 1, 2, 3, 4 and scrambled shRNA plasmids before the restriction digestion. The presence of 2 bands around 1000 and 4000 base pair range indicates successful amplification according to the manufacturer protocol.

### **6.2.2 Minimum effective dose determination**

Prior to transfection, the minimum neomycin concentration (also called minimum effective dose) that results in total cell killing of U89MG glioma cancer cell line was determined. U89MG was exposed to increasing dose of neomycin and a dose responses curve was plotted. As shRNA plasmids carry a neomycin resistance gene mammalian cells transfected with this plasmid will be resistant to neomycin compared to untransfected cells and should results in neomycin resistance and normal cell growth. A dose response curve for minimum effective dose of neomycin was generated as below.

U89MG cells were seeded in 12-well tissue culture plates at 10% confluence and incubated in a fresh media containing an increasing dose of neomycin at concentrations 0, 100, 200, 400, 600, 800, and 1000 µg/ml. The plates were then maintained in a humidified incubator at 37 °C and 5% CO<sub>2</sub>. The media was replaced every 2 days with neomycin. On day 6, the plate with neomycin reached confluence. The minimum concentration of neomycin that kills all the cells is the effective concentration that will be used for the selection. The cells in each well were counted and a dose response graph was plotted (Figure 6.2). 800 µg of neomycin was demonstrated to be the minimum killing dose of neomycin in U89MG cells. This concentration was used in the subsequent experiments for selection after transfection.



**Figure 6.2 A histogram showing the minimum effective dose determination of neomycin in glioma cell line.** U89MG cells were seeded into each well of 12-well plates to produce 10% confluence. A fresh media containing increasing dose of neomycin was added to the well and plates were incubated at 37 °C. When the zero dose well reached 100% confluence, cells were counted and a dose dependent toxicity was demonstrated. 800 μg of Neomycin was the minimum dose that resulted in 100% glioma cell death. This dose was considered as the effective dose and was used for subsequent experiment as a selective concentration. All experiments were performed in triplicates and the results represent the Mean ± S.E.

### 6.2.3 APE1 knock down in U89MG glioma cell line

Out of 3 shRNA plasmids supplied by manufacturer a study by an MSc student in the laboratory had identified one plasmid that was successful in knocking down APE1 in breast cancer cells. Therefore this plasmid was used in transfection experiment in U89MG glioma cells.

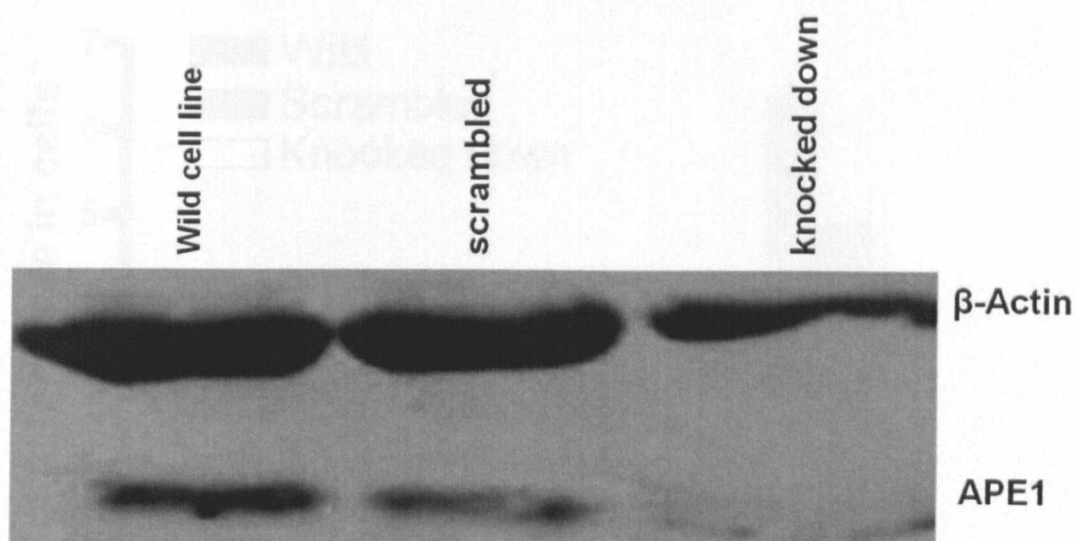
The transfection of U89MG with shRNA plasmids was performed as below: 100 μl of Opti-MEM™ I Reduced-Serum Medium was added into the appropriate well of a 24-well cell culture plate to which 0.4 μg of APE1 shRNA plasmid was then added and mixed by gently shaking. 3 μl of SureFECT (transfection reagent) was added and mixed gently and the plate

was incubated at room temperature for 20 minutes. U89MG cell line was prepared for transfection by washing them with Dulbecco's PBS without calcium and magnesium. The cells were trypsinised and harvested by centrifugation at 1000 rpm for 5 minutes, washed twice with Dulbecco's PBS without calcium and magnesium.

The cells were then counted by haemocytometer, recentrifuged and resuspended in a fresh DMEM growth medium containing 10% fetal bovine serum and 1% Non essential amino acids (NEAA), to a density of  $1.6 \times 10^6$  cells per ml. 500  $\mu$ l of the cell suspension was added into the wells containing the SureFECT-plasmid complexes. The suspension was mixed gently and the cells were incubated at 37 °C and 5% CO<sub>2</sub> for 48 hours. Cells were then harvested and transferred to 6-well tissue culture plates. Two wells were used per plasmid and each well was seeded at 10% confluent. A fresh media containing neomycin at concentration of 800  $\mu$ g/ml was added and the cells were maintained at 37 °C and 5% CO<sub>2</sub> for 6-7 days. The media with neomycin were replaced every 72 hours.

U89MG cells transfected with shRNA plasmids were maintained under neomycin antibiotic selection for about 6 weeks at a dose of 800  $\mu$ g/ml. The neomycin concentration was then lowered gradually from 800  $\mu$ g/ml to 400  $\mu$ g/ml and the cells were maintained under this selective concentration. In order to confirm APE1 knock down a western blot analysis was performed (Figure 6.3). Compared to wild type and cells treated with scrambled plasmids, cells transfected with APE1 shRNA showed more than 90% knock down in APE1 expression.



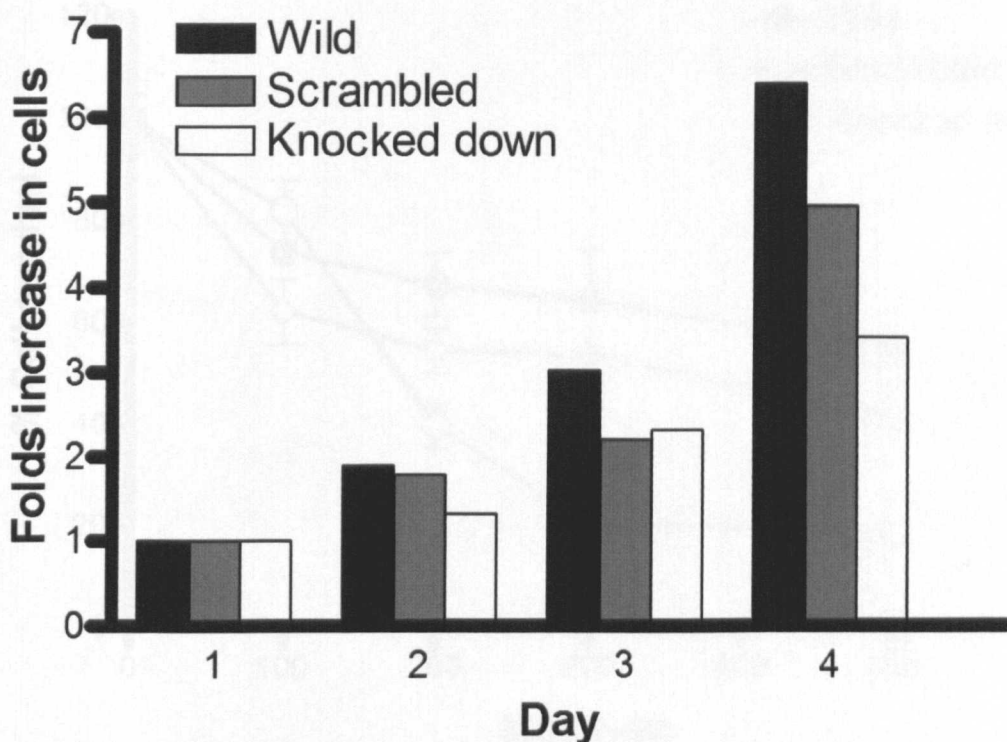


**Figure 6.3 Western blotting showing shRNA knock down of APE1 expression in U89MG cell line.** The first lane is the wild type U89MG cell line where APE1 protein is significantly expressed. The second lane is U89MG cell line transfected with scrambled shRNA plasmid (negative control). APE1 protein is still very well expressed in this cell line. However, the last lane is U89MG cell line transfected with APE1 shRNA plasmid. APE1 expression is decreased by more than 90% compared to wild type control.

## 6.2.5 Biological consequence of APE1 knock down in U89MG cells

### 6.2.5.1 Growth curve

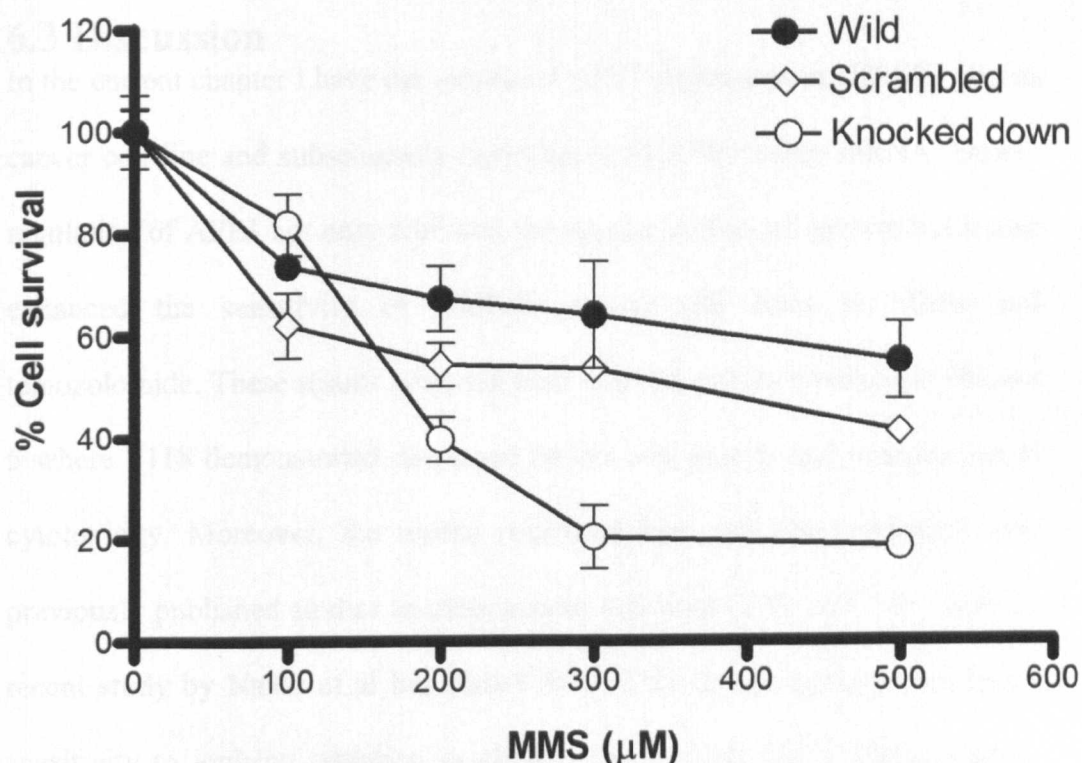
$10^5$  cells of wild type, scrambled and APE1 knocked down U89MG cells were seeded into T25 tissue culture flasks and the cellular proliferation and doubling time was monitored over four days incubation. The folds increase in cell numbers compared to day 1 was plotted. APE1 knocked down cells demonstrated reduced cell proliferation compared to wild type and scrambled control (Figure 6.4) this result is consistent with those seen with P118, a specific inhibitor of APE1 (Figure 5.14 d , chapter 5).



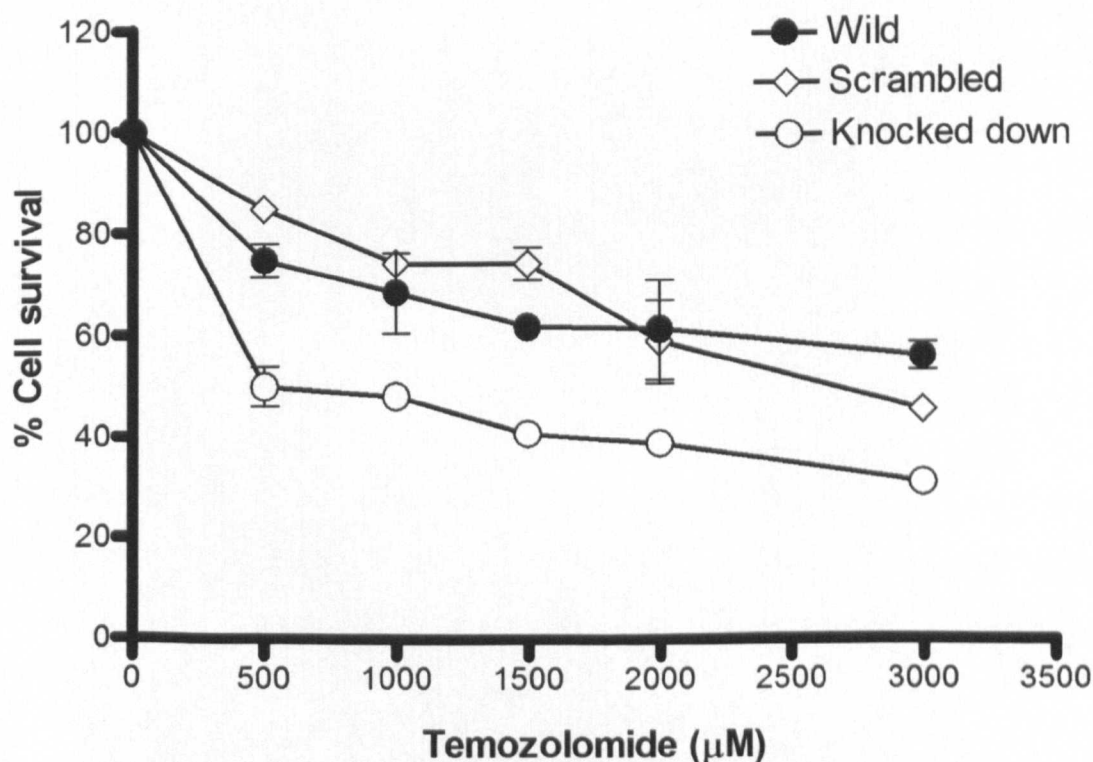
**Figure 6.4** Histograms shows the growth curve in wild type U89MG and U89MG cell line transfected with scrambled and shRNA plasmids.  $10^5$  of U89MG wild type, and U89MG transfected with scrambled and shRNA plasmids were seeded into T25 tissue culture flasks. The cell numbers were monitored over a period of four days incubation and the folds increase in cell number compared to day 1 were calculated. APE1 knock down in U89MG glioma cancer cell line results in significant decrease in the growth compared to wild type cells and negative control. All experiments were performed in triplicates and the results represent the Mean  $\pm$  S.E. (Note St Errors are very small numbers)

#### 6.2.5.2 CellTiter 96<sup>®</sup> AQueous Non-Radioactive Cell proliferation and survival Assay (MTS)

To investigate whether knock down of APE1 in U89MG glioma cells line had any biological consequence, MTS cell proliferation assay were undertaken and compared to cells with normal expression of APE1. APE1 knocked down cells were significantly more sensitive to MMS compared to wild type and scrambled U89MG (Figure 6.5). Similar sensitivity was also seen with temozolomide (Figure 6.6). This result is consistent with those seen using P118, a specific inhibitor of APE1 (Figure 5.7 and 5.11, chapter 5).



**Figure 6.5 MTS assay.** APE1 knock down in U89MG cell line resulted in significant increase in MMS toxicity compared to wild cell line and cells transfected with scrambled plasmid. All experiments were performed in triplicates and the results represent the Mean  $\pm$  S.E.



**Figure 6.6 MTS assay.** APE1 knock down in U89MG cell line resulted in significant increase in temozolomide toxicity compared to wild type cells and cells transfected with scrambled plasmid. All experiments were performed in triplicates and the results represent the Mean  $\pm$  S.E.



### **6.3 Discussion**

In the current chapter I have demonstrated APE1 expression in U89MG glioma cancer cell line and subsequently downregulated APE1 using shRNA. Down-regulation of APE1 not only inhibited the glioma cancer cell growth but it also enhanced the sensitivity of U89MG cancer cell lines to MMS and temozolomide. These results are consistent with the results obtained in chapter 5 where P118 demonstrated decreased cancer cell growth and potentiation of cytotoxicity. Moreover, the results presented here are also consistent with previously published studies in other cancer cell lines [178, 183, 201, 266]. A recent study by Naidu et al has shown that APE1 down regulation increases sensitivity to ionising radiation in glioma cancer cells [221]. These studies, including mine suggest that APE1 inhibition could be promising strategy to enhance chemotherapy and radiotherapy in glioma patients.

## ***Chapter 7***

### ***Biochemical analyses of P118 analogues***

---

## **7. Biochemical analyses of P118 analogues**

### **7.1 Introduction**

Structure-activity relationship (SAR) study is a key component to drug discovery [269]. In the process of hit series generation, focus on compound series with structural similarities can generate analogues that can be tested for SAR hypotheses. Computational models can be built to support the analogue design process and predict the activity of test compounds [270].

In the previous chapters it was shown that virtual screening and biochemical screening identified P118, a promising APE1 inhibitor. Structural features and predicted pharmacological properties suggest that P118 is a potential candidate for further drug development.

Furthermore, P118 resulted in decreased cancer cell growth, associated with AP site accumulation and potentiation of cytotoxicity of MMS and temozolomide in panel of cancer cell lines.

Therefore this PhD project was taken a step further to study P118 analogues

In virtual screening there are two types of techniques that can be used in SAR studies: ligand-based design and structure-based design. Ligand-based design methods capitalize on the fact that ligands similar to an active ligand are more likely to be active than random ligands. Ligand-based approaches commonly consider two- or three-dimensional chemistry, shape, electrostatic, and interaction points (e.g., Pharmacophore points) to assess similarity. On the other hand structure-based design attempts to use the 3D protein structure to predict which ligands will bind to the target. Ligand similarity approaches require only a single

active molecule, which may come from the literature, patents, or in-house experimental data. P118 was therefore selected for a ligand-based similarity search strategy.

Ligand-based Quantitative Structure-Activity Relationship (QSAR) approaches require a number of active molecules spanning a wide range of activity against the target receptor (three orders of magnitude is the minimum range). The quality of the QSAR model depends to a large extent on the quality of the activity data, such that they are reliable. QSAR models are usually built based on carefully acquired binding or inhibition data.

To conduct the similarity search, the zinc search tool available online (<http://zinc.docking.org/choose.shtml>) was used to sketch P118 structure in 2D. A 99% similarity search was chosen and the search resulted in fifty six P118 analogues.

## **7.2 Results**

### **7.2.1 Biochemical screening**

The structures of the fifty six P118 like analogues were physically examined by Dr Charlie Laughton Reader in Molecular Recognition, School of Pharmacy, University of Nottingham. Nine compounds were selected for biochemical analysis (Table 7.1). Initial screening was conducted at 100 $\mu$ M.

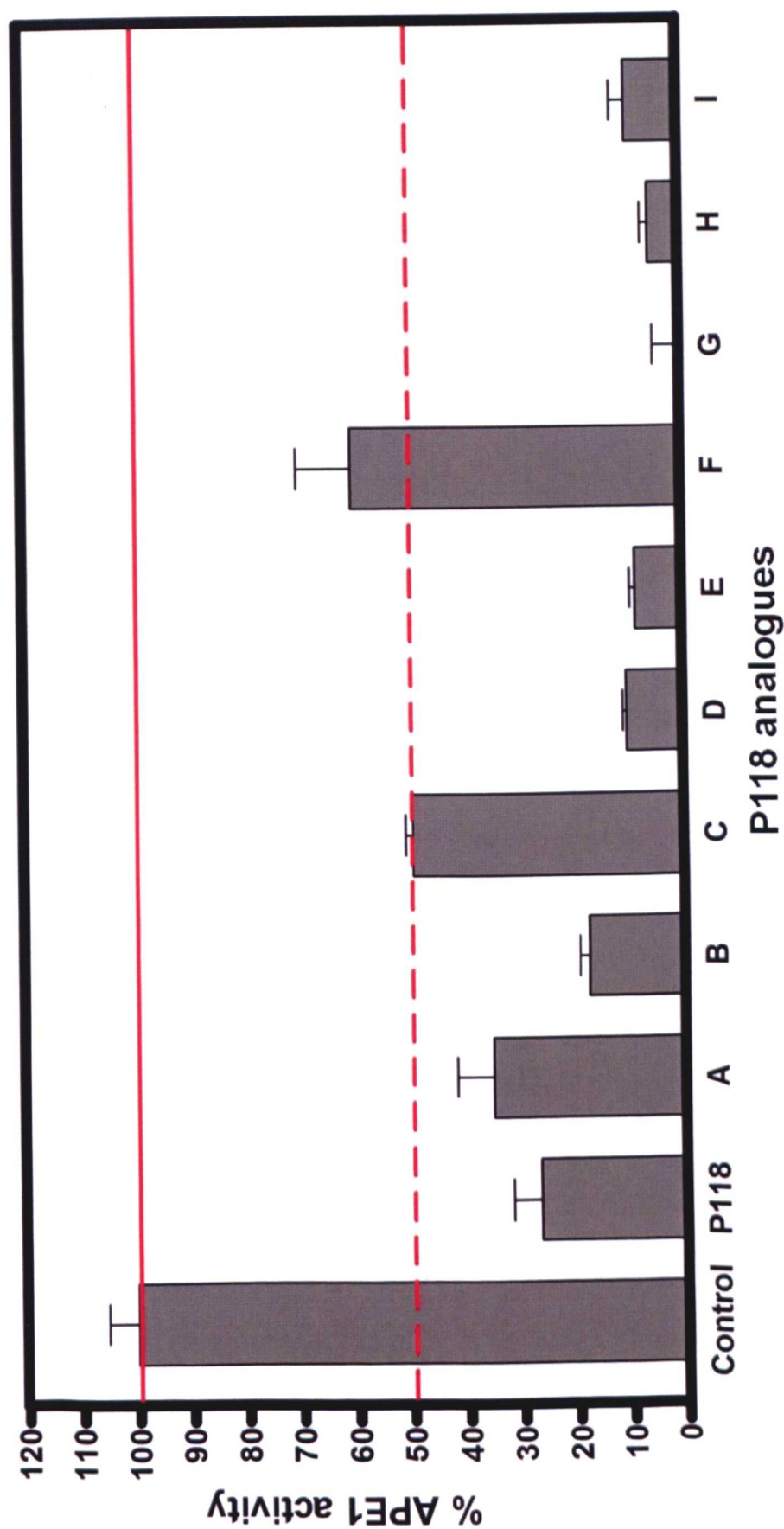
Compounds were purchased and screened using the fluorescence based APE1 AP-site cleavage assay (as described in chapter 4). Compounds D, E, G, H and I achieved more than 90% inhibition to AP endonuclease activity of APE1 (Figure 7.1 and Table 7.2). Compounds A, B and C could inhibit between 50-83% of the total APE1 activity (table 7.2). Whereas compound F showed less than 40%

inhibition of APE1 activity. The  $IC_{50}$  was estimated by expanding concentration as described previously (chapter 4).  $IC_{50}$  ranged from 100 nM to more than 100  $\mu$ M. Compounds D, E, G, H and I were more potent APE1 inhibitors and achieved 10-100 folds increase in APE1 inhibition compared to P118 (Table 7.2).

The compounds were then counter screened against endonuclease IV. All the nine screened compounds had no inhibitory activity against endonuclease IV implying that these compounds are specific for APE1 similar to P118 (Table 7.2). The compounds were then tested for any intrinsic fluorescence quenching activity and were all shown to be non quenchers (Figure 7.2). Therefore the data from the biochemical assay confirm that the nine P118 analogues are specific APE1 inhibitors with  $IC_{50}$  ranging from 100 nM to >100  $\mu$ M.

**Table 7. 1** A table shows the nine P118 analogues. XlogP = octanol/water partition coefficient, Mwt. = molecular weight.

Compound	xLogP	Mwt.
P118	5.41	482.558
A	6.22	561.454
B	6.09	517.003
C	5.86	496.585
D	5.26	494.594
E	5.29	524.62
F	6.07	492.622
G	5.13	486.521
H	5.41	482.558
I	4.96	468.531

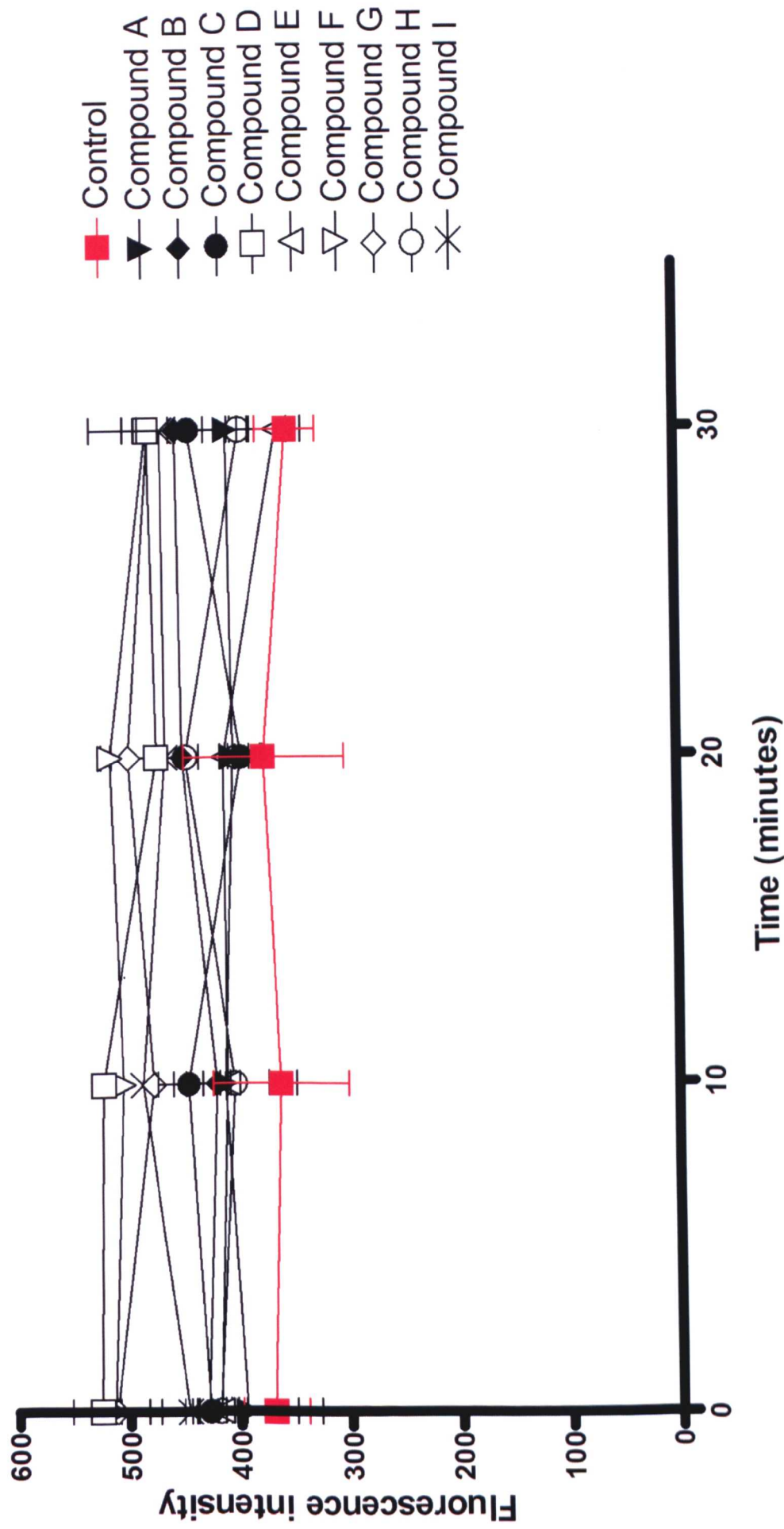


**Figure 7.1 Histograms showing the results of fluorescence based APE1 AP-site cleavage assay.** 100  $\mu$ M of P118 and P118 analogues were incubated in a reaction containing 5 nM of APE1, 5 nM Oligonucleotide DNA substrate under same buffering condition (in chapter 4). APE1 inhibition ranged from 40%- 99%. The continuous read line marks 100% APE1 activity, while the interrupted red line represents 50% APE1 activity. All experiments were performed in triplicates and the results represent the Mean  $\pm$  S.E.

Table 7.2 A table summarises the results of biochemical screening of P118 analogues.

<i>Hit name</i>	<i>% APE1 activity at 100µM</i>	<i>Endonuclease IV inhibition</i>	<i>Fluorescence quenching</i>	<i>IC<sub>50</sub></i>
A	35.0 ± 6.7	–	–	5 µM
B	17.6 ± 1.7	–	–	5 µM
C	49.5 ± 1.4	–	–	100 µM
D	10.3 ± 0.6	–	–	0.7 µM
E	8.6 ± 0.9	–	–	0.2 µM
F	60.3 ± 10	–	–	>100 µM
G	1.0 ± 4.9	–	–	0.5 µM
H	5.6 ± 1.3	–	–	0.2 µM
I	9.6 ± 2.7	–	–	0.1 µM
P118	12.0 ±3.5	–	–	11.6 µM





**Figure 7.2 Fluorescence quenching assay.** 100  $\mu$ M of P118 analogues incubated with 5 nM oligonucleotide DNA substrate and incubated under same buffering condition for APE1 AP-site cleavage assay. Serial measurement of fluorescence emission every 5 minutes were taken for 30min. P118 analogues did not show any fluorescence quenching effect. The red line with red points indicate the fluorescence emission of the control wells that contains the fluorescence tagged DNA substrates. All experiments were performed in triplicates and the results represent the Mean  $\pm$  S.E.

## 7.3 Discussion

There were a large number of P118 analogues in the ZINC database and a 99% similarity search identified 56 structural analogues.

Biochemical screening of the nine P118 analogues had shown that all the hits were able to block APE1 ( $IC_{50}$ : 100 nM - 100  $\mu$ M). This confirms that the pharmacophore of P118 is a consistent and potent APE1 inhibitor. Although the mechanism of action of these analogues is currently unknown, their mode of activity is very likely to be similar to P118. Kinetic analyses suggest uncompetitive inhibition for P118. Co-crystallization studies, currently underway in the laboratory, will provide further structural insights.

In conclusion, this small analogue series study provides convincing evidence for further series expansion to enable further SAR studies.

## ***Chapter 8***

### ***General discussion and conclusions***

---

## **8. General discussion and conclusions**

### **8.1 General discussion**

Monofunctional alkylating agents are routinely used in the treatment of patients with advanced melanoma and glioma. However, the response rate to chemotherapy is modest and the overall prognosis is poor. The cytotoxicity of alkylating agents is directly related to their propensity to induce genomic DNA damage. However, the ability of cancer cells to recognize this damage and initiate DNA repair is an important mechanism for therapeutic resistance that negatively impacts upon therapeutic efficacy. Pharmacological inhibition of DNA repair, therefore, has the potential to enhance the cytotoxicity of alkylating agents and improve patient outcomes[20, 267].

The BER pathway is critically involved in the repair of bases that have been damaged by alkylating agents such as temozolomide and dacarbazine [12]. Although there is more than one sub-pathway of BER, in most cases base excision is initiated by a DNA glycosylase, which recognizes a damaged base and cleaves the N-glycosidic bond, leaving a potentially cytotoxic AP site intermediate [107]. This product is a target for the human APE1. The DNA repair domain of APE1 cleaves the phosphodiester backbone on the 5' side of the AP site resulting in a single-strand break, which is further processed by proteins of the BER pathway. APE1 accounts for over 95% of the total AP endonuclease activity in human cell lines[120]. In addition to its DNA repair activity, APE1 also performs functions such as redox regulation (mediated through a separate redox domain) and transcriptional regulation [156, 164, 167]. APE 1 is a member of the highly conserved exonuclease III family of AP endonucleases, named after the *E. coli* homologue of APE1 [101]. The

endonuclease IV family of AP endonucleases, the prototypical member of which is *E. coli* endonuclease IV [108], is structurally unrelated to APE1, despite being able to carry out the comparable AP site incision reaction [103-105].

Using either antisense oligonucleotides or RNA interference approaches, several groups have reported that depletion of intracellular APE1 sensitizes mammalian cells to a variety of DNA damaging agents [157, 179, 180]. In melanoma cell lines, APE1 down-regulation led to increased apoptosis, whereas APE1 overexpression conferred protection from chemotherapy- or hydrogen peroxide-induced apoptosis [188]. Antisense oligonucleotides directed APE1 depletion in SNB19, a human glioma cell line lacking O(6)-methylguanine-DNA-methyltransferase, lead to potentiation of MMS and temozolomide cytotoxicity [180].

In patient tumours, APE1 expression may have prognostic and/or predictive significance. In a recent study by our group, APE1 expression was shown to have prognostic significance in ovarian, gastrooesophageal and pancreaticobiliary cancers [215]. APE1 is also aberrantly expressed in other human tumours and strong nuclear expression has consistently been observed in these studies [271]. In head and neck cancer, nuclear localisation of APE1 was associated with resistance to chemoradiotherapy and poor outcome [211], and in cervical cancer, an inverse relationship between intrinsic radiosensitivity and levels of APE1 has been demonstrated [218].

Preclinical and clinical studies suggest that APE1 is a viable anticancer drug target. A drug discovery programme was initiated in our laboratory to identify small molecule inhibitor-lead compounds of APE1 [23]. Fluorescence-based

high throughput screening of a chemical library, as well as biochemical and cellular investigations were undertaken. CRT0044876 (7-nitro-1Hindole- 2-carboxylic acid) was identified and characterised by our group as the first small molecule inhibitor of APE1 that potentiated the cytotoxicity of alkylating agents such as temozolomide [23]. The ability of CRT0044876 to block BER has also been demonstrated independently by other investigators [249, 251]. In a recent study, BER inhibition using CRT0044876 was shown to confer selectively enhanced cytotoxicity in an acidic tumour microenvironment [250]. However, the ability of CRT0044876 to block BER has not been consistently demonstrated by other groups [248] implying that further work needs to be done before a genuine lead inhibitor could emerge.

In the current PhD project I adopted a structure-based drug design strategy to identify APE1 inhibitors. In order to develop novel drug-like chemotypes, a virtual screening approach was taken. The architecture of the active site of APE1 in the absence and presence of bound AP-DNA indicates that there is little or no remodelling of the active site upon substrate binding, a feature that is suitable for a virtual screen [103, 104]. I have exploited the structural features of APE1 to develop an enhanced virtual screening strategy and identified several novel small molecule inhibitors for further drug development. Three new pharmacophore templates were designed *in silico* (M1, M2 and M3) and a total of 1679 virtual hits with similarities to the templates were identified (CRT template = 359, M1 template = 373, M2 template = 459 and M3 template = 488). Detailed biochemical screening showed that 17/147 (11.5%) of the chemical library screened were potent

APE1 inhibitors in the biochemical assay. This confirms the validity of using the virtual approach in identifying APE1 inhibitors compared to direct screening of a large chemical library approaches used in previous studies. In these studies the APE1 inhibitor identified represented 0.02% [23], 0.5% [252], 0.005%[255] of the chemical library screened. However, the majority of the compounds isolated in my PhD study belonged to the M3 template which bears an additional heteroaromatic side chain that can access a subsidiary cleft in one branch of the ligand-binding. Although the structural details of M3 template binding to APE1 active site is unknown, cocrytallization trials may provide structural insight to guide a rational drug-design strategy.

My approach allowed the identification of several novel APE1 inhibitors. The hits have potential for series expansion and further drug development. I have also presented preclinical data to support APE1 modulation as a particularly promising new strategy in melanoma and glioma where alkylating agents remain an important treatment modality. In addition, APE1 modulation may also be a promising strategy in pancreatic cancer.

In this study, I also provide evidence for the first time that certain APE1 inhibitors may be more effective in blocking the endonuclease activity of the APE1 D148E polymorph a common polymorph associated with cancer predisposition compared with the wild type. The inability of seventeen of the twenty four compounds examined to inhibit the activity of endonuclease IV provides presumptive evidence that the compounds indeed act by interaction with APE1 rather than by obscuring the abasic site on the DNA substrate. Moreover, the kinetics analysis has provided insight into the mechanism of action of the inhibitor. I have shown that P118 decreased  $K_M$ ,  $k_{cat}$  (compared

with no inhibitor) and decreased the  $k_{cat}/K_M$  implying uncompetitive inhibition. Future cocrystallization experiments in the presence of DNA are likely to provide further information regarding the exact mechanism of action of this compound. To assess potency and specificity of our compounds, I screened their ability to block AP-site cleavage activity using WCE. This is a good system to screen for compounds that may have non-specific binding to other cellular proteins. 6/17 (35.3%) specific inhibitors identified by fluorescence-based APE1 AP-site, (P96, P111, P118, P126, P128 and P147), exhibited more than 80% inhibition in the WCE assays, implying strong potency and specificity.

In order to provide preclinical evidence that blocking the repair domain of APE1 is a potential treatment strategy, I have conducted studies in glioma, melanoma and pancreatic cancer cell lines. I confirmed APE1 expression in these cancer cell lines. I then confirmed accumulation of AP sites *in vivo* in cells exposed to inhibitor, providing direct evidence of target inhibition *in vivo*. Intrinsic cytotoxicity for several of the inhibitors was demonstrated in glioma, melanoma and pancreatic cancer cell lines, a finding consistent with the observation that APE1 down-regulation in melanoma cell lines promotes apoptosis, although non-specific toxicity at higher doses of the compound cannot be excluded in our study [188]. Interestingly, the inhibitors were relatively non-toxic to HUVEC cells implying selectivity to cancer cells.

In a recent study, BER inhibition using CRT0044876 was shown to confer selectively enhanced cytotoxicity in an acidic tumour microenvironment [250] suggesting a further novel opportunity to target tumours. I then showed potentiation of MMS and temozolomide cytotoxicity in glioma, melanoma and



pancreatic cancer cell lines. However, P118 did not potentiate doxorubicin toxicity in these cell lines implying that APE1 inhibitor potentiates chemotherapy that induce base damage and repaired through BER. Moreover, potentiation of cytotoxicity was not demonstrated in HUVEC cells, again implying selectivity to cancer cells. These studies indicate that APE1 inhibitors, either alone or in combination with chemotherapy, may be a promising strategy in cancer. To complement studies using small molecule APE1 inhibitors, APE1 knockdown in U89MG was performed using shRNA approach. The results were consistent with previously published studies in other cancer cell lines[178, 183, 201, 266]. Studies of P118 like analogues showed that most of these analogues were consistent in their inhibition of APE1 suggesting that P118 is a suitable target for further synthetic drug design.

Following the initial identification of APE1 inhibitor by our group, a number of other groups have been working on the development of APE1 DNA repair inhibitors. Seiple et al. have identified the potential of arylstibonic acids, which possess inherent inhibitory activity in a fluorescence-based high-throughput screen [252]. Simeonov et al. utilized a similar fluorescence screening assay to identify three compounds (6-hydroxy-DL-DOPA, Reactive Blue 2 and myricetin) which potentiate MMS cytotoxicity in HeLa cells associated with a quantifiable increase in AP site accumulation. Modelling studies of 6-hydroxy-DL-DOPA suggest that it docks to the APE1 active site in a manner similar to CRT0044876 [256]. Bapat *et al.* modified the previously-described fluorescence assay to identify the novel inhibitor AR02, which is able to selectively block APE1 DNA repair function in glioma cells and

potentiate cytotoxicity of alkylating agents [255]. Zawahir et al. performed an *in silico* pharmacophore model-based screen to identify 21 potent and specific inhibitors. It is interesting to note that APE1 inhibitors identified to date share some common features such as one or two carboxylate groups arranged around a hydrophobic core bearing structural similarity to the 3'- and 5'-deoxyribosephosphate groups on abasic DNA [252, 254].

In conclusion, these studies including two reports from our group [215, 272], confirm the validity of APE1 as an emerging anti-cancer drug target.

## **8.2 Summary of key findings**

1. Three potential APE1 inhibitor templates (M1, M2, and M3) were designed based on APE1 active site crystal structure and CRT0044876 (first identified APE1 inhibitor).
2. Virtual screening of (2.6 million) chemical library identified 1679 hits with similar structures to the designed templates.
3. 1679 hits were ranked based on their binding affinity calculated by virtual docking onto APE1 active site.
4. The top 25% of hits (n = 420) were selected. 250/420 were shortlisted based on their pharmaceutical properties. 147/250 chemical compounds were available for biochemical analyses.
5. Biochemical screening of 147 drug-like candidates identified 38 potential hits. 6/38 were potent and specific APE1 inhibitors (P96, P111, P118, P126, P128 and P147). The IC<sub>50</sub> for these hits ranged from 50 nM- 16  $\mu$ M for inhibition of APE1 activity.
6. Kinetic analysis conducted on P118 suggests an uncompetitive inhibition for the DNA repair domain of APE1.
7. P118 potentiated the cytotoxicity of DNA damaging agents in a panel of cancer cell lines.
8. P118 was relatively non toxic to HUVEC endothelial cells implying specificity to cancer cell lines.
9. P118 did not have any effect on damaging agents that are repaired in pathways other than BER (doxorubicin).
10. Potentiation of cytotoxicity of base damaging agents was associated with a delay in S-phase progression and G2M accumulation.

11. P118 alone caused significant accumulation of AP sites in the genomic DNA compared to untreated cells. In combination with methylating agents, P118 caused further accumulation of AP sites.
12. P118 decreased pancreatic cancer cell migration in a dose dependant manner.
13. Biochemical screening of P118 analogues confirmed that the pharmacophore of P118 was consistent in blocking APE1 endonuclease activity.
14. P118 and its analogues represent the second generation of APE1-targeting compounds for blocking BER during cancer chemotherapy.
15. My PhD project provides further confirmatory evidence that APE1 is an emerging anti-cancer drug target.

### 8.3 Suggestions for future studies

- Synthetic chemical design of P118 analogues is necessary to create more powerful structure–activity relationship profiles and subsequently high-affinity selective compounds.
- Characterization of the binding mode of one or more of the current inhibitors by X-ray crystallography to facilitate the rational design of APE1 inhibitors that enhanced potency.
- Evaluate P118 inhibitor or its analogue in tumour xenograft models to confirm activity *in vivo*.
- Evaluate APE1 inhibitors as radio-sensitizers in glioma and other cancer models.
- Evaluate APE1 inhibitors as agents for synthetic lethality strategy in tumours that are deficient in homologous recombination.

## • References

1. WHO, <http://www.who.int/mediacentre/factsheets/fs297/en/>. 2009.
2. WHO, [http://www.who.int/mediacentre/events/annual/world\\_cancer\\_day/en/](http://www.who.int/mediacentre/events/annual/world_cancer_day/en/). 2010.
3. Longley, D.B. and P.G. Johnston, *Molecular mechanisms of drug resistance*. J Pathol, 2005. **205**(2): p. 275-92.
4. Sancar, A., et al., *Molecular mechanisms of mammalian DNA repair and the DNA damage checkpoints*. Annu Rev Biochem, 2004. **73**: p. 39-85.
5. Gerson, S.L., *MGMT: its role in cancer aetiology and cancer therapeutics*. Nat Rev Cancer, 2004. **4**(4): p. 296-307.
6. Dianov, G., et al., *Mammalian Base Excision Repair*, in *Eukaryotic DNA Damage Surveillance and Repair*, K.W. Caldecott, Editor. 2003, Kluwer Academic/Plenium Publishers. p. 1-22.
7. Bassing, C.H. and F.W. Alt, *The cellular response to general and programmed DNA double strand breaks*. DNA Repair (Amst), 2004. **3**(8-9): p. 781-96.
8. Willers, H., J. Dahm-Daphi, and S.N. Powell, *Repair of radiation damage to DNA*. Br J Cancer, 2004. **90**(7): p. 1297-301.
9. Costa, R.M., et al., *The eukaryotic nucleotide excision repair pathway*. Biochimie, 2003. **85**(11): p. 1083-99.
10. Schofield, M.J. and P. Hsieh, *DNA mismatch repair: molecular mechanisms and biological function*. Annu Rev Microbiol, 2003. **57**: p. 579-608.
11. Gros, L., et al., *The major human AP endonuclease (Ape1) is involved in the nucleotide incision repair pathway*. Nucleic Acids Res, 2004. **32**(1): p. 73-81.
12. Hoeijmakers, J.H., *Genome maintenance mechanisms for preventing cancer*. Nature, 2001. **411**(6835): p. 366-74.
13. Goode, E.L., C.M. Ulrich, and J.D. Potter, *Polymorphisms in DNA repair genes and associations with cancer risk*. Cancer Epidemiol Biomarkers Prev, 2002. **11**(12): p. 1513-30.
14. Frosina, G., *Commentary: DNA base excision repair defects in human pathologies*. Free Radic Res, 2004. **38**(10): p. 1037-54.
15. Gurubhagavatula, S., et al., *XPD and XRCC1 genetic polymorphisms are prognostic factors in advanced non-small-cell lung cancer patients treated with platinum chemotherapy*. J Clin Oncol, 2004. **22**(13): p. 2594-601.
16. Camps, C., et al., *Assessment of nucleotide excision repair XPD polymorphisms in the peripheral blood of gemcitabine/cisplatin-treated advanced non-small-cell lung cancer patients*. Clin Lung Cancer, 2003. **4**(4): p. 237-41.
17. Zhou, W., et al., *Excision repair cross-complementation group 1 polymorphism predicts overall survival in advanced non-small cell lung cancer patients treated with platinum-based chemotherapy*. Clin Cancer Res, 2004. **10**(15): p. 4939-43.
18. Roses, A.D., *Pharmacogenetics and the practice of medicine*. Nature, 2000. **405**(6788): p. 857-65.
19. Schmith, V.D., et al., *Pharmacogenetics and disease genetics of complex diseases*. Cell Mol Life Sci, 2003. **60**(8): p. 1636-46.

20. Madhusudan, S. and I.D. Hickson, *DNA repair inhibition: a selective tumour targeting strategy*. Trends Mol Med, 2005. 11(11): p. 503-11.
21. Farmer, H., et al., *Targeting the DNA repair defect in BRCA mutant cells as a therapeutic strategy*. Nature, 2005. 434(7035): p. 917-21.
22. Bryant, H.E., et al., *Specific killing of BRCA2-deficient tumours with inhibitors of poly(ADP-ribose) polymerase*. Nature, 2005. 434(7035): p. 913-7.
23. Madhusudan, S., et al., *Isolation of a small molecule inhibitor of DNA base excision repair*. Nucleic Acids Res, 2005. 33(15): p. 4711-24.
24. Wyatt, M.D., et al., *3-methyladenine DNA glycosylases: structure, function, and biological importance*. Bioessays, 1999. 21(8): p. 668-76.
25. Parikh, S.S., C.D. Putnam, and J.A. Tainer, *Lessons learned from structural results on uracil-DNA glycosylase*. Mutat Res, 2000. 460(3-4): p. 183-99.
26. Nilsen, H., et al., *Excision of deaminated cytosine from the vertebrate genome: role of the SMUG1 uracil-DNA glycosylase*. Embo J, 2001. 20(15): p. 4278-86.
27. Matsubara, M., et al., *Mutational analysis of the damage-recognition and catalytic mechanism of human SMUG1 DNA glycosylase*. Nucleic Acids Res, 2004. 32(17): p. 5291-302.
28. An, Q., et al., *5-Fluorouracil incorporated into DNA is excised by the Smug1 DNA glycosylase to reduce drug cytotoxicity*. Cancer Res, 2007. 67(3): p. 940-5.
29. Waters, T.R. and P.F. Swann, *Thymine-DNA glycosylase and G to A transition mutations at CpG sites*. Mutat Res, 2000. 462(2-3): p. 137-47.
30. Bellacosa, A., *Role of MED1 (MBD4) Gene in DNA repair and human cancer*. J Cell Physiol, 2001. 187(2): p. 137-44.
31. Hazra, T.K., et al., *Identification and characterization of a human DNA glycosylase for repair of modified bases in oxidatively damaged DNA*. Proc Natl Acad Sci U S A, 2002. 99(6): p. 3523-8.
32. Hazra, T.K., et al., *Identification and characterization of a novel human DNA glycosylase for repair of cytosine-derived lesions*. J Biol Chem, 2002. 277(34): p. 30417-20.
33. Barnes, D.E. and T. Lindahl, *Repair and genetic consequences of endogenous DNA base damage in mammalian cells*. Annu Rev Genet, 2004. 38: p. 445-76.
34. Dianov, G.L., *Monitoring base excision repair by in vitro assays*. Toxicology, 2003. 193(1-2): p. 35-41.
35. Izumi, T., et al., *Mammalian DNA base excision repair proteins: their interactions and role in repair of oxidative DNA damage*. Toxicology, 2003. 193(1-2): p. 43-65.
36. Nilsen, H. and H.E. Krokan, *Base excision repair in a network of defence and tolerance*. Carcinogenesis, 2001. 22(7): p. 987-98.
37. Hegde, M.L., T.K. Hazra, and S. Mitra, *Early steps in the DNA base excision/single-strand interruption repair pathway in mammalian cells*. Cell Res, 2008. 18(1): p. 27-47.
38. Dogliotti, E., et al., *The mechanism of switching among multiple BER pathways*. Prog Nucleic Acid Res Mol Biol, 2001. 68: p. 3-27.
39. Fromme, J.C., A. Banerjee, and G.L. Verdine, *DNA glycosylase recognition and catalysis*. Curr Opin Struct Biol, 2004. 14(1): p. 43-9.
40. McCullough, A.K., M.L. Dodson, and R.S. Lloyd, *Initiation of base excision repair: glycosylase mechanisms and structures*. Annu Rev Biochem, 1999. 68: p. 255-85.

41. Drablos, F., et al., *Alkylation damage in DNA and RNA--repair mechanisms and medical significance*. DNA Repair (Amst), 2004. 3(11): p. 1389-407.
42. De Bont, R. and N. van Larebeke, *Endogenous DNA damage in humans: a review of quantitative data*. Mutagenesis, 2004. 19(3): p. 169-85.
43. Sweasy, J.B., T. Lang, and D. DiMaio, *Is base excision repair a tumor suppressor mechanism?* Cell Cycle, 2006. 5(3): p. 250-9.
44. Kow, Y.W., *Repair of deaminated bases in DNA*. Free Radic Biol Med, 2002. 33(7): p. 886-93.
45. Krokan, H.E., et al., *Properties and functions of human uracil-DNA glycosylase from the UNG gene*. Prog Nucleic Acid Res Mol Biol, 2001. 68: p. 365-86.
46. Longerich, S. and U. Storb, *The contested role of uracil DNA glycosylase in immunoglobulin gene diversification*. Trends Genet, 2005. 21(5): p. 253-6.
47. Ide, H. and M. Kotera, *Human DNA glycosylases involved in the repair of oxidatively damaged DNA*. Biol Pharm Bull, 2004. 27(4): p. 480-5.
48. Dou, H., S. Mitra, and T.K. Hazra, *Repair of oxidized bases in DNA bubble structures by human DNA glycosylases NEIL1 and NEIL2*. J Biol Chem, 2003. 278(50): p. 49679-84.
49. Idriss, H.T., O. Al-Assar, and S.H. Wilson, *DNA polymerase beta*. Int J Biochem Cell Biol, 2002. 34(4): p. 321-4.
50. Sobol, R.W., et al., *Requirement of mammalian DNA polymerase-beta in base-excision repair*. Nature, 1996. 379(6561): p. 183-6.
51. Starcevic, D., S. Dalal, and J.B. Sweasy, *Is there a link between DNA polymerase beta and cancer?* Cell Cycle, 2004. 3(8): p. 998-1001.
52. Lee, S.H., et al., *Studies on the activator 1 protein complex, an accessory factor for proliferating cell nuclear antigen-dependent DNA polymerase delta*. J Biol Chem, 1991. 266(1): p. 594-602.
53. Stucki, M., et al., *Mammalian base excision repair by DNA polymerases delta and epsilon*. Oncogene, 1998. 17(7): p. 835-43.
54. Kim, J. and S.A. MacNeill, *Genome stability: a new member of the RFC family*. Curr Biol, 2003. 13(22): p. R873-5.
55. Maga, G. and U. Hubscher, *Proliferating cell nuclear antigen (PCNA): a dancer with many partners*. J Cell Sci, 2003. 116(Pt 15): p. 3051-60.
56. Liu, Y., H.I. Kao, and R.A. Bambara, *Flap endonuclease 1: a central component of DNA metabolism*. Annu Rev Biochem, 2004. 73: p. 589-615.
57. Johnson, A. and M. O'Donnell, *DNA ligase: getting a grip to seal the deal*. Curr Biol, 2005. 15(3): p. R90-2.
58. Montecucco, A., et al., *DNA ligase I is recruited to sites of DNA replication by an interaction with proliferating cell nuclear antigen: identification of a common targeting mechanism for the assembly of replication factories*. Embo J, 1998. 17(13): p. 3786-95.
59. Timson, D.J., M.R. Singleton, and D.B. Wigley, *DNA ligases in the repair and replication of DNA*. Mutat Res, 2000. 460(3-4): p. 301-18.
60. Cappelli, E., et al., *Involvement of XRCC1 and DNA ligase III gene products in DNA base excision repair*. J Biol Chem, 1997. 272(38): p. 23970-5.
61. Nash, R.A., et al., *XRCC1 protein interacts with one of two distinct forms of DNA ligase III*. Biochemistry, 1997. 36(17): p. 5207-11.
62. Critchlow, S.E., R.P. Bowater, and S.P. Jackson, *Mammalian DNA double-strand break repair protein XRCC4 interacts with DNA ligase IV*. Curr Biol, 1997. 7(8): p. 588-98.



63. Kubota, Y., et al., *Reconstitution of DNA base excision-repair with purified human proteins: interaction between DNA polymerase beta and the XRCC1 protein*. *Embo J*, 1996. **15**(23): p. 6662-70.
64. Caldecott, K.W., et al., *An interaction between the mammalian DNA repair protein XRCC1 and DNA ligase III*. *Mol Cell Biol*, 1994. **14**(1): p. 68-76.
65. Vidal, A.E., et al., *XRCC1 coordinates the initial and late stages of DNA abasic site repair through protein-protein interactions*. *Embo J*, 2001. **20**(22): p. 6530-6539.
66. Tebbs, R.S., et al., *Requirement for the Xrcc1 DNA base excision repair gene during early mouse development*. *Dev Biol*, 1999. **208**(2): p. 513-29.
67. Hung, R.J., et al., *Genetic polymorphisms in the base excision repair pathway and cancer risk: a HuGE review*. *Am J Epidemiol*, 2005. **162**(10): p. 925-42.
68. Jagtap, P. and C. Szabo, *Poly(ADP-ribose) polymerase and the therapeutic effects of its inhibitors*. *Nat Rev Drug Discov*, 2005. **4**(5): p. 421-40.
69. Bouchard, V.J., M. Rouleau, and G.G. Poirier, *PARP-1, a determinant of cell survival in response to DNA damage*. *Exp Hematol*, 2003. **31**(6): p. 446-54.
70. Khodyreva, S.N., et al., *Apurinic/apyrimidinic (AP) site recognition by the 5'-dRP/AP lyase in poly(ADP-ribose) polymerase-1 (PARP-1)*. *Proc Natl Acad Sci U S A*, 2010. **107**(51): p. 22090-5.
71. Haince, J.F., et al., *PARP1-dependent kinetics of recruitment of MRE11 and NBS1 proteins to multiple DNA damage sites*. *J Biol Chem*, 2008. **283**(2): p. 1197-208.
72. Wang, M., et al., *PARP-1 and Ku compete for repair of DNA double strand breaks by distinct NHEJ pathways*. *Nucleic Acids Res*, 2006. **34**(21): p. 6170-82.
73. Kraus, W.L. and J.T. Lis, *PARP goes transcription*. *Cell*, 2003. **113**(6): p. 677-83.
74. Masutani, M., et al., *The response of Parp knockout mice against DNA damaging agents*. *Mutat Res*, 2000. **462**(2-3): p. 159-66.
75. Durkacz, B.W., et al., *(ADP-ribose)<sub>n</sub> participates in DNA excision repair*. *Nature*, 1980. **283**(5747): p. 593-6.
76. Nosh, K., et al., *Overexpression of poly(ADP-ribose) polymerase-1 (PARP-1) in the early stage of colorectal carcinogenesis*. *Eur J Cancer*, 2006. **42**(14): p. 2374-81.
77. Valeria Ossovskaya, C.A., Eric Kaldjian and Barry Sherman, *PARP1 gene over-expression in primary human cancers: A potential marker for PARP inhibition*. AACR-NCI-EORTC International Conference: Molecular Targets and Cancer Therapeutics, 2007. – Oct 22-26, 2007; San Francisco, CA.
78. Staibano, S., et al., *Poly(adenosine diphosphate-ribose) polymerase 1 expression in malignant melanomas from photoexposed areas of the head and neck region*. *Hum Pathol*, 2005. **36**(7): p. 724-31.
79. Shiobara, M., et al., *Enhanced polyadenosine diphosphate-ribosylation in cirrhotic liver and carcinoma tissues in patients with hepatocellular carcinoma*. *J Gastroenterol Hepatol*, 2001. **16**(3): p. 338-44.
80. Molinete, M., et al., *Overproduction of the poly(ADP-ribose) polymerase DNA-binding domain blocks alkylation-induced DNA repair synthesis in mammalian cells*. *Embo J*, 1993. **12**(5): p. 2109-17.

81. de Murcia, J.M., et al., *Requirement of poly(ADP-ribose) polymerase in recovery from DNA damage in mice and in cells*. Proc Natl Acad Sci U S A, 1997. **94**(14): p. 7303-7.
82. Southan, G.J. and C. Szabo, *Poly(ADP-ribose) polymerase inhibitors*. Curr Med Chem, 2003. **10**(4): p. 321-40.
83. Komjati, K., et al., *Poly(ADP-ribose) polymerase inhibition protect neurons and the white matter and regulates the translocation of apoptosis-inducing factor in stroke*. Int J Mol Med, 2004. **13**(3): p. 373-82.
84. Beneke, S., J. Diefenbach, and A. Burkle, *Poly(ADP-ribosyl)ation inhibitors: promising drug candidates for a wide variety of pathophysiologic conditions*. Int J Cancer, 2004. **111**(6): p. 813-8.
85. Bowman, K.J., et al., *Potentiation of anti-cancer agent cytotoxicity by the potent poly(ADP-ribose) polymerase inhibitors NU1025 and NU1064*. Br J Cancer, 1998. **78**(10): p. 1269-77.
86. Plummer, R., et al., *Phase I study of the poly(ADP-ribose) polymerase inhibitor, AG014699, in combination with temozolomide in patients with advanced solid tumors*. Clin Cancer Res, 2008. **14**(23): p. 7917-23.
87. Rouleau, M., et al., *PARP inhibition: PARP1 and beyond*. Nat Rev Cancer. **10**(4): p. 293-301.
88. Lindahl, T. and B. Nyberg, *Rate of depurination of native deoxyribonucleic acid*. Biochemistry, 1972. **11**(19): p. 3610-8.
89. Lindahl, T. and O. Karlstrom, *Heat-induced depyrimidination of deoxyribonucleic acid in neutral solution*. Biochemistry, 1973. **12**(25): p. 5151-4.
90. Lindahl, T., *Instability and decay of the primary structure of DNA*. Nature, 1993. **362**(6422): p. 709-15.
91. Atamna, H., I. Cheung, and B.N. Ames, *A method for detecting abasic sites in living cells: age-dependent changes in base excision repair*. Proc Natl Acad Sci U S A, 2000. **97**(2): p. 686-91.
92. Nakamura, J. and J.A. Swenberg, *Endogenous apurinic/aprimidinic sites in genomic DNA of mammalian tissues*. Cancer Res, 1999. **59**(11): p. 2522-6.
93. Hickson, I.D., *Base Excision Repair of DNA Damage*. Molecular Biology Intelligence unit, ed. I.D. Hickson. 1997: Landes Bioscience.
94. Wilson, D.M., 3rd and D. Barsky, *The major human abasic endonuclease: formation, consequences and repair of abasic lesions in DNA*. Mutat Res, 2001. **485**(4): p. 283-307.
95. Kingma, P.S. and N. Osheroff, *The response of eukaryotic topoisomerases to DNA damage*. Biochim Biophys Acta, 1998. **1400**(1-3): p. 223-32.
96. Pourquier, P., et al., *Effects of uracil incorporation, DNA mismatches, and abasic sites on cleavage and religation activities of mammalian topoisomerase I*. J Biol Chem, 1997. **272**(12): p. 7792-6.
97. Fung, H. and B. Dimple, *A vital role for Ape1/Ref1 protein in repairing spontaneous DNA damage in human cells*. Mol Cell, 2005. **17**(3): p. 463-70.
98. Calleja, F., et al., *Modulation of the toxic and mutagenic effects induced by methyl methanesulfonate in Chinese hamster ovary cells by overexpression of the rat N-alkylpurine-DNA glycosylase*. Mutat Res, 1999. **425**(2): p. 185-94.
99. Liu, L. and S.L. Gerson, *Therapeutic impact of methoxyamine: blocking repair of abasic sites in the base excision repair pathway*. Curr Opin Investig Drugs, 2004. **5**(6): p. 623-7.

100. Yu, S.L., et al., *The stalling of transcription at abasic sites is highly mutagenic*. Mol Cell Biol, 2003. **23**(1): p. 382-8.
101. Barzilay, G. and I.D. Hickson, *Structure and function of apurinic/apyrimidinic endonucleases*. Bioessays, 1995. **17**(8): p. 713-9.
102. Evans, A.R., M. Limp-Foster, and M.R. Kelley, *Going APE over ref-1*. Mutat Res, 2000. **461**(2): p. 83-108.
103. Gorman, M.A., et al., *The crystal structure of the human DNA repair endonuclease HAP1 suggests the recognition of extra-helical deoxyribose at DNA abasic sites*. Embo J, 1997. **16**(21): p. 6548-58.
104. Mol, C.D., et al., *Structure and function of the multifunctional DNA-repair enzyme exonuclease III*. Nature, 1995. **374**(6520): p. 381-6.
105. Hosfield, D.J., et al., *Structure of the DNA repair enzyme endonuclease IV and its DNA complex: double-nucleotide flipping at abasic sites and three-metal-ion catalysis*. Cell, 1999. **98**(3): p. 397-408.
106. Saporito, S.M., B.J. Smith-White, and R.P. Cunningham, *Nucleotide sequence of the xth gene of Escherichia coli K-12*. J Bacteriol, 1988. **170**(10): p. 4542-7.
107. Hickson, I.D., Michael A.Gorman., Paul S.Freemont., *Structure and Functions of the Major Human AP Endonuclease HAP1/Ref-1*. DNA Damage and Repair, Vol3 : Advances from Phage to Humans, ed. J.A. Nickoloff, Hoekstra, M.F. 2000: Humana Press Inc., Totowa, NJ. 87-105.
108. Ramotar, D., *The apurinic-apyrimidinic endonuclease IV family of DNA repair enzymes*. Biochem Cell Biol, 1997. **75**(4): p. 327-36.
109. Robson, C.N. and I.D. Hickson, *Isolation of cDNA clones encoding a human apurinic/apyrimidinic endonuclease that corrects DNA repair and mutagenesis defects in E. coli xth (exonuclease III) mutants*. Nucleic Acids Res, 1991. **19**(20): p. 5519-23.
110. Robson, C.N., et al., *Structure of the human DNA repair gene HAP1 and its localisation to chromosome 14q 11.2-12*. Nucleic Acids Res, 1992. **20**(17): p. 4417-21.
111. Xanthoudakis, S., G.G. Miao, and T. Curran, *The redox and DNA-repair activities of Ref-1 are encoded by nonoverlapping domains*. Proc Natl Acad Sci U S A, 1994. **91**(1): p. 23-7.
112. Luo, M., et al., *Role of the Multifunctional DNA Repair and Redox Signaling Protein Ape1/Ref-1 in Cancer and Endothelial Cells: Small-Molecule Inhibition of the Redox Function of Ape1*. Antioxid Redox Signal, 2008.
113. McNeill, D.R. and D.M. Wilson, 3rd, *A dominant-negative form of the major human abasic endonuclease enhances cellular sensitivity to laboratory and clinical DNA-damaging agents*. Mol Cancer Res, 2007. **5**(1): p. 61-70.
114. Izumi, T. and S. Mitra, *Deletion analysis of human AP-endonuclease: minimum sequence required for the endonuclease activity*. Carcinogenesis, 1998. **19**(3): p. 525-7.
115. Georgiadis, M.M., et al., *Evolution of the redox function in mammalian apurinic/apyrimidinic endonuclease*. Mutat Res, 2008.
116. Fritz, G., *Human APE/Ref-1 protein*. Int J Biochem Cell Biol, 2000. **32**(9): p. 925-9.
117. Robbins, J., et al., *Two interdependent basic domains in nucleoplasmin nuclear targeting sequence: identification of a class of bipartite nuclear targeting sequence*. Cell, 1991. **64**(3): p. 615-23.

118. Jackson, E.B., et al., *Analysis of nuclear transport signals in the human apurinic/apyrimidinic endonuclease (APE1/Ref1)*. *Nucleic Acids Res*, 2005. **33**(10): p. 3303-12.
119. Li, M., et al., *Identification and characterization of mitochondrial targeting sequence of human apurinic/apyrimidinic endonuclease 1*. *J Biol Chem*, 2010. **285**(20): p. 14871-81.
120. Demple, B., T. Herman, and D.S. Chen, *Cloning and expression of APE, the cDNA encoding the major human apurinic endonuclease: definition of a family of DNA repair enzymes*. *Proc Natl Acad Sci U S A*, 1991. **88**(24): p. 11450-4.
121. Chen, D.S., T. Herman, and B. Demple, *Two distinct human DNA diesterases that hydrolyze 3'-blocking deoxyribose fragments from oxidized DNA*. *Nucleic Acids Res*, 1991. **19**(21): p. 5907-14.
122. Barzilay, G., et al., *Site-directed mutagenesis of the human DNA repair enzyme HAP1: identification of residues important for AP endonuclease and RNase H activity*. *Nucleic Acids Res*, 1995. **23**(9): p. 1544-50.
123. Barzilay, G., et al., *Identification of critical active-site residues in the multifunctional human DNA repair enzyme HAP1*. *Nat Struct Biol*, 1995. **2**(7): p. 561-8.
124. Rothwell, D.G. and I.D. Hickson, *Asparagine 212 is essential for abasic site recognition by the human DNA repair endonuclease HAP1*. *Nucleic Acids Res*, 1996. **24**(21): p. 4217-21.
125. Erzberger, J.P. and D.M. Wilson, 3rd, *The role of Mg<sup>2+</sup> and specific amino acid residues in the catalytic reaction of the major human abasic endonuclease: new insights from EDTA-resistant incision of acyclic abasic site analogs and site-directed mutagenesis*. *J Mol Biol*, 1999. **290**(2): p. 447-57.
126. Mundle, S.T., et al., *Novel role of tyrosine in catalysis by human AP endonuclease 1*. *DNA Repair (Amst)*, 2004. **3**(11): p. 1447-55.
127. Fritz, G., et al., *APE/Ref-1 and the mammalian response to genotoxic stress*. *Toxicology*, 2003. **193**(1-2): p. 67-78.
128. Parsons, J.L., Dianova, II, and G.L. Dianov, *APE1 is the major 3'-phosphoglycolate activity in human cell extracts*. *Nucleic Acids Res*, 2004. **32**(12): p. 3531-6.
129. Chou, K.M. and Y.C. Cheng, *An exonucleolytic activity of human apurinic/apyrimidinic endonuclease on 3' mispaired DNA*. *Nature*, 2002. **415**(6872): p. 655-9.
130. Jiricny, J., *An APE that proofreads*. *Nature*, 2002. **415**(6872): p. 593-4.
131. Wong, D., M.S. DeMott, and B. Demple, *Modulation of the 3'→5'-exonuclease activity of human apurinic endonuclease (Ape1) by its 5'-incised Abasic DNA product*. *J Biol Chem*, 2003. **278**(38): p. 36242-9.
132. Chou, K.M., M. Kukhanova, and Y.C. Cheng, *A novel action of human apurinic/apyrimidinic endonuclease: excision of L-configuration deoxyribonucleoside analogs from the 3' termini of DNA*. *J Biol Chem*, 2000. **275**(40): p. 31009-15.
133. Das, A., et al., *NEIL2-initiated, APE-independent repair of oxidized bases in DNA: Evidence for a repair complex in human cells*. *DNA Repair (Amst)*, 2006. **5**(12): p. 1439-48.
134. Wiederhold, L., et al., *AP endonuclease-independent DNA base excision repair in human cells*. *Mol Cell*, 2004. **15**(2): p. 209-20.
135. Gelin, A., et al., *Genetic and biochemical characterization of human AP endonuclease 1 mutants deficient in nucleotide incision repair activity*. *PLoS One*, 2010. **5**(8).

136. Maher, R.L. and L.B. Bloom, *Pre-steady-state kinetic characterization of the AP endonuclease activity of human AP endonuclease 1*. J Biol Chem, 2007. **282**(42): p. 30577-85.
137. Kanazhevskaya, L.Y., et al., *Conformational transitions in human AP endonuclease 1 and its active site mutant during abasic site repair*. Biochemistry, 2010. **49**(30): p. 6451-61.
138. Yang, H., et al., *Enhanced activity of adenine-DNA glycosylase (Myh) by apurinic/apyrimidinic endonuclease (Ape1) in mammalian base excision repair of an A/GO mismatch*. Nucleic Acids Res, 2001. **29**(3): p. 743-52.
139. Baldwin, M.R. and P.J. O'Brien, *Nonspecific DNA binding and coordination of the first two steps of base excision repair*. Biochemistry, 2010. **49**(36): p. 7879-91.
140. Hill, J.W., et al., *Stimulation of human 8-oxoguanine-DNA glycosylase by AP-endonuclease: potential coordination of the initial steps in base excision repair*. Nucleic Acids Res, 2001. **29**(2): p. 430-8.
141. Marenstein, D.R., et al., *Substrate specificity of human endonuclease III (hNTH1). Effect of human APE1 on hNTH1 activity*. J Biol Chem, 2003. **278**(11): p. 9005-12.
142. Parikh, S.S., et al., *Base excision repair initiation revealed by crystal structures and binding kinetics of human uracil-DNA glycosylase with DNA*. Embo J, 1998. **17**(17): p. 5214-26.
143. Waters, T.R., et al., *Human thymine DNA glycosylase binds to apurinic sites in DNA but is displaced by human apurinic endonuclease 1*. J Biol Chem, 1999. **274**(1): p. 67-74.
144. Bennett, R.A., et al., *Interaction of human apurinic endonuclease and DNA polymerase beta in the base excision repair pathway*. Proc Natl Acad Sci U S A, 1997. **94**(14): p. 7166-9.
145. Masuda, Y., R.A. Bennett, and B. Dimple, *Dynamics of the interaction of human apurinic endonuclease (Ape1) with its substrate and product*. J Biol Chem, 1998. **273**(46): p. 30352-9.
146. Dianova, II, V.A. Bohr, and G.L. Dianov, *Interaction of human ap endonuclease 1 with flap endonuclease 1 and proliferating cell nuclear antigen involved in long-patch base excision repair*. Biochemistry, 2001. **40**(42): p. 12639-44.
147. Ranalli, T.A., S. Tom, and R.A. Bambara, *AP endonuclease 1 coordinates flap endonuclease 1 and DNA ligase I activity in long patch base excision repair*. J Biol Chem, 2002.
148. Gaiddon, C., N.C. Moorthy, and C. Prives, *Ref-1 regulates the transactivation and pro-apoptotic functions of p53 in vivo*. Embo J, 1999. **18**(20): p. 5609-21.
149. Marsin, S., et al., *Role of XRCC1 in the coordination and stimulation of oxidative DNA damage repair initiated by the DNA glycosylase hOGG1*. J Biol Chem, 2003. **278**(45): p. 44068-74.
150. Zhou, J., et al., *A role for p53 in base excision repair*. Embo J, 2001. **20**(4): p. 914-23.
151. Hanson, S., E. Kim, and W. Deppert, *Redox factor 1 (Ref-1) enhances specific DNA binding of p53 by promoting p53 tetramerization*. Oncogene, 2005. **24**(9): p. 1641-7.
152. Busso, C.S., T. Iwakuma, and T. Izumi, *Ubiquitination of mammalian AP endonuclease (APE1) regulated by the p53-MDM2 signaling pathway*. Oncogene, 2009. **28**(13): p. 1616-25.
153. Chung, U., et al., *The interaction between Ku antigen and REF1 protein mediates negative gene regulation by extracellular calcium*. J Biol Chem, 1996. **271**(15): p. 8593-8.

154. Ahn, B., et al., *Regulation of WRN helicase activity in human base excision repair*. J Biol Chem, 2004. **279**(51): p. 53465-74.
155. Mendez, F., et al., *Specific stimulation of human apurinic/aprimidinic endonuclease by heat shock protein 70*. DNA Repair (Amst), 2003. **2**(3): p. 259-71.
156. Xanthoudakis, S., et al., *Redox activation of Fos-Jun DNA binding activity is mediated by a DNA repair enzyme*. Embo J, 1992. **11**(9): p. 3323-35.
157. Walker, L.J., et al., *A role for the human DNA repair enzyme HAP1 in cellular protection against DNA damaging agents and hypoxic stress*. Nucleic Acids Res, 1994. **22**(23): p. 4884-9.
158. Tell, G., et al., *The intracellular localization of APE1/Ref-1: more than a passive phenomenon?* Antioxid Redox Signal, 2005. **7**(3-4): p. 367-84.
159. Walker, L.J., et al., *Identification of residues in the human DNA repair enzyme HAP1 (Ref-1) that are essential for redox regulation of Jun DNA binding*. Mol Cell Biol, 1993. **13**(9): p. 5370-6.
160. Hirota, K., et al., *AP-1 transcriptional activity is regulated by a direct association between thioredoxin and Ref-1*. Proc Natl Acad Sci U S A, 1997. **94**(8): p. 3633-8.
161. Qin, J., et al., *The solution structure of human thioredoxin complexed with its target from Ref-1 reveals peptide chain reversal*. Structure, 1996. **4**(5): p. 613-20.
162. Flaherty, D.M., M.M. Monick, and G.W. Hunninghake, *AP endonucleases and the many functions of Ref-1*. Am J Respir Cell Mol Biol, 2001. **25**(6): p. 664-7.
163. Zou, G.M., et al., *Ape1 regulates hematopoietic differentiation of embryonic stem cells through its redox functional domain*. Blood, 2007. **109**(5): p. 1917-22.
164. Okazaki, T., et al., *A redox factor protein, ref1, is involved in negative gene regulation by extracellular calcium*. J Biol Chem, 1994. **269**(45): p. 27855-62.
165. Fuchs, S., et al., *Implication of Ref-1 in the repression of renin gene transcription by intracellular calcium*. J Hypertens, 2003. **21**(2): p. 327-35.
166. McHaffie, G.S. and S.H. Ralston, *Origin of a negative calcium response element in an ALU-repeat: implications for regulation of gene expression by extracellular calcium*. Bone, 1995. **17**(1): p. 11-4.
167. Bhakat, K.K., et al., *Role of acetylated human AP-endonuclease (APE1/Ref-1) in regulation of the parathyroid hormone gene*. Embo J, 2003. **22**(23): p. 6299-309.
168. Yamamori, T., et al., *SIRT1 deacetylates APE1 and regulates cellular base excision repair*. Nucleic Acids Res, 2010. **38**(3): p. 832-45.
169. Fantini, D., et al., *APE1/Ref-1 regulates PTEN expression mediated by Egr-1*. Free Radic Res, 2008. **42**(1): p. 20-9.
170. Chattopadhyay, R., et al., *Regulatory Role of Human AP-endonuclease (APE1/Ref-1) in YB-1-Mediated Activation of Multi Drug Resistance (MDR1) Gene*. Mol Cell Biol, 2008.
171. Sengupta, S., et al., *Human AP endonuclease (APE1/Ref-1) and its acetylation regulate YB-1-p300 recruitment and RNA polymerase II loading in the drug-induced activation of multidrug resistance gene MDR1*. Oncogene, 2010.
172. Xanthoudakis, S., et al., *The redox/DNA repair protein, Ref-1, is essential for early embryonic development in mice*. Proc Natl Acad Sci U S A, 1996. **93**(17): p. 8919-23.

173. Ludwig, D.L., et al., *A murine AP-endonuclease gene-targeted deficiency with post-implantation embryonic progression and ionizing radiation sensitivity*. *Mutat Res*, 1998. **409**(1): p. 17-29.
174. Meira, L.B., et al., *Heterozygosity for the mouse Apex gene results in phenotypes associated with oxidative stress*. *Cancer Res*, 2001. **61**(14): p. 5552-7.
175. Ordway, J.M., D. Eberhart, and T. Curran, *Cysteine 64 of Ref-1 is not essential for redox regulation of AP-1 DNA binding*. *Mol Cell Biol*, 2003. **23**(12): p. 4257-66.
176. Izumi, T., et al., *Two essential but distinct functions of the mammalian abasic endonuclease*. *Proc Natl Acad Sci U S A*, 2005. **102**(16): p. 5739-43.
177. Robertson, K.A., et al., *Down-regulation of apurinic/aprimidinic endonuclease expression is associated with the induction of apoptosis in differentiating myeloid leukemia cells*. *Cell Growth Differ*, 1997. **8**(4): p. 443-9.
178. Fishel, M.L., et al., *Knockdown of the DNA repair and redox signaling protein Ape1/Ref-1 blocks ovarian cancer cell and tumor growth*. *DNA Repair (Amst)*, 2008. **7**(2): p. 177-86.
179. Chen, D.S. and Z.L. Olkowski, *Biological responses of human apurinic endonuclease to radiation-induced DNA damage*. *Ann N Y Acad Sci*, 1994. **726**: p. 306-8.
180. Silber, J.R., et al., *The apurinic/aprimidinic endonuclease activity of Ape1/Ref-1 contributes to human glioma cell resistance to alkylating agents and is elevated by oxidative stress*. *Clin Cancer Res*, 2002. **8**(9): p. 3008-18.
181. Ono, Y., et al., *Stable expression in rat glioma cells of sense and antisense nucleic acids to a human multifunctional DNA repair enzyme, APEX nuclease*. *Mutat Res*, 1994. **315**(1): p. 55-63.
182. Wang, D., M. Luo, and M.R. Kelley, *Human apurinic endonuclease 1 (APE1) expression and prognostic significance in osteosarcoma: enhanced sensitivity of osteosarcoma to DNA damaging agents using silencing RNA APE1 expression inhibition*. *Mol Cancer Ther*, 2004. **3**(6): p. 679-86.
183. Xiong, G.S., et al., *Small interfering RNA against the apurinic or apyrimidinic endonuclease enhances the sensitivity of human pancreatic cancer cells to gemcitabine in vitro*. *J Dig Dis*, 2010. **11**(4): p. 224-30.
184. Wang, D., et al., *APE1 overexpression is associated with cisplatin resistance in non-small cell lung cancer and targeted inhibition of APE1 enhances the activity of cisplatin in A549 cells*. *Lung Cancer*, 2009. **66**(3): p. 298-304.
185. Wilson, D.M., 3rd, et al., *Trans-complementation by human apurinic endonuclease (Ape) of hypersensitivity to DNA damage and spontaneous mutator phenotype in apn1-yeast*. *Nucleic Acids Res*, 1995. **23**(24): p. 5027-33.
186. Hansen, W.K., et al., *Creation of a fully functional human chimeric DNA repair protein. Combining O6-methylguanine DNA methyltransferase (MGMT) and AP endonuclease (APE/redox effector factor 1 (Ref 1)) DNA repair proteins*. *J Biol Chem*, 1998. **273**(2): p. 756-62.
187. Robertson, K.A., et al., *Altered expression of Ape1/ref-1 in germ cell tumors and overexpression in NT2 cells confers resistance to bleomycin and radiation*. *Cancer Res*, 2001. **61**(5): p. 2220-5.
188. Yang, S., et al., *Alterations in the expression of the apurinic/aprimidinic endonuclease-1/redox factor-1 (APE/Ref-1) in*

- human melanoma and identification of the therapeutic potential of resveratrol as an APE/Ref-1 inhibitor. Mol Cancer Ther, 2005. 4(12): p. 1923-35.*
189. Bobola, M.S., et al., *Apurinic/apyrimidinic endonuclease is inversely associated with response to radiotherapy in pediatric ependymoma. Int J Cancer, 2011.*
  190. Hadi, M.Z., et al., *Functional characterization of Ape1 variants identified in the human population. Nucleic Acids Res, 2000. 28(20): p. 3871-9.*
  191. Lu, J., et al., *Functional characterization of a promoter polymorphism in APE1/Ref-1 that contributes to reduced lung cancer susceptibility. FASEB J, 2009.*
  192. Gu, D., et al., *The DNA repair gene APE1 T1349G polymorphism and cancer risk: a meta-analysis of 27 case-control studies. Mutagenesis, 2009.*
  193. Li, C., et al., *Genetic variants of the ADPRT, XRCC1 and APE1 genes and risk of cutaneous melanoma. Carcinogenesis, 2006. 27(9): p. 1894-901.*
  194. Li, D.H., et al., *Effects of base excision repair gene polymorphisms on pancreatic cancer survival. International Journal of Cancer, 2007. 120(8): p. 1748-1754.*
  195. Farkasova, T., et al., *Significance of amino acid substitution variants of DNA repair genes in radiosusceptibility of cervical cancer patients; a pilot study. Neoplasma, 2008. 55(4): p. 330-7.*
  196. Agachan, B., et al., *Apurinic/apyrimidinic endonuclease (APE1) gene polymorphisms and lung cancer risk in relation to tobacco smoking. Anticancer Res, 2009. 29(6): p. 2417-20.*
  197. Hu, J.J., et al., *Amino acid substitution variants of APE1 and XRCC1 genes associated with ionizing radiation sensitivity. Carcinogenesis, 2001. 22(6): p. 917-22.*
  198. Chang-Claude, J., et al., *Association between polymorphisms in the DNA repair genes, XRCC1, APE1, and XPD and acute side effects of radiotherapy in breast cancer patients. Clinical Cancer Research, 2005. 11(13): p. 4802-4809.*
  199. Fung, H., R.A. Bennett, and B. Dimple, *Key Role of a Downstream Specificity Protein 1 Site in Cell Cycle-regulated Transcription of the AP Endonuclease Gene APE1/APEX in NIH3T3 Cells. J Biol Chem, 2001. 276(45): p. 42011-7.*
  200. Bobola, M.S., et al., *Apurinic/Apyrimidinic endonuclease activity is elevated in human adult gliomas. Clin Cancer Res, 2001. 7(11): p. 3510-8.*
  201. Jiang, Y., et al., *Reduced expression of DNA repair and redox signaling protein APE1/Ref-1 impairs human pancreatic cancer cell survival, proliferation, and cell cycle progression. Cancer Invest, 2010. 28(9): p. 885-95.*
  202. Kelley, M.R., et al., *Elevated and altered expression of the multifunctional DNA base excision repair and redox enzyme Ape1/ref-1 in prostate cancer. Clin Cancer Res, 2001. 7(4): p. 824-30.*
  203. Yoo, D.G., et al., *Alteration of APE1/ref-1 expression in non-small cell lung cancer: The implications of impaired extracellular superoxide dismutase and catalase antioxidant systems. Lung Cancer, 2008. 60(2): p. 277-284.*
  204. Kakolyris, S., et al., *Human apurinic endonuclease 1 expression in a colorectal adenoma-carcinoma sequence. Cancer Res, 1997. 57(9): p. 1794-7.*



205. Tell, G., et al., *TSH controls Ref-1 nuclear translocation in thyroid cells*. J Mol Endocrinol, 2000. **24**(3): p. 383-90.
206. Di Maso, V., et al., *Subcellular localization of APE1/Ref-1 in human hepatocellular carcinoma: possible prognostic significance*. Mol Med, 2007. **13**(1-2): p. 89-96.
207. Moore, D.H., et al., *Alterations in the expression of the DNA repair/redox enzyme APE/ref-1 in epithelial ovarian cancers*. Clin Cancer Res, 2000. **6**(2): p. 602-9.
208. Xu, Y., et al., *The apurinic/aprimidinic endonuclease (APE/ref-1) DNA repair enzyme is elevated in premalignant and malignant cervical cancer*. Anticancer Res, 1997. **17**(5B): p. 3713-19.
209. Sak, S.C., et al., *APE1 and XRCC1 protein expression levels predict cancer-specific survival following radical radiotherapy in bladder cancer*. Clin Cancer Res, 2005. **11**(17): p. 6205-11.
210. Thomson, B., et al., *Histology-specific expression of a DNA repair protein in pediatric rhabdomyosarcomas*. J Pediatr Hematol Oncol, 2001. **23**(4): p. 234-9.
211. Koukourakis, M.I., et al., *Nuclear expression of human apurinic/aprimidinic endonuclease (HAP1/Ref-1) in head-and-neck cancer is associated with resistance to chemoradiotherapy and poor outcome*. Int J Radiat Oncol Biol Phys, 2001. **50**(1): p. 27-36.
212. Puglisi, F., et al., *Prognostic significance of Ape1/ref-1 subcellular localization in non-small cell lung carcinomas*. Anticancer Res, 2001. **21**(6A): p. 4041-9.
213. Kakolyris, S., et al., *Nuclear localization of human AP endonuclease 1 (HAP1/Ref-1) associates with prognosis in early operable non-small cell lung cancer (NSCLC)*. J Pathol, 1999. **189**(3): p. 351-7.
214. Bobola, M.S., et al., *Apurinic/aprimidinic endonuclease activity is associated with response to radiation and chemotherapy in medulloblastoma and primitive neuroectodermal tumors*. Clin Cancer Res, 2005. **11**(20): p. 7405-14.
215. Al-Attar, A., et al., *Human apurinic/aprimidinic endonuclease (APE1) is a prognostic factor in ovarian, gastro-oesophageal and pancreaticobiliary cancers*. Br J Cancer, 2010. **102**(4): p. 704-9.
216. Kakolyris, S., et al., *Human AP endonuclease 1 (HAP1) protein expression in breast cancer correlates with lymph node status and angiogenesis*. Br J Cancer, 1998. **77**(7): p. 1169-73.
217. Puglisi, F., et al., *Prognostic role of Ape/Ref-1 subcellular expression in stage I-III breast carcinomas*. Oncol Rep, 2002. **9**(1): p. 11-7.
218. Herring, C.J., et al., *Levels of the DNA repair enzyme human apurinic/aprimidinic endonuclease (APE1, APEX, Ref-1) are associated with the intrinsic radiosensitivity of cervical cancers*. Br J Cancer, 1998. **78**(9): p. 1128-33.
219. Qing, Y., et al., *[The expression of APE1 and its correlation with prognostic significance after 252Cf radiotherapy in cervical cancer]*. Sichuan Da Xue Xue Bao Yi Xue Ban, 2009. **40**(1): p. 125-8.
220. Xiang, D.B., et al., *Chimeric adenoviral vector Ad5/F35-mediated APE1 siRNA enhances sensitivity of human colorectal cancer cells to radiotherapy in vitro and in vivo*. Cancer Gene Ther, 2008.
221. Naidu, M.D., et al., *Radiation resistance in glioma cells determined by DNA damage repair activity of ape1/ref-1*. J Radiat Res (Tokyo), 2010. **51**(4): p. 393-404.
222. Avellini, C., et al., *Apurinic apyrimidinic endonuclease/redox effector factor 1 immunoreactivity and grading in hepatocellular carcinoma risk*

- of relapse after liver transplantation. *Transplant Proc*, 2010. **42**(4): p. 1204-8.
223. Lau, J.P., et al., *Effects of gemcitabine on APE/ref-1 endonuclease activity in pancreatic cancer cells, and the therapeutic potential of antisense oligonucleotides*. *Br J Cancer*, 2004. **91**(6): p. 1166-73.
  224. Lord, C.J. and A. Ashworth, *Targeted therapy for cancer using PARP inhibitors*. *Current Opinion in Pharmacology*, 2008. **8**(4): p. 363-369.
  225. Fong, P.C., et al., *Inhibition of Poly(ADP-Ribose) Polymerase in Tumors from BRCA Mutation Carriers*. *New England Journal of Medicine*, 2009. **361**(2): p. 123-134.
  226. Rehman, F.L., C.J. Lord, and A. Ashworth, *Synthetic lethal approaches to breast cancer therapy*. *Nature Reviews Clinical Oncology*, 2010. **7**(12): p. 718-724.
  227. Miki, Y., et al., *A Strong Candidate for the Breast and Ovarian-Cancer Susceptibility Gene Brca1*. *Science*, 1994. **266**(5182): p. 66-71.
  228. Venkitaraman, A.R., *Cancer susceptibility and the functions of BRCA1 and BRCA2*. *Cell*, 2002. **108**(2): p. 171-82.
  229. Turner, N., A. Tutt, and A. Ashworth, *Hallmarks of 'BRCAness' in sporadic cancers*. *Nature Reviews Cancer*, 2004. **4**(10): p. 814-819.
  230. Giorgetti, G., et al., *Brcaness phenotype and methylation of BRCA1 promoter in sporadic breast cancers*. *Annals of Oncology*, 2007. **18**: p. 52-52.
  231. Shen, W.H., et al., *Essential role for nuclear PTEN in maintaining chromosomal integrity*. *Cell*, 2007. **128**(1): p. 157-170.
  232. Mendes-Pereira, A.M., et al., *Synthetic lethal targeting of PTEN mutant cells with PARP inhibitors*. *Embo Molecular Medicine*, 2009. **1**(6-7): p. 315-322.
  233. Shaheen, M., et al., *Synthetic lethality: exploiting the addiction of cancer to DNA repair*. *Blood*, 2011. **117**(23): p. 6074-82.
  234. Delaney, C.A., et al., *Potentiation of temozolomide and topotecan growth inhibition and cytotoxicity by novel poly(adenosine diphosphoribose) polymerase inhibitors in a panel of human tumor cell lines*. *Clin Cancer Res*, 2000. **6**(7): p. 2860-7.
  235. Miknyczki, S.J., et al., *Chemopotentiation of temozolomide, irinotecan, and cisplatin activity by CEP-6800, a poly(ADP-ribose) polymerase inhibitor*. *Mol Cancer Ther*, 2003. **2**(4): p. 371-82.
  236. Liuzzi, M. and M. Talpaert-Borle, *A new approach to the study of the base-excision repair pathway using methoxyamine*. *J Biol Chem*, 1985. **260**(9): p. 5252-8.
  237. Liu, L., Y. Nakatsuru, and S.L. Gerson, *Base excision repair as a therapeutic target in colon cancer*. *Clin Cancer Res*, 2002. **8**(9): p. 2985-91.
  238. Taverna, P., et al., *Methoxyamine potentiates DNA single strand breaks and double strand breaks induced by temozolomide in colon cancer cells*. *Mutat Res*, 2001. **485**(4): p. 269-81.
  239. Fishel, M.L., et al., *Manipulation of base excision repair to sensitize ovarian cancer cells to alkylating agent temozolomide*. *Clin Cancer Res*, 2007. **13**(1): p. 260-7.
  240. Taverna, P., et al., *Inhibition of base excision repair potentiates iododeoxyuridine-induced cytotoxicity and radiosensitization*. *Cancer Res*, 2003. **63**(4): p. 838-46.
  241. Anthony, S.P., L. S. Rosen, G. J. Weiss, M. S. Gordon, B. J. Adams, S. L. Gerson, D. Alvarez, C. P. Theuer, and B. R. Leigh., *A phase I study of daily oral TRC102 (methoxyamine) to enhance the therapeutic*

- effects of pemetrexed in patients with advanced refractory cancer. *J Clin Oncol (Meeting Abstracts)* 2009. **27**( 15S)): p. 2552.
242. Sawides, P., Y. Xu, L. Liu, J. A. Bokar, P. Silverman, A. Dowlati, and S. L. Gerson. , *Pharmacokinetic profile of the base-excision repair inhibitor methoxyamine-HCl (TRC102; MX) given as an one-hour intravenous infusion with temozolomide (TMZ) in the first-in-human phase I clinical trial.* *J Clin Oncol (Meeting Abstracts)* 2010. **28**((15S)): p. e13662.
  243. Shekhar, K.C., *Schistosomiasis drug therapy and treatment considerations.* *Drugs*, 1991. **42**(3): p. 379-405.
  244. Bases, R.E. and F. Mendez, *Topoisomerase inhibition by lucanthone, an adjuvant in radiation therapy.* *Int J Radiat Oncol Biol Phys*, 1997. **37**(5): p. 1133-7.
  245. Luo, M. and M.R. Kelley, *Inhibition of the human apurinic/apyrimidinic endonuclease (APE1) repair activity and sensitization of breast cancer cells to DNA alkylating agents with lucanthone.* *Anticancer Res*, 2004. **24**(4): p. 2127-34.
  246. Mendez, F., J.D. Goldman, and R.E. Bases, *Abasic sites in DNA of HeLa cells induced by lucanthone.* *Cancer Invest*, 2002. **20**(7-8): p. 983-91.
  247. Del Rowe, J.D., et al., *Accelerated regression of brain metastases in patients receiving whole brain radiation and the topoisomerase II inhibitor, lucanthone.* *Int J Radiat Oncol Biol Phys*, 1999. **43**(1): p. 89-93.
  248. Fishel, M.L. and M.R. Kelley, *The DNA base excision repair protein Ape1/Ref-1 as a therapeutic and chemopreventive target.* *Mol Aspects Med*, 2007. **28**(3-4): p. 375-95.
  249. Guikema, J.E., et al., *APE1- and APE2-dependent DNA breaks in immunoglobulin class switch recombination.* *J Exp Med*, 2007. **204**(12): p. 3017-26.
  250. Seo, Y. and T.J. Kinsella, *Essential role of DNA base excision repair on survival in an acidic tumor microenvironment.* *Cancer Res*, 2009. **69**(18): p. 7285-93.
  251. Koll, T.T., et al., *HSP90 inhibitor, DMAG, synergizes with radiation of lung cancer cells by interfering with base excision and ATM-mediated DNA repair.* *Mol Cancer Ther*, 2008. **7**(7): p. 1985-92.
  252. Seiple, L.A., et al., *Potent inhibition of human apurinic/apyrimidinic endonuclease 1 by arylstibonic acids.* *Mol Pharmacol*, 2008. **73**(3): p. 669-77.
  253. Wilson, D.M., 3rd and A. Simeonov, *Small molecule inhibitors of DNA repair nuclease activities of APE1.* *Cell Mol Life Sci*, 2010.
  254. Zawahir, Z., et al., *Pharmacophore guided discovery of small-molecule human apurinic/apyrimidinic endonuclease 1 inhibitors.* *J Med Chem*, 2009. **52**(1): p. 20-32.
  255. Bapat, A., et al., *Novel small-molecule inhibitor of apurinic/apyrimidinic endonuclease 1 blocks proliferation and reduces viability of glioblastoma cells.* *J Pharmacol Exp Ther*, 2010. **334**(3): p. 988-98.
  256. Simeonov, A., et al., *Identification and characterization of inhibitors of human apurinic/apyrimidinic endonuclease APE1.* *PLoS One*, 2009. **4**(6): p. e5740.
  257. Humphrey, W., A. Dalke, and K. Schulten, *VMD: visual molecular dynamics.* *J Mol Graph*, 1996. **14**(1): p. 33-8, 27-8.
  258. Grant, J.A.G., M. A.; Pickup, B. T., *A fast method of molecular shape comparison: A simple application of a Gaussian description of molecular shape.* *J. Comput. Chem*, 1996(17): p. 1653-1666.

259. Kitchen, D.B., et al., *Docking and scoring in virtual screening for drug discovery: methods and applications*. Nat Rev Drug Discov, 2004. 3(11): p. 935-49.
260. Mol, C.D., et al., *DNA-bound structures and mutants reveal abasic DNA binding by APE1 and DNA repair coordination [corrected]*. Nature, 2000. 403(6768): p. 451-6.
261. <http://www.pdb.org/pdb/explore/explore.do?structureId=2ISI>, 2006.
262. Beernink, P.T., et al., *Two divalent metal ions in the active site of a new crystal form of human apurinic/apyrimidinic endonuclease, Ape1: implications for the catalytic mechanism*. J Mol Biol, 2001. 307(4): p. 1023-34.
263. Hartshorn, M.J., et al., *Diverse, high-quality test set for the validation of protein-ligand docking performance*. J Med Chem, 2007. 50(4): p. 726-41.
264. Engelward, B.P., et al., *A chemical and genetic approach together define the biological consequences of 3-methyladenine lesions in the mammalian genome*. J Biol Chem, 1998. 273(9): p. 5412-8.
265. Gewirtz, D.A., *A critical evaluation of the mechanisms of action proposed for the antitumor effects of the anthracycline antibiotics adriamycin and daunorubicin*. Biochem Pharmacol, 1999. 57(7): p. 727-41.
266. Vascotto, C., et al., *APE1/Ref-1 interacts with NPM1 within nucleoli and plays a role in the rRNA quality control process*. Mol Cell Biol, 2009.
267. Madhusudan, S. and M.R. Middleton, *The emerging role of DNA repair proteins as predictive, prognostic and therapeutic targets in cancer*. Cancer Treat Rev, 2005. 31(8): p. 603-17.
268. Liu, F., Y. Fu, and F.L. Meyskens, Jr., *MtTF regulates cellular response to reactive oxygen species through transcriptional regulation of APE-1/Ref-1*. J Invest Dermatol, 2009. 129(2): p. 422-31.
269. Gribbon, P., et al., *Evaluating real-life high-throughput screening data*. J Biomol Screen, 2005. 10(2): p. 99-107.
270. Esposito, E.X., A.J. Hopfinger, and J.D. Madura, *Methods for applying the quantitative structure-activity relationship paradigm*. Methods Mol Biol, 2004. 275: p. 131-214.
271. Abbotts, R. and S. Madhusudan, *Human AP endonuclease 1 (APE1): from mechanistic insights to druggable target in cancer*. Cancer Treat Rev, 2010. 36(5): p. 425-35.
272. Mohammed, M.Z., et al., *Development and evaluation of human AP endonuclease inhibitors in melanoma and glioma cell lines*. Br J Cancer, 2011. 104(4): p. 653-63.